



University  
of Glasgow

Thakur, Teena (2025) *Investigating drug resistance in RAS-driven models of colon cancer*. PhD thesis.

<https://theses.gla.ac.uk/84890/>

Copyright and moral rights for this work are retained by the author

A copy can be downloaded for personal non-commercial research or study,  
without prior permission or charge

This work cannot be reproduced or quoted extensively from without first  
obtaining permission in writing from the author

The content must not be changed in any way or sold commercially in any  
format or medium without the formal permission of the author

When referring to this work, full bibliographic details including the author,  
title, awarding institution and date of the thesis must be given

Enlighten: Theses

<https://theses.gla.ac.uk/>  
[research-enlighten@glasgow.ac.uk](mailto:research-enlighten@glasgow.ac.uk)

# Investigating Drug Resistance in RAS-driven Models of Colon Cancer

Teena Thakur,  
B.Tech

Student ID: XXXXXXXX

Supervisors: Ross Cagan, Owen Sansom and Andrew Campbell

Thesis Submitted to the University of Glasgow for the  
Degree of Doctor of Philosophy (PhD)

College of Medical, Veterinary, and Life Sciences

November 2024



University  
of Glasgow



CANCER  
RESEARCH  
UK

Scotland  
Institute

CRUK Beatson Institute  
Garscube Estate  
Switchback Road  
Glasgow  
G61 1BD  
United Kingdom

# Abstract

Colorectal cancer (CRC) is the second leading cause of cancer-related mortality in the world, accounting for more than 900,000 deaths in 2020. A disproportionate number of these deaths are due to KRAS-mutant CRCs, which account for ~40% of all CRC cases and are notoriously resistant to most therapies. Despite showing great promise in preclinical studies, targeted therapies have performed sub-optimally in clinical trials for KRAS mutant cancers. The mechanisms by which RAS pathway inhibitors have failed to reduce tumour progression remains poorly understood and presents a huge clinically unmet need. This research addresses the significant gap in effective treatments for KRAS-mutant CRC by delving into the mechanisms underlying drug resistance, using advanced CRC models. Several studies have reported that drug resistance is an emergent feature of genetically complex tumours.

To capture tumour genome complexity, I used a diverse panel of CRC models reflecting multigenic and heterogeneous nature of tumours. Our patient-specific *Drosophila avatars* and transgenic mouse models are designed to explore how genome complexity impacts drug response. Our models comprise alterations in at least three primary pathways implicated in CRCs- APC, KRAS and TP53, providing a robust platform for studying the cellular and molecular dynamics driven by oncogenic Ras signalling.

Key findings demonstrate that CRC tumour complexity significantly impacts the efficacy of RAS-pathway inhibitors, which have shown limited success clinically. By characterizing these models, this research has uncovered that different stages of tumour development exhibit varying dependencies on the MAPK pathway, offering insights into the failure of existing therapies. Additionally, the study identifies and validates the upregulation of the glucuronidation detoxification pathway as a novel resistance mechanism, showing that targeted combination therapies can enhance drug efficacy within tumours.

This comprehensive study not only deepens the understanding of CRC pathogenesis and resistance mechanisms but also opens avenues for developing more effective targeted therapies.

# Table of Contents

<b>ABSTRACT</b> .....	<b>1</b>
<b>TABLE OF CONTENTS</b> .....	<b>2</b>
<b>LIST OF FIGURES</b> .....	<b>5</b>
<b>ACKNOWLEDGMENT</b> .....	<b>7</b>
<b>AUTHOR'S DECLARATION</b> .....	<b>10</b>
<b>DEFINITIONS /ABBREVIATIONS</b> .....	<b>11</b>
<b>CHAPTER 1 INTRODUCTION</b> .....	<b>13</b>
<b>1.1 COLORECTAL CANCER - GLOBAL INCIDENCE AND SURVIVAL</b> .....	<b>13</b>
<b>1.2 TREATMENT STRATEGIES</b> .....	<b>13</b>
<b>1.3 CRC INITIATION AND PROGRESSION</b> .....	<b>16</b>
1.3.1 <i>Sequential theory</i> .....	<b>16</b>
1.3.2 <i>The Big Bang Theory</i> .....	<b>17</b>
<b>1.4 MAJOR PATHWAY ALTERATIONS IN CRC</b> .....	<b>19</b>
1.4.1 <i>The Canonical Wnt Signalling Pathway</i> .....	<b>20</b>
1.4.1.1 Pathophysiology of the canonical Wnt pathway.....	<b>21</b>
1.4.1.2 Challenges in targeting the Wnt pathway.....	<b>21</b>
1.4.2 <i>The RAS Signalling Pathway</i> .....	<b>22</b>
1.4.2.1 Pathophysiology of the RAS pathway .....	<b>23</b>
1.4.2.2 Challenges in targeting the RAS pathway .....	<b>24</b>
1.4.3 <i>The P53 pathway</i> .....	<b>25</b>
1.4.3.1 Pathophysiology of the p53 pathway .....	<b>26</b>
1.4.3.2 Challenges in targeting the p53 pathway.....	<b>26</b>
<b>1.5 DISEASE MODELLING IN MOUSE AND DROSOPHILA</b> .....	<b>27</b>
1.5.1 <i>Spatio-temporal transgene regulation in mice models</i> .....	<b>29</b>
1.5.2 <i>Spatio-temporal transgene regulation in Drosophila models</i> .....	<b>31</b>
<b>1.6 GENETIC COMPLEXITY AND DRUG RESISTANCE IN CRC</b> .....	<b>33</b>
<b>1.7 AIMS</b> .....	<b>34</b>
<b>CHAPTER 2 MATERIALS AND METHODS</b> .....	<b>35</b>
<b>2.1 FLY MODELS OF RAS-DRIVEN COLON CANCER</b> .....	<b>35</b>
2.1.1 <i>Optimising Developmental Temperature for Flies</i> .....	<b>35</b>
2.1.2 <i>Drug Treatment</i> .....	<b>36</b>
2.1.3 <i>Rescue-from-lethality assay</i> .....	<b>36</b>
2.1.4 <i>RNA isolation and RNA Sequencing</i> .....	<b>36</b>
<b>2.2 MOUSE MODELS OF RAS DRIVEN COLON CANCER</b> .....	<b>37</b>
2.2.1 <i>Mouse Housing and Ethics</i> .....	<b>37</b>
2.2.2 <i>Genetic Alleles</i> .....	<b>37</b>
2.2.3 <i>Treatment groups and Drug Formulations:</i> .....	<b>38</b>
2.2.4 <i>Inductions, Treatment Regime and Sample processing</i> .....	<b>38</b>
2.2.4.1 Short-term Model .....	<b>39</b>
2.2.4.2 Long-term Model .....	<b>40</b>
2.2.4.3 Colon Tumour Model.....	<b>40</b>
2.2.4.4 Intracolonic Transplantation Model .....	<b>41</b>
2.2.5 <i>Histoprocessing</i> .....	<b>42</b>
2.2.6 <i>Tumour Scoring</i> .....	<b>42</b>
2.2.7 <i>In vivo proliferation Assay</i> .....	<b>43</b>
2.2.8 <i>Immunohistochemistry and RNA in situ hybridisation</i> .....	<b>44</b>
2.2.9 <i>Slide Scanning</i> .....	<b>44</b>
<b>2.3 CRYPT ISOLATION AND ORGANOID CULTURE</b> .....	<b>44</b>

2.3.1	<i>Determination of IC<sub>50</sub></i> .....	45
2.3.2	<i>Western blot and antibodies used</i> .....	46
2.3.3	<i>Cell cycle analysis</i> .....	46
2.4	STATISTICAL ANALYSES .....	46
2.5	ILLUSTRATIONS.....	46
<b>CHAPTER 3 CHARACTERISATION OF MODELS TO STUDY DRUG RESPONSE IN RAS DRIVEN COLON CANCER .....</b>		<b>47</b>
3.1	GENETICALLY COMPLEX FRUIT-FLY MODELS OF RAS-DRIVEN COLORECTAL CANCER.....	47
3.1.1	<i>Oncogenic Ras signalling in larval hindgut results in enlarged hindgut proliferation zone</i> .....	47
3.1.2	<i>Spatio-temporal regulation of transgenes in a patient-specific fly avatar mirrors clinical response</i> .....	48
3.2	MOUSE MODELS OF KRAS-DRIVEN COLORECTAL CANCER .....	51
3.2.1	<i>Short-term Model</i> .....	53
3.2.2	<i>Long-term model</i> .....	56
3.2.2.2	<i>Oncogenic Ras signalling enhances tumour development in the colon</i> .....	58
3.2.2.3	<i>Loss of p53 further increases the overall tumour burden and impacts overall survival</i> ....	60
3.2.2.4	<i>Discussion</i> .....	62
3.2.3	<i>Colon tumour model</i> .....	63
3.3	<i>Intestinal organoids</i> .....	66
3.3	DISCUSSION .....	67
<b>CHAPTER 4 TARGETING THE MAPK PATHWAY IN OUR CRC MODELS .....</b>		<b>70</b>
4.1	INVESTIGATION OF MAPK DEPENDENCY IN DROSOPHILA MODEL OF CRC .....	70
4.1.1	<i>Response of patient-specific fly avatar to targeted therapies</i> .....	70
4.1.2	<i>Screening of genetically complex Drosophila models on trametinib</i> .....	71
4.2.1	<i>Determination of IC<sub>50</sub> value</i> .....	73
4.2.2	<i>Qualitative analysis of key signalling pathways</i> .....	74
4.2.3	<i>Cell cycle analysis of Ras-driven small intestinal organoids</i> .....	76
4.3	INVESTIGATING MAPK DEPENDENCY IN MOUSE MODELS OF CRC .....	77
4.3.1	<i>Targeting MAPK in Kras driven hyperproliferation model</i> .....	77
4.3.2	<i>Targeting the RAS pathway in Kras driven intestinal tumour model</i> .....	80
4.3.2.1	<i>Response to MEK inhibition in Kras driven intestinal tumour model with functional p53</i> .80	
4.3.2.2	<i>Response to MEK inhibition in Kras driven intestinal tumour model with loss of p53</i> .....	83
4.3.3	<i>Targeting the RAS pathway in Kras driven colon tumour model</i> . .....	88
4.4	DISCUSSION .....	94
<b>CHAPTER 5 COMBINATION STRATEGIES TO TARGET VULNERABILITIES OF KRAS MUTANT CRCs</b>		<b>96</b>
5.1	DOSE TITRATION OF TRAMETINIB .....	97
5.1.1	<i>Dose titration of trametinib in short-term model</i> .....	97
5.1.2	<i>Dose titration of trametinib in orthotopic transplantation model</i> .....	99
5.2	CRC ORTHOTOPIC TRANSPLANTATION FOR MASS SPEC ANALYSIS OF TRAMETINIB AND ITS METABOLITES...	101
5.3	COMBINATION OF TRAMETINIB AND VORINOSTAT IN SHORT-TERM MODEL .....	102
5.4	COMBINATION OF TRAMETINIB AND VORINOSTAT IN LONG-TERM MODEL .....	104
5.4.1	<i>Combination of vorinostat and standard-dose trametinib offers no survival advantage</i> .....	104
5.4.2	<i>Combination of vorinostat and low-dose trametinib improves survival</i> .....	107
5.5	DISCUSSION .....	109
<b>CHAPTER 6 DISCUSSION AND OUTLOOK .....</b>		<b>111</b>
6.1	ONCOGENIC RAS SIGNALLING PERTURBS INTESTINAL HOMEOSTASIS .....	111
6.2	ONCOGENIC KRAS ACCELERATES TUMOUR DEVELOPMENT IN THE MOUSE COLON .....	112
6.3	ONCOGENIC KRAS DOES NOT ACCELERATE PROLIFERATION IN ESTABLISHED COLON TUMOURS IN MICE .....	112
6.4	GENETICALLY COMPLEX RAS-DRIVEN TUMOURS ARE RESISTANT TO MAPK SUPPRESSION .....	113
6.5	MAPK DEPENDENCY CHANGES DURING THE COURSE OF TUMOUR DEVELOPMENT IN MICE.....	113

6.6	TUMOUR MICROENVIRONMENT IMPACTS RESPONSE TO MAPK SUPPRESSION.....	113
6.7	COLON TUMOURS EVADE DRUG RESPONSE BY UPREGULATING A TOXIN-CLEARANCE PATHWAY .....	114
<b>7</b>	<b>BIBLIOGRAPHY .....</b>	<b>117</b>

# List of Figures

Figure 1-1: The Sequential theory of CRC initiation and progression. ....	17
Figure 1-2: The Big Bang model of CRC initiation and progression (Sottoriva et al., 2015)....	18
Figure 1-3: Illustration of the canonical Wnt Signalling Pathway .....	20
Figure 1-4: Overview of RAS Signalling Pathway.....	22
Figure 1-5: Illustration of Tamoxifen-inducible Cre-Lox system in mice.....	30
Figure 2-1: Illustration of study plan in Drosophila.....	36
Figure 2-2: Illustration showing transgene activation and treatment plan for different Ras-driven intestinal tumour models of CRC .....	39
Figure 3-1:Transgene activation in fly hindgut leads to expansion of Hindgut Proliferation Zone.....	48
Figure 3-2: Characterisation of fly hindgut as a model of human CRC. ....	50
Figure 3-3:Illustration of different Kras-driven mouse intestinal tumour models utilised in this thesis. ....	53
Figure 3-4: Changes in intestinal crypt pathology upon tamoxifen administration in short-term model. (Representative images) .....	54
Figure 3-5: Oncogenic Ras activation leads to rapid hyperproliferation of intestinal crypts..	55
Figure 3-6: Figure 3-5: Loss of Apc predisposes tumour formation in the small intestine. ....	57
Figure 3-7: Oncogenic Kras shortens survival in mice by increasing colonic tumour burden.	59
Figure 3-8: Further loss of p53 reduces median survival by increasing overall tumour burden. ....	61
Figure 3-9: Oncogenic Kras signalling accelerates tumour development in the colon and loss of p53 accelerates overall tumour burden. ....	62
Figure 3-10: Brightfield images of intracolonic tumors stained with haematoxylin & eosin. ....	63
Figure 3-11: Analysis of key signalling pathways in colon tumour model.....	64
Figure 3-12: Loss of Apc results in altered cellular organisation in organoids. ....	66
Figure 3-13: Orthotopic transplantation of mouse derived intestinal organoids in the colon.	67
Figure 4-1: Genetically complex Drosophila avatar is resistant towards most targeted therapies. ....	71
Figure 4-2: Passenger mutations impact response to trametinib. ....	72
Figure 4-3: Genetic complexity impacts response to MEK inhibition in intestinal organoids..	73
Figure 4-4: Trametinib suppresses MAPK activity in Kras driven intestinal organoids.....	74
Figure 4-5: Trametinib suppresses MAPK activity and induces cell death.....	75
Figure 4-6: Organoids with loss of p53 arrest at G0/G1 upon MEK inhibition with trametinib. ....	77
Figure 4-7: Trametinib suppresses proliferation of hyperproliferative small intestinal and colon crypts of AK-HOM mice. ....	78
Figure 4-8: Trametinib suppresses proliferation of hyperproliferative small intestinal and colon crypts of AKP-HOM mice. ....	79
Figure 4-9: Trametinib treatment results in up to 30% survival extension in mice bearing Kras driven intestinal tumours with functional p53. ....	81
Figure 4-10: Survival extension in Trametinib treated in AK-HET mice is due to reduction of tumour burden in colon but not small intestine. ....	82
Figure 4-11: Distribution of tumour burden by size in small intestine and colon. ....	83
Figure 4-12: Trametinib treatment results in up to 75% survival extension in mice bearing Kras driven intestinal tumours with loss of p53. ....	85
Figure 4-13: Survival extension in Trametinib treated AKP-HET mice is due to reduction in overall tumour burden. While this reduction in tumour burden is dose-dependent, it is more pronounced in the colon. ....	86
Figure 4-14: Extension of survival causes progression to adenocarcinoma in some intestinal tumours. ....	87

Figure 4-15: Trametinib treatment does not suppress proliferation in Ras-driven colon tumour model. ....	89
Figure 4-16: Trametinib suppresses MAPK activity in Kras driven colon tumour model. ....	90
Figure 4-17: Trametinib treatment alters Wnt signalling activity based on p53 status. ....	91
Figure 4-18: Trametinib treatment induces p21 in Ras driven colon tumour with functional p53. ....	92
Figure 4-19: Trametinib treatment induces double strand breaks in Ras driven colon tumour with functional p53. ....	93
Figure 5-1: Glucuronidation pathway induces trametinib resistance in Drosophila and mouse intestinal organoids. ....	96
Figure 5-2: Schematic summary of targeting trametinib glucuronidation by blocking deacetylation step. ....	97
Figure 5-3: Trametinib has a dose-dependent effect on suppressing proliferation and MAPK activity in the intestinal crypts. ....	98
Figure 5-4: Trametinib has a modest effect on suppressing proliferation in orthotopically transplanted model. ....	100
Figure 5-5: LC-MS analysis revealed low-levels of Trametinib in colon tumour compared to adjacent normal intestine in mice that received trametinib as a single-agent. ....	102
Figure 5-6: Combination of Trametinib and vorinostat moderately suppresses proliferation in acute hyperplastic intestinal crypts. ....	103
Figure 5-7: Addition of vorinostat does not contribute to survival extension at standard-dose of Trametinib. ....	104
Figure 5-8: Addition of vorinostat has no additional impact on tumour burden at standard-dose of Trametinib. ....	105
Figure 5-9: Emergence of drug-resistant lesions is observed in the small intestine of AKP-HET mice. ....	106
Figure 5-10: Addition of vorinostat has a modest impact on extension of survival at low-dose Trametinib. ....	107
Figure 5-11: Addition of vorinostat has a modest impact on reduction in tumour burden at low-dose Trametinib. ....	108

# Acknowledgment

During my first day in a cancer research lab at National University of Singapore in 2014, I found myself exploring the COSMIC database to analyse BRCA mutations in over 50 ovarian cancer cell lines. I was struck by the sheer number of mutations present—sometimes exceeding 3,000—in these cancer lines. While the existence of multiple mutations in cancer was already known, my deep dive into each cell line's mutations, beyond just the BRCA status, sparked a profound curiosity in me. I began to wonder how these other mutations might influence drug responses, particularly in terms of homologous recombination proficiency and sensitivity to PARP inhibitors.

Over the next four years, my research focused on the implications of DNA repair proficiency in response to chemotherapy and PARP inhibition, examining the deregulation of DNA repair pathways in ovarian cancer cell lines. I realized that cancer cells are not simply defined by a few mutations but are often composed of thousands, driven by a handful of key genes. Throughout this process, I couldn't help but question the roles of other mutations in therapy responses—whether they contributed to sensitivity or resistance.

Until then, my research had primarily focused on cancer models with deregulation in single pathways, leading to a reductionist approach to a complex disease. However, I was deeply intrigued by how various mutations could affect drug resistance and tumour progression. I often pondered whether therapy responses are simply the sum of all mutations or an integration of them, how different signalling pathways interact under normal and cancerous conditions, and how we could study such intricate models.

In 2020, I seized the opportunity to study the impact of genetic complexity in Ras mutant colon cancers. I was well aware that pursuing a PhD would be challenging. I had already experienced the feelings of imposter syndrome, the frustration of experimental results that contradicted my initial hypotheses, and the difficulty of transforming projects into publishable papers. I decided that selecting a project rooted in genuine curiosity—questions that kept me awake at night—would be essential.

This PhD project represented that opportunity. Moving halfway across the world during a pandemic to work with the Sansom group and Cagan lab felt worthwhile. I was excited about delving into what is known and unknown in the field. While Ras pathway inhibitors have shown promise in other Ras mutant cancers, colorectal cancer (CRC) has remained resistant to these therapies. This PhD allowed me to explore genetically complex models and investigate some of the most pressing challenges in CRC.

I am immensely grateful to **Owen Sansom** and **Ross Cagan** for granting me this opportunity to study drug resistance in these models. The foundation they built in their lab enabled me to pose intriguing—and sometimes seemingly absurd—questions. My heartfelt thanks to them for their guidance throughout my thesis journey, helping me lay a solid foundation with mouse and fruit fly models, allowing me to ask compelling questions, however unconventional.

I extend my gratitude to **Andrew Campbell** for countless discussions and brainstorming sessions about my project. His reassurance during moments of self-doubt about my experimental design and the questions I was probing helped me greatly. I am thankful for his valuable advice, support, and for critically reviewing this thesis prior to submission.

I am also grateful to **Rachel Ridgway** and **Catriona Ford** for training me on the mouse models and for their invaluable support with mouse experiments during the final months of my thesis writing. A special thanks to **Bojie Cong**, who taught me about *Drosophila*

genetics and the intricacies of larval dissections. His unwavering commitment to scientific pursuit inspired me and I learned the importance of resilience in the face of setbacks.

Interactions with the Cagan lab and Sansom group enriched my experience; each lab meeting left me eager to learn more. I am thankful to all members of both laboratories for the stimulating discussions during journal meetings and lunches.

I especially want to thank **Alexandra McLaren** for taking the time to guide me through cancer pathology and the similarities and differences between mouse tumours and human cancers. Until then, I struggled to decipher H&E sections, but thanks to her, I developed a newfound appreciation for tissue architecture and the resilience of poorly structured tumours against aggressive treatments.

Much of the critical data included in this thesis was generated in the last year, and I am immensely grateful to **the Histology Team** and **the BSU team** for their support with histology and animal experiments, which involved over 100 mice and countless blocks. Their willingness to accommodate my urgent requests amid the busy demands of the institute was invaluable. Colin's histology team and the BSU mice facility provided the exceptional quality of support that enabled me to pursue compelling research questions.

I owe a special debt of gratitude to **Akhilesh Gaharwar** at Texas A&M University for giving me my first break into academia. My internship in his lab during 2014-2015 was pivotal; without it, I might not have pursued a career in academic research. It was there that I realized the potential of what science can achieve. I also owe thanks to the talented scientists I worked with, including Dr Prachi Desai and Dr Janet Xavier, with whom I spent many nights in the lab building biomimetics and dreaming of creating groundbreaking biomaterials.

Finally, I am immensely grateful to **Dr Anand Jeyasekharan** and **Sir David Lane** for providing a rewarding and enriching experience in their laboratory, where I honed my skills in meticulous experimental planning and attention to detail. David's infectious curiosity about signalling pathways and the role of p53 in drug resistance deepened my desire to understand the fundamentals of cancer biology.

## ***To my family,***

Everything I am and all that I aspire to be, I owe it to my family.

My journey into cancer research was profoundly personal, ignited by my beloved aunt's courageous battle with stage III-B lung cancer. Witnessing her vibrant spirit face the brutal realities of chemotherapy and radiotherapy shocked us all. As a family, we clung to hope with each PET/CT scan, only to be met with the heartbreaking truth that the aggressive treatments had little impact on her tumour. This experience left me with a deep sense of wonder and confusion—how could something so chaotic and out of place not only survive but also thrive in such harsh conditions? I entered cancer research hoping that understanding the disease would help me cope with the grief of losing a loved one. While my parents cared for family members fighting cancer, I found myself miles away, immersing in scientific experiments, feeling helpless but driven to contribute in whatever way I could.

This journey would have been unimaginable without the unwavering support of my mom, dad, brother, and my loving partner, Abhishek. They have weathered long distances and the challenges of different time zones for over a decade, all so that I could pursue my scientific dreams and develop into the scientist I am today.

To my wonderful in-laws and my incredibly supportive friends—Gee, Jan, Dur, Kasthu, Mani, Anj, and Shree—you are the wind beneath my wings. You have patiently endured countless hours of my musings and theories on cancer, always encouraging my quest to communicate science more effectively. Your belief in my potential to make a meaningful impact in the cancer community continues to inspire me every day.

Science, at its core, is a relentless pursuit of curiosity. As I reflect on a decade spent in research, I dedicate this thesis—undoubtedly one of my most significant scientific endeavours—to my beloved **dad, grandpa, and my beautiful aunt.**

The love and support I have received from my family this year have been a guiding light, even as we navigate the heartache of one less beating heart among us.

## Author's Declaration

I confirm that the contents of this thesis are my own work unless stated otherwise. The work contained in this thesis does not form part of any other degree.

# Definitions / Abbreviations

APC - Adenomatous Polyposis Coli

CBC - Crypt Base Columnar Cells

CMS - Consensus Molecular Subtype

CRC - Colorectal Cancer

CRIS - CRC Intrinsic Subtypes

DMSO - Dimethyl sulfoxide

DUSP - Dual Specific Phosphatase

DVL - Dishevelled

EGFR - Epidermal Growth Factor

ERBB - Epidermal Growth Factor Receptor Family

ERK - Extracellular Signal Regulated Kinase

FAP - Familial Adenomatous Polyposis

FOX - Forkhead Box Transcription Factor Family

FZD - Frizzled

GEF - Guanine Nucleotide Exchange Factors

GEMM - Genetically Engineered Mouse Model

GOF - Gain of Function

GPCR - G-Protein Coupled Receptor

GRB2 - Growth Factor Receptor-Bound Protein 2

GSK3 - Glycogen Synthase Kinase 3

H&E - Hematoxylin and Eosin

HPMC - Hydroxypropyl Methylcellulose

IP - Intraperitoneal

ISH - In-situ hybridisation

JNK - c-Jun N-terminal Kinases

KRAS - Kirsten Rat Sarcoma Virus

LGR5 - Leucine-rich Repeat-containing G-protein Coupled Receptor 5

LOF - Loss of Function

LRP5/6 - Low-density Lipoprotein Receptor-related Proteins 5/6

MAPK - Mitogen Activated Protein Kinase

mCRC - metastatic CRC

NSCLC - Non-Small Cell Lung Cancer

PI3-K - Phosphatidylinositol-3-phosphate Kinase

PIP3 - phosphatidylinositol(3,4,5)phosphate; PI(3,4,5)P3

PTEN - Phosphatase and Tensin Homolog

p.o. - per os or oral gavage

q.d - quaque die or once daily

RBD - Ras Binding Domain

RTK - Receptor Tyrosine Kinase

Ri - RNA Interference

SI - Small Intestine

SOS1 - Son of Sevenless Homolog 1

SLS - Scientific Laboratory Supplies

TA - Transit Amplifying

TCF/ LEF - T-cell factor/Lymphoid Enhancer-binding Factor

TGFβ - Transforming Growth Factor Beta

TP53 - Tumour Protein 53

UAS - Upstream Activating Sequence

VDRC - Vienna Drosophila Research Centre

WES - Whole Exome Sequencing

# Chapter 1 Introduction

## 1.1 Colorectal Cancer - Global Incidence and Survival

Colorectal cancer (CRC) remains one of the most prevalent cancers globally and is a leading cause of cancer-related deaths. According to the GLOBOCAN 2020 database, there were an estimated 1.9 million new cases of CRC in 2022, resulting in approximately 900,000 deaths (Bray et al., 2024). The survival rate for CRC depends largely on the stage at diagnosis. About 20% of cases are metastatic at diagnosis, with a similar proportion progressing to metastasis during the course of the disease. Patients diagnosed at an early stage have a five-year survival rate of 90%, but this rate drops to below 15% once the cancer has metastasized, primarily due to decreased therapeutic response and increased drug resistance.

Despite these challenging statistics, there has been gradual progress in combating CRC. In the United Kingdom, for example, the age-standardized incidence rate has remained stable over the past two decades, accompanied by a notable improvement in survival rates. The five-year survival rate has increased from 41% in the 1990s to 59% in the 2010s, marking a significant 18 percentage point improvement (Cancer Research UK). This improvement is largely attributable to advancements in early detection and the development of targeted therapies.

Recent studies indicate a decline in CRC incidence among individuals aged 65 and older, with annual decreases of 3.3% between 2011 and 2016 (Siegel et al., 2020). In contrast, incidence rates are rising among younger populations, with an annual increase of 1% among those aged 50 to 64 and 2% among those under 50 years in age. This increase might be due to changes in lifestyle and diet. Mortality trends also vary by age group, with annual decreases of 3% among those aged 65 and over, but only a 0.6% decrease among those aged 50 to 64, and a concerning 1.3% annual increase in mortality rates for individuals under 50 (Meng et al., 2023). The Surveillance, Epidemiology, and End Results (SEER) registry projects that by 2030, incidence rates for colon and rectal cancers will rise by 90.0% and 124.2%, respectively, among those aged 20 to 34. This alarming trend, noted in younger CRC patients, is linked to poorer survival outcomes and unique adverse event profiles, potentially related to distinct genetic markers (Meng et al., 2023).

## 1.2 Treatment Strategies

### **Surgery:**

As per the latest National Comprehensive Cancer Network (NCCN) guidelines (Version 10 Aug 2024) for patients with colorectal cancer presenting as invasive adenoma in a pedunculated polyp, no further surgery is needed if the polyp is fully removed and exhibits

favourable histological characteristics (Yoshii et al., 2014). Conversely, for sessile polyps, even those with favourable histology, a colectomy is typically recommended due to a higher risk of recurrence, metastasis, and mortality compared to pedunculated polyps. This recommendation stems from the higher likelihood of incomplete removal and positive margins in sessile polyps (Cooper, 2007, Hassan et al., 2005). For visual reference of pedunculated and sessile adenomas, see Section 2.2.6, Figure 2-2.

#### **Adjuvant therapy:**

Apart from surgery, anti-metabolite 5-fluorouracil, a pyrimidine analog that disrupts DNA and RNA synthesis was the backbone of CRC chemotherapy until late 20<sup>th</sup> century (Longley et al., 2003). Although effective as a single agent, its efficacy and survival outcomes improved in metastatic CRC (mCRC) patients upon combination with oxaliplatin or irinotecan; FOLFOX, FOLFIRI or CAPEOX regimen. These combinations have improved response rate (50% vs 22.3%) and overall survival (9 months vs 6.2 months) when compared to 5-FU alone (De Gramont et al., 2000, Köhne et al., 2005).

#### **Biomarkers for targeted therapy:**

The application of targeted therapies has become critical for treating advanced or metastatic CRC. Current guidelines by National Comprehensive Cancer Network (NCCN) recommend assessing tumour gene status, including KRAS/NRAS and BRAF mutations, along with HER2 amplifications and MSI/MMR status, to tailor treatments (Ciombor et al., 2015). Monoclonal antibodies targeting EGFR (e.g., cetuximab and panitumumab) and VEGF (e.g., bevacizumab) are particularly effective when used in conjunction with chemotherapy. Notably, anti-EGFR therapies are only effective in patients without mutations in KRAS, PTEN, and PI3K, as these components are downstream of EGFR, precluding the efficacy of anti-EGFR therapies (Sorich et al., 2015, Tejpar et al., 2012). In patients with wild-type KRAS pathway, these agents have not only improved response rates when combined with cytotoxic drugs but are also beneficial as maintenance therapies in treating metastatic CRC (Simkens et al., 2015). Patients with KRAS- or NRAS-mutant tumours do not benefit from anti-EGFR therapies, and the associated toxicities and costs are unjustifiable (Cutsem et al., 2009). An exception exists for the use of cetuximab or panitumumab combined with sotorasib or adagrasib in patients with the KRAS<sup>G12C</sup> mutation where improved response has been noted in patients that received combination of KRAS<sup>G12C</sup> inhibitor and anti-EGFR therapy (CodeBreak101 and KRYSTAL-1 trial) (Yaeger et al., 2023, Kuboki et al., 2024). Response rate from Sotorasib and Adagrasib was high in Non-Small cell lung cancers (NSCLC) but limited in colorectal cancer patients (CRC) due to adaptive response selectively triggered in CRC. Moreover, both the inhibitors bind to KRAS<sup>G12C</sup> in its GDP-bound state studies have revealed that EGFR signals

can maintain the newly expressed KRAS<sup>G12C</sup> protein in the active GTP-bound form, thereby evading treatment (Xue et al., 2020).

Approximately 5-10% of CRCs have BRAF<sup>V600E</sup> mutation and is often associated with poor prognosis and aggressive cancer (Van Cutsem et al., 2010). Similarly, KRAS is mutated in approximately 40% of CRCs and is also associated with poor prognosis and resistance towards most targeted treatments. KRAS mutation is believed to be an early event in tumorigenesis and results in constitutive signalling and activation of downstream phosphoinositide 3-kinase (PI3K)- and mitogen-activated protein kinase (MAPK)-dependent pathways (Yoon et al., 2014).

Recently, immunotherapy has shown remarkable results in a subset of patients with deficiency in mismatch repair (dMMR) or microsatellite instability (MSI). Based on KEYNOTE 028 phase Ib (Hansen et al., 2018) and Checkmate 142 phase II (Overman et al., 2017) trials pembrolizumab (anti-PD1 antibody) and nivolumab (anti-CTLA-4 antibody) has been approved by the FDA for use in MSI-high and dMMR patients who have progressed through first line chemotherapy.

#### **Unmet needs in KRAS mutant CRC**

KRAS mutations, found in about 40% of mCRC are predominantly in codons 12 and 13 (Jones et al., 2017). Of these mutations, KRAS G12D was most commonly found (36%), followed by G12V (22%), and G13D (19%) (Neumann et al., 2009). KRAS G12C has been reported in approximately 17% of KRAS-mutated mCRCs (Schirripa et al., 2020). Presence of codon 12 mutations in KRAS have been associated with adverse prognosis in aggregate CRC population of diverse disease stages (Modest et al., 2016, Henry et al., 2021) (Andreyev et al., 2001, Imamura et al., 2012, Yoon et al., 2014). It might be speculated that the reason for differing outcomes could be mediated by differing activation of KRAS-dependant pathways by distinct mutation variants.

Apart from cancer relapse, the inability to accurately predict patient survival with mCRC or response to any given regimen of chemotherapy or biologic agents remains a significant obstacle. The discovery of KRAS status as a predictive biomarker for anti-EGFR therapy has been helpful in guiding treatment regimens, however it is insufficient to predict efficacy. There is an unmet need to identify more biomarkers that can predict patient suitability to a particular regimen and guide treatments for patients with distinct genetic underpinnings.

## 1.3 CRC Initiation and Progression

There are two prominent theories explaining the progression of colon cancer: the Sequential theory (Fearon and Vogelstein, 1990) and the more recent Big Bang theory (Sottoriva et al., 2015). These models provide contrasting perspectives on how mutations accumulate and drive CRC development.

### 1.3.1 Sequential theory

The Sequential Theory, also known as the adenoma-carcinoma sequence, posits that tumor initiation is characterised by sequential and step-wise accumulation of somatic mutations, leading to the expansion of clones with selective growth advantages, such that the fittest clone eventually survives (Fearon and Vogelstein, 1990, Vogelstein et al., 2013) (Figure 1-1). By increasing the fitness of a target cell relative to other premalignant cells, driver events can result in clonal expansions and selectively sweep through the resident population. This model suggests that colon cancer begins with the benign growth of an adenoma due to genetic mutations in specific genes, such as APC, KRAS, and TP53. Over time, further mutations accumulate, leading to increased dysplasia and eventually transforming the adenoma into an adenocarcinoma. This theory is characterized by a stepwise progression (Luebeck and Moolgavkar, 2002):

1. Initiation: Small benign adenomas form due to mutations in the APC gene.
2. Proliferation: Additional mutations, such as those in the KRAS gene, lead to the growth and progression of these adenomas.
3. Progression: Further genetic changes, including mutations in TP53 and other genes, drive the transition from advanced adenoma to invasive carcinoma.

This pattern of tumor development is often seen in cancers, such as Barrett's esophagus where tumor initiation often occurs over a span of many years (Maley, 2007). The sequential theory, well corroborated by epidemiological data on CRC incidence (Luebeck and Moolgavkar, 2002), is often regarded as a cornerstone in understanding colorectal cancer progression. According to this model, numerous drivers of tumor growth are anticipated in an established tumor. However, relatively few putative driver mutations have been identified in individual tumors (Lawrence et al., 2013).

Recently, several studies involving large scale lineage tracing and sequencing approaches in primary CRCs indicate that selective sweeps and large clonal expansions are less frequent after transformation and predict star-shaped phylogenies (Siegmond et al., 2009, Humphries et al., 2013, Kostadinov et al., 2013). Investigations of other cancer types similarly highlight branched phylogenies and punctuated clonal evolution (Navin et al., 2010, Baca et al., 2013, Burrell et al., 2013). These studies highlighted that sequential

clonal evolution may not accurately describe patterns of intra-tumoral heterogeneity found in most established human cancers (Davis et al., 2017, Hu et al., 2017).

High levels of intra-tumoral heterogeneity at the genomic, transcriptomic, cellular, and phenotypic levels have been reported in diverse cancers and pose challenges for targeted therapy with implications for patient stratification and the efficacy of targeted therapy.

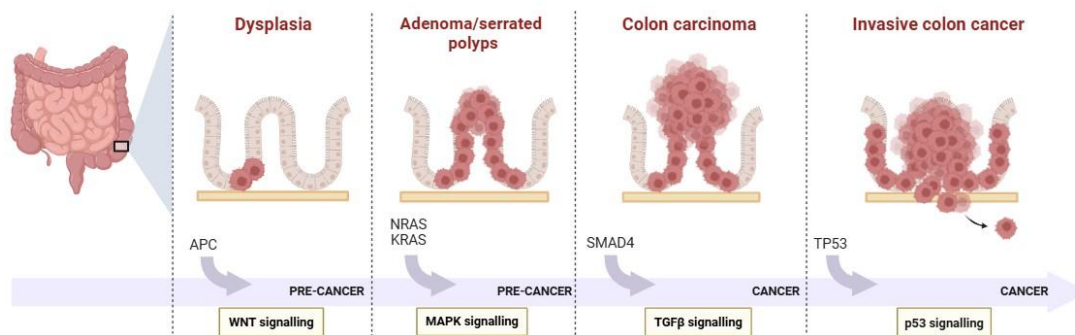


Figure 1-1: The Sequential theory of CRC initiation and progression.

The Sequential model or the adenoma-carcinoma sequence depicts an approximate order of morphological changes that appear at different stages of tumour development, starting with steps that promote benign tumour formation (adenomas), followed by steps that promote progression toward histologically more advanced tumours (colon carcinoma), and finally steps associated with tumour transformation into an invasive carcinoma (invasive colon carcinoma). This illustration was adapted from (Fearon and Vogelstein, 1990) and created with Biorender.com.

### 1.3.2 The Big Bang Theory

Contrasting sharply with the Sequential Theory, the Big Bang theory asserts that cancer does not follow a linear, stepwise progression. Instead, it suggests that once a mutation occurs, cancer cells proliferate rapidly and heterogeneously from a very early stage, even before the tumour is detectable (Sottoriva et al., 2015). According to this model, the timing of mutation dictates its cellular prevalence in the fully established tumor. As such, most detectable sub-clonal alterations occur early during tumor expansion, whereas late-arising mutations will be undetectable as they are diluted by population growth (Figure 1-2). Thus, subclone composition remains relatively homogenous with major clones persisting tumor growth. Key characteristics of this model includes:

1. **Single Mutational Event:** The tumour originates from a single mutational event, and all subsequent growth is effectively a clonal expansion of these initially mutated cells.
2. **Heterogeneity from the Start:** The genetic diversity within the tumour is established early on and remains relatively constant throughout its development. This early heterogeneity results in a variety of cells with different mutations, some of which may confer a more aggressive cancer phenotype.
3. **Spatial Distribution:** The growth of the tumour is more akin to an explosion (hence "Big Bang"), with the bulk of the mutation and the establishment of the tumour architecture occurring early, followed by expansion without further significant evolution.

The predictions generated by the Big Bang model were examined through detailed sampling of distant tumor regions, single gland, and single cell profiling at the mutational and copy-number levels. These studies revealed uniform intra-tumoral heterogeneity at multiple scales. Moreover, glands from distant tumor regions were found to have similar mitotic ages suggesting they derived from the same clonal expansion (Siegmund et al., 2011, Sottoriva et al., 2013). Particularly, patterns of genetic variegation or subclone mixing were observed in glands from distant tumor regions (>3cm apart). These regions were found to harbour identical sub-clonal somatic single nucleotide variants (sSNV) or copy number alteration (CNA) breakpoints (Sottoriva et al., 2015). Using deep targeted sequencing, evidence for subclone mixing was also reported in colorectal cancers (Suzuki et al., 2017) and breast cancers (Yates et al., 2015).

The Big Bang growth dynamics in CRC have been corroborated by several multiregion sequencing (MRS) studies (Bozic et al., 2016, Uchi et al., 2016, Sievers et al., 2017, Suzuki et al., 2017), suggesting that this mode of tumor growth and effective neutrality may be relatively common.

This shift away from a linear gradualist view of the sequential theory towards the punctuated clonal evolution also has clinical ramifications. The conventional linear model implied that aggressive cancers evolve gradually and only become invasive and detectable late during the evolutionary course. However, recent data suggests that early cataclysmic events initiate many such tumors with early specification of malignant potential.

The mice and *Drosophila* models of CRC investigated in my thesis represents the Big Bang model of tumor initiation.

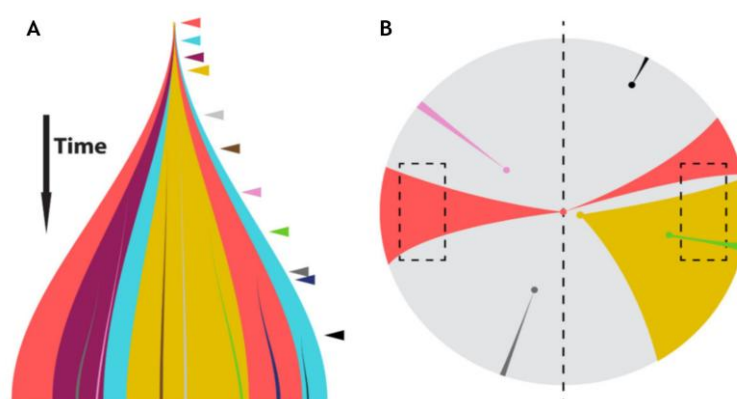


Figure 1-2: The Big Bang model of CRC initiation and progression (Sottoriva et al., 2015).

(A) Post initiation, a tumour grows predominantly as a single expansion populated by numerous heterogenous sub-clones. Intratumoral heterogeneity results from clonal mutations (depicted by coloured arrowheads) accumulating due to replication errors. The clonal mutations acquired early persist and become pervasive in the final tumor, while remaining non-dominant (coloured segments). Late-arising mutations are only present in small regions of the tumor. (B) In the Big Bang model, the pervasiveness of the clonal mutations depends on when the mutation occurs during growth, rather than selection for that mutation. Due to aberrant sub-clone mixing in the primordial tumor, followed by scattering during expansion, sub-clonal mutations are pervasive despite remaining non-dominant (depicted in red and yellow). Late alterations are restricted to small regions (depicted in black) and are essentially undetectable by conventional whole exome sequencing (WES). Illustration from (Sottoriva et al., 2015).

## 1.4 Major Pathway alterations in CRC

CRC being an extremely complex and heterogenous disease, progresses from adenoma to malignant carcinoma through multiple stages with coalescence of multiple signalling pathways. The cumulative accumulation of clonal and sub-clonal mutations varies not only between patients but also between tumours (Tai et al., 2018, Punt et al., 2017). Commonly affected pathways include Wnt, TP53, RTK/RAS, PI3K/AKT, TGFBR1I signalling pathways, along with CpG island methylation, microsatellite instability and chromosomal mutations. Most patients have mutations in at least two or more of these pathways. APC has been identified as the key driver mutation for initiation of CRC tumourigenesis (Fearon and Vogelstein, 1990). Other commonly affected genes include TP53, KRAS, BRAF, NRAS, PIK3CA, FBXW7, SMAD4 and TCF7L2 (TCGA, 2012).

Although genomic sequencing efforts and the identification of key driver mutations have enhanced our understanding of the mechanisms underlying colorectal cancer (CRC) development and progression, they have so far been relatively ineffective in predicting prognosis or therapeutic response. To tackle this limitation, recent research has shifted towards transcriptional profiling of human tumor samples, aiming to achieve a more comprehensive understanding of the molecular biology driving CRC.

In this context, Guinney et al. utilized RNA sequencing on clinical CRC samples and identified four consensus molecular subtypes (CMS) (Guinney et al., 2015). CMS1 tumors were characterized by hypermutation, inclusion of most microsatellite-unstable samples, and a pronounced immune infiltration. CMS2 tumors exhibited high Wnt and Myc signaling activity and epithelial differentiation. CMS3, known as the metabolic subtype, showed enrichment for KRAS mutations and multiple metabolism-related gene signatures. CMS4 tumors, linked to the poorest patient prognosis, demonstrated elevated levels of epithelial-to-mesenchymal transition (EMT) and increased infiltration of non-cancerous cells such as fibroblasts. Since these analyses were performed on bulk tumor samples, the transcriptional profiles included contributions from stromal cells.

Building upon this framework, Joanito et al. conducted single-cell and bulk transcriptome sequencing to further refine the CMS classification. Their study revealed two intrinsic epithelial subtypes, iCMS2 and iCMS3, which provided a more nuanced understanding of tumor heterogeneity. Notably, iCMS3 included both microsatellite unstable (MSI-H) cancers and a subset of microsatellite-stable (MSS) tumors, with the latter exhibiting transcriptomic similarities to MSI-H cancers. This refined classification has significant implications for prognosis and therapeutic strategies (Joanito et al., 2022).

Briefly, the research outlined in this thesis focusses upon three key signalling pathways, each of which plays a crucial role in CRC initiation and progression. These are the Wnt

signalling pathway, the mitogen-activated protein kinase (MAPK) pathway and the p53 pathway. The focus of this thesis was to understand how these pathways interact to drive intestinal cancer in mouse and *Drosophila* models.

### 1.4.1 The Canonical Wnt Signalling Pathway

The Wnt signalling pathway is crucial in both normal cellular functions and the pathology of diseases, including CRC. It plays a significant role in cell growth, differentiation, and migration. Aberrations in Wnt signalling are among the most common molecular changes driving CRC initiation and progression (Rim et al., 2022).

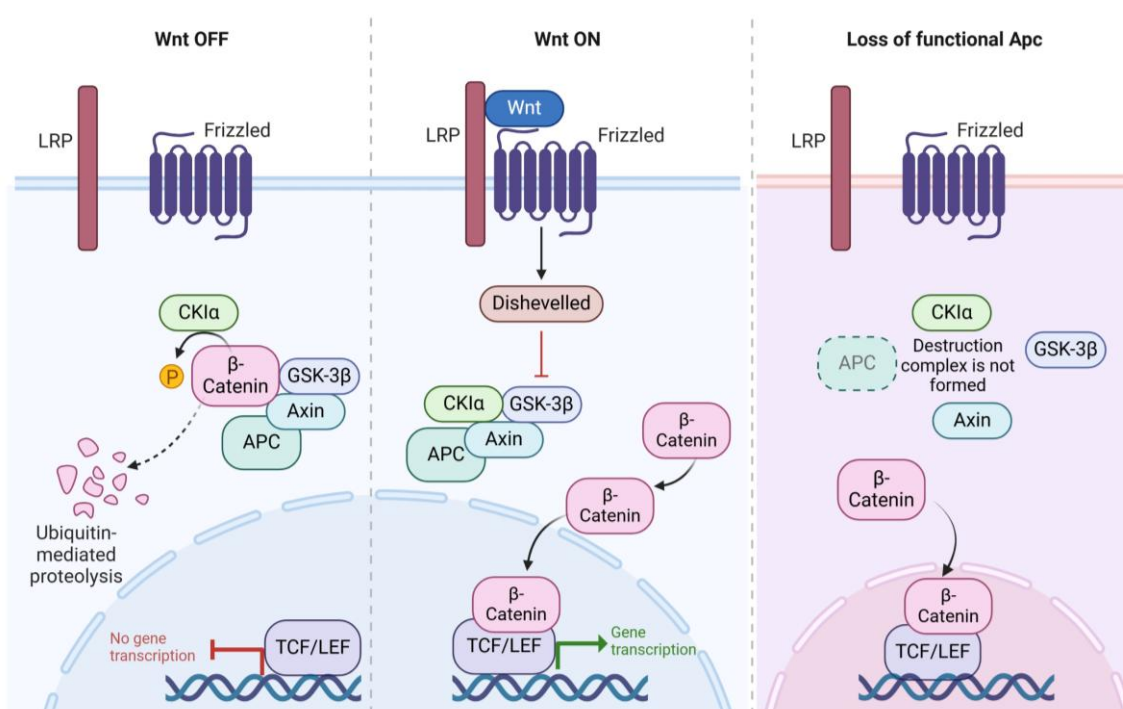


**Figure 1-3: Illustration of the canonical Wnt Signalling Pathway**

Wnt OFF state: In the absence of Wnt signalling,  $\beta$ -Catenin is degraded by the destruction complex (DC), which consists of AXIN, APC, GSK-3 $\beta$ , and CK1. Wnt ON state: Wnt signalling is activated when Wnt ligands bind to receptors (Frizzled and LRP), leading to disruption of the  $\beta$ -Catenin destruction complex. This stabilizes  $\beta$ -Catenin, allowing it to translocate to the nucleus and activate TCF/LEF transcription factors, promoting gene transcription. Upon loss of functional Apc, the DC is not formed, resulting in  $\beta$ -Catenin accumulation.  $\beta$ -Catenin then translocates to the nucleus, where it supports transcription of Wnt target genes. (Adapted from (Zhang and Wang, 2020), created using Biorender.com)

The Wnt pathway involves several key components, including Wnt proteins (which are secreted lipid-modified signalling proteins), Frizzled receptors (which bind to Wnt proteins), LRP5/6 co-receptors, and a set of intracellular proteins that transmit the signal from the cell surface to the nucleus.

Under normal circumstances, in the absence of Wnt proteins, a destruction complex that includes the proteins Axin, APC (adenomatous polyposis coli), GSK-3 (glycogen synthase kinase 3), and CK1 (casein kinase 1) degrades  $\beta$ -catenin, a central player in the Wnt

pathway.  $\beta$ -catenin is marked for degradation by being phosphorylated by GSK-3 and CK1 (Liu et al., 2002, van Noort et al., 2002).

When Wnt proteins are present, they bind to Frizzled receptors and LRP5/6 co-receptors on the cell surface (Bhanot et al., 1996, Cong et al., 2004, Pinson et al., 2000). This binding disrupts the destruction complex (DC), preventing the phosphorylation of  $\beta$ -catenin. As a result,  $\beta$ -catenin is not degraded by the proteasome. Stabilized  $\beta$ -catenin accumulates in the cytoplasm and then translocates into the nucleus. In the nucleus,  $\beta$ -catenin binds to TCF/LEF family of transcription factors. This complex then acts as a transcriptional activator for various target genes such as *MYC*, *AXIN2*, *NOTUM* and *CCND1* (Hernández *et al.*, 2012). The genes activated by  $\beta$ -catenin are involved in numerous processes including cell proliferation, survival, and differentiation. Some of the key genes include *MYC*, which drives cell proliferation, and *CCND1*, which encodes cyclin D1, are crucial for cell cycle progression.

#### 1.4.1.1 Pathophysiology of the canonical Wnt pathway

In CRC, mutations in components of the Wnt pathway, particularly the APC gene, are frequently observed (TCGA, 2012). Mutations in the APC gene result in a truncated APC protein that cannot effectively participate in the  $\beta$ -catenin destruction complex. Consequently,  $\beta$ -catenin is not properly degraded, leading to its accumulation and constant activation of Wnt target genes, even in the absence of Wnt ligands.

Mutations in  $\beta$ -catenin within CRC frequently affect conserved phosphorylation sites on exon 3, leading to protein stabilization. In the proximal small intestine, where Wnt-ligand levels are highest, stable  $\beta$ -catenin expression led to high-grade dysplasia and nuclear localization of  $\beta$ -catenin (Leedham et al., 2013). The severity of these effects gradually decreased moving toward the distal end of the gut. Interestingly, APC truncating mutations in human patients are found in specific regions, suggesting that the extent of APC truncation may be selectively influenced by these regional differences in Wnt signalling (Leedham et al., 2013).

#### 1.4.1.2 Challenges in targeting the Wnt pathway

Over the last three decades, targeting the Wnt signalling pathway has been a significant focus for drug development due to its aberrant activation in numerous cancers. Despite this, no therapies targeting this pathway have yet been approved, although recent clinical trials are testing potential drugs in various hematologic and solid tumours. A major concern with inhibiting the Wnt-beta catenin pathway is its critical role in maintaining stem cells and tissue regeneration (Staal and Sen, 2008). Specifically, there are worries that such inhibition could adversely impact the normal populations of Wnt-dependent stem cells, particularly in regions with rapid cellular turnover, such as hair follicles and the gastrointestinal tract. Early trials with tankyrase inhibitors indicate that

gastrointestinal toxicity could be a dose-limiting factor, potentially restricting their clinical use (Zhong et al., 2016). Furthermore, understanding the extensive interplay among cellular signalling pathways that are frequently mutated in CRC such as the RAS and p53 pathways will be vital for developing effective treatments.

### 1.4.2 The RAS Signalling Pathway

The RAS/MAPK pathway is a critical signalling cascade that regulates various cellular processes including proliferation, survival, growth, migration, and differentiation. It is particularly significant in the development and progression of many cancers, such as CRC.

RAS proteins are members of a family of small guanosine triphosphate (GTP) phosphatases (GTPases) regulating many intracellular networks, which are fundamental in cell proliferation, migration, differentiation, senescence, and apoptosis. Activation of this pathway begins when growth factors bind to receptor tyrosine kinases (RTKs) on the cell surface, such as the epidermal growth factor receptor (EGFR) (Figure 1-2). This binding triggers the RTKs to dimerize and autophosphorylate, for the formation of signalling complexes. RAS proteins are turned off if guanosine diphosphate (GDP)-bound and turned

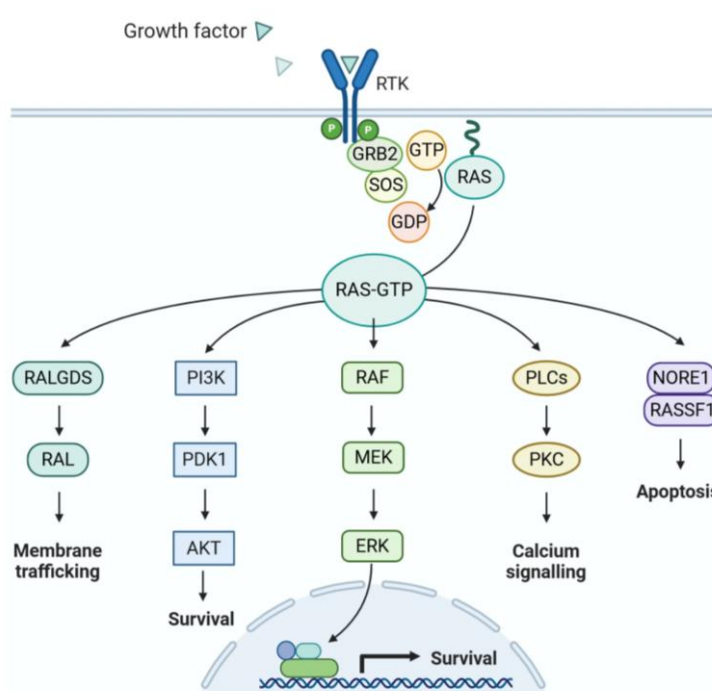


**Figure 1-4: Overview of RAS Signalling Pathway**

In its active, GTP-bound state, RAS interacts with various effector proteins, stimulating their catalytic activities. Major effectors: **RAF protein kinases** initiate the MAP kinase cascade, leading to ERK activation. ERK acts on numerous cytoplasmic and nuclear substrates, including ETS transcription factors like ELK1, to regulate cell-cycle progression. **(PI3Ks)** produce second-messenger lipids, such as phosphatidylinositol-3,4,5-trisphosphate, activating downstream targets, including the survival kinase AKT/PKB. **RALGDS proteins** function as guanine nucleotide exchange factors (GEFs) for RAL, a RAS-related protein, with downstream targets like Forkhead transcription factors. **Phospholipase Cε (PLCε)** catalyzes the hydrolysis of phosphatidylinositol-4,5-bisphosphate, generating diacylglycerol and inositol trisphosphate. This results in protein kinase C (PKC) activation and mobilizes calcium from intracellular stores. Illustration was generated using Biorender.

on when GTP-bound. Despite RAS intrinsic capability of GTP hydrolysis and nucleotide exchange, this process is mainly regulated by extrinsic guanine nucleotide exchange factors (GEF) such as son of sevenless homologue 1 (SOS1) for GDP-to-GTP transition, and GTPase-activating proteins (GAP) such as neurofibromin for GTP hydrolysis (Lowenstein et al., 1992, Pierre et al., 2011). This activation leads to the recruitment and activation of the RAS GTPase, a small protein that acts as a molecular switch, cycling between an inactive GDP-bound state and an active GTP-bound state.

Once activated, RAS engages multiple binding partners, triggering various downstream signalling pathways. These pathways include the canonical MAPK signalling (RAS/RAF/ERK) through interaction with RAF (Matallanas et al., 2011), PI3-Kinase signalling via its catalytic p110 subunit (Cuesta et al., 2021), and activation of RAL-GTPases (Koyama and Kikuchi, 2001) and Rac (Lambert et al., 2002) through their respective GEFs.

In the RAS/RAF/ERK pathway, active RAS-GTP (dimer) activates the RAF kinase family members (ARAF, BRAF, CRAF) (Lavoie and Therrien, 2015), which in turn phosphorylate and activate MEK1 and MEK2 (MAPK/ERK kinases). MEK proteins are dual-specificity kinases that specifically phosphorylate the ERK1 and ERK2 (extracellular signal-regulated kinases) (Braicu et al., 2019, Fanger et al., 1997). Phosphorylated ERKs translocate to the nucleus where they phosphorylate a variety of transcription factors that regulate gene expression. The genes activated by ERK signalling include those involved in cell cycle progression, survival, and differentiation, notably MYC, ELK1, and FOS.

This intricate network of signals plays a vital role in modulating cellular responses to external stimuli, highlighting the complexity and importance of the RAS/RAF/ERK pathway in cellular function and oncogenesis.

#### 1.4.2.1 Pathophysiology of the RAS pathway

Mutations in components of the RAS/RAF/ERK pathway are common in colon cancer. The most frequent mutations occur in the KRAS gene, affecting approximately 40-45% of colon cancer cases. These mutations result in a constitutively active RAS protein, which continuously signals to RAF, MEK, and ERK, regardless of external growth signals.

BRAF mutations are also significant but less common, occurring in about 10% of colon cancers, often signifying a more aggressive disease and a poorer prognosis. *BRAF<sup>V600E</sup>* mutations in CRC often develop primaries in the right-side of the colon and are often associated with decreased response to chemotherapy (Kayhanian et al., 2018). In addition to its poor prognosis, *BRAF<sup>V600E</sup>* mutant CRC patients have worse health-related quality of life (Thomsen et al., 2017).

Continuous activation of the RAS/RAF/ERK pathway leads to uncontrolled cell division and survival, contributing to the initiation and progression of colon cancer. This pathway also influences the tumour microenvironment, promoting angiogenesis (formation of new blood vessels) and metastasis, further complicating the disease progression.

#### 1.4.2.2 Challenges in targeting the RAS pathway

Five main strategies have been identified for targeting the RAS pathway: direct RAS targeting, targeting the RAS pathway, harnessing RAS through immunotherapy combinations, RAS targeting through metabolic pathways. Despite its significance in colon cancer, directly targeting the RAS component of the RAS/RAF/ERK pathway has been challenging. This difficulty arises from the high affinity of RAS proteins for GTP/GDP and their structural complexity, which lacks appropriate binding pockets for effective inhibition. Recent strides have been made with *KRAS*<sup>G12C</sup> inhibitors such as sotorasib or adagrasib in patients with the *KRAS*<sup>G12C</sup> mutation where improved response has been noted in patients that received combination of *KRAS*<sup>G12C</sup> inhibitor and anti-EGFR therapy (CodeBreak101 and KRYSTAL-1 trial) (Yaeger et al., 2023, Kuboki et al., 2024). Response rate from Sotorasib and Adagrasib was high in Non-Small cell lung cancers (NSCLC) but limited in CRC patients due to adaptive response selectively triggered in CRC. Moreover, both the inhibitors bind to *KRAS*<sup>G12C</sup> in its GDP-bound state studies have revealed that EGFR signals can maintain the newly expressed *KRAS*<sup>G12C</sup> protein in the active GTP-bound form, thereby evading treatment (Xue et al., 2020, Awad et al., 2021).

Inhibition of pathway effectors other than RAS represents a further strategy targeting RAS mutant CRC, mainly in the form of combination therapies targeting multiple downstream kinases or upstream membrane RTK (Tolcher et al., 2018). Successful interventions have been achieved with inhibitors targeting downstream elements like BRAF and MEK. For example, *BRAF*<sup>V600E</sup> inhibitors such as vemurafenib, dabrafenib, and encorafenib have shown efficacy with *BRAF*<sup>V600</sup> tumors. However, targeted inhibition of mutant BRAF led to paradoxical activation of EGFR/MAPK pathway through ERK-mediated regulatory feedback (Prahallad et al., 2012). Following this, MEK inhibitors were established as a cornerstone for targeting the RAS pathway, favoured over BRAF inhibitors. MEK inhibitors such as trametinib, binimetinib, and cobimetinib, prevent MEK phosphorylation of ERK ½, thus avoiding its dimerization and nuclear translocation. However, MEK inhibitors have not proved effective in CRC clinical trials as a single-agent (Rosen et al., 2016, Infante et al., 2012) and are currently under investigation in combination with other therapeutic modalities to enhance effectiveness and counteract resistance mechanisms. Here are some challenges for targeting the p53 pathway:

**Resistance and Combination Therapies:** Resistance to therapies targeting the RAS/RAF/ERK pathway is a frequent obstacle, leading to the exploration of combination

treatments that may include BRAF or MEK inhibitors paired with other targeted therapies, chemotherapy, or immunotherapy. This approach aims to improve outcomes by addressing multiple aspects of tumour biology simultaneously.

**Structural Complexity and Redundancy:** The structural complexity of RAS proteins complicates the development of direct inhibitors. Furthermore, the pathway's redundancy and extensive feedback loops mean that inhibiting one part often triggers compensatory mechanisms through alternative pathways, undermining therapeutic efficacy (Xue et al., 2020, Awad et al., 2021).

The ongoing evolution in our understanding of the RAS/RAF/ERK pathway's role in colon cancer underscores the complexity of targeting this essential signalling mechanism. Effective treatment development requires an in-depth understanding of pathway dynamics and its interactions with other cellular processes, highlighting the necessity for comprehensive biomarker-driven strategies in cancer therapy.

### 1.4.3 The P53 pathway

More than forty years ago, four research laboratories across the world independently uncovered the existence of the p53 protein (Linzer and Levine, 1979, Lane and Crawford, 1979, Kress et al., 1979, DeLeo et al., 1979).

p53, often referred to as "the guardian of the genome," is a tumour suppressor protein that is activated in response to various cellular stresses, including DNA damage, oxidative stress, and oncogene activation (Levine, 2019a). The p53 pathway plays a critical role in maintaining genomic stability and preventing tumorigenesis by regulating cell cycle progression, DNA repair, apoptosis, and senescence (Levine, 2019a, Vogelstein et al., 2000).

Under normal conditions, p53 levels are kept low through its interaction with MDM2, a protein that promotes the degradation of p53 (Wu et al., 1993). When cellular stress is detected, p53 is stabilized and accumulates in the cell, primarily due to post-translational modifications that prevent MDM2-mediated degradation (Oren et al., 1982).

Once activated, p53 can function as a transcription factor that regulates the expression of a wide range of genes involved in critical cellular processes, such as cell cycle arrest, apoptosis, senescence and DNA repair (Vogelstein et al., 2000). p53 can induce the expression of p21, a cyclin-dependent kinase inhibitor that blocks cell cycle progression, allowing time for DNA repair or activation of other protective mechanisms (Shieh et al., 1997, Kastan et al., 1992). If DNA damage is irreparable, p53 promotes apoptosis through transcriptional activation of pro-apoptotic genes such as BAX, PUMA, and NOXA. p53 can also induce cellular senescence (a permanent state of cell cycle arrest) and upregulate genes involved in DNA repair mechanisms (Mallette and Ferbeyre, 2007).

#### 1.4.3.1 Pathophysiology of the p53 pathway

p53 is one of the most mutated genes in human cancers, including colon cancer (Nigro et al., 1989, Baker et al., 1989). Approximately 50-60% of colon cancer cases harbour mutations in the TP53 gene, resulting in loss of functions (LOFs) necessary for tumor suppression and even the gain-of-functions (GOFs) necessary for tumor growth (Sabapathy and Lane, 2018). Loss of functional p53 has been reported to cause:

- **Enhanced proliferation:** The inability to arrest the cell cycle or induce apoptosis allows cells with damaged DNA to continue dividing, enhancing tumour growth (Drosten et al., 2014).
- **Resistance to Therapy:** The loss of p53 function contributes to resistance against chemotherapy and radiation therapy, which often rely on p53-mediated apoptosis to kill cancer cells (Chang et al., 2023, Cao et al., 2020, Hientz et al., 2017, Keshelava et al., 2001, Drosten et al., 2014).
- **Increased Tumour Aggressiveness and Poor Prognosis:** Studies have shown that tumours with p53 mutations are often more aggressive and associated with a worse prognosis compared to those with functional p53 (Russo et al., 2005, Hientz et al., 2017, Stiewe and Haran, 2018, Olivier et al., 2010, Zhou et al., 2019).

Despite extensive research, effective targeting of p53 in cancer therapy remains challenging due to the complexity of its regulation and the varied nature of its mutations. Advances in understanding the specific mechanisms of p53 inactivation and restoration in colon cancer will be crucial for developing effective treatments.

#### 1.4.3.2 Challenges in targeting the p53 pathway

Since mutations in p53 contribute to cancer proliferation and metastasis, targeting the signalling pathways altered by p53 mutation appears to be an attractive strategy. Depending on the p53 status, therapeutic strategies may include preventing the degradation of wildtype p53, inhibiting mutant p53, or restoring the wildtype functionality of mutant p53 (Zhu et al., 2020, Levine, 2019b, Zhou et al., 2019). Agents that stabilise wildtype p53 primarily achieve this by disrupting its interactions with negative regulators like MDM2, thereby preventing ubiquitination (Vassilev et al., 2004). Elevated wildtype p53 levels are sufficient to induce tumor-suppressive responses. Additionally, p53 GOF mutations endow cancer cells with oncogenic properties, and thus targeting these specific mutations may inhibit cancer cell proliferation (Schulz-Heddergott and Moll, 2018). However, the development of p53-targeted drugs is particularly challenging as these agents must specifically target mutant p53 in cancer cells while having no effect on normal cells harbouring wildtype p53. Here are some approaches for targeting the p53 pathway:

**Stabilisation of wildtype p53 using small molecule inhibitors:** The degradation of p53 is primarily mediated by ubiquitination via the E3 ubiquitin ligase MDM2, leading to proteasomal degradation. This process has spurred the development of small molecules that inhibit the MDM2-p53 interaction, stabilizing p53. The first inhibitors identified were nutlins, a class of cis-imidazolines (Vassilev et al., 2004).

**Targeting p53 GOF mutant tumors:** Over the years many mutant p53-reactivating drugs have been described such as PRIMA-1, MIRA-1, and STIMA-1 which can potentially modify cysteines in the p53 protein to stabilise the wildtype conformation and prevent mutant p53 unfolding (Zache et al., 2008, Lambert et al., 2009, Saha et al., 2014). Despite demonstrating p53-dependent effects in vitro and in vivo, none have entered clinical trials, owing to solubility issues and toxicity in normal cells (Zache et al., 2008, Bou-Hanna et al., 2015).

**Targeting truncated p53:** While most cancer-associated TP53 mutations are missense mutations, approximately 10% result in nonsense mutations that produce truncated p53 proteins. These truncated proteins are often rapidly degraded by the nonsense-mediated mRNA decay (NMD) pathway, making reactivation approaches less feasible. Instead, alternative methods have been proposed to activate the p53 pathway in cells with truncating mutations. One approach involves promoting translational readthrough, enabling ribosomes to bypass stop codons and produce full-length p53. Aminoglycoside antibiotics like gentamicin and its derivatives (e.g., G418 and NB124) have shown promise in this regard, as they restore full-length p53 synthesis and promote cancer cell apoptosis (Bidou et al., 2017, Floquet et al., 2011). Another strategy focuses on inhibiting the NMD pathway, with compounds like NMD14 targeting components such as SMG7 (Martin et al., 2014). Drugs like ataluren, already in phase III trials for cystic fibrosis, may also hold potential as anticancer agents. However, the toxicity of these compounds raises concerns about their viability as selective p53-targeted therapies (Dabrowski et al., 2018).

As with targeting the Wnt and RAS pathways, a major concern regarding p53-based therapy is the emergence of resistance (Michaelis et al., 2011, Chapeau et al., 2017). Moreover, p53-targeted drugs are unlikely to succeed as standalone treatments in clinical settings.

## 1.5 Disease modelling in mouse and drosophila

While genetics give a central perspective about the nature of cancer, understanding tumour interactions with its surrounding environment gives us a systemic view of the disease. Given all the information on the common mutations that occur in CRC, mouse and *Drosophila* models can be developed that are based on the genetic make-up of tumors, generating realistic models of the human disease. We have made tremendous

progress in our understanding of colorectal cancer with the help of ex-vivo and whole animal models. Mouse, flies and organoids throw light on how tumours interact with surrounding micro- and macroenvironment and promote complex phenotypes such as drug resistance and metastasis. Patient-derived organoids implanted in mouse capture tumour complexity at organismic level - allowing strong preservation of tumoral and stromal architecture with high degree of fidelity to donor tumour. However, these samples represent late carcinoma and are usually taken from patients with highly advanced tumours who have undergone several cycles of chemotherapy. Moreover, the amount of viable tumour engrafted may not accurately represent intra-tumoural heterogeneity.

One of the commonly used models is the multiple intestinal neoplasia (MIN) model (referred to as  $APC^{Min+/-}$ ). This model was generated by *N*-ethyl-*N*-nitrosourea (ENU) mutagenesis which causes loss of function of *Apc* gene at codon 850. These mice predominantly develop multiple adenomas in the small intestine and a smaller number of colonic polyps (Moser et al., 1990, Moser et al., 1993).  $APC^{Min+/-}$  mice with *SMAD4* and *SMAD2* deletion, key proteins of TGF- $\beta$  signalling pathway, showed advanced adenocarcinoma without any changes in number of polyps, suggesting this pathway is critical in adenoma to carcinoma progression. The development of genetically engineered mouse and fly models enabled us to understand the significance of individual and collective genetic alterations in CRC. *KRAS* mutation coupled with *APC* loss showed accelerated tumour formation and metastatic progression to lungs and liver in mice. Subsequent restoration of *KRAS* led to extinction of metastases and spontaneous regression of tumour (Boutin et al., 2017). While mutated *KRAS* is reported in 40% of human CRCs, the study showed that *KRAS* alone is insufficient to induce tumourigenesis but increases the susceptibility of intestinal mucosa to carcinogens (Haigis et al., 2008, Calcagno et al., 2008). Similarly, loss and gain-of-function *TP53* mutations are found in approximately 40-60% of human CRCs (Nakayama and Oshima, 2019). When coupled with *APC* loss, intestinal tumours in *p53* mutant mice show increased invasiveness and Epithelial Mesenchymal Transition (EMT). Restoration of *APC* led to spontaneous tumour regression in mice. Loss of *p53* in mice with constitutively active Notch signalling background led to intestinal tumour formation and metastasis (Chanrion et al., 2014). *FBXW7* is critical for degradation of *c-myc*, *ccne1*, *jun* and *notch* and is reported to be regulated in sizeable proportion of human cancers. Intestinal deletion of *FBXW7* in  $APC^{Min+/-}$  mice leads to aggressive tumour development and double knockout mice models of *TP53* and *FBXW7* show more aggressive intestinal cancers with lymph node and liver metastasis (Sancho et al., 2010, Grim et al., 2012). *PI3/AKT* pathway dysregulation is reported in 60-70% of colorectal cancers (Faes and Dormond, 2015). Constitutively active *PIK3ca* has been reported as a driver mutation causing rapid tumourigenesis and invasion of adjacent organs. This coupled with loss of *Apc* leads to adenoma to carcinoma

progression and metastasis (Leystra et al., 2012). Moreover, maintaining transgenic mice colonies is laborious and resource intensive. Fly models help complement mouse models by accommodating multiple mutations in a resource and time-efficient manner. Bangi et al., developed a 9-hit (KRAS-TP53-APC-FBXW7-TGF $\beta$ R2-SMARCA4-FAT4-MAPK14-CDH1) personalised fly avatar to mimic the genetic profile of a patient with advanced KRAS mutant pT3N2a colon carcinoma (Bangi et al., 2019) for developing personalised targeted therapy as a part of a clinical trial. Such a bench-to-bedside clinical trial for late-stage patients would not be possible using mouse models. This study identified trametinib plus zoledronate as a candidate treatment combination which led to significant response in the patient: target and non-target lesions displayed a strong partial response and remained stable for 11 months (Bangi et al., 2019).

### 1.5.1 Spatio-temporal transgene regulation in mice models

The development of Cre-Lox (Cre) technologies in the 1990s enabled researchers to delete any gene in any tissue of interest (Nagy, 2000). This system involves interaction between two major components: a Cre recombinase and *LoxP* sites. In this method, mice carrying a *Cre* transgene (under the control of an inducible tissue specific promoter) are crossed to mice bearing an inducible allele in which the target region is flanked by *LoxP* recombination sites (Figure 1-5). Cre Recombinase is an enzyme derived from bacteriophage P1, that can recognize and interact with specific DNA sequences known as *LoxP* sites which are specific 34 base-pair sequences. When two *LoxP* sites flank a gene or DNA segment of DNA, Cre-mediated recombination can excise or modify this segment depending on the orientation and position of the *LoxP* sites. This can be either an essential exon(s) of a gene, to produce a conditional knockout, or a Stop motif to activate an oncogene, eg *Kras*, within adult tissue. The inducibility of Cre recombinases is achieved by coupling the Cre enzyme to the estrogen receptor (generating CreER), leading to activation of *Cre* with an estrogen agonist. To address the limitations of non-specific activation of CreER by endogenous estrogens, CreERT2 was developed (Zhao et al., 2006). The CreERT2 recombinase is a fusion protein that contains three mutations in the human ER, so that the complex is efficiently activated by synthetic estrogen-like agonists tamoxifen (Zhao et al., 2006). However, this approach still has some limitations including "leakiness," where Cre activity can occur without an inducer, leading to unintended recombination. Additionally, mosaicism may arise if not all targeted cells undergo recombination, resulting in a heterogeneous population of cells.

I have utilised this system to generate the transgenic mouse models described in this thesis. Briefly, tamoxifen inducible Cre-recombinase was expressed under the control of the epithelium-specific *Villin1* promoter (*Villin*<sup>CreERT2</sup>), allowing targeted genetic recombination throughout the intestine (El Marjou et al., 2004). To target the most

frequently altered pathways in CRC - Wnt, RAS and p53 - I used *Apc<sup>fl</sup>* (Shibata et al., 1997), *Kras<sup>G12D</sup>* (Jackson et al., 2001), *Trp53<sup>fl</sup>* (Jonkers et al., 2001) alleles respectively, to generate compound mutant mice.

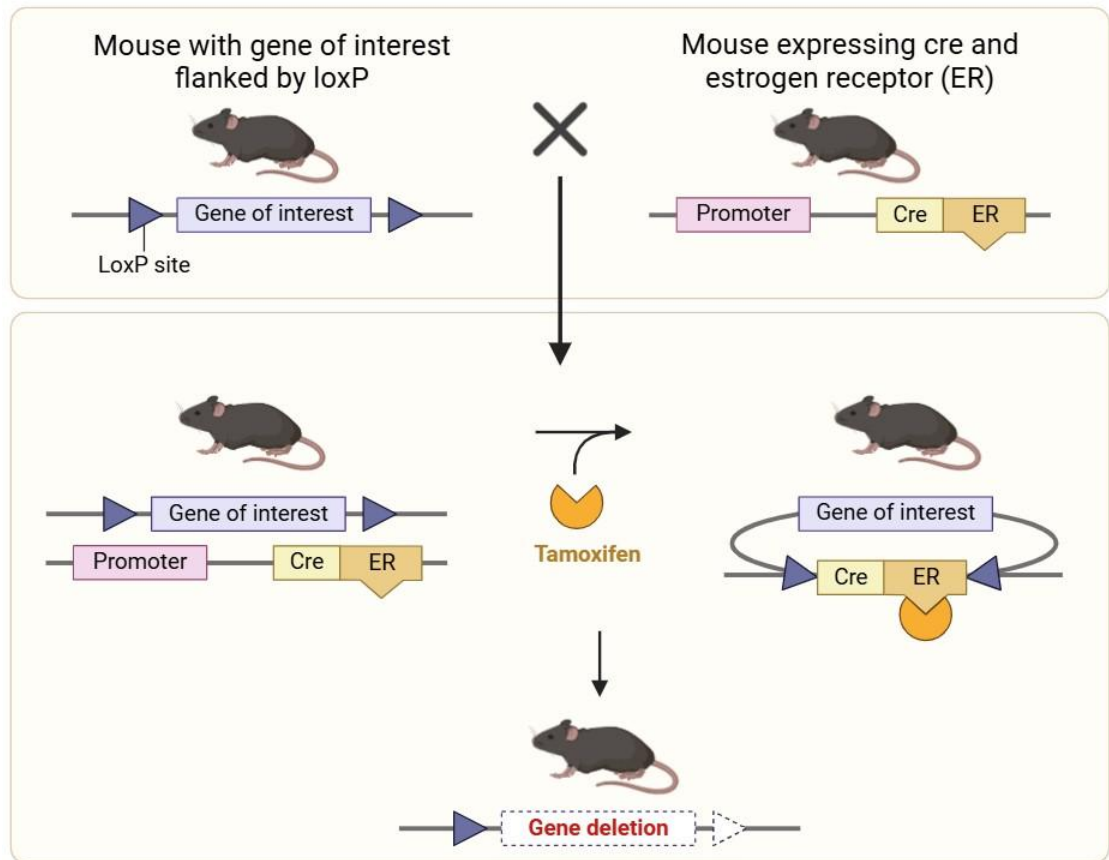


**Figure 1-5: Illustration of Tamoxifen-inducible Cre-Lox system in mice.**

In an inducible Cre line, Cre is fused to mutated hormone-binding domains of the estrogen receptor. Cre-ER is inactive until tamoxifen is added. Inducible lines allow for both spatial and temporal control by combining the tissue-specific expression of Cre-ER by CD31 and its tamoxifen-dependent activity of the enzyme. Illustration was generated using Biorender.com.

It has been shown that acute deletion of both copies of *Apc* results in a crypt progenitor phenotype characterized by increased proliferation and altered migration and differentiation (Sansom et al., 2004, Andreu et al., 2005). Site-directed activation of *Apc* using 4-hydroxy tamoxifen resulted in development of colonic adenomas (discussed in Chapter 3). Our mouse models, combining mutation of *Apc* with aberrant expression of mutated *Kras<sup>G12D/wt</sup>* resulted in higher number of intestinal adenomas compared to mice bearing loss of *Apc* alone (discussed in Chapter 3). This observation is also corroborated by other groups (Sansom et al., 2006, Janssen et al., 2006). Expression of *Kras<sup>G12D/wt</sup>* alone did not accelerate tumorigenesis in mice, as these mice developed adenomas and adenocarcinomas at very long latencies (>500 days) (Sansom et al., 2006). In these mouse models, *Apc* mutation seems to act as an initiator, reducing latency and increasing tumor burden. However, this is a problem as compound mutant mice *Apc<sup>fl/wt</sup> Kras<sup>G12D/wt</sup>* develop multiple tumors and thus need to be euthanized earlier due to higher tumor burden,

before any tumors have had the opportunity to invade or metastasize (discussed in Chapter 3).

Similar to mutant  $Kras^{G12D/wt}$  mice, loss of p53 alone does not drive intestinal tumorigenesis in mice. This is also noted in patients with Li-Fraumeni syndrome who carry germline mutations in the p53 gene usually develop soft tissue sarcomas of mesenchymal origin (Strong et al., 1992). In mouse intestines, an increase in tumor burden and progression was observed with concomitant loss of Apc in  $Apc^{Min/+} Tp53^{-/-}$  compound mice (Halberg et al., 2000). Similarly, I have also observed increased intestinal tumor burden in mice bearing mutations in Apc, Kras and p53 genes ( $Apc^{fl/wt} Kras^{G12D/wt} Trp53^{fl/fl}$ , discussed in Chapter 3).

Collectively, nearly all the common human mutations in CRC lead to increased tumor burden and tumor progression, although alone these mutations do not provoke rapid tumorigenesis. I used these models to study the interplay between aberrations in Apc, Kras and p53 in tumorigenesis and tumor progression.

### 1.5.2 Spatio-temporal transgene regulation in *Drosophila* models

The GAL4/UAS system, a workhorse of *Drosophila* genetics for spatiotemporal regulation of transgenes, was developed by Brand and Perrimon (Duffy, 2002, Brand and Perrimon, 1993). This bipartite system consists of two main components: the GAL4 transcriptional activator, identified in the yeast *Saccharomyces cerevisiae* (Laughon and Gesteland, 1984) and a transgene controlled by an Upstream Activating Sequences (UAS) promoter that is largely silent in the absence of GAL4 (Brand and Perrimon, 1993).

A modification of this system, Gal80<sup>ts</sup>, is a temperature-sensitive variant of Gal80 that allows conditional control over Gal4 activity. At lower, permissive temperatures, Gal80<sup>ts</sup> represses Gal4; however at higher, restrictive temperatures, it becomes inactive, allowing Gal4 to activate transcription. This feature is particularly useful when combined with specific promoters, such as the *byn*, which is active in the hindgut of *Drosophila*, enabling targeted gene expression to these tissues (Figure 1-6).

This system is highly versatile and can be used for cell- or tissue- specific genetic mutant rescue, gene overexpression, RNA interference (Ri) screens, and many other applications. It has been extensively employed in developmental studies in various tissues, including the hindgut (*byn*: (Lengyel and Iwaki, 2002)), and midgut (*esg*: (Micchelli and Perrimon, 2006, Potten, 1998)).

**Expression of transgenes in *Drosophila* hindgut using *byn* promoter:** In *Drosophila*, *byn* is expressed in the ring of cells that will internalize to form the hindgut and continues to be expressed in the hindgut throughout embryogenesis. *Byn* specifically regulates

transgene expression specifically in the drosophila hindgut (Fox and Spradling, 2009, Takashima et al., 2008, Lengyel and Iwaki, 2002).

To investigate which aspects of tumorigenesis are recapitulated by mutations in the RAS, WNT and p53 pathways, I targeted transgenes specifically to the *Drosophila* hindgut epithelium. The *Drosophila* hindgut which functions as the equivalent of mammalian colon, is a single layer of epithelium divided into three main sections along its anterior-posterior axis (Fox and Spradling, 2009, Takashima et al., 2008, Lengyel and Iwaki, 2002). The pylorus is the anterior-most region of the hindgut that controls the passage of gut contents from the midgut to the hindgut. The ileum contains differentiated enterocytes and the rectum sits most posteriorly.

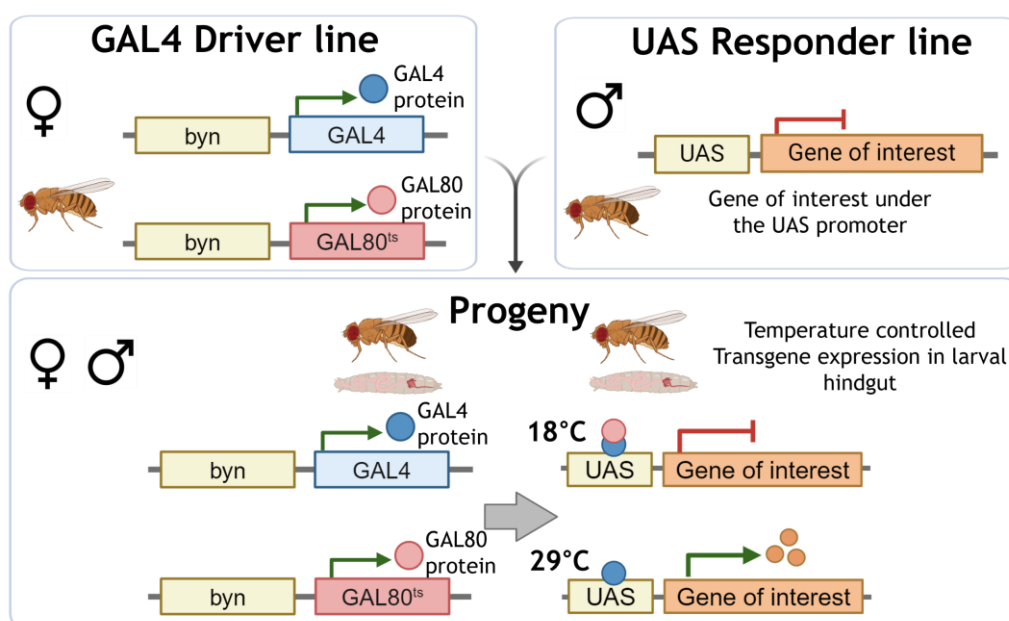


**Figure 1-6: GAL4 and UAS system for spatiotemporal transgene expression in fruit-flies.** Female virgins bearing GAL4 under a tissue-specific promoter (*byn*: hindgut), are crossed with male flies bearing gene of interest under the control of upstream activating sequence (UAS). In the parental line, gene of interest is not expressed in the absence of GAL4. Gene of interest is expressed only in the F1 progenies that carry both UAS and GAL4 proteins. GAL80<sup>ts</sup> allows temporal control of transgene expression; at 18°C transcription is blocked by GAL80<sup>ts</sup>; at 29°C GAL80<sup>ts</sup> is inactive, allowing GAL4 to activate transcription of gene of interest.

For my thesis, I employed the temperature-sensitive GAL4/GAL80<sup>ts</sup> system in combination with the hindgut-specific *byn* promoter to control the timing and location of transgene expression. This model has been well-characterized by Bangi et al. for recapitulating key features of tumorigenesis (Hanahan and Weinberg, 2011): disruption of normal tissue architecture, evasion of apoptosis, oncogene-induced senescence, migration and metastasis (Bangi et al., 2016).

**Drosophila Stock Maintenance Using Balancer Chromosomes:** One of key advantages of *Drosophila* as a model organism is the availability of balancer chromosomes. These chromosomes suppress recombination with their homologues, enabling the maintenance of lethal and sterile mutants as balanced heterozygotes. All balancers carry dominant

markers that unambiguously distinguish homozygous mutants from their heterozygous siblings. The TM6B balancer (Craymer, 1984) carries the *Tb*<sup>1</sup> dominant mutation, is characterized by a distinct phenotype in which the flies exhibit a rounded and somewhat bloated abdomen, which makes them appear "tubby". This balancer is particularly useful during examination of suitable mutant larvae for dissection and analysis.

## 1.6 Genetic Complexity and drug resistance in CRC

Although tremendous progress has been made in modelling human cancers in mouse and flies, we still lack models representing an integrated view of the genetic and genomic changes and their significance for colorectal tumorigenesis (Ocana et al., 2010, Caponigro and Sellers, 2011). Only 6% of cancer clinical trials lead to FDA approval, highlighting a huge disconnect between pre-clinical response and clinical outcome (Hay et al., 2014). This suggests that our current models albeit powerful are insufficient to understand the complex disease biology of cancer and its treatment. Development of new treatment options requires development of novel screening methodologies. Current models of drug screening including *in vitro* cell systems, orthotopic models and genetically engineered mouse and fly models fail to capture patient tumour complexity and heterogeneity. The efficacy of any therapeutic strategy is highly dependent on tumour burden and its growth kinetics; tumour heterogeneity, physical barriers, immune system and microenvironment, undruggable cancer drivers, and the consequence of therapy pressure (Grizzi and Chiriva-Internati, 2006). Many of the mouse models cannot be used to analyse large scale drug screening as they are not only resource intensive but also not the ideal models to study metastasis. While fly models provide scalability for whole-animal screening and help exploration of cancer processes at the level of single cells, they lack adaptive immune system and cannot be used to study certain types of cancer. It is an established fact that tumours are comprised of a heterogeneous population of cells and is complex system that continuously evolves during disease progression. However, there are very few models that capture this complexity of cancer in its true essence. Indeed, cancer models focussing on single-gene or single pathways have provided us with deeper understanding of signalling pathways involved and facilitated significant breakthroughs in the field. To develop effective therapeutic strategies, we need more innovative *in vitro* and *in vivo* models that can encapsulate the complexity of this disease.

## 1.7 Aims

Despite numerous clinical studies, there remains a significant unmet need for effective treatments in patients with KRAS-mutant colorectal cancer (CRC). The differential responses observed in clinical settings suggest variations in MAPK pathway dependency in KRAS-mutant colorectal cancers, warranting a detailed investigation. Several studies have implicated genetic complexity in imparting drug resistance. This thesis posits that a deeper understanding of current CRC models is essential to study the mechanisms of drug resistance effectively.

Transgenic mouse models developed by the Sansom group and patient-specific fly avatars from the Cagan lab, provide a unique opportunity to explore the interplay between multiple deregulated pathways across species. My thesis leverages *Drosophila* and mouse models to dissect the cellular and molecular dynamics of CRC driven by oncogenic Ras signalling, offering critical insights into the interaction of signalling pathways.

Utilizing transgenic mouse models from the Sansom group and patient-specific *Drosophila* models from the Cagan lab, my research focuses on the following key aims:

### **AIM 1: Characterization of Ras-Driven Models of Colorectal Cancer:**

In Chapter 3, I aim to characterize *Drosophila* and mouse models that incorporate relevant mutations in the WNT, KRAS, and P53 pathways. This involves studying how these mutations disrupt tissue homeostasis and contribute to tumour initiation and progression, as well as exploring the interactions between multiple oncogenic mutations.

### **AIM 2: Investigate MAPK Dependency in Ras-Driven CRC Models:**

In Chapter 4, I will examine the MAPK pathway's role in genetically complex *Drosophila* and mouse CRC models. Understanding how these models respond to Ras pathway inhibition at various tumour stages will provide insights into why Ras inhibitors have been unsuccessful in clinical settings.

### **AIM 3: Identify and Target Resistance Mechanisms:**

In Chapter 5, I investigated and validated the upregulation of a toxin clearance pathway—glucuronidation—in mouse models of colorectal cancer (CRC). This mechanism was initially identified in *Drosophila* models in collaboration with Dr. Bojie Cong. My goal was to determine whether this resistance mechanism is conserved in mammals. I demonstrated that genetically complex Ras-driven colon tumours exhibit lower drug concentrations compared to adjacent normal tissues. By employing a combinatorial strategy, I was able to enhance drug accumulation specifically within the tumour. I then assessed whether increasing the drug concentration in the tumours would lead to tumour regression and improved survival in mice bearing intestinal tumours.

# Chapter 2 Materials and Methods

## 2.1 Fly models of Ras-driven colon cancer

*Drosophila melanogaster* (fly) lines were cultured at room temperature or 25-29°C on standard fly media. Our fly media consisted of: Tayo agar 10g, Soya flour 5g, Sucrose 15g, Glucose 33g, Maize meal 15g, Wheat germ 10g, Treacle molasses 30g, Yeast 35g, Nipagin 10ml, Propionic acid 5ml prepared in 1 litre water. All reagents were purchased from Scientific Laboratory Supplies (SLS).

Fly lines used in this study are: *UAS-ras<sup>G12V</sup>* (second chromosome, G. Halder), *UAS - arm<sup>S10</sup>*, *UAS-p53<sup>Ri</sup>* (second chromosome, VDRC), *byn-Gal4* (third chromosome, V-Hartenstein) and *byn-Gal4/Gal80<sup>ts</sup>* (third chromosome, Bloomington). The following fly lines were made by Cagan lab at Mount Sinai, USA.

Fly Line	Genotype	Human Ortholog
CPCT036	<i>UAS - ras<sup>G12V</sup> apc<sup>Ri</sup> p53<sup>Ri</sup> ago<sup>Ri</sup> chico<sup>Ri</sup> smox<sup>Ri</sup> eva<sup>Ri</sup> sdhA<sup>Ri</sup> rassf<sup>Ri</sup> efa6<sup>Ri</sup></i>	KRAS <sup>G12V</sup> , APC, P53, IRS1, FBXW7, SMAD4, SDHA, RASSF, PSD
RAP-P1-M3B	<i>UAS - ras<sup>G12V</sup> apc<sup>Ri</sup> p53<sup>Ri</sup> ago<sup>Ri</sup> wts<sup>Ri</sup> CG7742<sup>Ri</sup> atg2<sup>Ri</sup></i>	KRAS, APC, P53, FBXW7, LATS1, TBC1D19, ATG2B/2A
RAP-P2-M1B	<i>UAS - ras<sup>G12V</sup> apc<sup>Ri</sup> p53<sup>Ri</sup> vrp1<sup>Ri</sup> ry<sup>Ri</sup> khc-73<sup>Ri</sup></i>	KRAS, APC, P53, WIPF1, XDH, KIF13A
RAP-P5-M4A	<i>UAS - ras<sup>G12V</sup> apc<sup>Ri</sup> p53<sup>Ri</sup> amy-p<sup>Ri</sup> bt<sup>Ri</sup> ppk26<sup>Ri</sup></i>	KRAS <sup>G12V</sup> , APC, P53, AMY2B, TTN, ASIC1
RAP-P7-M2B	<i>UAS - ras<sup>G12V</sup> apc<sup>Ri</sup> p53<sup>Ri</sup> kn<sup>Ri</sup> CG12730<sup>Ri</sup> CG4733<sup>Ri</sup></i>	KRAS, APC, P53, EBF3, CMTM4, PPP2R3B
RAP-P13-M1A	<i>UAS - ras<sup>G12V</sup> apc<sup>Ri</sup> p53<sup>Ri</sup> tefu<sup>Ri</sup> CG31223<sup>Ri</sup> ida<sup>Ri</sup></i>	KRAS <sup>G12V</sup> , APC, P53, ATM, ZNHIT2, ANAPC5
RAP-P19-M1A	<i>UAS - ras<sup>G12V</sup> apc<sup>Ri</sup> p53<sup>Ri</sup> pten<sup>Ri</sup> tet<sup>Ri</sup> mor<sup>Ri</sup></i>	KRAS, APC, P53, PTEN, TET1, SMARCC2

### 2.1.1 Optimising Developmental Temperature for Flies

Developmental temperature for fly lines - RAP-P1-M3B, RAP-P2-M1B, RAP-P7-M2B and RAP-P19-M1A were optimised by colleagues in Cagan laboratory. To optimise the developmental temperature for the CPCT036 fly line for subsequent rescue-from-lethality assays, a breeding stock population consisting of 12 female virgins (driver lines) of either *byn-Gal4* or *byn-Gal4/Gal80<sup>ts</sup>* and 4 males (responder flies) per vial was established. Flies were allowed to acclimatise by culturing for 48 - 72 hours at room temperature. After acclimatisation, breeding population were transferred into fresh vials containing fly

media and placed in an 18°C incubator for egg laying. This temperature was chosen to minimise transgene expression during embryogenesis, thereby preventing embryonic defects or lethality. Post embryogenesis, larvae were raised at 25°C, 27°C and 29°C respectively until eclosion. Once all the flies had eclosed, the number of empty pupal cases were counted to determine viability.

### 2.1.2 Drug Treatment

The following drugs were used in this study: trametinib (Selleckchem), Regorafenib (Selleckchem), Rapamycin (Selleckchem), Pyrvinium (Selleckchem), LY294002 (LC Labs), Dabrafenib (Selleckchem), Bortezomib (Selleckchem), and Simvastatin (Selleckchem). All compounds were reconstituted in DMSO and mixed with fly media to make drug-food (0.1% final DMSO concentration). Drug media was prepared by diluting drug stocks in semi-defined fly media to a final concentration of 0.1% DMSO.

### 2.1.3 Rescue-from-lethality assay

A breeding population consisting of 12 female virgins (*bynGal4/Gal80<sup>ts</sup>*) and at least 4 males (flies with gene of interest) per vial were transferred into vials with fly media. Flies were allowed to acclimatise by culturing for 48 - 72 hours at room temperature. Post acclimatisation, the breeding population was transferred to vials with drug media and transferred to 18°C for egg laying. Egg laying was performed at 18°C to minimize transgene expression during embryogenesis and to prevent defects or lethality that could not be rescued by drug feeding. Vials containing eggs and embryos were allowed to age at 18°C for 72 hours to complete embryogenesis before transferring them to incubators set to optimised temperatures for the assay. Larvae were reared on drug media, which took approximately 11 to 14 days to reach adulthood, depending on the temperature. Once all flies had eclosed, the number of empty pupal cases was counted to calculate viability.

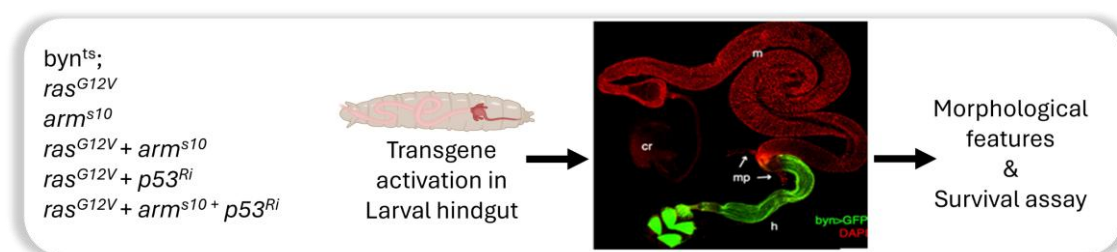


Figure 2-1: Illustration of study plan in *Drosophila*

### 2.1.4 RNA isolation and RNA Sequencing

Hindguts from twenty third-instar larvae were dissected and collected in microcentrifuge tubes containing RNAlater™ Stabilization Solution (Qiagen, #AM7020). For sample processing, fly hindguts were washed with an equal volume of PBS and centrifuged at

1000 rpm for 10 minutes. Total RNA was extracted according to the manufacturer's instructions (Qiagen RNeasy Kit, #740106).

Quality control of all RNA samples was performed using the Agilent TapeStation 4200 High Sensitivity RNA screentape. RNA concentrations were determined with a Qubit Fluorometer using the Qubit RNA Broad Range assay (both Thermo Fisher), with an initial input of 500 ng of total RNA. Libraries were prepared following standard procedures (Illumina Stranded mRNA) using IDT for Illumina RNA UD Indexes to index the libraries. Post-library quality control was conducted using High Sensitivity D1000 screentape (Agilent) for sizing and profiling, with quantification using the Qubit High Sensitivity DNA assay. The libraries were pooled equimolar to a final concentration of 4 nM prior to sequencing on an Illumina NextSeq 500 instrument, utilizing a High-Output 150 cycle run with paired-end 74 bp read length.

The reference genome used was *Drosophila melanogaster* (BDGP6.46.110, Ensembl). Reads underwent quality checks using FastQC, followed by trimming with Trim Galore to remove adapters and low-quality reads (Phred score < 20). Aligned reads were processed using Hisat2, and gene-level counts were obtained using featureCounts. Differential expression analyses were conducted in R using DESeq2, which employs a Wald test to assess significance between groups. Graphs were generated using the ggplot2 package in R. Downregulated genes were marked in blue (Adjusted p-values < 0.05 & log2Fold change < -1), while upregulated genes were marked in red (Adjusted p-values < 0.05 & log2Fold change > 1).

## 2.2 Mouse models of Ras driven colon cancer

### 2.2.1 Mouse Housing and Ethics

All mouse experiments were performed according to the UK Home Office regulations (project licenses: PP3908577 and 70/9112) with approval from the University of Glasgow Animal Welfare and Ethical Review Board. Male and female mice between 12 to 16 weeks of age and weighing  $\geq 20$  g were utilized. Mice were housed in conventional cages within an animal room at a constant temperature (19 to 23°C) and humidity (55%  $\pm$  10%), maintained under a 12-hour light-dark cycle and were fed a standard chow diet and water at *ad libitum*. Mice were euthanized humanely at predefined time points or when exhibiting clinical signs such as hunching, progressive weight loss, or anemia, indicative of intestinal tumour burden.

### 2.2.2 Genetic Alleles

Mice used were on a C57BL/6J background for the following alleles: Villin<sup>CreERT2</sup> transgene (El Marjou et al., 2004), *Apc*<sup>fl</sup> (Shibata et al., 1997), *Kras*<sup>G12D</sup> (Jackson et al., 2001), *Trp53*

(Jonkers et al., 2001). For genotyping, mice were ear notched upon weaning and ear punches were sent to Transnetyx (Cordova, TN) where samples were genotyped using the established genotyping procedure for the individual alleles.

### 2.2.3 Treatment groups and Drug Formulations:

trametinib (LC Laboratories), a selective MEK1/2 inhibitor, was reconstituted in 0.5% hydroxypropyl methylcellulose (HPMC) + 0.1% Tween-80 and mice were dosed as described below. Duration of treatment which depended on model and study plan has been noted in the subsequent sections.

T<sub>L</sub> - trametinib<sub>(low-dose)</sub> - dosed at 0.2mg/kg and formulated as 0.05mg/ml trametinib, administered once daily by oral gavage.

T<sub>M</sub> - trametinib<sub>(mid-dose)</sub> - dosed at 0.4mg/kg and formulated as 0.1mg/ml trametinib, administered once daily by oral gavage.

T<sub>S</sub> - trametinib<sub>(standard-dose)</sub> - dosed at 0.8mg/kg and formulated as 0.2mg/ml trametinib, administered once daily by oral gavage.

Vor - vorinostat (Selleckchem) - was reconstituted in 0.5% hydroxypropyl methylcellulose (HPMC) + 0.1% Tween-80 and mice were dosed at 50mg/kg and formulated as 12.5mg/ml, administered once daily by oral gavage.

For combination treatments, drugs were reconstituted together at appropriate concentrations and co-administered at the same frequency. For example:

T<sub>L</sub> + Vor (trametinib<sub>(low-dose)</sub> + vorinostat) treated mice received trametinib at 0.2mg/kg and vorinostat at 50mg/kg, administered once daily by oral gavage. Drug formulation contained trametinib (0.05mg/ml) and vorinostat (12.5mg/ml).

T<sub>S</sub> + Vor (trametinib<sub>(standard-dose)</sub> + vorinostat) treated mice received trametinib at 0.8mg/kg and vorinostat at 50mg/kg, administered once daily by oral gavage. Drug formulation contained trametinib (0.2mg/ml) and vorinostat (12.5mg/ml).

Upon reconstitution, drugs were stored at 4°C and replenished fortnightly where applicable.

### 2.2.4 Inductions, Treatment Regime and Sample processing

Cre recombination was activated across the whole intestine using Tamoxifen (for Short-term model and Long-term model) or spatially localised using 4-Hydroxy Tamoxifen (for Colon Tumour model).

Tamoxifen (#T5648, Merck) was dissolved in Absolute Ethanol to a stock solution of 100mg/ml. This was diluted in corn oil (#C8267, Merck) to a final working concentration of 10mg/ml for intraperitoneal injection.

4-Hydroxy Tamoxifen (#H6278, Merck) was dissolved in Absolute Ethanol to a stock solution of 10mg/ml or 25mM. This was diluted in PBS to a final working concentration of 100µM for intracolonic injection.

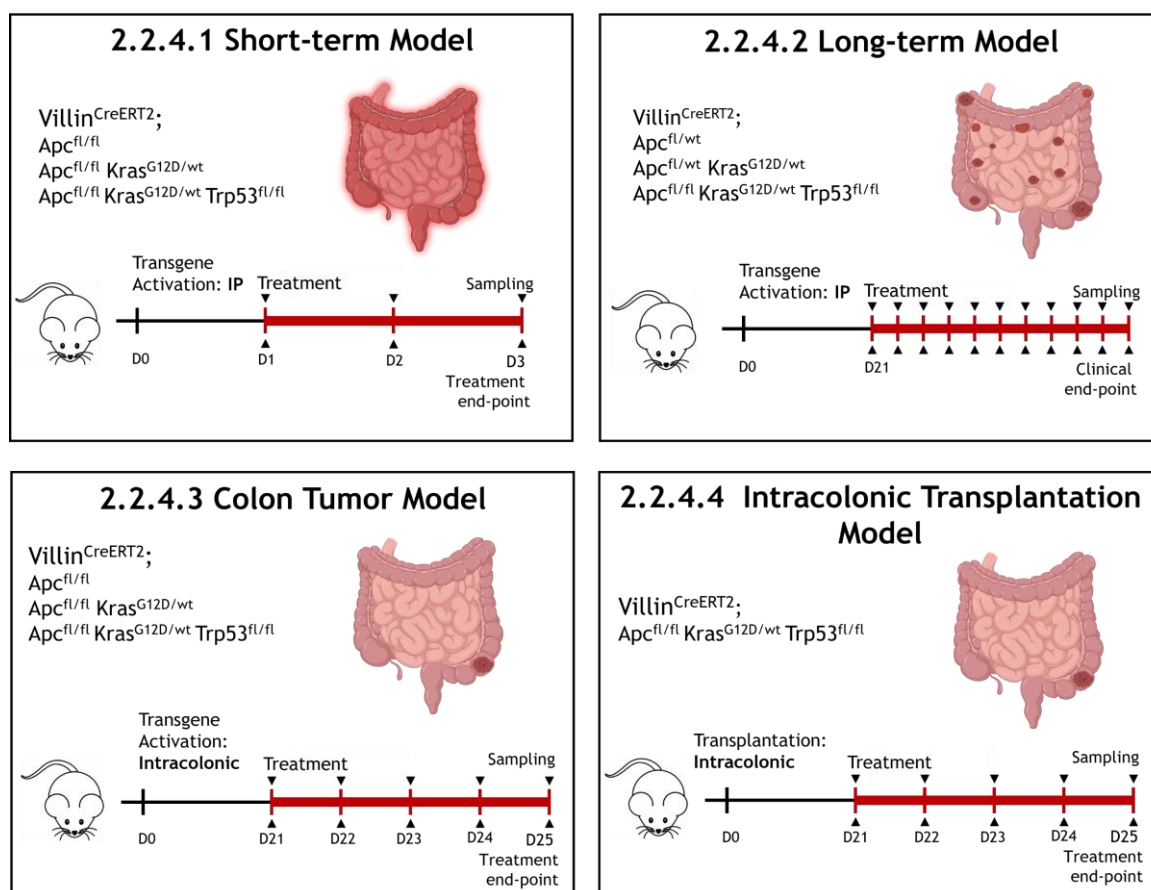


**Figure 2-2:** Illustration showing transgene activation and treatment plan for different Ras-driven intestinal tumour models of CRC

### 2.2.4.1 Short-term Model

**Transgene Activation and Treatment Regime:** In mice with homozygous lox-flanked Apc allele (Apc<sup>fl/fl</sup>), robust Cre recombination across the entire intestine was achieved via a single administration of Tamoxifen (80mg/kg, i.p.) on Day 0. Mice were randomly assigned to treatment groups starting Day 1 and culled on Day 3. Drugs were administered once daily by oral gavage (p.o.), and BrdU (0.25ml, 10mM) was given two hours prior to culling on Day 3.

**Sample Processing:** Upon dissection, intestines were flushed with water and fixed using the following methods:

**Methacarn fixation:** This method is optimal for assaying proliferation in intestinal crypts, as it preserves the three-dimensional structure of the gut with minimal cross-cuts. Methacarn fixation is ideal for BrdU staining but less suitable for other immunohistochemical stains. The proximal small intestine (first 7 cm) was opened longitudinally on Whatman filter paper and submerged overnight at room temperature in freshly prepared Methacarn solution consisting of absolute methanol (Sigma, #32213), chloroform (Fisher Scientific, #C4960/PB17), and glacial acetic acid (Sigma, #695092) in 4:2:1 ratio. The following day, guts were rolled and transferred to 10% Neutral Buffered Formalin (NBF) for further histological processing.

**Quick Fixation:** Entire colon and part of proximal SI is fixed using this method for immunohistochemical assays that cannot be done on Methacarn fixed samples. This method is ideal for B-catenin IHC. Longitudinally cut Colon was pinned out on wax plates while part of proximal SI was cut into 1cm lengths and bundled with surgical tape. Tissues were fixed in 10% NBF at 4°C for no more than 24h. The following day samples were transferred to 70% ethanol for further histoprocessing.

#### 2.2.4.2 Long-term Model

**Transgene Activation and Treatment Regime:** In mice with heterozygous lox-flanked Apc allele ( $Apc^{fl/wt}$ ), Cre recombination across the entire intestine was achieved by a single administration of Tamoxifen (80mg/kg, i.p.) on Day 0. Mice were allocated to treatment groups from Day 21 and aged until clinical end-point (progressive weight loss, hunching, anaemia). Drugs were administered once daily by oral gavage (p.o.), and BrdU (0.25ml, 10mM) was given two hours prior to sampling at clinical end-point.

**Sample Processing:** Upon dissection, intestines were flushed with water and “optimal-fixed” in 10% NBF. This fixation is suitable for all immunohistochemical stains.

**Optimal Fixation:** Small intestine, colon and caecum were cut open longitudinally and pinned on wax plates. Samples were submerged in 10% NBF for 24-72 hours at room temperature. Post-fixation, guts were rolled and transferred to 70% ethanol for further histological processing.

#### 2.2.4.3 Colon Tumour Model

**Transgene Activation and Treatment Regime:** To drive spatially resolved Cre recombination in the colon, mice with homozygous lox-flanked allele ( $Apc^{fl/fl}$ ) received colonoscope-guided injection of 4-hydroxy Tamoxifen (70µl, 100nM) into the colonic submucosa under general anaesthesia (Roper et al., 2017). Post confirmation of tumour establishment by colonoscopy, mice were assigned to treatment groups. Drugs were administered once daily by oral gavage (p.o.) for 5 days and BrdU (0.25ml, 10mM) was administered 2h before sampling on Day 5.

**Sample processing:** Upon dissection, colon was flushed with water and cut open longitudinally to reveal tumour and adjacent normal tissue. Both colon tumour and adjacent normal tissue were optimally fixed on Whatman filter paper in 10% NBF for 24 to 72 hours, after which they were transferred to 70% ethanol for further histological processing.

#### 2.2.4.4 Intracolonic Transplantation Model

**Organoid transplantation and Treatment Regime:** Wild-type C57BL/6 mice were purchased from Charles River Laboratories. Intestinal organoids with the genotype  $Apc^{fl/fl}$   $KRas^{G12D/wt}$   $p53^{fl/fl}$  were transplanted into the colonic submucosa via colonoscopy (Roper et al., 2017). Post confirmation of tumour establishment by colonoscopy, mice were assigned to treatment groups. Drugs were administered once daily by oral gavage (p.o.) for 5 days and mice were sampled on Day 5.

**Sample Processing:** Samples were collected for histological processing and metabolite analysis using LC/MS. Upon dissection, the intestines were flushed with ice-cold PBS, and tissues of interest were collected for histological processing and metabolite analysis, as follows:

- A. **Histological processing:** The colon was cut open longitudinally to reveal tumour and adjacent normal tissue. Both colon tumour and adjacent normal tissue were optimally fixed on Whatman filter paper in 10% NBF for 24 to 72 hours, after which they were transferred to 70% ethanol for further histological processing.
- B. **Sample processing for LC/MS analysis of drug metabolites:** Upon dissection, the intestines were flushed with ice-cold PBS, and tissues of interest (~20 mg) such as tumor, adjacent normal tissue, liver, serum, and stool were collected and snap-frozen in Precellys tubes (CK28-R, Bertin Technologies) for further analysis. Metabolites were extracted from the frozen tissue fragments using an ice-cold polar solvent mixture (Methanol:Acetonitrile:Water, 5:3:2) at a concentration of 20 mg/ml. The tissues were homogenized using a Precellys homogenizer. Samples were then centrifuged to remove any debris and prepared for LC/MS analysis.

Samples were analysed using reverse phase chromatography (ZORBAX Eclipse Plus C18, 2.1x50mm, 1.8-micron) using water 0.1% formic acid as mobile phase A and acetonitrile 0.1% formic acid as mobile phase B. Elution started at 99% A (one minute), followed by a linear increase to 92% A for 12 minutes, a washing step of 1% A for 5 minutes and a final re-equilibration step to 99% A for 3 minutes. Column oven was set to 35 °C and flow rate to 250  $\mu$ l min<sup>-1</sup>.

Metabolite analysis was performed using a Q Exactive Orbitrap mass spectrometer (Thermo Fisher Scientific) equipped with electrospray ionization in positive ionisation mode. Resolution (RES) was set to 70,000 at 200 m/z, with a scan range of 100 to

1000 m/z (automatic gain control (AGC) target of  $3 \times 10^6$  and maximal injection time (IT) of 200 ms). Data analysis was carried out in Skyline (version 24.1.0.199).

### 2.2.5 Histoprocessing

Following fixation, samples were processed by the CRUK Scotland Institute Histology Department and embedded into paraffin wax using standard histological techniques. 3-4 $\mu$ m sections were cut for Haematoxylin and Eosin (H&E), and IHC or *in situ* hybridisation techniques (RNAscope®). H&E staining was performed according to standard protocols.

### 2.2.6 Tumour Scoring

Tumours were characterised and scored using H&E-stained sections on HALO™ (Indica Labs). Briefly, small intestinal and colon tumours were annotated, and their area was calculated using a tissue classifier module. Tumours were sorted by size: small (0.001 - 0.1mm<sup>2</sup>), medium (0.1 - 1.5mm<sup>2</sup>) and large (>1.5mm<sup>2</sup>). Pathologically they were categorised as dysplastic adenomas (low-grade vs high-grade) or adenocarcinomas. Histologically, adenomas are preinvasive pedunculated or sessile lesions. More advanced adenomas, characterized by architectural complexity, increased cytologic atypia, and loss of tumour cell polarity, are categorized as high-grade dysplastic adenomas.

Adenocarcinomas, on the other hand, are malignant neoplasms of glandular epithelium that penetrate through the muscularis mucosa. They can be subclassified based on several criteria, including degree of differentiation (well-differentiated, moderately differentiated, or poorly differentiated) and histologic type. Pseudo-invasion, a common finding in the mouse intestine, can occur independently of cancer development and is likely due to the relatively thin muscularis mucosae. In mice, this muscular layer is only a few cells thick, allowing the mucosa to penetrate the muscle with relative ease.

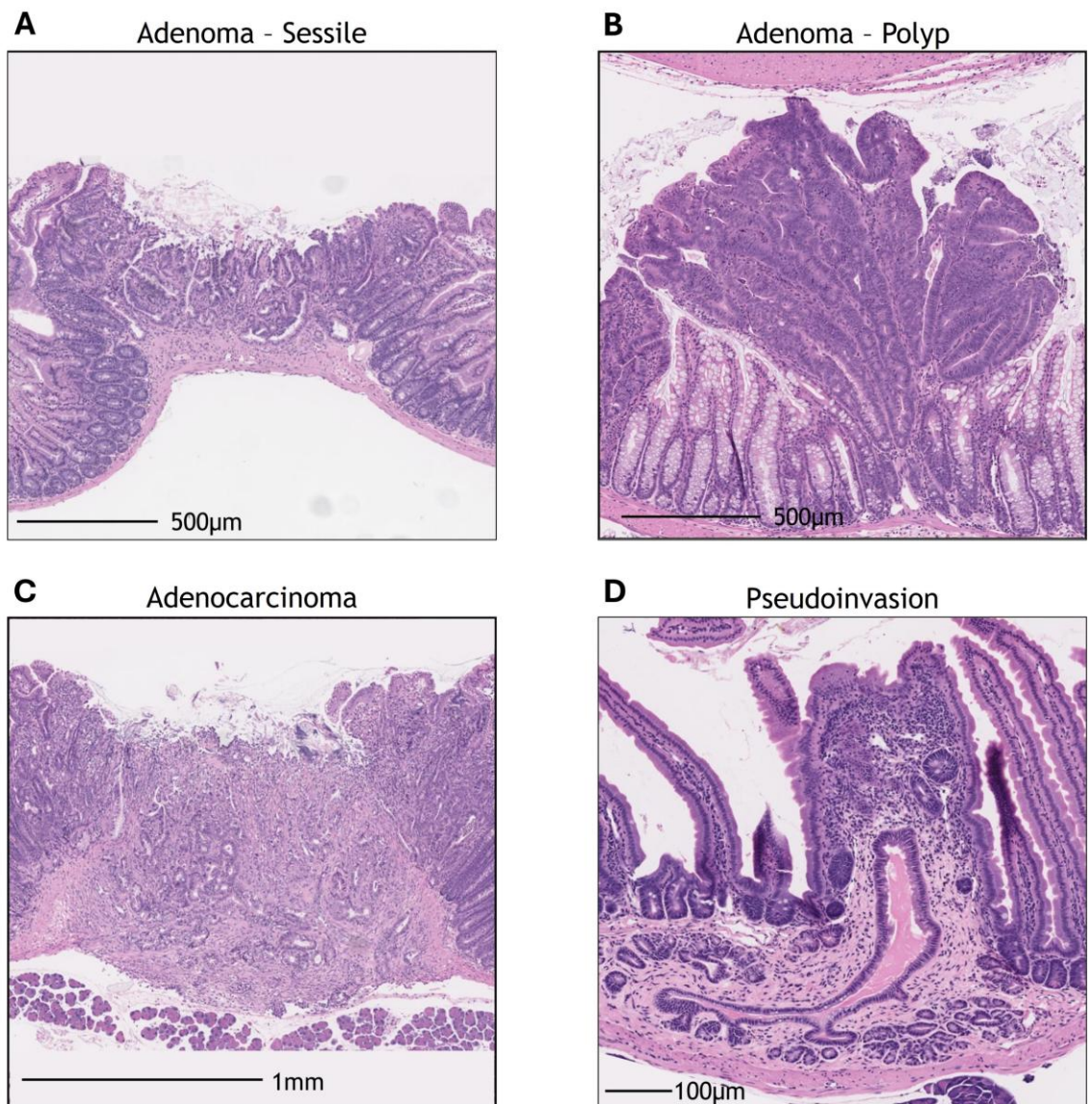


**Figure 2-2. Histopathological features of mouse intestinal tumours.** A-B, Adenomas have an intact basal membrane with conserved glandular structure with high grade of differentiation and little stromal infiltrate. C- Adenocarcinomas are characterized by broken basal membrane, rich stromal infiltrate and loss of crypt architecture. D- Pseudoinvasion caused by displacement of adenomatous epithelium due to torsion or trauma to the lesion.

### 2.2.7 *In vivo* proliferation Assay

Proliferation levels were assessed by measuring BrdU incorporation. Briefly, mice were administered with 0.25ml BrdU (10mM, Amersham Biosciences) 2h before sampling. IHC staining for BrdU was performed using the anti-BrdU (#347580, BD Biosciences) antibody.

For intestinal crypts, BrdU scores were determined by counting number of BrdU positive cells per half crypt using Aperio™ (Leica Biosystems). For tumours, BrdU scores were assessed counting number of BrdU positive cells per 1000 dysplastic cells. This was done using an adaptation of the CytoNuclear V 2.0.9 algorithm in HALO™.

## 2.2.8 Immunohistochemistry and RNA in situ hybridisation

IHC staining was performed by the CRUK Scotland Institute, Histology Department using the following primary antibodies as listed in Table 2-1:  $\beta$ -catenin, BrdU, Cleaved PARP, p21, p53, gH2Ax, p16, cyclin D1.

Table 2-1:

Antibody	Cat#	Supplier	Secondary	Antigen Retrieval	Dilution
BrdU	347580	BD Biosciences	Envision Mouse	TRS High	1:250
cleaved PARP	ab32064	Abcam	Envision Rb	TRS High	1:1000
p21	ab10709	Abcam	Immpress Rat	ER2 20min	1:250
p53	NCL-L- p53CM5p	Leica	Envision Rb	TRS High	1:750
gH2Ax	#9718	Cell Signalling Technology	Envision Rb	ER2 10min	1:120
cyclin D1	#55506S	Cell Signalling Technology	Envision Rb	ER2 30min	1:150

RNAscope®:

RNA *in situ* hybridisation (ISH) or RNAscope® was performed by the CRUK Scotland Institute Histology Department on a Leica Biosystems BOND RX automated IHC/ISH stainer using the RNAscope™ 2.5 LS Reagent Kit-BROWN (Advanced Cell Diagnostics, #322100). Mm-PPIB probe (Advanced Cell Diagnostics, #313918) were run as a positive control to confirm integrity of RNA. dabP probe (Advanced Cell Diagnostics, #312038) was used as a negative control. RNAscope® probes used: Dusp6 (Advanced Cell Diagnostics, #429328), Notum (Advanced Cell Diagnostics, #428988), Axin2 (Advanced Cell Diagnostics, #400338), Anxa1 (Advanced Cell Diagnostics, #509298).

## 2.2.9 Slide Scanning

Slides were scanned by the CRUK Beatson Institute Histology Department using a SCN400F Leica Slide Scanner at 20x magnification for IHC and 40x magnification for RNAscope® analysis.

## 2.3 Crypt isolation and organoid culture

Intestinal crypts were isolated and cultured as organoids following an adapted protocol (Sato et al., 2011). Small intestines were flushed with cold water and longitudinally cut open on a paper towel. Villi were gently scraped out using a glass coverslip at 45° angle. The villi-free intestine was cut into 1cm fragments and washed twice with ice-cold sterile

PBS, with subsequent steps performed in a biosafety cabinet. Tissues were washed 10 times with 50ml ice-cold PBS to remove digested food. Tissues were then rolled at 60rpm for 30 minutes in the cold room, in PBS supplemented with 25mM EDTA to help detach crypts from the surrounding tissue. After gently washing the intestinal bits with PBS, crypts were isolated by mechanical hard pipetting. Crypt fractions were combined with 50ml Advanced DMEM/F12 (ADF) and filtered through a 70µm cell strainer to isolate crypts and remove any villi or tissue bits. To eliminate single cells from the fraction, the crypt suspension was centrifuged at lower speed 600rpm for 5 minutes.

The pellet was re-suspended with growth factor reduced Matrigel® (Merck, #CLS356231) at 2000crypts/ml and plated on 6-well plates as 20µl domes, supplemented with organoid culture media (OCM) that consisted: Advanced DMEM/F12 (Gibco, #12634-028) supplemented with 100U/ml penicillin/streptomycin (Thermo Fisher Scientific, #15140122), 10mM HEPES (Thermo Fisher Scientific, #15630080), 2 mM L-glutamine (Thermo Fisher Scientific, #25030081). Additional supplements: 1:100 N2-supplement (Thermo Fisher Scientific, #17502001) and 1:50 B27-supplement (Thermo Fisher Scientific, #17504044), 100 ng/ml recombinant murine Noggin (Peprotech, #250-38). Organoid media for wildtype organoids was additionally supplemented with a growth factor mix comprising: 50ng/ml recombinant murine EGF (Peprotech, #AF-100-15), 500 ng/ml recombinant mouse Rspodin-1 (R&D systems, #3474-RS), 2.5µM CHIR99021 (GSK3 inhibitor) (Sigma, #SML1046), and 10 µM 62Y-27632 (ROCK inhibitor) (Cambridge Bioscience, #SMO2-1).

Organoids were passaged 1-2 times per week. For passaging, Matrigel domes were scraped off the plate using a P1000 pipette and sterile PBS. They were dissociated into fragments and washed in PBS, followed by centrifugation at 1200 rpm for 5 minutes. After one more wash in sterile PBS, the organoids were re-suspended and seeded in fresh Matrigel.

### 2.3.1 Determination of IC<sub>50</sub>

To determine IC<sub>50</sub> of crypt organoids against trametinib, organoids were dissociated into single cells following incubation in 0.25% TrypLE at 37°C for 7 minutes, with frequent pipetting in between. Post incubation, TrypLE was neutralised with OCM and passed through 40µm filter to eliminate multicellular clusters. Cell density was determined using Countess automated cell counter (Thermo Fisher Scientific). 6µl of Matrigel containing 1000 cells were seeded in standard 96-well black-walled cell culture plates, and plates were incubated for 10 min in a 37°C and 5% CO<sub>2</sub> cell culture incubator to allow jellification of Matrigel before adding 100 µl of organoid growth media (OCM). Cells were allowed to form organoids for 24 hours prior to initiating drug treatment. At treatment endpoint, media was supplemented with 20µl CellTiter-Glo® 3D Cell viability assay (Promega, #G9681) and viability was measured after 4hours as per manufacturer's instructions.

### 2.3.2 Western blot and antibodies used

Two wells of a 6-well plate, typically containing 6 organoid domes/well were harvested as described in Section 2.2.10. Cells were lysed at 4°C for 45 minutes using RIPA buffer supplemented with phosphatase and proteinase inhibitors. The lysate was centrifuged at maximum speed for 45 minutes to pellet cellular debris. The protein concentration of the supernatant was determined using a BCA assay according to the manufacturer's instructions.

Protein samples (20 µg) were mixed with a 10X reducing agent and 4X loading buffer, then adjusted to a final volume of 30 µl. Samples were heated to 95 °C for 5 minutes before loading onto NuPAGE 4-12% gradient Bis-Tris gels. MOPS buffer was used to fill the running tank. Gels were run at 200 V for approximately 50 minutes. Following electrophoresis, proteins were transferred to nitrocellulose membranes using a semi-dry transfer method at 15 V for 1.5 hours. Membranes were blocked with 5% BSA in TBS-T for 1 hour at room temperature to reduce non-specific binding. After blocking, membranes were cut into horizontal strips and incubated with appropriate primary antibodies, followed by the corresponding secondary antibodies. Membranes were reassembled for signal detection. For signal detection, Immobilon Chemiluminescent horseradish peroxidase substrate (Merck) was used according to the manufacturer's instructions.

### 2.3.3 Cell cycle analysis

Intestinal organoids were treated 5nM trametinib or 0.1% DMSO as Vehicle control for a period of 72hours. Post-treatment, organoids were dissociated into single cells and fixed with 70% ice-cold ethanol drop-wise while vortexing to prevent clumping. Cells were washed thrice using ice-cold PBS at 1200 rpm for 5 minutes at 4°C to remove residual ethanol. Cells were then resuspended in 500µl FxCycle PI/RNase (Thermo Fisher Scientific, #F10797). Cell cycle analysis was performed on Attune using YL1 to detect PI.

## 2.4 Statistical analyses

All statistical analyses except for differential expression analysis in DESeq2 was performed using GraphPad Prism V10. Further details on exact statistical test have been mentioned in the figures.

## 2.5 Illustrations

Some illustrations were generated using Biorender.com, which was indicated in the figure caption where applicable.

# Chapter 3 Characterisation of models to study drug response in Ras driven colon cancer

The Fruit-fly intestine has a lot of similarities with mammalian intestine, both at the cellular and molecular levels. Our intestine is similar to that of the fly, not only in function but also in its development and maintenance.

Modelling colorectal cancer using *Drosophila melanogaster*, the common fruit-fly, offers several advantages due to their genetic versatility and rapid life cycle. I used patented patient-specific fruit fly avatars where fruit flies are genetically modified to carry mutations that mirror the genetic profile of human colorectal cancer patients, allowing precise simulation of the disease progression and tumour response. Incorporating patient's genetic mutations into fly genome, allowed us to model patient tumours in a manner that is both biologically relevant and cost-effective.

In recent years, there has been a growing interest in using fruit-flies as a drug discovery platform as it provides a unique opportunity to screen small molecules or FDA approved drugs against complex diseases in a whole animal setting.

## 3.1 Genetically complex fruit-fly models of Ras-driven colorectal cancer

Key similarities between fruit-fly hindgut and mammalian intestinal crypts have been explored in depth in Section 1.5. Briefly, the proximal part of fly hindgut, the hindgut proliferation zone (HPZ) is reminiscent of transit-amplifying zone (TAZ) in mammalian intestinal crypts. The interplay between key signalling pathways is well conserved between fly hindgut and mouse intestine, wherein hyperactivated Wnt signalling results in expansion of HPZ in the fly hindgut and enlargement of crypts in mouse intestine.

### 3.1.1 Oncogenic Ras signalling in larval hindgut results in enlarged hindgut proliferation zone.

I studied how mutations in Ras, Wnt and p53 - the most deregulated pathways in CRC, affect homeostasis in the larval hindgut using data generated by Dr Bojie Cong. Transgene expression in larval hindguts was induced by a temperature regulated hindgut specific driver: *byn<sup>ts</sup>-Gal4* (hereafter *byn<sup>ts</sup>*). Oncogenic Ras signalling in larval hindgut (*byn<sup>ts</sup>>ras<sup>G12V</sup>*) resulted in an enlarged hindgut proliferation zone (HPZ) (Figure 3.1, C) compared to wildtype animals that served as control. Similarly, hyperactivated Wnt

signalling (*byn<sup>ts</sup>* > *arm<sup>S10</sup>*) also resulted in expansion of the HPZ (Figure 3.1, D). Simultaneous perturbation of Ras-Wnt signalling (*byn<sup>ts</sup>* > *ras<sup>G12V</sup>* *arm<sup>S10</sup>*) or Ras-p53 signalling (*byn<sup>ts</sup>* > *ras<sup>G12V</sup>* *p53<sup>Ri</sup>*) or Ras-Apc-p53 signalling (*byn<sup>ts</sup>* > *ras<sup>G12V</sup>* *arm<sup>S10</sup>* *p53<sup>Ri</sup>*, hereafter *byn*>*RAP*) also resulted in an enlarged HPZ in the larval hindgut. This expansion of HPZ was only observed in larvae that had *ras<sup>G12V</sup>* suggesting hyperproliferation of HPZ is an emergent property of oncogenic *ras* activity. Due to disruption of hindgut homeostasis, none of the larvae survived to adulthood.

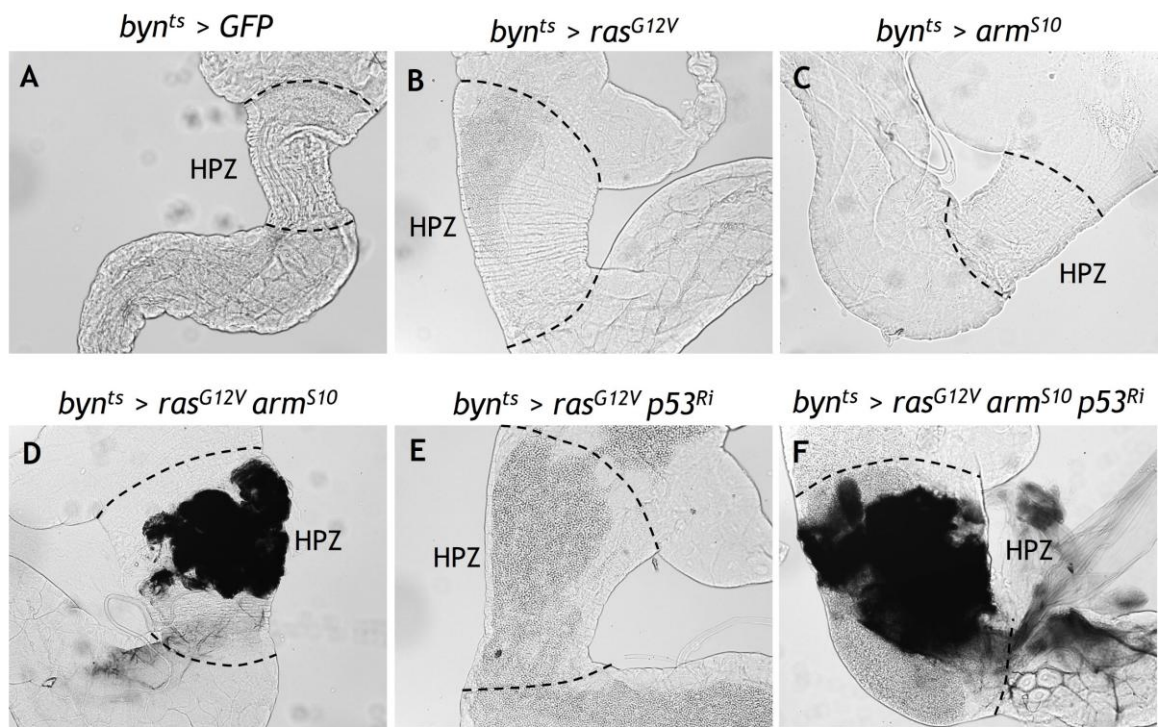


**Figure 3-1: Transgene activation in fly hindgut leads to expansion of Hindgut Proliferation Zone**

Bright-field images of Hindgut Proliferation Zone (HPZ, marked by dotted lines) of fly hindguts in - (A) *byn<sup>ts</sup>* > *GFP* (wildtype), (B) *byn<sup>ts</sup>* > *ras<sup>G12V</sup>*, (C) *byn<sup>ts</sup>* > *arm<sup>S10</sup>*, (D) *byn<sup>ts</sup>* > *ras<sup>G12V</sup>* *arm<sup>S10</sup>*, (E) *byn<sup>ts</sup>* > *ras<sup>G12V</sup>* *p53<sup>Ri</sup>*, (F) *byn<sup>ts</sup>* > *ras<sup>G12V</sup>* *arm<sup>S10</sup>* *p53<sup>Ri</sup>*. These data were generated by Dr. Bojie Cong in the Cagan Laboratory, University of Glasgow.

### 3.1.2 Spatio-temporal regulation of transgenes in a patient-specific fly avatar mirrors clinical response

Having established the hyperproliferation phenotype in the larval HPZ in single- and multi-hit fly models, I studied the patient-specific fly avatar (UAS-CPCT036) developed by the Cagan Laboratory for modelling human colorectal cancer (Bangji et al., 2016). Briefly, a patient tumour was modelled in a fruit-fly hindgut. RNA interference (Ri) lines were used to knockdown tumour suppressor genes, and a *ras<sup>G12V</sup>* transgene to model the oncogenic isoform of *KRAS<sup>G12V</sup>*. Mutational profile of UAS-CPCT036 is listed in Table 3-1 below.

**Table 3-1** : Mutations in fly avatar and its human ortholog

Fly Avatar	Genotype	Human Ortholog
CPCT006 9-hit model	UAS - <i>ras</i> <sup>G12V</sup> <i>apc</i> <sup>Ri</sup> <i>p53</i> <sup>Ri</sup> <i>ago</i> <sup>Ri</sup> <i>ahg</i> <sup>Ri</sup> <i>put</i> <sup>Ri</sup> <i>p38a</i> <sup>Ri</sup> <i>ft</i> <sup>Ri</sup> <i>brm</i> <sup>Ri</sup>	<i>KRas</i> <sup>G12V</sup> , <i>Apc</i> , <i>p53</i> , <i>Fbxw7</i> , <i>Acvr2a</i> , <i>Fat4</i> , <i>Smarca2</i>
CPCT036 10-hit model	UAS - <i>ras</i> <sup>G12V</sup> <i>apc</i> <sup>Ri</sup> <i>p53</i> <sup>Ri</sup> <i>ago</i> <sup>Ri</sup> <i>chico</i> <sup>Ri</sup> <i>smox</i> <sup>Ri</sup> <i>eva</i> <sup>Ri</sup> <i>sdhA</i> <sup>Ri</sup> <i>rassf</i> <sup>Ri</sup> <i>efa6</i> <sup>Ri</sup>	<i>KRas</i> <sup>G12V</sup> , <i>Apc</i> , <i>p53</i> , <i>Irs1</i> , <i>Fbxw7</i> , <i>Smad4</i> , <i>Sdha</i> , <i>Rassf</i> , <i>Psd</i>

I utilised the temperature-sensitive Gal4/Gal80<sup>ts</sup> system (Described in Chapter 1.7) and hindgut-specific promoter *byn* or *byn*<sup>ts</sup> for spatio-temporal regulation of transgene expression (Brand and Perrimon, 1993). The temperature-sensitive Gal4/Gal80<sup>ts</sup> system allows for the management of transgene expression, where gene activity is controlled via temperature regulation. At high temperatures such as 29 °C, Gal80<sup>ts</sup> is inactive, resulting in robust Gal4 activity under the *byn* promoter. Conversely, at lower temperatures such as 18 °C, Gal80<sup>ts</sup> actively engages with Gal4, completely repressing its activity.

Male flies bearing patient-specific mutations (*UAS-CPCT036*) were crossed with 15-20 *byn* or *byn*<sup>ts</sup> virgin females to generate desired progenies - *byn*>*CPCT036* or *byn*<sup>ts</sup>>*CPCT036* respectively. I used the *tubby* marker, characterized by a visibly distinct rounded abdomen, to facilitate the selection of desired F1 progeny in genetic crosses. Specifically, in my experiment, the desired F1 progeny, which carry the patient-specific fly avatar (*UAS-CPCT036*) were identified by the *absence* of this tubby phenotype. These non-tubby larvae and pupae, with their standard *Drosophila* morphology, lack the bloated appearance typical of tubby mutants, allowing them to be easily distinguished (Figure 3.2, A). Other progenies that displayed tubby phenotype (Figure 3-2, A) served as internal controls to evaluate potential temperature or drug related toxicities. Survival to adulthood was calculated by counting the number of empty experimental and control pupal cases (indicating an adult fly has successfully eclosed).

I tested various development temperatures ranging from 25 °C to 29 °C to optimise Gal4/Gal80<sup>ts</sup> activity in the larval hindgut, aiming to determine the ideal temperature for baseline survival rates between 10-20%. The idea is that a subsequent therapeutic intervention would improve survival rates by restoring homeostasis in the HPZ. Constitutive expression of transgenes in larval hindgut (*byn*>*CPCT036*) was embryonically lethal; as no larvae survived to adulthood due to disruption of hindgut homeostasis at any of the temperatures tested (Figure 3-2, C). However, when transgene expression was regulated both spatially and temporally (*byn*<sup>ts</sup>>*CPCT036*), improvements in larval-to-adulthood survival rates were evident (Figure 3-2, D). Specifically, *byn*<sup>ts</sup>>*CPCT036* larvae that developed at 25 °C had almost 100% survival compared to tubby controls, which might be due to sub-optimal transgene expression. Whereas *byn*<sup>ts</sup>>*CPCT036* progenies that

developed at 27°C had 43% survival and those that developed at 29°C had 0% survival. Since the survival rate at 27°C was too high for baseline and 29°C was lethal, 28°C was estimated as a better temperature for transgene regulation.

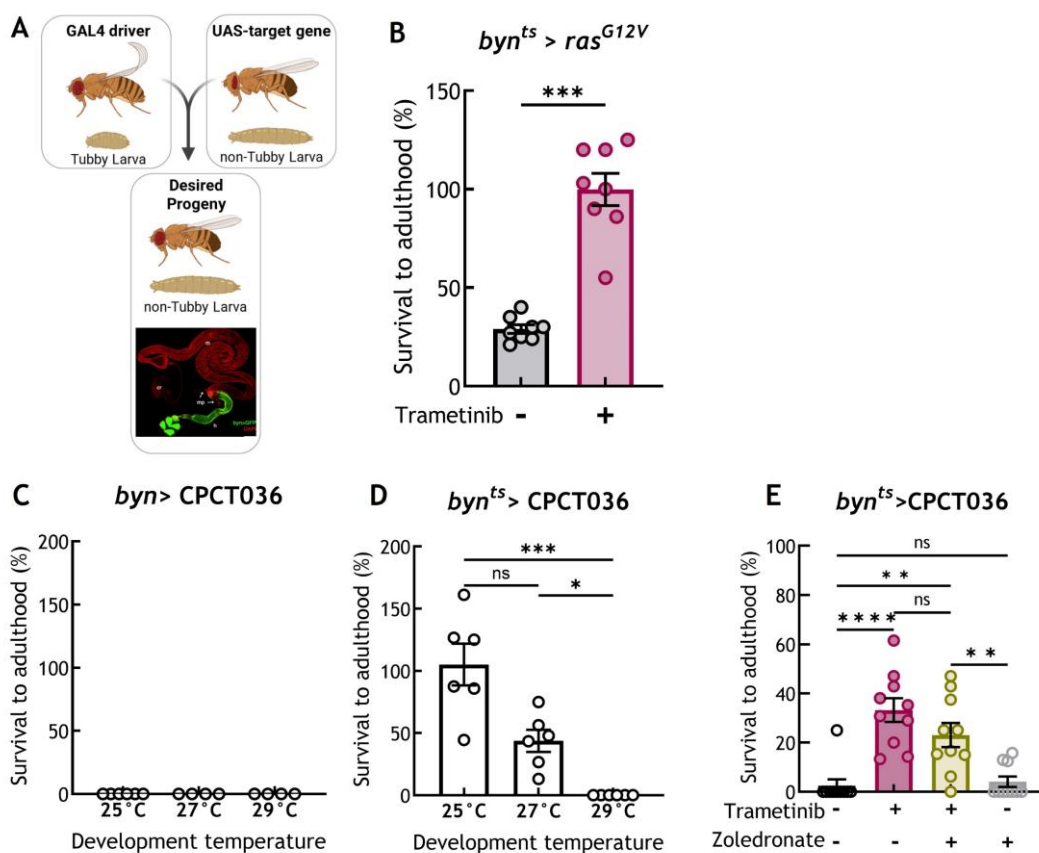


**Figure 3-2: Characterisation of fly hindgut as a model of human CRC.**

(A) Illustration of fly cross. (B) Trametinib improves survival of *byn<sup>ts</sup>>ras<sup>G12V</sup>* fly line, (Mann-Whitney test). (C) Larvae with constitutive transgenes expression under hindgut-specific *byn* promoter fail to reach adulthood. (D) Larvae under spatiotemporal regulation of transgene expression (*byn<sup>ts</sup>*) demonstrate a temperature dependent survival to adulthood. (E) Rescue from lethality assay demonstrates a significant survival benefit in larvae treated with Trametinib as a single agent and in combination with Zoledronate. Asterisks represent *P* values obtained from One-way ANOVA, Kruskal-Wallis test followed by Dunn's correction; ns *P*(>0.05), \* *P*(<0.05), \*\* *P*(<0.005), \*\*\* *P*(<0.001), and \*\*\*\* *P*(<0.0001).

A recent fly-to-bedside clinical trial (Bangli et al., 2019), demonstrated that combination of trametinib and zoledronate significantly improved survival, in a specific fly avatar - *byn<sup>ts</sup>>CPCT006*, when compared to single-agent trametinib. Trametinib is a MEK inhibitor that suppresses MAPK pathway and zoledronate is a bisphosphonate prescribed to patients with bone resorption disorders, with no known anti-cancer activity. The response was also translated in the patient for whom the fly avatar was generated. Target lesions in the patient reduced by 45% and remained stable for several months before new lesions emerged that were non-responsive to the combination therapy (Bangli et al., 2019). Seeking to uncover the synergy between trametinib and zoledronate, I tested this drug combination on *byn<sup>ts</sup>>CPCT036*, which also exhibits mutations in the Ras-Apc-p53 pathway among others (Table 3-1). Briefly, crosses for the drug screen were set up at 28°C as

described earlier in this section. Egg lays were performed on drug laden fly media which consisted of trametinib (1 $\mu$ M) with or without zoledronate (0.7 $\mu$ M). 0.1% DMSO and zoledronate (0.7 $\mu$ M) treated flies served as controls. Single-hit fly line, *byn*> *ras*<sup>G12V</sup> that showed 70% improvement in survival when treated with trametinib (Figure 3-2, B). In contrast, *byn*<sup>ts</sup>>*CPCT036* larvae treated with trametinib as a single agent or in combination with zoledronate had a moderate improvement in survival (33.2% & 23% vs 05,  $p < 0.005$ ,  $n = 10$ ) (Figure 3.2, E). Flies that received Vehicle (0.1% DMSO) failed to reach adulthood. This variation observed between single-hit and multi-hit fly lines emphasises what is observed in clinics - resistance to targeted therapies. Our multi-hit fly models capture key features of human colon tumours which show complex multigenic regulation.

## 3.2 Mouse Models of Kras-driven colorectal cancer

Unlike fruit-fly models, oncogenic Kras signalling or loss of p53 alone exert minimal effects on mouse intestinal homeostasis (Sansom et al., 2006). However, acute loss of Apc precipitates rapid hyperproliferation of crypts accompanied by altered proliferation, differentiation and apoptosis (Sansom et al., 2004). This study explores impact of oncogenic KRas in the background of loss of p53 and/or loss of Apc. For spatio-temporal regulation, our model incorporates a tamoxifen-inducible Cre-recombinase under the control of the intestinal epithelium-specific Villin1 promoter (Villin<sup>CreERT2</sup>) (El Marjou et al., 2004), allowing targeted genetic recombination at specific genetic sequences (“loxP” sites). The following alleles were used for targeting Apc<sup>fl</sup> (Shibata et al., 1997), KRas<sup>L5L-G12D</sup> (Jackson et al., 2001), and p53<sup>fl</sup> (Jonkers et al., 2001).

**Short-term Model:** To assess how oncogenic Kras disrupts intestinal homeostasis, mice expressing Villin<sup>CreERT2</sup> were crossed with mice harbouring conditional alleles of oncogenic Kras (Kras<sup>G12D/wt</sup>), inactivated Apc (Apc<sup>fl/fl</sup>) and/or inactivated p53 (p53<sup>fl/fl</sup>). This generated single mutant - Villin<sup>CreERT2</sup>; Apc<sup>fl/fl</sup> (hereafter **A-HOM**) or compound mutants - Villin<sup>CreERT2</sup>; Apc<sup>fl/fl</sup> Kras<sup>G12D/wt</sup> (hereafter **AK-HOM**) and Villin<sup>CreERT2</sup>; Apc<sup>fl/fl</sup> Kras<sup>G12D/wt</sup> p53<sup>fl/fl</sup> (hereafter **AKP-HOM**). Note that -HOM refers to homozygosity of Apc<sup>fl</sup> allele. Acute loss of Apc by Tamoxifen administration (80mg/kg, i.p.) results in rapid hyperproliferation of the crypt-villus axis upon Cre recombination in both single and compound mutants (Figure 3-3, A). Due to rapid expansion of the crypt and a hyperproliferative phenotype, this model has a shorter latency, and mice must be culled at 3 days post transgene activation.

I have utilised the short-term models to investigate the effects of acute loss of Apc, p53 and oncogenic Kras on intestinal homeostasis (Chapter 3.2.1) and to explore whether targeting the MAPK pathway could abrogate the hyperproliferative phenotype (Chapter

3.2 and 3.3). A primary limitation of this model is its short latency, which precludes the development of adenoma.

**Long-term Model:** To assess the role of oncogenic Kras in intestinal tumourigenesis, we generated compound mutants bearing a single-copy of lox-flanked Apc allele - Villin<sup>CreERT2</sup>; Apc<sup>fl/wt</sup> KRas<sup>G12D/wt</sup> (hereafter **AK-HET**) and Villin<sup>CreERT2</sup>; Apc<sup>fl/wt</sup> KRas<sup>G12D/wt</sup> p53<sup>fl/fl</sup> (hereafter **AKP-HET**). I also studied Villin<sup>CreERT2</sup>; Apc<sup>fl/wt</sup> (hereafter **A-HET**) mice were used to understand baseline tumourigenesis by loss of Apc. Administration of Tamoxifen (80mg/kg, i.p.) induces a heterozygous loss of Apc throughout the intestine. The sporadic loss of the second Apc allele drives subsequent tumour formation. 21 days after transgene activation, mice are randomly allocated to treatment groups and monitored until clinical endpoint (hunching, progressive weight loss and anaemia) (Figure 3-3, B).

Due to its extended latency, this model is particularly useful for studying tumour initiation, progression and overall survival (Chapter 3.1). In Chapters 3.2 and 3.3, I have investigated whether targeting the MAPK pathway can reduce tumour burden and increase overall survival (Chapter 3.2 and 3.3). A caveat of this model is that transgene activation across the whole intestine results in multiple tumours which can have a significant impact on the overall health of the mice. Mice predisposed to forming fewer tumours might live longer, despite experiencing progressive tumourigenesis. Conversely, mice with multiple tumours may succumb earlier, though with less advanced tumours. Furthermore, it is challenging to ascertain the tumour burden at the onset of therapy; thus, tumours assessed at the clinical endpoint may have initiated at different points.

**Colon tumour Model:** Villin<sup>CreERT2</sup> mice bearing homozygous lox-flanked Apc allele (Apc<sup>fl/fl</sup>) receive intracolonic administration of 4-Hydroxy Tamoxifen into the colonic submucosa as described by (Roper et al., 2017). Cre recombination at the site of tamoxifen administration results in formation of a single tumour at the distal colon, extending latency of this model. Mice are allocated into treatment groups after confirmation of tumour establishment by colonoscopy. Mice are treated for 5 days and sampled at treatment endpoint (Figure 3-3, C). This model allows us to study signalling networks in fully established tumours. A big advantage of our intracolonic model is that treatment is begun after confirmation of tumour establishment, allowing us to study treatment response in fully established tumours. Since time of tumour initiation is known and a single tumour has a lower impact on the overall health of the mouse, I used this model to study how mutations in colon tumours impact response to targeted therapy in Chapters 3.2.3 and 4.3.3.

**Intracolonic Transplantation Model:** This model involves intracolonic transplantation of sex-matched intestinal organoids into the colonic submucosa (Roper et al., 2017) (Figure

3-3, D). I used this model to corroborate my *in vitro* drug metabolism studies (Cong et al., 2023) at a whole animal level. While the intracolonic model allows the study of colon tumour at the distal end of colon, this approach allows transplantation of organoids of interest into the colonic sub-mucosa. The only caveat of the study is that p53 loss is required for successful transplantation. We found limited success in transplanting organoids with wildtype p53.

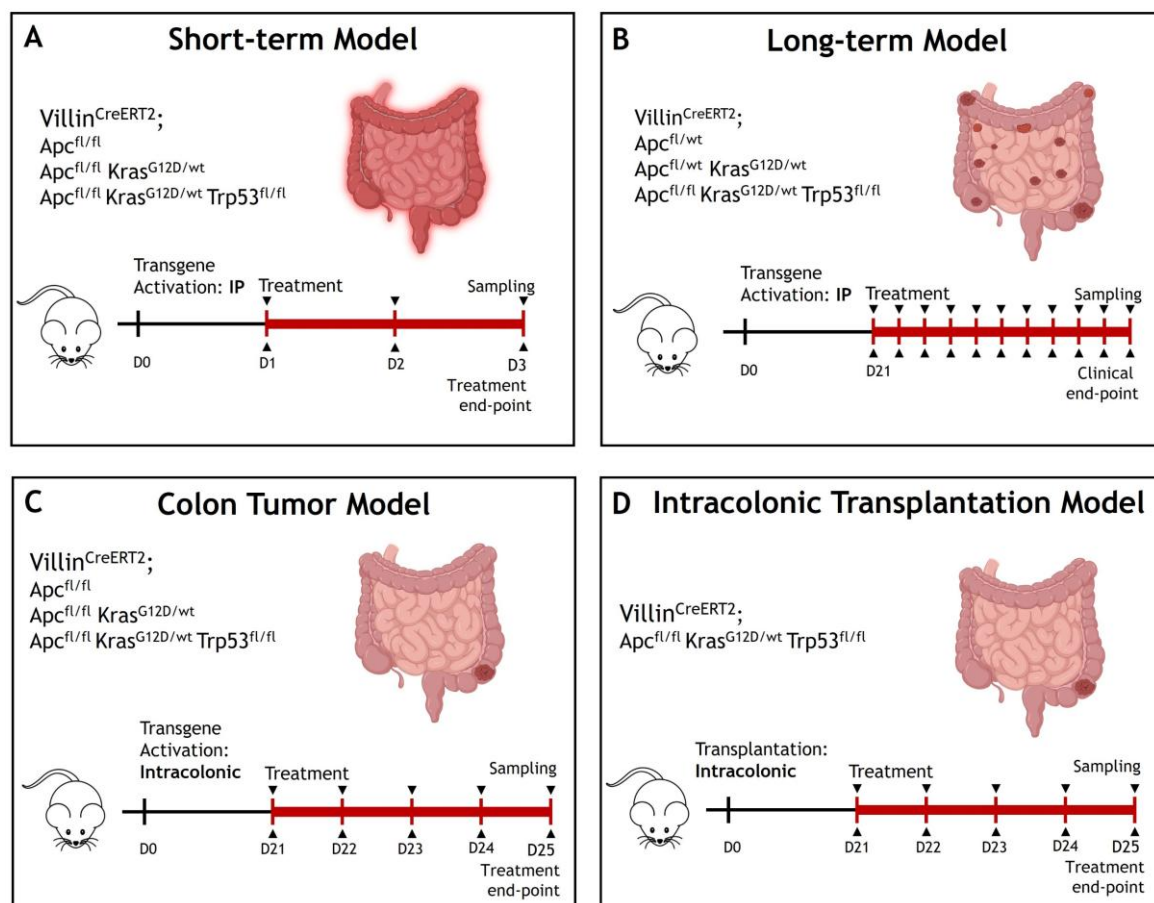


**Figure 3-3: Illustration of different Kras-driven mouse intestinal tumour models utilised in this thesis.**

(A) Short-term model, (B) Long-term model, (C) Colon tumour model, (D) Intracolonic transplantation model.

### 3.2.1 Short-term Model

Transgene activation in A-HOM, AK-HOM and AKP-HOM mice was carried out with Tamoxifen administration (80mg/kg, i.p.) on Day 0. Mice were then treated with 0.5% HPMC + 0.1% Tween (Vehicle control) from Day 1 to 3. BrdU (0.25ml, 10mM) was administered 2h before sampling. This is a shorter latency model as homozygous loss of Apc leads to rapid hyperproliferation of crypt across the whole intestine and mice must be culled at day 3 post-induction due to ethical reasons. Wildtype mice subjected to tamoxifen administration served as controls to understand baseline proliferation rate. I studied haematoxylin and eosin (H&E) stained sections to assess alterations in crypt architecture following hyperactivation of the Wnt and MAPK pathways and the loss of p53.

The analysis revealed a significant increase in crypt length along the crypt-villus axis, with densely packed, morphologically atypical 'crypt- progenitor like' cells predominating this region, suggestive of enhanced proliferation and altered differentiation (Figure 3-4). Comparatively, crypts were more densely packed than those in wildtype mice, resulting in a higher number of crypts per unit area (Figure 3-4).

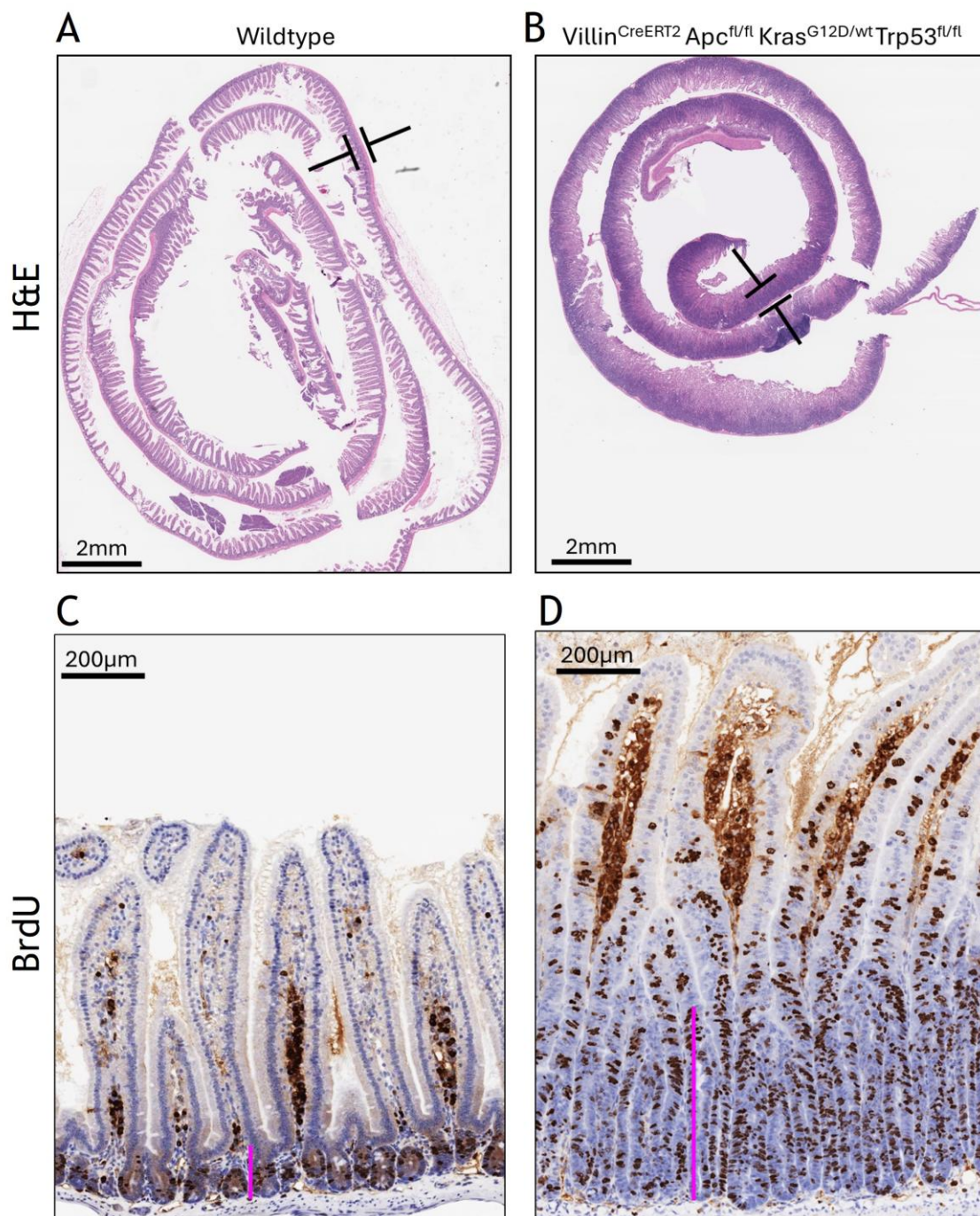


**Figure 3-4: Changes in intestinal crypt pathology upon tamoxifen administration in short-term model. (Representative images)**

H&E-stained section of a small intestinal (proximal) gut roll of (A) wildtype and, (B) AKP-HOM mouse, showing thickening of the gut epithelium in AKP-HOM mouse. Transgene activation results in altered proliferation. BrdU-positive cells in (C) wildtype and (D) AKP-HOM proximal small intestinal crypts 2h post BrdU injection are confined to a transit amplifying zone (TAZ) within the crypts.

The Transit Amplifying Zone (TAZ) within the normal crypt has been well characterised by previous studies, where cycling cells are confined to the mid-crypt region (Figure 3.4, A-B). In my analysis, BrdU labelling was used to quantify the number of S-phase cells per half-crypt in the proximal small intestine and mid-colon of A-HOM, AK-HOM, and AKP-HOM mice.

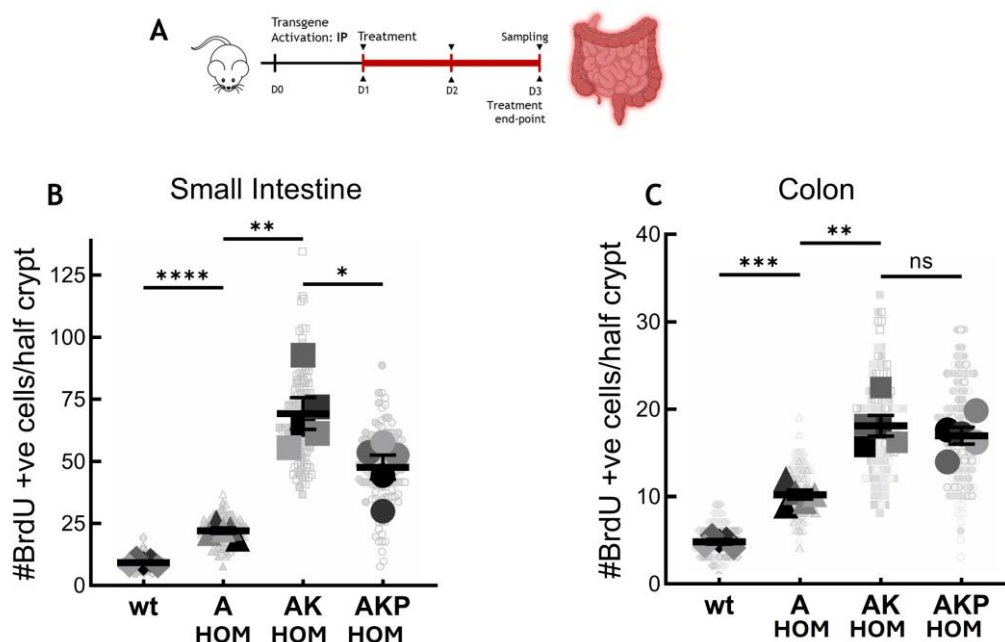


Table 3-2: BrdU score in Small Intestine and Colon

	wt	A HOM	AK HOM	AKP HOM
Small Intestine	9	22	69	48
Colon	5	10	18	17

**Figure 3-5: Oncogenic Ras activation leads to rapid hyperproliferation of intestinal crypts.**

A-HOM (N=5), AK-HOM (N=5), and AKP-HOM (N=5) mice were administered with tamoxifen (80mg/kg, i.p) on Day 0 and sampled on day 3. BrdU (0.25ml, 10mM) was administered 2h before sampling. (A) Illustration of study plan. (B-C) BrdU score was calculated by counting number of BrdU-positive cells per half crypt (n = 25) from small intestine and colon. Small dots represent single half-crypts, large dots represent mean of biological replicates. Asterisks represent *P* values obtained from One-way ANOVA, Kruskal-Wallis test followed by Dunn's correction; ns *P*(>0.05), \* *P*(<0.05), \*\* *P*(<0.005), \*\*\* *P*(<0.001), and \*\*\*\* *P*(<0.0001). Table 3-2: summary of BrdU score in small intestine and colon.

Loss of *Apc* alone doubled proliferation rates in the small intestine (22 vs 9 BrdU positive cells per half crypt, A-HOM vs wt, n = 5, p <0.0001). Further activation of oncogenic *Kras* (AK-HOM) led to 200% increase in proliferation rate (69 vs 22 BrdU positive cells per half crypt, AK-HOM vs A-HOM, n = 5, p < 0.005). Loss of *p53* has been implicated in increased tumour proliferation in several studies. I hypothesised that additional loss of *p53* would increase proliferation due to deregulation of cell cycle checkpoints and apoptosis. Interestingly, the additional loss of *p53* resulted in 30% lower proliferation rates than its wildtype counterpart suggesting complex interactions between these pathways (48 vs 69 BrdU positive cells per half crypt, AKP-HOM vs AK-HOM, n = 5, p < 0.05) (Figure 3-4, B). This increase in cellular proliferation in cells with functional *p53* (AK-HOM) might be due

to compensatory cell proliferation activated by JNK and Wnt pathways (Ryoo et al., 2004). However, this warrants further investigation. In the colon, proliferation rate was similar between AK- and AKP-HOM. Suggesting, loss of p53 did not affect proliferation in the colon (Figure 3-4, C). Differences in proliferation between the small intestine and the colon has also been reported by other studies (Andreu et al., 2005, Gândara et al., 2012). In summary, our short-term models are good for studying the effects of acute activation of Wnt signalling in the background of oncogenic Ras signalling with or without functional p53. Our group has (Sansom et al., 2004) shown that acute activation of Wnt produces many of the phenotypes associated with early colorectal lesions: failure to differentiate and increased proliferation. Overall, this serves as a good model for pre-adenoma stage, and I will be exploring this model further in section 3.2 to understand MAPK dependency. I have also utilised intestinal organoids generated from this model for *in vitro* studies, which is discussed in section 3.3.

### 3.2.2 Long-term model

I next wanted to check how oncogenic Ras signalling impacts intestinal tumour burden and survival in a hyperactivated Wnt background. I utilised the long-term model to study this in detail which has been described in section 3.1.2. Transgene activation in A-HET, AK-HET, and AKP-HET mice was carried out with tamoxifen administration (80mg/kg, i.p.) on Day 0 and mice were aged until they showed clinical signs of distress such as hunching, progressive weight loss and anaemia. While A-HET mice were aged until clinical end-point post transgene induction, AK- and AKP-HET mice were treated with 0.5% HPMC + 0.1% Tween (Vehicle control) once daily by oral gavage (p.o, q.d) from Day 21 post transgene induction and aged until clinical endpoint. This is a longer latency model as loss of heterozygosity of the Apc allele is required for dysplasia and subsequent tumour formation.

#### 3.2.2.1 Loss of Apc leads to tumour formation predominantly in the SI

To understand the impact of constitutive Ras signalling in a High-Wnt background, it was important to establish a baseline of intestinal cancer initiation and progression driven solely by functional loss of Apc. I studied the baseline survival profile and histopathological features of tumours arising from A-HET mice. Unlike the short-term model described in the earlier section (Section 3.2.1), Tamoxifen administration (80 mg/kg, i.p) resulted in a loss of one copy of Apc throughout the intestinal epithelium and drove a predisposition to tumour formation in the intestine by loss of heterozygosity. Following induction, mice were aged up to a defined clinical end-point for this model which included signs of weight loss, anaemia, and hunching, and then sampled.

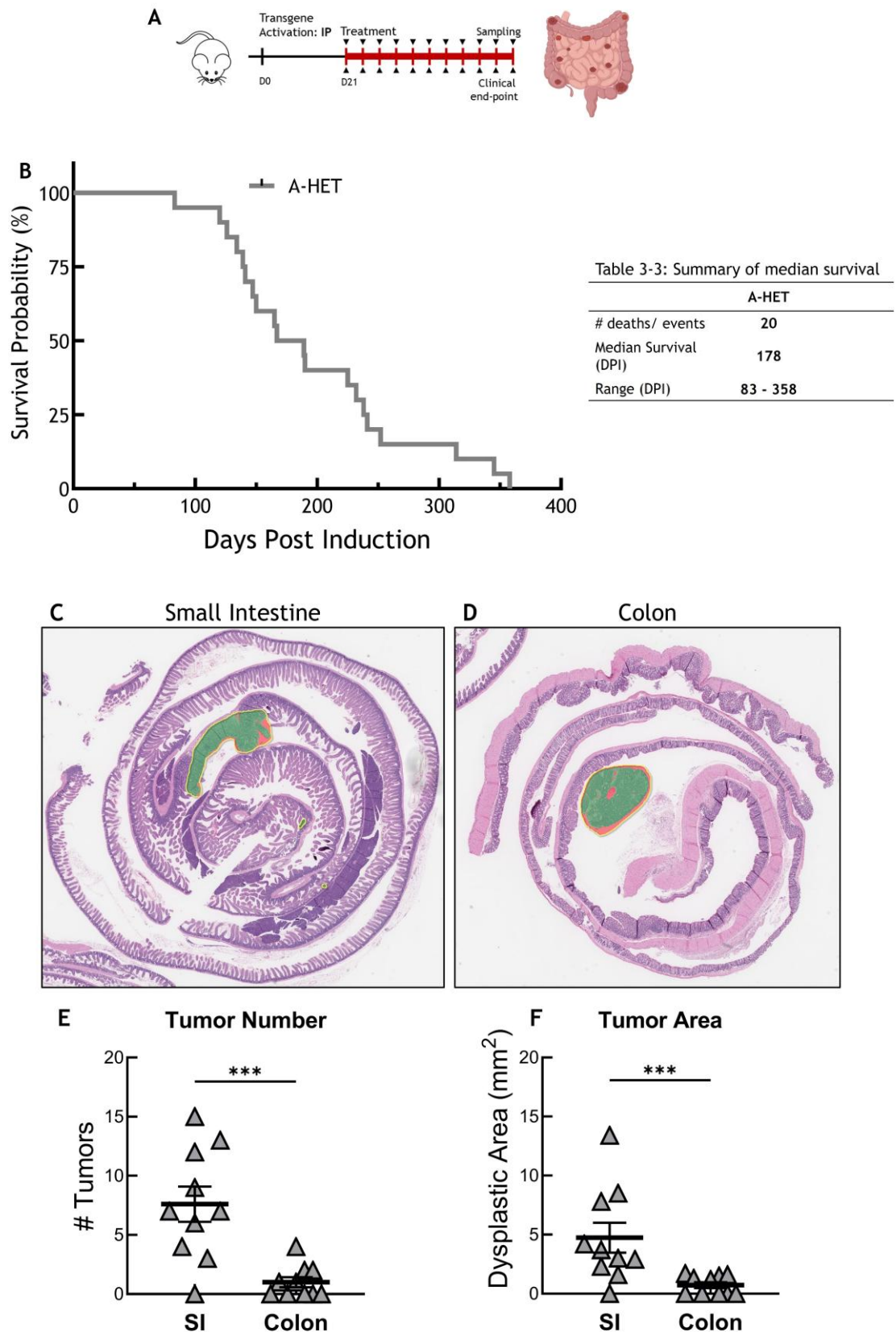


**Figure 3-6: Figure 3-5: Loss of Apc predisposes tumour formation in the small intestine.**

(A) Illustration of study plan. (B) Survival probability of A-HET mice ( $n = 20$ ) post transgene activation by administration of tamoxifen (80mg/kg, i.p). Mice are aged until clinical endpoint: hunching, anaemia and/or weight loss. Median survival: 178 days post induction. Table 3-2, Summary of median survival. Representative images of H&E-stained sections of gut roll depicting tumour burden **in green** (C) proximal small intestine, (D) colon. Tumour burden calculated by (E) number of tumours and (F) total dysplastic area. Mann-Whitney test. Asterisks represent  $P$  values; ns  $P(>0.05)$ , \*  $P(<0.05)$ , \*\*  $P(<0.005)$ , \*\*\*  $P(<0.001)$ , and \*\*\*\*  $P(<0.0001)$ .

A-HET mice had a median survival of 178 days post induction (DPI) (Range: 83 - 358 DPI, n = 20) (Figure 3-5, B).

Upon dissection, macroscopic tumours were noted predominantly in the small intestine and only occasional formation of colonic adenomas (Figure 3.5, C-F). Only one of the 20 mice developed adenocarcinoma in the small intestine, perhaps longer latency contributed towards tumour progression. To further understand the tumour burden, I characterised them by size and number using HALO™. A-HET mice developed an average of 7 small intestinal tumours and occasional colon tumours. By area, small intestinal tumours were the largest with a median size of 0.2mm<sup>2</sup> and reaching upto 7mm<sup>2</sup>. Colonic tumours on the other hand were relatively small not exceeding 2mm<sup>2</sup>.

### 3.2.2.2 Oncogenic Ras signalling enhances tumour development in the colon

Having established a baseline model incorporating Apc loss in the intestinal epithelium, I then went on to assess the impact of oncogenic Kras activation. To do this, Villin<sup>CreERT2</sup>; Apc<sup>fl/wt</sup> mice were crossed with mice bearing a conditional Kras<sup>LSL-G12D</sup> allele (hereafter Kras<sup>G12D</sup>), thus generating Villin<sup>CreERT2</sup>; Apc<sup>fl/wt</sup> Kras<sup>G12D/wt</sup> (AK-HET) mice. As described previously for this model, Tamoxifen administration (80mg/kg, i.p.) induced Cre recombination across the whole intestinal epithelium resulting in loss of one copy of Apc and activation of Kras<sup>G12D</sup> allele. Loss of heterozygosity of Apc leads to tumour formation with cells comprising Apc<sup>fl/fl</sup> and Kras<sup>G12D/wt</sup> alleles. To understand the phenotype of oncogenic Kras signalling in high-Wnt background, I studied mice treated with Vehicle (p.o, q.d) from 21 days post induction (DPI) and aged until clinical endpoint. Median survival of AK-HET mice on Vehicle treatment was 74.5 DPI (Range: 64 - 96 DPI, n = 10) (Figure 3.6, A). Upon dissection, macroscopic tumours were noted predominantly in the proximal and distal part of the colon and in the proximal small intestine. Thickening and widening of the whole gut was also noted during dissection. I used (H&E) stained tissue sections to histologically characterise these tumours. Activation of oncogenic Kras signalling led to a 15-fold increase in overall tumour number (Figure 3.6, B). Number of colonic tumours were on average twice small intestinal tumours Figure 3.6, E (92 vs 50 tumours, Colon vs SI, n = 10, p = 0.054). Tumours in the SI ranged from low- to high- grade dysplasia and colonic tumours were all low-grade dysplasia. Tumours in the small intestine were sessile in their architecture while colonic tumours were mostly adenomatous polyps. None of the tumours in the SI or colon had invasive features, hence all tumours were categorised as dysplastic adenomas. Interestingly, colonic tumour burden accounted for more than 80% of the overall tumour burden in these mice. This is in contrast with our A-HET mice where tumour burden was predominantly in the small intestine, suggesting oncogenic Kras drives tumour development in the colon.

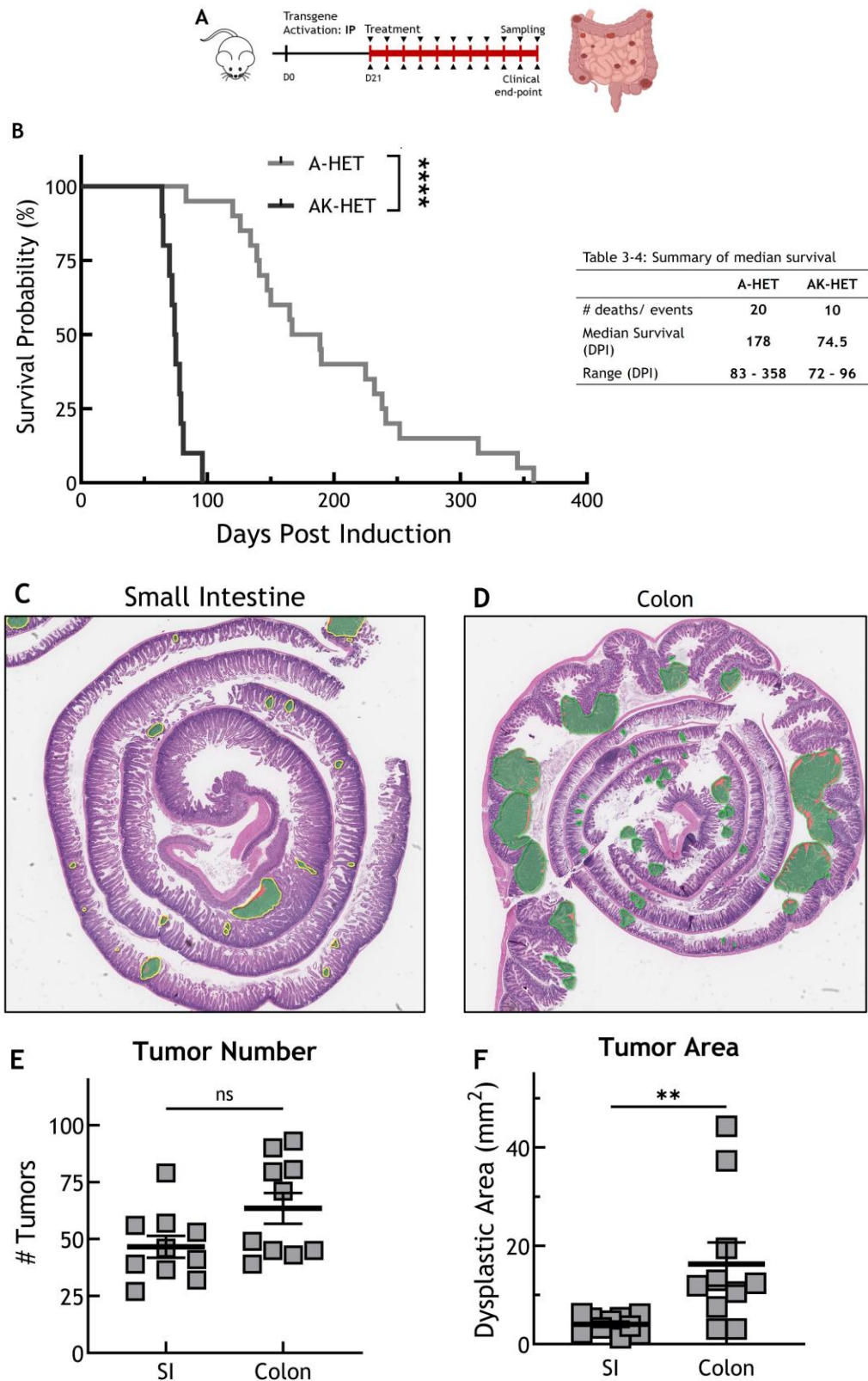


**Figure 3-7: Oncogenic Kras shortens survival in mice by increasing colonic tumour burden.**

(A) Illustration of study plan. (B) Survival probability of A-HET mice (grey,  $n = 20$ ) and AK-HET mice (black,  $n = 10$ ) post transgene activation by administration of tamoxifen (80mg/kg, i.p). Mice are aged until clinical endpoint: hunching, anaemia and/or weight loss. Median Survival (MS) reduces by 58% upon activation of  $Kras^{G12D/wt}$  (MS: 178 vs 74.5 DPI,  $p < 0.005$ , Log rank test). Table 3-3, Summary of median survival. Representative images of H&E-stained sections of gut roll depicting tumour burden in (C) proximal small intestine, (D) colon. Tumour burden calculated by (E) number of tumours and (F) total dysplastic area. Mann-Whitney test. Asterisks represent  $P$  values; ns  $P(>0.05)$ , \*  $P(<0.05)$ , \*\*  $P(<0.005)$ , \*\*\*  $P(<0.001)$ , and \*\*\*\*  $P(<0.0001)$ .

### 3.2.2.3 Loss of p53 further increases the overall tumour burden and impacts overall survival

Approximately 20% of all KRAS-driven CRCs are accompanied by concomitant loss of Apc and p53. Several studies have implicated loss of p53 in drug resistance. To understand the impact of loss of p53 in tumours driven by hyperactivated Wnt and MAPK signalling, mice bearing  $Apc^{fl/wt}$  and  $Kras^{G12D/wt}$  alleles were crossed with mice bearing  $p53^{fl/fl}$  allele, thus generating  $Villin^{CreERT2}; Apc^{fl/wt} Kras^{G12D/wt} p53^{fl/fl}$  (AKP-HET) mice. As described previously for this model, Tamoxifen administration (80mg/kg, i.p.) induced Cre recombination across the whole intestinal epithelium resulting in loss of one copy of Apc and homozygous loss of p53 along with activation of oncogenic Kras. As loss of heterozygosity of Apc is required for tumour formation, tumours arising from the intestine of these mice have homozygous loss of Apc, p53 and oncogenic Kras activation. Similar to AK-HET mice, AKP-HET mice were also treated with Vehicle (p.o., q.d.) from 21 days post induction and aged until clinical endpoint as described previously for this model.

AKP-HET mice reached median clinical endpoint at 44 DPI (Range: 33 - 66 DPI, n = 9) which was significantly lower than AK-HET mice (74.5 DPI, n = 10,  $p < 0.0001$ , Log-rank test) (Figure 3-7, B).

Like AK-HET mice, macroscopic tumours were noted predominantly in the proximal and distal colon and in the proximal small intestine (Figure 3-7, C-F). Histopathological assessment revealed colonic tumour burden contributed to majority of the overall tumour burden. While the colonic tumour burden was similar in AK-HET and AKP-HET mice, it should be noted that AKP-HET mice showed clinical signs much earlier, suggesting tumour growth in a shorter span of time. Like AK-HET mice, tumours in the small intestine were sessile in their architecture while colonic tumours were mostly adenomatous polyps. A notable increase in SI tumour burden was observed (Figure 3-8, E-F).

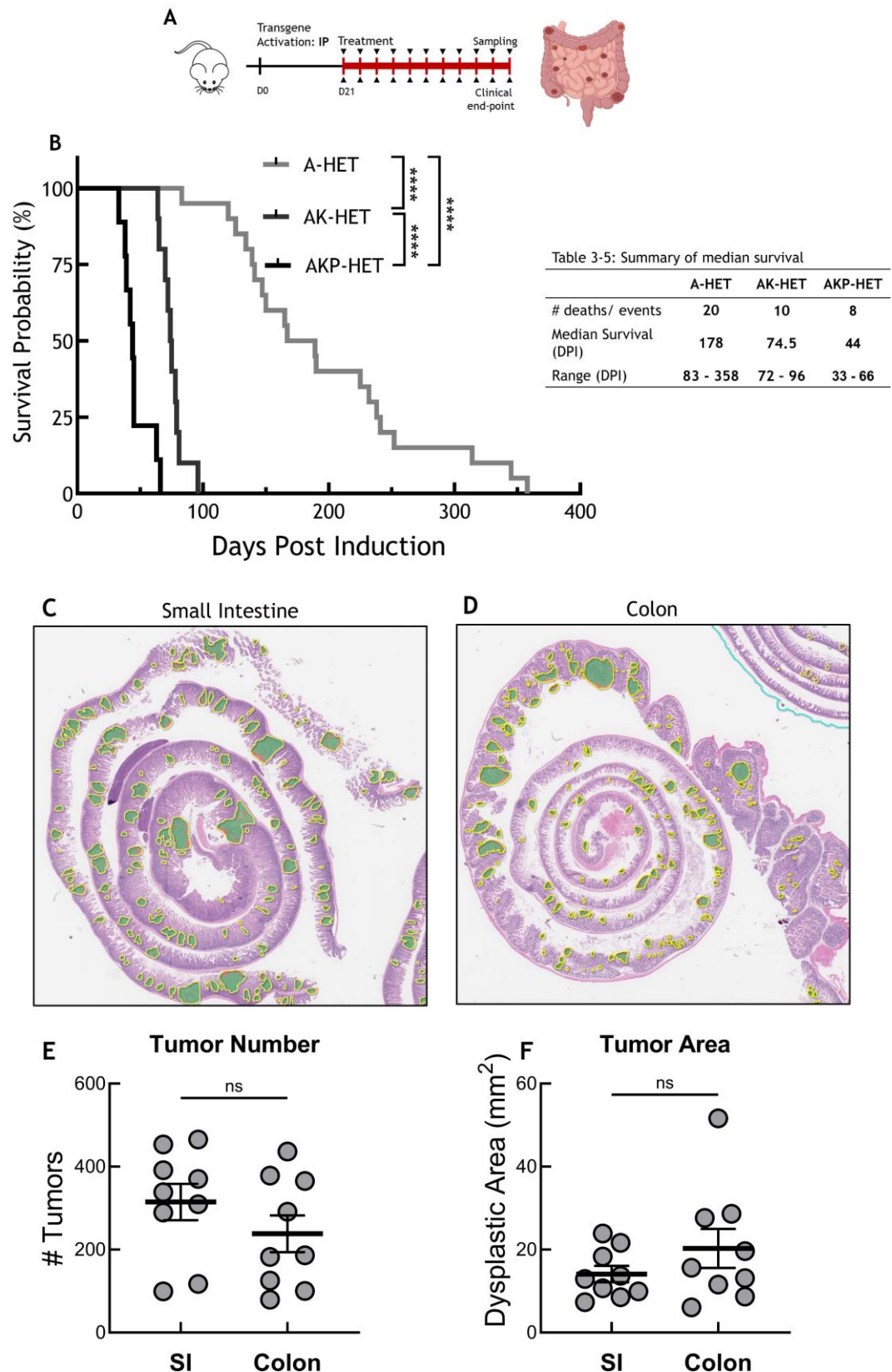


**Figure 3-8: Further loss of p53 reduces median survival by increasing overall tumour burden.**

(A) Illustration of study plan. (B) Survival probability of A-HET mice (light grey,  $n = 20$ ), AK-HET mice (grey,  $n = 10$ ) and AKP-HET mice (black,  $n = 9$ ) post transgene activation by administration of tamoxifen (80mg/kg, i.p). Mice are aged until clinical endpoint: hunching, anaemia and/or weight loss. Median Survival (MS) further reduces by 40% upon loss of p53 (MS: 44 vs 74.5 DPI, AKP-HET vs AK-HET,  $p < 0.005$ , Log rank test). Table 3-4, Summary of median survival. Representative images of H&E-stained sections of gut roll depicting tumour burden in (C) proximal small intestine, (D) colon. Tumour burden calculated by (E) number of tumours and (F) total dysplastic area. Mann-Whitney test. Asterisks represent  $P$  values; ns  $P(>0.05)$ , \*  $P(<0.05)$ , \*\*  $P(<0.005)$ , \*\*\*  $P(<0.001)$ , and \*\*\*\*  $P(<0.0001)$ .

### 3.2.2.4 Discussion

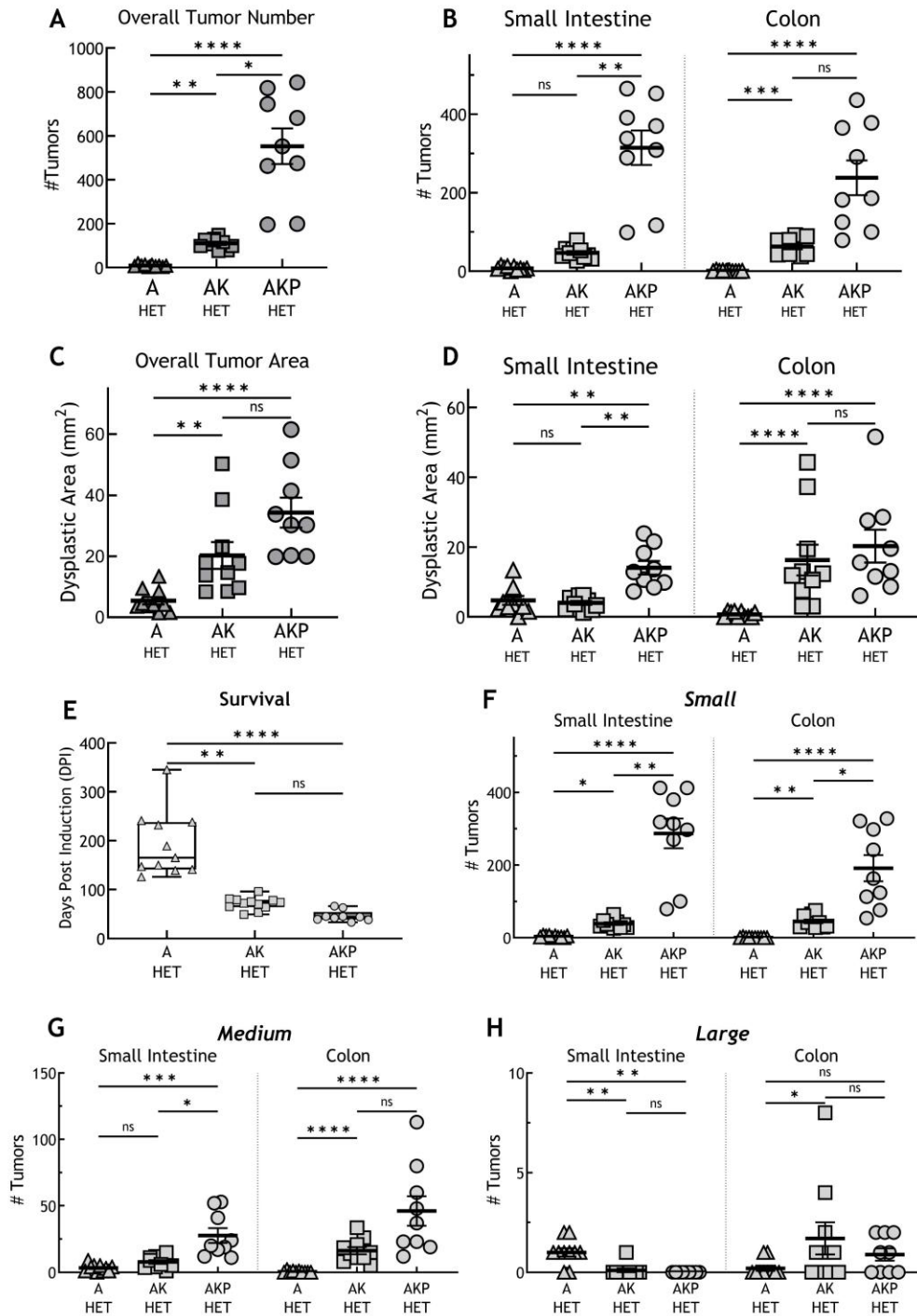


**Figure 3-9: Oncogenic Kras signalling accelerates tumour development in the colon and loss of p53 accelerates overall tumour burden.**

Overall tumour burden in A-, AK- and AKP-HET mice at clinical endpoint quantified by (A) total number of tumours and, (C) total dysplastic area. (B&D) Tumour burden in small intestine and colon. (E) Box-plot of median survival of A-, AK- and AKP-HET mice scored for tumour burden. (F-H) Tumours sorted by size, small (<0.1mm<sup>2</sup>), medium (0.1-1.5mm<sup>2</sup>) and large (>1.5mm<sup>2</sup>). One-way ANOVA, Kruskal-Wallis test. . Asterisks represent P values; ns P(>0.05), \* P(<0.05), \*\* P(<0.005), \*\*\* P(<0.001), and \*\*\*\* P(<0.0001).

In summary, I have shown that loss of Apc predisposes tumour formation predominantly in the small intestine, with occasional colonic polyps. These mice typically develop fewer than 20 tumours and exhibit longer median survival (178 days post-induction, A-HET). The activation of Kras<sup>G12D/wt</sup> significantly reduces survival by approximately 60% (median

survival of 74.5 days post-induction, AK-HET) due to a significant increase in tumour burden, particularly in the colon. Notably, the further loss of p53 shifts the balance towards the formation of more small intestinal tumours (median survival of 44 days post-induction, AKP-HET). However, the shorter duration of these tumours does not allow them to develop into invasive adenocarcinomas.

### 3.2.3 Colon tumour model

Our short-term models are good for studying early stages of tumour initiation and progression. Long term models develop multiple tumours throughout the intestine including the small intestine. Human colon cancer has little similarity with small intestinal cancer. In our long-term models, I observed that small intestinal tumours progress faster than colon tumours. At clinical endpoint, colon tumours were low-grade well-differentiated adenomas with no high grade or invasive features. Another approach to induce colon tumours is with induction of single colon tumour with injection of 4-hydroxy Tamoxifen into the colonic submucosa guided by colonoscopy. Development of single tumour extends latency of this model and gives an opportunity for tumour progression.

To generate a single colonic tumour, tamoxifen (4-OHT) was injected into the colonic sub-mucosa of A-HOM, AK-HOM and AKP-HOM mice to induce focal transgene induction. Tumours resulting from these mice are referred as A, AK and AKP colon tumours respectively. Mice were monitored for tumour growth by colonoscopy 21-days post induction. Upon confirmation of tumour establishment, mice were treated with Vehicle (0.5% HPMC + 0.1% Tween) for 5 days (p.o, q.d.) and sampled at treatment endpoint. In short, tumours in these models had a similar time for initiation and progression.

Histopathological assessment showed well-differentiated tubular adenomas with no detectable invasion, reminiscent of human adenomas. This model recapitulates key features of colonic adenomas in a fully immunocompetent environment, allowing

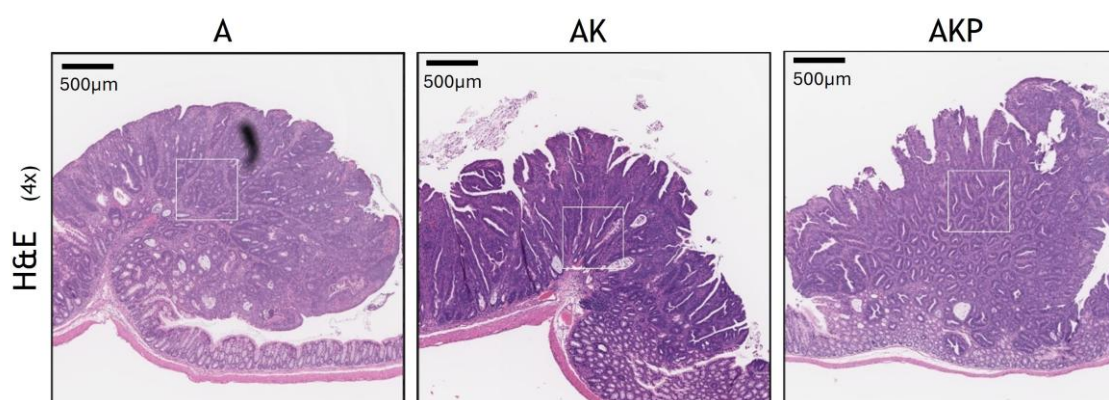


**Figure 3-10: Brightfield images of intracolonic tumors stained with haematoxylin & eosin.**

Bright-field images of A-, AK-, and AKP colon tumour sampled at 5 days post-tumour confirmation. Tissue sections stained with Haematoxylin & Eosin (4x magnification), show well-differentiated adenomatous polyps.

fundamental questions of tumour initiation and dependency on key signalling pathways. A-, AK and AKP intracolonic tumours look similar in histology. Notably, p53 loss was not sufficient to cause invasive tumours in the colon (Figure 3-10).

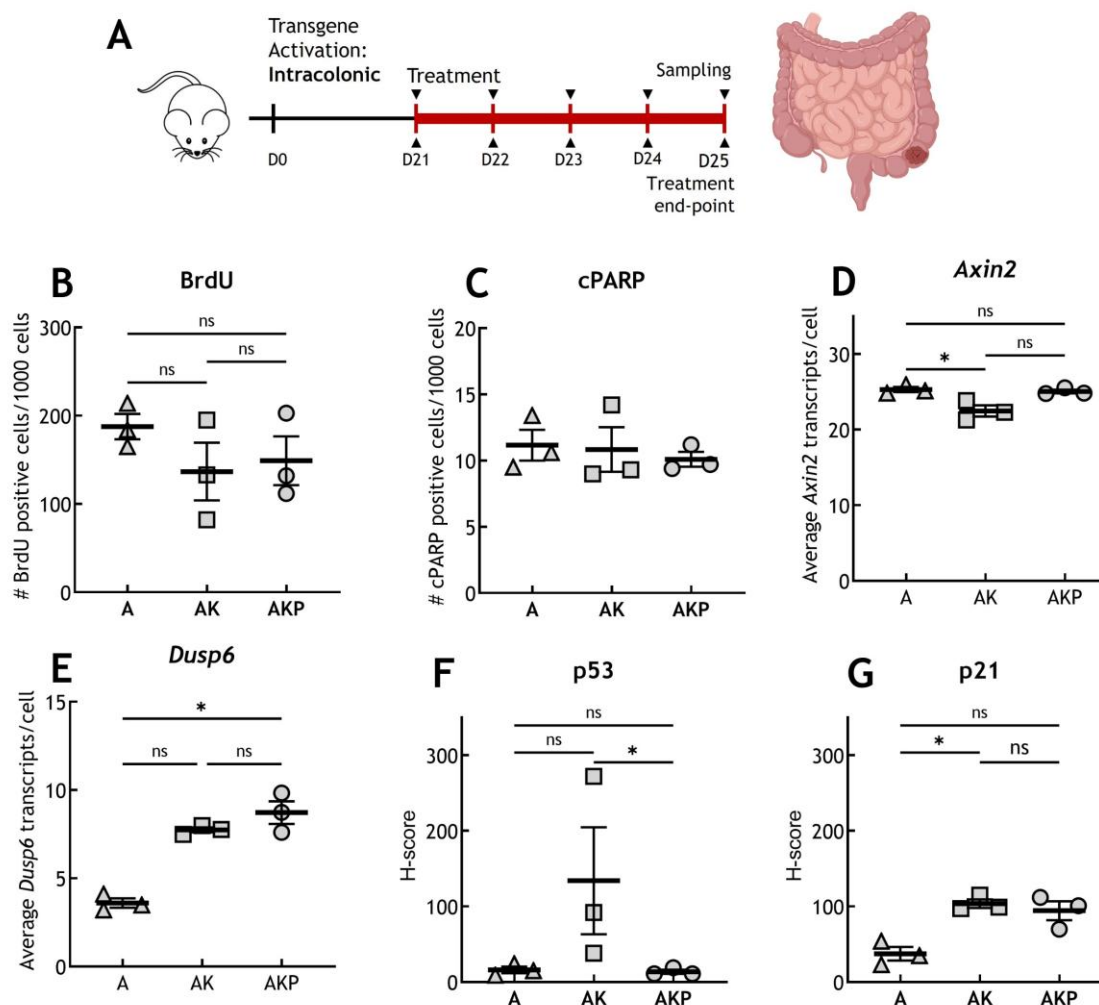


**Figure 3-11: Analysis of key signalling pathways in colon tumour model.**

A-, AK- and AKP- colon tumours (N=3) were generated by intracolonic induction of 4-hydroxy Tamoxifen in A-, AK- and AKP-HOM mice guided by colonoscopy. Post confirmation of tumour, mice were treated with Vehicle for 5 days (p.o. q.d) and BrdU (0.25ml, 10mM) was administered 2h before sampling. (A) Brightfield images of colon tumours. (B) Rate of proliferation assessed by counting number of BrdU positive cells/ 1000 dysplastic cells. (C) Cell death assessed by counting number of cPARP positive cells/ 1000 dysplastic cells. (D) Wnt status assessed by RNAscope analysis of Axin2. (E) MAPK status assessed by RNAscope analysis of Dusp6. (F-G) p53 status assessed immunohistochemical analysis of p53 and p21. One-way ANOVA Kruskal-Wallis test. Asterisks represent P values; ns P(>0.05), \* P(<0.05), \*\* P(<0.005), \*\*\* P(<0.001), and \*\*\*\* P(<0.0001).

**Homeostasis:** I studied homeostasis by assessing the rate of proliferation and cell death in the colon tumour models. To assess rate of proliferation and cell death, I assessed BrdU and cPARP of the intracolonic tumours by counting number of positive cells per 1000 dysplastic epithelial cells. Interestingly, Ras driven tumours (AK and AKP) had a non-significant reduction (<25%) in proliferation rate compared to its wildtype counterpart (A) (Figure 3-9, B). This reduction in proliferation might be attributed to oncogene-induced senescence that is reported by several groups in Ras driven tumours. Moreover, rate of cell death remained similar across the different tumours (Figure 3-9, C).

**Wnt, MAPK and P53 status:** I next assessed status of Wnt, MAPK and p53 pathway by studying Axin2 RNAscope (Wnt marker), Dusp6 RNAscope (MAPK marker), and p53 and p21 immunohistochemistry. Axin2 RNAscope analysis revealed Wnt status remained largely similar across the tumours (Figure 3-9, D), suggesting oncogenic Kras does not perturb the Wnt signalling pathway. As anticipated, the number of Dusp6 transcripts per cell almost doubled in tumours with oncogenic Kras<sup>G12D/wt</sup> suggesting activation of MAPK pathway (Figure 3-9, E).

To assess p53 activity, I looked for p53 and p21 staining pattern in the tumour. P53 has a very short half-life (<15 minutes) and is often undetectable in the absence of stress signals. Hence, I also studied tumour sections stained for p21 as it is directly regulated by p53. Loss of Apc alone was not sufficient to activate p53 and p21 as observed in A colon tumours, suggesting hyperactive Wnt signalling alone is not sufficient to induce p53 (Figure 3-9, F&G). However, in AK colon tumour, oncogenic Kras triggers p53 activity as seen by high levels of p53 as well as p21 in the dysplastic tumours (Figure 3-9, F&G). Interestingly, AKP colon tumours, without functional p53, had high p21 levels compared to tumours with loss of Apc alone, suggesting p21 is induced by mechanisms independent of p53. (Figure 3-9, F&G).

### 3.3 Intestinal organoids

The development of gut organoid cultures has significantly advanced our understanding of tissue dynamics by replicating many aspects of *in situ* tissue structures and functions (Sato et al., 2009). For our *in vitro* studies, organoids were generated from the small intestinal crypts of wildtype (wt),  $Kras^{G12D/wt}$  (K),  $Apc^{fl/fl}$  (A),  $Apc^{fl/fl} Kras^{G12D/wt}$  (AK), and  $Apc^{fl/fl} Kras^{G12D/wt} Trp53^{fl/fl}$  (AKP). These organoids were maintained in organoid culture media and routinely passaged as outlined in Section 2.3. The organoids derived from wt, K, and A models required additional supplementation with EGF and R-spondin to support growth.

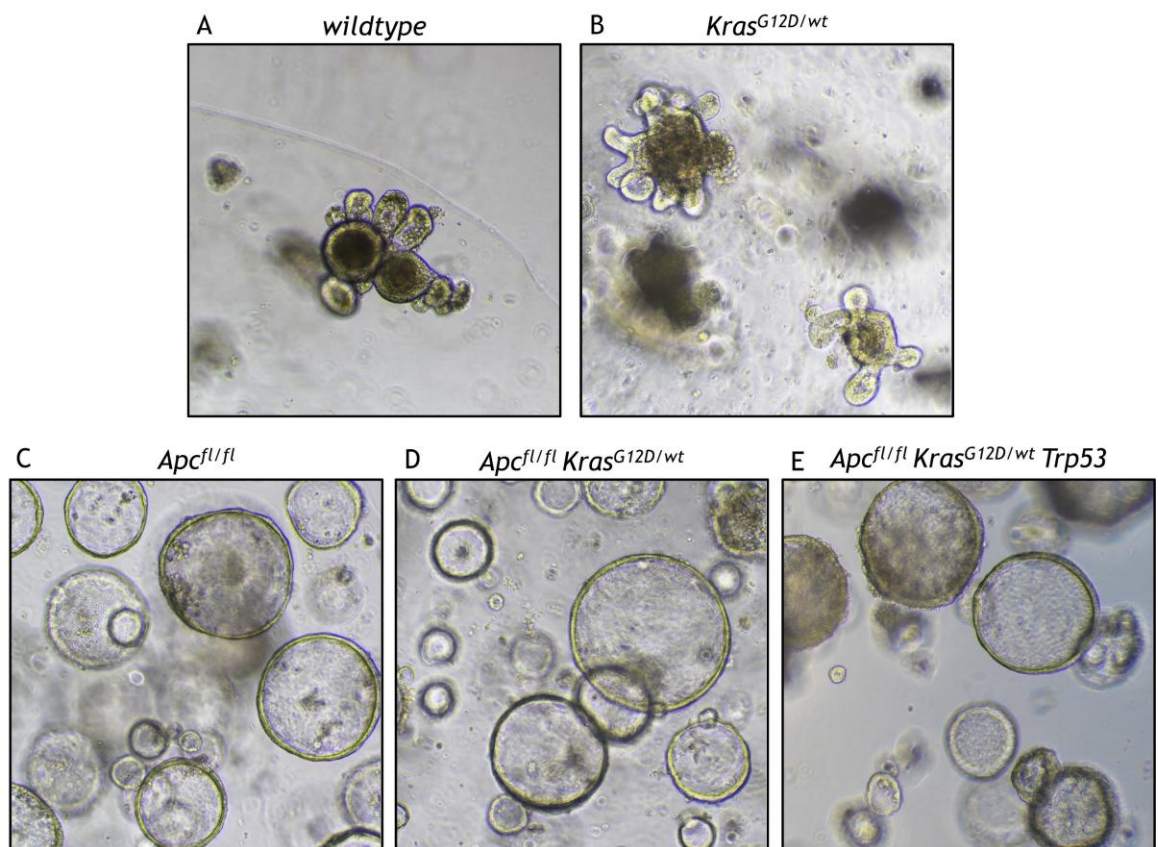


**Figure 3-12: Loss of *Apc* results in altered cellular organisation in organoids.**

Bright field images of small intestinal organoids derived from crypts of (A) wildtype, (B)  $Kras^{G12D/wt}$ , (C)  $Apc^{fl/fl}$ , (D)  $Apc^{fl/fl} Kras^{G12D/wt}$ , (E)  $Apc^{fl/fl} Kras^{G12D/wt} Trp53^{fl/fl}$  mice. Organoids were imaged 48 hours post seeding at 10x magnification. Wildtype and *Kras* organoids form highly branched morphology that mimics tissue organisation *in situ* whereas organoids with deficient *Apc* form cystic structures. Dark patches visible in the organoids are created by dying cells that were shed into the lumen of the cyst.

The structural organization and cellular hierarchy of the wildtype and  $Kras^{G12D/wt}$  organoids closely mimic that of the native intestinal epithelium. Within these organoids, stem cells and highly proliferative transit-amplifying cells are localized within crypt-like domains (Figure 3-10, A-B), closely resembling their *in vivo* counterparts as described by (Sato et al., 2009). Dying cells are typically observed in the central region of the organoid. Organoids exhibiting loss of *Apc* function display a distinctive non-budding stem cell morphology, highlighting significant alterations architecture (Figure 3-10, C-E).

### 3.2.4 Orthotopic Transplantation Model

I sought to utilise the orthotopic transplantation approach to develop an *in vivo* model of intestinal organoids where cultured intestinal organoids are grown in the native colon environment of wildtype (C57BL/6J) recipient mouse. For this, sex-matched intestinal organoids derived from the crypts of AKP-HOM mice were transplanted into the colonic sub-mucosa of wildtype guided by colonoscopy. Transplanted organoids engraft into the colonic submucosa and form glandular architecture reminiscent of colonic adenomas observed in the colon tumour model.

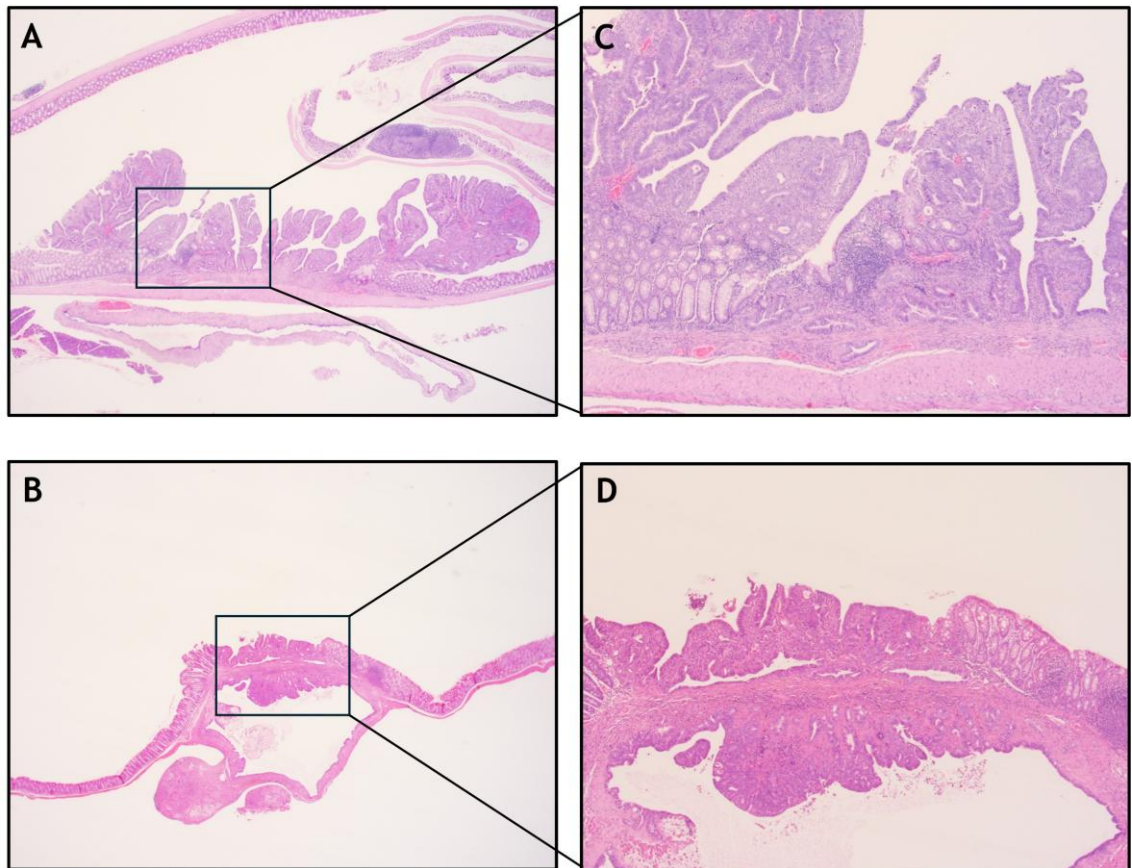


**Figure 3-13: Orthotopic transplantation of mouse derived intestinal organoids in the colon.** C57BL/6J mice were intracolonicly transplanted with AKP-HOM intestinal organoids. Post tumour establishment mice were treated with or Vehicle (0.5% HPMC + 0.1% Tween20, p.o, q.d) control for 5 days and sampled at treatment endpoint. Bright-field images of tumour stained with Haematoxylin & Eosin to study tumour architecture at (A &B) 4x magnification, (C&D) 20x magnification.

## 3.3 Discussion

Understanding the mechanisms underlying Ras-driven colon cancer is crucial for developing effective therapies, as these pathways play significant roles in tumour initiation and progression. In this chapter, I extensively characterized Ras-driven colon cancer models - specifically *Drosophila* and mouse models - to elucidate the key signalling pathways involved in human CRC.

The findings from this research highlight a conserved mechanistic link across species, evidenced by the hyperproliferation observed in both the hindgut of fruit flies and the intestinal crypts of mice following the activation of oncogenic Ras, alongside mutations in Apc and p53. The *Drosophila* hindgut serves as a genetically tractable model system for studying colon cancer development and progression, recapitulating essential features of human colorectal cancer (CRC). These include increased proliferation, disruption of tissue architecture, evasion of apoptosis and senescence, epithelial-mesenchymal transition (EMT), and dissemination to distant sites (Bangji et al., 2016).

In my experiments, oncogenic Ras signaling led to hyperproliferation in the Hindgut Proliferation Zone (HPZ) of larval hindguts. This disruption in hindgut homeostasis resulted in larval lethality unless the phenotype was resolved. I utilized this approach to perform rescue screens, demonstrating that trametinib strongly rescues single-mutant *byn<sup>ts</sup>>ras<sup>G12V</sup>* larvae but only modestly improves survival in the genetically complex patient-specific fly avatar (*byn<sup>ts</sup>>CPCT036*). This suggests that drug resistance is an emergent feature of genetically complex tumours, mirroring challenges faced in clinical settings.

Similar to the observations in *Drosophila* models, oncogenic Ras signaling accelerates hyperproliferation in intestinal crypts in mice. In my short-term models, the acute loss of Apc alone doubled the proliferation rate in the mouse intestinal crypts, while further activation of *Kras<sup>G12D/wt</sup>* resulted in a nearly 300% increase. However, contrary to my expectations, the additional loss of p53 resulted in significantly lower proliferation rates compared to its wild-type counterpart. This finding indicates complex interactions between these pathways and suggests that loss of p53 may have unanticipated regulatory effects on cell proliferation, possibly due to feedback mechanisms that warrant further investigation. Our short-term models are good for studying the effects of acute activation of Wnt signalling in the background of oncogenic Ras signalling with or without functional p53. (Sansom et al., 2004) showed that acute activation of Wnt produces many of the phenotypes associated with early colorectal lesions: failure to differentiate and increased proliferation. Overall, this serves as a good model for pre-adenoma stage, and I will be exploring this model further in Chapter 4 to understand MAPK dependency. I have also utilised intestinal organoids generated from this model for *in vitro* studies, which is discussed in (Section 4.2).

In mice that develop tumours throughout the intestine, as observed in our long-term model, loss of Apc predisposes tumour formation predominantly in the small intestine, with occasional colonic polyps. These mice typically develop fewer than 20 tumours and

exhibit longer median survival (178 days post-induction, A-HET). The activation of  $Kras^{G12D/wt}$  significantly reduces survival by approximately 60% (median survival of 74.5 days post-induction, AK-HET) due to an increased tumour burden, primarily in the colon, while small intestinal tumours remain consistent. Notably, the further loss of p53 shifts the balance towards the formation of more small intestinal tumours (median survival of 44 days post-induction, AKP-HET). However, the shorter duration of these tumours does not allow them to develop into invasive adenocarcinomas.

A key limitation of our long-term models is the development of multiple tumours throughout the intestine, a phenomenon that is less common in human CRC. Since loss of heterozygosity of the  $Apc^{fl}$  allele is required for tumour initiation, these tumours arise at different time points following transgene induction, complicating the correlation between tumour burden and clinical outcomes.

To overcome this limitation, I investigated intracolonic induced tumours, representing a more refined colon tumour model. In contrast to our short-term models, which depict the pre-adenoma stage, proliferation rates remained similar across A-, AK-, and AKP colon tumours. This suggests distinct tumour dynamics during the pre-adenoma versus early adenoma stages. Histologically, these colon tumours exhibited highly differentiated architecture and represented low-grade adenomas, aligning closely with human adenomatous lesions.

In the next chapter, I will further investigate the MAPK dependency of these tumours using trametinib, aiming to elucidate therapeutic strategies that may enhance treatment efficacy in Ras-driven colon cancer.

## Chapter 4

# Targeting the MAPK pathway in our CRC models

The MAPK pathway plays a critical role in colorectal cancer (CRC) by regulating cell growth and survival, often activated by KRAS mutations. Trametinib, a selective MEK1/2 inhibitor, offers advantages over other MEK inhibitors by minimizing off-target effects and providing a favorable pharmacokinetic profile. While clinical trials have shown mixed results for trametinib in CRC, ongoing studies are exploring its efficacy in combination therapies. My models facilitate the investigation of MAPK dependency in KRAS mutant CRC at various tumour stages, enhancing our understanding of tumour dynamics.

## 4.1 Investigation of MAPK dependency in Drosophila model of CRC

### 4.1.1 Response of patient-specific fly avatar to targeted therapies

Having observed a modest yet favourable response of patient-specific fly avatar (*byn<sup>ts</sup>>CPCT036*) to trametinib (MEK inhibitor) (Chapter 3.1.2), I investigated if treatment with other Ras pathway inhibitors and other poly-pharmacological drugs which have known significance downstream of RAS signalling pathway, would elicit a similar, if not better response than trametinib. Most of these drugs were candidate hits during a largescale screening for the fly-to-bedside clinical trial (Bangi et al., 2016, Bangi et al., 2019). Dabrafenib, a selective BRAF inhibitor, targets MAPK signalling pathway. Several studies have suggested that combined inhibition of BRAF and MEK leads to improved suppression of MAPK signalling. Regorafenib is a multi-kinase inhibitor that targets and inhibits receptor tyrosine kinases (RTKs) in the Ras/Raf/MEK/ERK pathway, which participates in the signalling of oncogenesis, angiogenesis, and cancer proliferation and metastasis. Pyrvinium, a recognized inhibitor of  $\beta$ -catenin in Wnt signalling pathway was a consistent candidate hit in the fly-to-bedside clinical trial (Bangi et al., 2019). Several reports have suggested simultaneous down-regulation of both  $\beta$ -catenin and KRAS to induce significant cell death and tumour growth inhibition. Oncogenic RAS signalling is known to affect cell metabolism, stress resistance and signalling in colon tumours (Najumudeen et al., 2021). LY294002 is a PI3K inhibitor that increases drug accumulation and initiates apoptosis by activation of caspases 9 and 3 in RAS activated colorectal tumours.

Seeking to uncover if treatment with other RAS pathway inhibitors and poly-pharmacological drugs would improve survival outcomes in genetically complex fly avatar,

**CPCT036 genotype:** *UAS-ras<sup>G12V</sup> apc<sup>Ri</sup> p53<sup>Ri</sup> chico<sup>Ri</sup> ago<sup>Ri</sup> smox<sup>Ri</sup> eva<sup>Ri</sup> sdhA<sup>Ri</sup> rassf<sup>Ri</sup> efa6<sup>Ri</sup>*

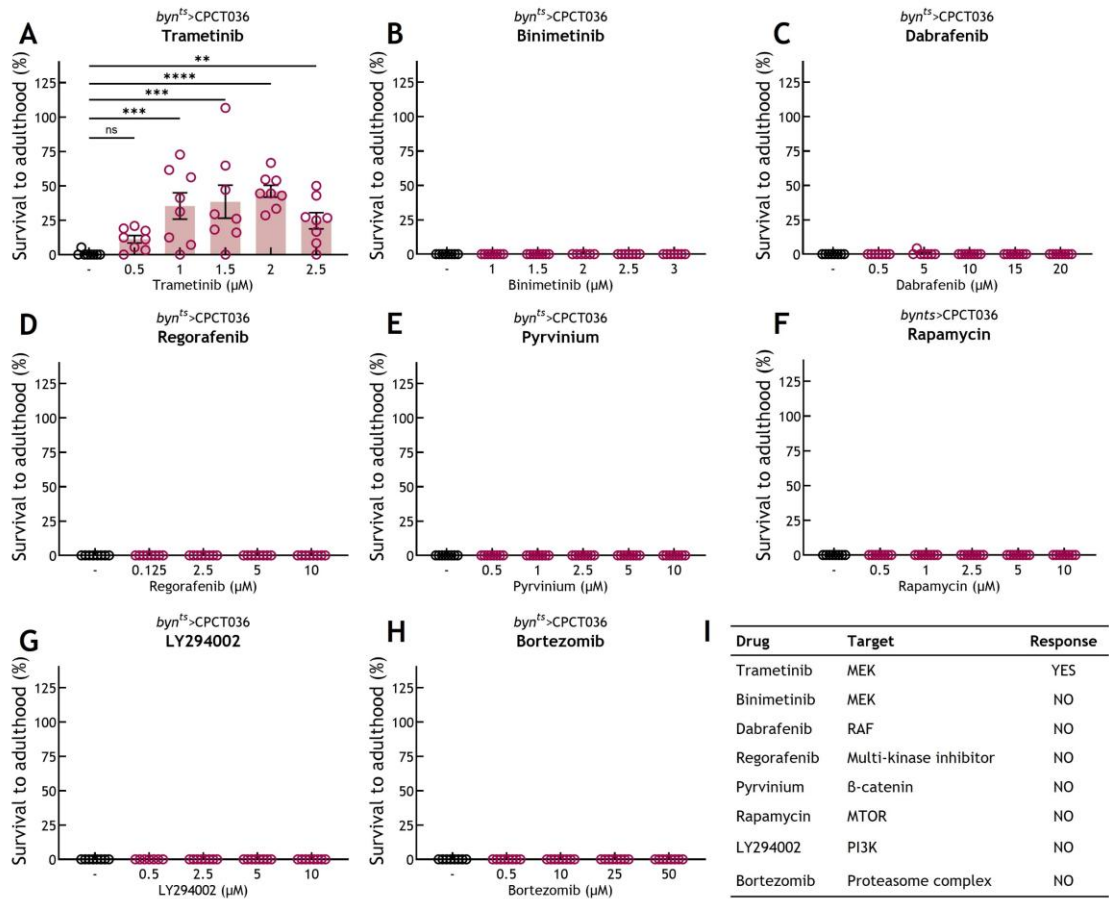


**Figure 4-1: Genetically complex *Drosophila* avatar is resistant towards most targeted therapies.**

Rescue-from-lethality assay demonstrates a significant survival benefit in *byn<sup>ts</sup>>CPCT036* larvae treated with (A) Trametinib. No other drug offers survival benefit in these larvae (B) Binimetinib, (C) Dabrafenib, (D) Regorafenib, (E) Pyrvinium, (F) Rapamycin, (G) LY294002, (H) Bortezomib. One-way ANOVA, Kruskal-Wallis test. Asterisks represent *P* values; ns *P*(>0.05), \* *P*(<0.05), \*\* *P*(<0.005), \*\*\* *P*(<0.001), and \*\*\*\*

I performed rescue-from-lethality assay on *byn<sup>ts</sup>>CPCOT36* larvae. Intriguingly, only larvae treated with trametinib showed significant dose-dependent rescue (Figure 4-1, A). No notable rescue was observed in flies treated with Regorafenib, Pyrvinium, Rapamycin, Bortezomib, LY294002, Dabrafenib and Simvastatin (Figure 4-1, B-H).

## 4.1.2 Screening of genetically complex *Drosophila* models on trametinib

Following the response of patient-specific fly avatars to combination of trametinib as a single agent and in combination with zoledronate (Figure 3-2, E), I studied if other fly avatars have a similar response. I utilised fly avatars developed based on the mutational profile from the TCGA database. I picked fly avatars that share mutations in *Apc*, *Kras* and *p53* among other passenger mutations. Rescue-from-lethality survival assay revealed varied response among these models to trametinib as a single agent or in combination with zoledronate. For instance, RAP-P1-M3B responded better to trametinib as a single

agent compared to combination with zoledronate (66 vs 42% survival,  $p < 0.005$ ) (Figure 4-2, A). Whereas, RAP-P2-M1B responded better to combination therapy compared to trametinib as a single agent (48 vs 19% survival,  $p < 0.005$ ) (Figure 4-2, B). This variation in drug response might be due to additional passenger mutations that warrant further investigation.

Table 4-2: Genotype of patient specific fly avatars and its human ortholog

Fly Line	Genotype	Human Ortholog
RAP-P1-M3B	UAS - <i>ras</i> <sup>G12V</sup> <i>apc</i> <sup>Ri</sup> <i>p53</i> <sup>Ri</sup> <i>ago</i> <sup>Ri</sup> <i>wts</i> <sup>Ri</sup> <i>CG7742</i> <sup>Ri</sup> <i>atg2</i> <sup>Ri</sup>	KRAS <sup>G12V</sup> , APC, P53, FBXW7, LATS1, TBC1D19, ATG2B/2A
RAP-P2-M1B	UAS - <i>ras</i> <sup>G12V</sup> <i>apc</i> <sup>Ri</sup> <i>p53</i> <sup>Ri</sup> <i>vrp1</i> <sup>Ri</sup> <i>ry</i> <sup>Ri</sup> <i>khc-73</i> <sup>Ri</sup>	KRAS <sup>G12V</sup> , APC, P53, WIPF1, XDH, KIF13A
RAP-P5-M4A	UAS - <i>ras</i> <sup>G12V</sup> <i>apc</i> <sup>Ri</sup> <i>p53</i> <sup>Ri</sup> <i>amy-p</i> <sup>Ri</sup> <i>bt</i> <sup>Ri</sup> <i>ppk26</i> <sup>Ri</sup>	KRAS <sup>G12V</sup> , APC, P53, AMY2B, TTN, ASIC1
RAP-P7-M2B	UAS - <i>ras</i> <sup>G12V</sup> <i>apc</i> <sup>Ri</sup> <i>p53</i> <sup>Ri</sup> <i>kn</i> <sup>Ri</sup> <i>CG12730</i> <sup>Ri</sup> <i>CG4733</i> <sup>Ri</sup>	KRAS <sup>G12V</sup> , APC, P53, EBF3, CMTM4, PPP2R3B
RAP-P13-M1A	UAS - <i>ras</i> <sup>G12V</sup> <i>apc</i> <sup>Ri</sup> <i>p53</i> <sup>Ri</sup> <i>tefu</i> <sup>Ri</sup> <i>CG31223</i> <sup>Ri</sup> <i>ida</i> <sup>Ri</sup>	KRAS <sup>G12V</sup> , APC, P53, ATM, ZNHIT2, ANAPC5
RAP-P19-M1A	UAS - <i>ras</i> <sup>G12V</sup> <i>apc</i> <sup>Ri</sup> <i>p53</i> <sup>Ri</sup> <i>pten</i> <sup>Ri</sup> <i>tet</i> <sup>Ri</sup> <i>mor</i> <sup>Ri</sup>	KRAS <sup>G12V</sup> , APC, P53, PTEN, TET1, SMARCC2

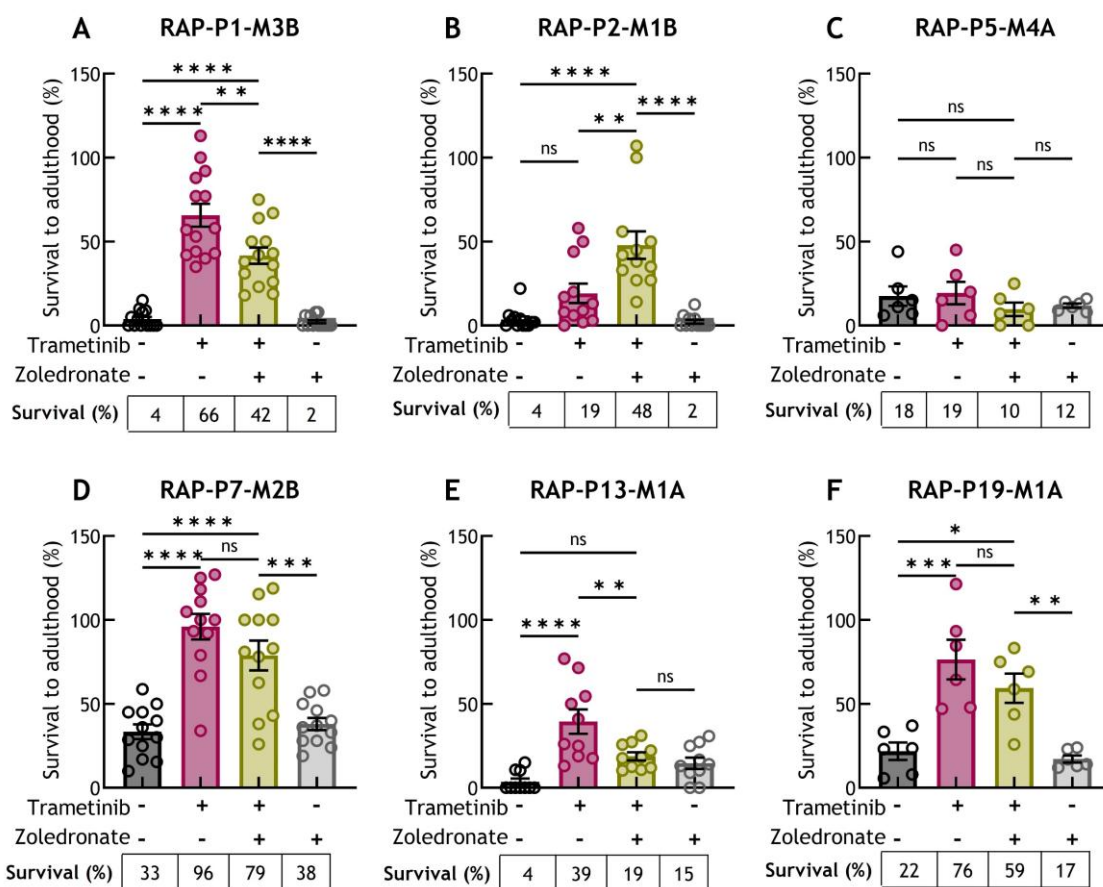


**Figure 4-2: Passenger mutations impact response to trametinib.**

Patient-specific fly avatars designed using the TCGA database that have additional mutations apart from Ras-Apc-p53 show varied response to Trametinib as a single agent and in combination with Zoledronate. Larval eclosion data of (A) *byn*<sup>ts</sup>>RAP-P1-M3B, (B) *byn*<sup>ts</sup>> RAP-P2-M1B, (C) *byn*<sup>ts</sup>> RAP-P5-M4A, (D) *byn*<sup>ts</sup>>RAP-P7-M2B, (E) *byn*<sup>ts</sup>>RAP-P13-M1A, (F) *byn*<sup>ts</sup>>RAP-P19-M1A. One-way ANOVA, Kruskal-Wallis test. Asterisks represent *P* values; ns ( $P > 0.05$ ), \* ( $P < 0.05$ ), \*\* ( $P < 0.005$ ), \*\*\* ( $P < 0.001$ ), and \*\*\*\* ( $P < 0.0001$ ).

## 4.2 Investigating MAPK dependency in mouse intestinal organoids

In Chapter 3.1.2.1, I showed that oncogenic KRAS contributes to a rapid hyperproliferative phenotype in mouse intestinal crypts of AK-HOM and AKP-HOM mice (Short-term model). I studied MAPK dependency of intestinal organoids derived from the small intestinal crypts of AK- and AKP-HOM mice.

### 4.2.1 Determination of IC50 value

I generated dose-response curves for wildtype,  $KRAS^{G12D/wt}$ , AK- and AKP-HOM organoids against trametinib. Organoids were seeded as fragments in Matrigel into a 96-well plate and allowed to grow with organoid culture media supplemented with Noggin and N2-B27. Wild-type and  $Kras^{G12D/wt}$  organoids were additionally supplemented with EGF and R-spondin. 48h post-seeding, organoids were treated with various concentrations of trametinib (10nM to 10 $\mu$ M). 0.1% DMSO treated organoids served as vehicle control and Staurosporin (0.25 $\mu$ M) treated organoids were taken as positive control for cell death. Proliferation rate and organoid forming efficacy was monitored 72h post drug treatment using CellTiter-Blue Cell viability assay (Promega, G8080).

Much like what has been reported in fly CRC models (Bangji et al., 2016), presence of additional mutations made Ras-driven organoids less sensitive to trametinib. Overall, AK- and AKP-HOM organoids were less sensitive to trametinib compared to  $Kras^{G12D/+}$  and wildtype organoids with an IC50 value of 6.4nM and 14.3nM respectively. This

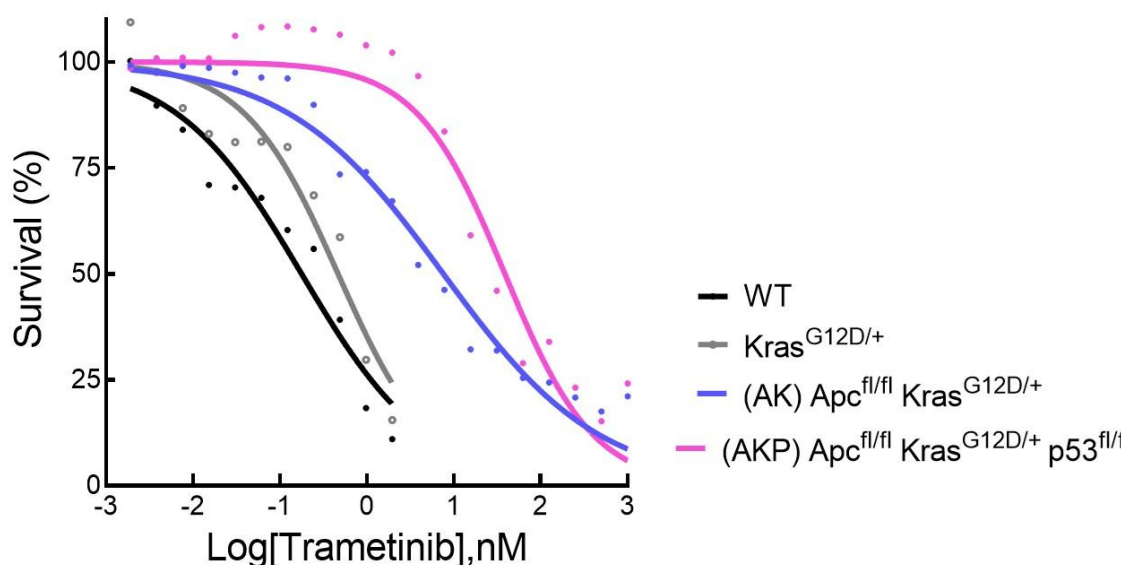


Figure 4-3: Genetic complexity impacts response to MEK inhibition in intestinal organoids. Small intestinal organoids (wildtype, Villin<sup>CreERT2</sup>;  $Kras^{G12D/wt}$ , Villin<sup>CreERT2</sup>;  $Apc^{fl/fl} Kras^{G12D/wt}$  or Villin<sup>CreERT2</sup>;  $Apc^{fl/fl} Kras^{G12D/wt} p53^{fl/fl}$  crypts) were seeded in 96-well plates and viability was determined using CellTiter Blue Assay. Dose-response curves (IC50) of RAS-driven small intestinal organoids treated with trametinib reveals drug resistance in genetically complex organoids.

corroborates our earlier findings that drug sensitivity decreases with increasing mutational burden. Much like the *Kras*<sup>G12D/+</sup>, WT organoids had an IC50 value of 0.2nM (Figure 4-3). Whether the reduced drug efficacy is due to impaired apoptotic pathway (p53 loss) or aberrant Wnt signalling pathway (Apc loss), remains to be elucidated.

#### 4.2.2 Qualitative analysis of key signalling pathways

I investigated the status of MAPK and apoptosis pathways to check if additional mutations impair response to MEK inhibition. AK- and AKP-HOM organoids were treated with trametinib or 0.1% DMSO for 6- and 18-hours and sampled for western blot analysis. Cisplatin treated organoids served as positive control for the apoptosis pathway.

##### Trametinib treatment leads to suppression of MAPK pathway

Trametinib treatment led to accumulation of phospho-MEK in both AK- and AKP-HOM organoids at 6h and 18h. In line with that, phospho-ERK levels remain suppressed in both AK- and AKP-HOM organoids at 6h. Intriguingly, phospho-ERK levels return to baseline

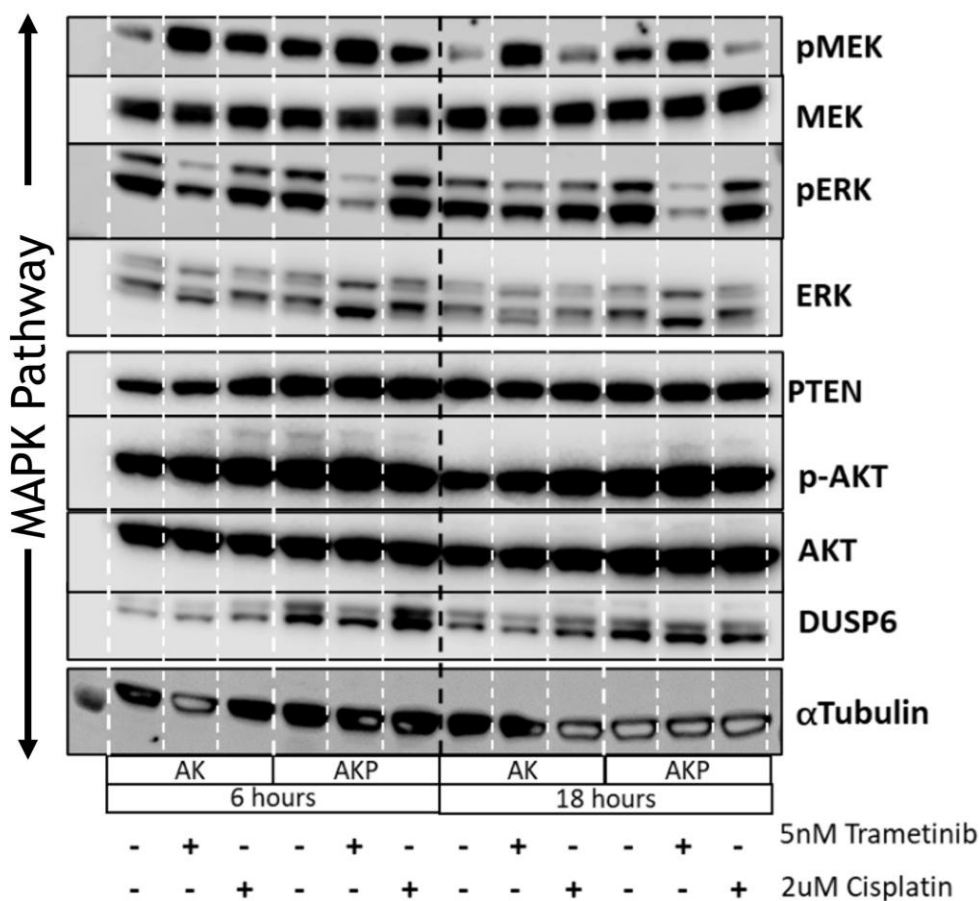


**Figure 4-4: Trametinib suppresses MAPK activity in *Kras* driven intestinal organoids**

AK- and AKP-HOM organoids were treated with Trametinib or cisplatin for 6h or 18h. Protein was then extracted and analysed by western blotting for key proteins involved in the RAS pathway. \*cisplatin treated organoids were taken as a positive control to check for proteins involved in p53-dependent apoptosis pathway.

levels in AK-HOM line at 18h, while remaining suppressed in the AKP-HOM organoids.

Higher levels of phospho-ERK were observed in AKP-HOM compared to AK-HOM (Figure 4-4). Suppression of RAS/RAF/ERK pathway is also corroborated by levels of Dual specificity phosphatase 6 (Dusp6), which is a feedback regulator activated by phospho-ERK. Dusp6 levels were higher in AKP-HOM compared to AK-HOM, suggesting increased activation of RAS pathway under loss of p54. Activated Kras can also lead to phosphorylation of AKT (phospho-AKT), through the PI3K pathway. AKP-HOM organoids had higher phospho-AKT levels compared to AK-HOM organoids. Moreover, trametinib treatment resulted in a slight increase in levels of phospho-AKT, suggesting that suppression of RAS/RAF/ERK pathway led to acute compensatory activation of RAS/PI3K/AKT pathway (Figure 4-4).

We surmised that loss of p53 might have a varied impact on drug response, given the impaired apoptotic pathway. We also observed a p53-dependent activation of apoptotic machinery with increase in the protein levels of p21, cleaved PARP and PUMA in AK-HOM and a lack thereof in AKP-HOM. The levels of cleaved caspase-3 were significantly higher in AK lines at 6h and 18h post trametinib treatment, while there was only a mild increase in AKP line at 18h. Our data suggests that inhibition of the MAPK pathway causes apoptosis in a p53-dependent manner.

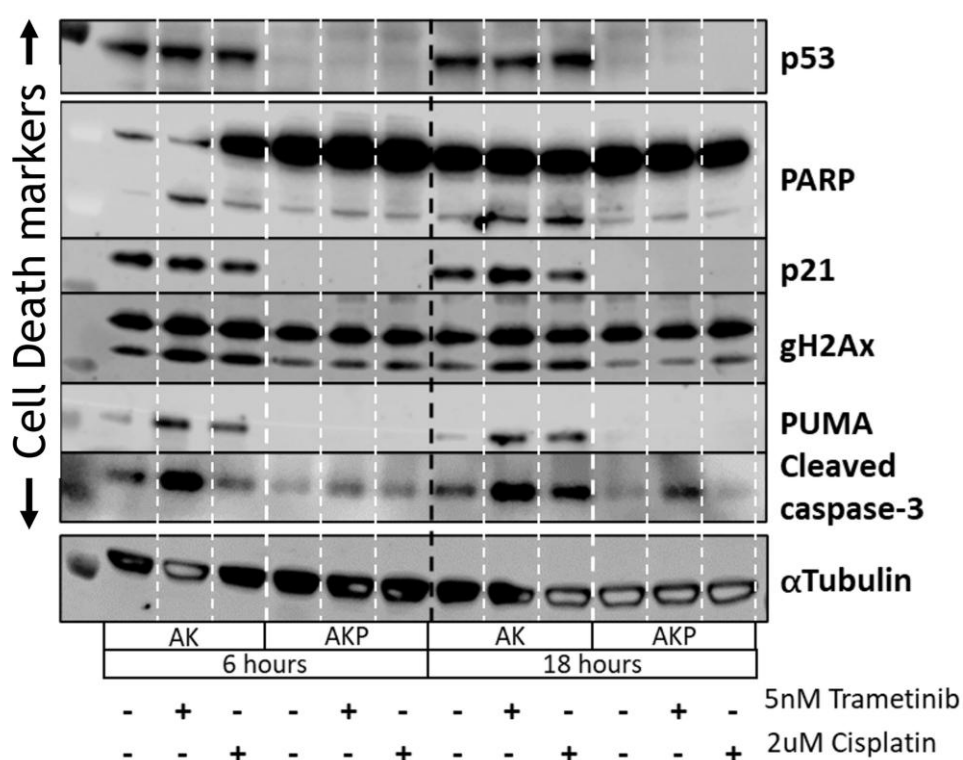


**Figure 4-5: Trametinib suppresses MAPK activity and induces cell death.**

AK- and AKP-HOM organoids were treated with Trametinib or cisplatin for 6h or 18h. Protein was then extracted and analysed by western blotting for key proteins involved in the apoptosis pathway. Intestinal organoids with loss of p53 have reduced cell death activity compared to its wildtype p53 counterpart. \*cisplatin treated organoids were taken as a positive control to check for proteins involved in p53-dependent apoptosis pathway.

### 4.2.3 Cell cycle analysis of Ras-driven small intestinal organoids

Our studies so far show that MAPK suppression upon trametinib treatment is quite effective in both AK and AKP *in vitro* and *in vivo* models. However, the apoptosis pathway is dysregulated in the AKP model due to loss of p53. I utilised AKPT intestinal organoids derived from the crypts of Villin<sup>CreERT2</sup>; Apc<sup>fl/fl</sup> Kras<sup>G12D/wt</sup> Trp53<sup>fl/fl</sup> Tgfbr2<sup>fl/fl</sup> to understand cell cycle dynamics under p53 loss.

Understanding the cell cycle dynamics of AKP organoids upon MEKi, could give a clue about therapy response in these cells. I performed cell-cycle analysis using FACS. Briefly, AK, AKP, and AKPT organoids were seeded as fragments in matrigel domes in 6-well plates. They were treated with or without 5nM trametinib for a period of 72hours. Post-treatment, matrigel domes were dissociated to harvest organoids. Organoids were treated with TrypLE for 7 mins at 37°C in a water bath to dissociate them into single cells. Single cell suspension was passed through a 40µM cell strainer to remove clumps. Cells were fixed with 70% ice-cold ethanol drop-wise whilst vortexing to avoid clumping. Cells were washed thrice using ice-cold PBS at 850g for 5 minutes at 4°C to remove residual ethanol. Cells were then resuspended in 500ul FxCycle PI/RNase (Thermo Fisher Scientific, F10797). Cell cycle analysis was performed on the Attune using YL1 to detect PI.

There were no significant differences in the cell cycle dynamics across AK, AKP and AKPT at baseline following Vehicle treatment. For instance, the average percentage of cells across all genotypes were 43.7% ± 1.6% in G0/G1, 25.3% ± 2.7% in G2/M, 28.4% ± 2.9% in S and 2.7% ± 1.1% in sub-G0. Similarly, percentage of cells in G2/M phase did not differ significantly across genotypes and between treatments (Figure 4-6). Upon trametinib treatment, the percentage of cells in S phase contracted by more than 50% in AKP and AKPT organoids, compared to less than 30% in AK organoids. Thus, demonstrating the anti-proliferative effects of MEK inhibition. We also observed accumulation of cells in G0/G1 stage in both AKP and AKPT organoids. In contrast, AK cells had accumulated in sub-G0 (Figure 4-6). This observation reiterates our early observations that p53 impacts the ability of cells to undergo apoptosis. These cells, we believe, are primarily arrested in G1 phase of the cell cycle. It would be interesting to see if these undergo quiescence or senescence. As both these phenotypes have been implicated in development of drug resistance mechanisms. To understand what happens to AKP cells after G1 arrest, we sought to look for markers of quiescence. Studies from other labs have demonstrated that cyclin-dependent kinase (CDK) inhibitor, p27 inhibits CDK1, 2, 4 and 6 via interaction with cyclin-CDK complex and inhibits cell cycle progression at the G0-G1 and G1-S transitions. Its expression is strictly regulated by atleast two kinds of ubiquitin ligases; KPC promotes

proteolysis of p27 at G0-G1 transition and SCF<sup>Skp2</sup> promotes its proteolysis at the S/G2/M phase.

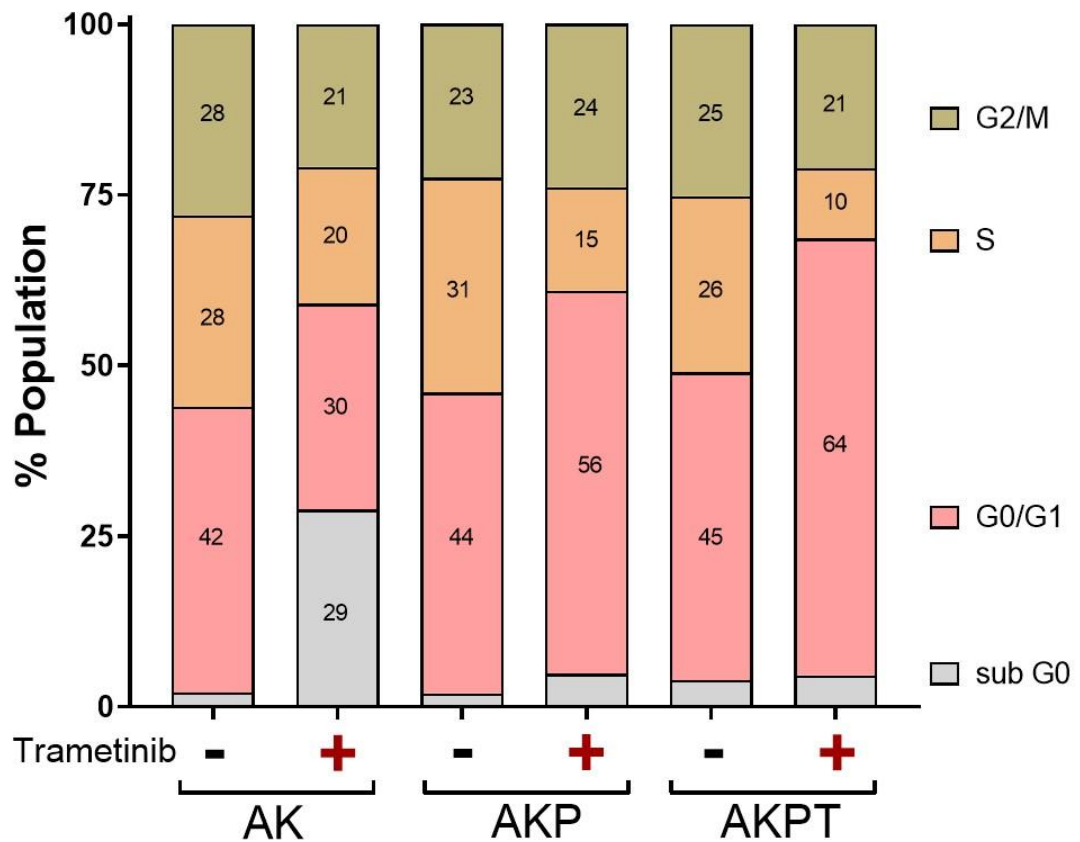


**Figure 4-6: Organoids with loss of p53 arrest at G0/G1 upon MEK inhibition with trametinib.**

AK-, AKP-, and AKPT- intestinal organoids were treated with trametinib or vehicle control (DMSO) for 72h before dissociating into single-cells for cell-cycle analysis using FACS. At least 10000 cells were analysed for each condition and percentage of cells in each phase - subG0 (grey), G0/G1 (pink), S (yellow), and G2/M (green) was calculated relative to total number of cells. Organoids with functional p53 (AK) underwent apoptosis upon trametinib treatment, whereas organoids with loss of p53 predominantly arrested at G0/G1.

## 4.3 Investigating MAPK dependency in mouse models of CRC

### 4.3.1 Targeting MAPK in Kras driven hyperproliferation model

As described in the section earlier, our short-term models are useful to check acute effects of drug treatment. Transgene induction by administration of Tamoxifen (80mg/kg, i.p.) leads to homozygous loss of Apc and activation of oncogenic Kras<sup>G12D/wt</sup> in case of AK-HOM mice. Combined loss of Apc and oncogenic activation of Kras<sup>G12D/+</sup> (AK-HOM) leads to hyperproliferation of epithelial cells along the crypt-villus axis.

While a wildtype crypt has around 20 BrdU positive cells/half crypt on average, it was noted that AK-HOM mice had an average of 60 BrdU positive cells/half crypt in the

proximal small intestine and 17 BrdU positive cells / half crypt in the mid-colon. Upon MEK inhibition with trametinib at 1mg/kg (p.o, q.d) for 3 days post tamoxifen induction, significant reduction in crypt cell proliferation was observed. Proximal region of small intestine had about 41 BrdU positive cells/half crypt and 11 BrdU positive cells/ half crypt in the colon. I also analysed if the increase in proliferation burden would also trigger cell death and scored dying cells with cleaved-PARP staining in small intestine and colon (Figure 4-7, B).

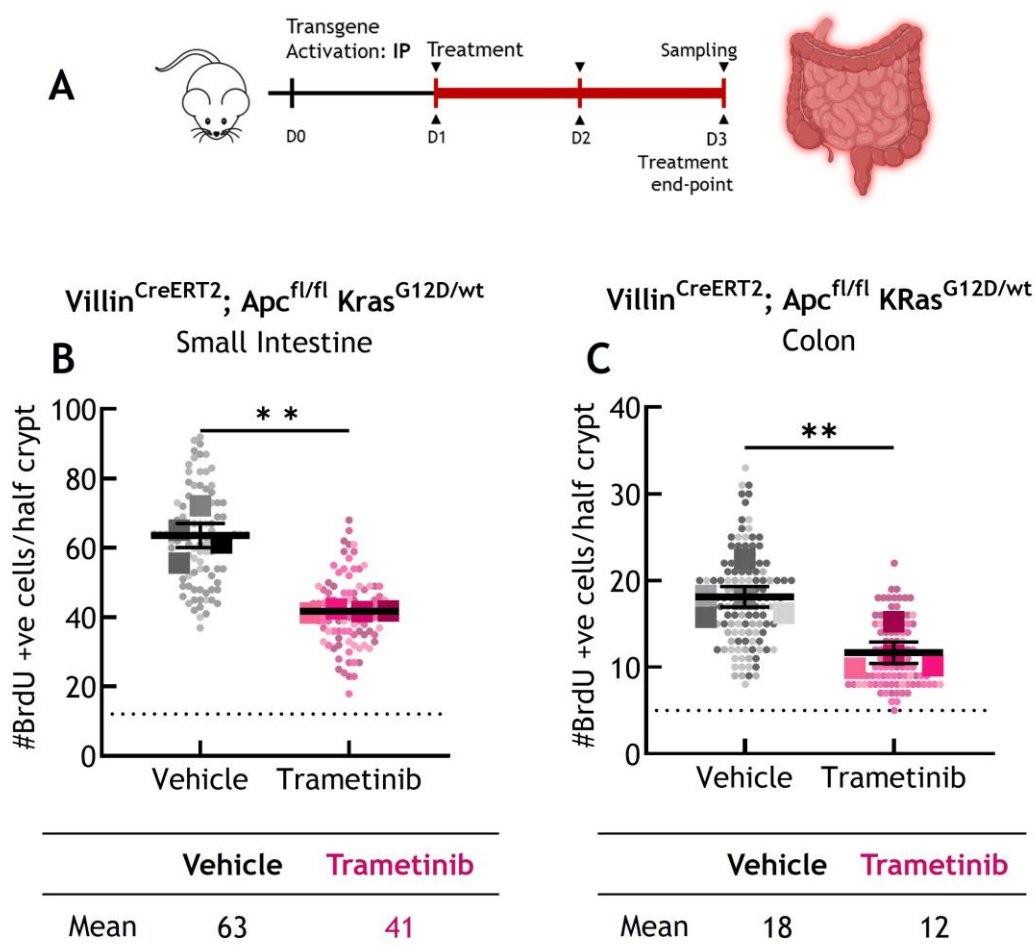


**Figure 4-7: Trametinib suppresses proliferation of hyperproliferative small intestinal and colon crypts of AK-HOM mice.**

AK-HOM mice were administered with Tamoxifen (80mg/kg, i.p) on Day 0 and treated with either Vehicle or Trametinib (1mg/kg) once daily by oral gavage from Day 1 -3. BrdU was administered 2h before sampling. (A) Illustration of study plan. To assess proliferative potential, number of BrdU positive cells per half crypt (n =25) were quantified from the proximal SI and mid colon. (B) BrdU score in small intestine. (C) BrdU score in colon. Dotted lines are mean BrdU positive cells per half crypt in wildtype crypt. Small dots represent single half-crypts, large dots are means of biological replicates. Small dots represent single half-crypts, large dots are means of biological replicates. Mann-Whitney test. Asterisks represent P values; ns P(>0.05), \* P(<0.05), \*\* P(<0.005), \*\*\* P(<0.001), and \*\*\*\* P(<0.0001).

I hypothesised that additional loss of p53 would lead to more rapid hyperproliferation and exacerbate the phenotype so far observed with the combination of Apc and Kras. Similar to the AK-HOM mice, transgene induction in AKP-HOM mice was done by Tamoxifen injection at 80mg/kg on Day0. Mice were treated with trametinib (1mg/kg, p.o, q.d) or

Vehicle (0.5% HPMC + 0.1% Tween, p.o, q.d) for 3 days. BrdU (0.25ml, 10mM) was administered 2 hours before sampling (Figure 4-8, A).

As described in the earlier section, Vehicle treated mice had an average of 46 BrdU positive cells/half crypt. Upon treatment with trametinib, the rate of proliferation reduced to 33 BrdU positive cells/half crypt. Although this difference was not significant, it must be noted that the BrdU proliferation rate in AKP-HOM mice were already at a lower rate to begin with in comparison to BrdU proliferation rate of AK-HOM mice treated with Vehicle (Figure 4-8, B).

Trametinib significantly suppresses proliferation in both AK- and AKP-HOM hyperproliferation CRC model. It must be noted that this model does not represent a CRC tumour. Due to a shorter latency, these mice need to be culled within a maximum of 3 days post transgene induction. However, it is a good model to study acute effects of

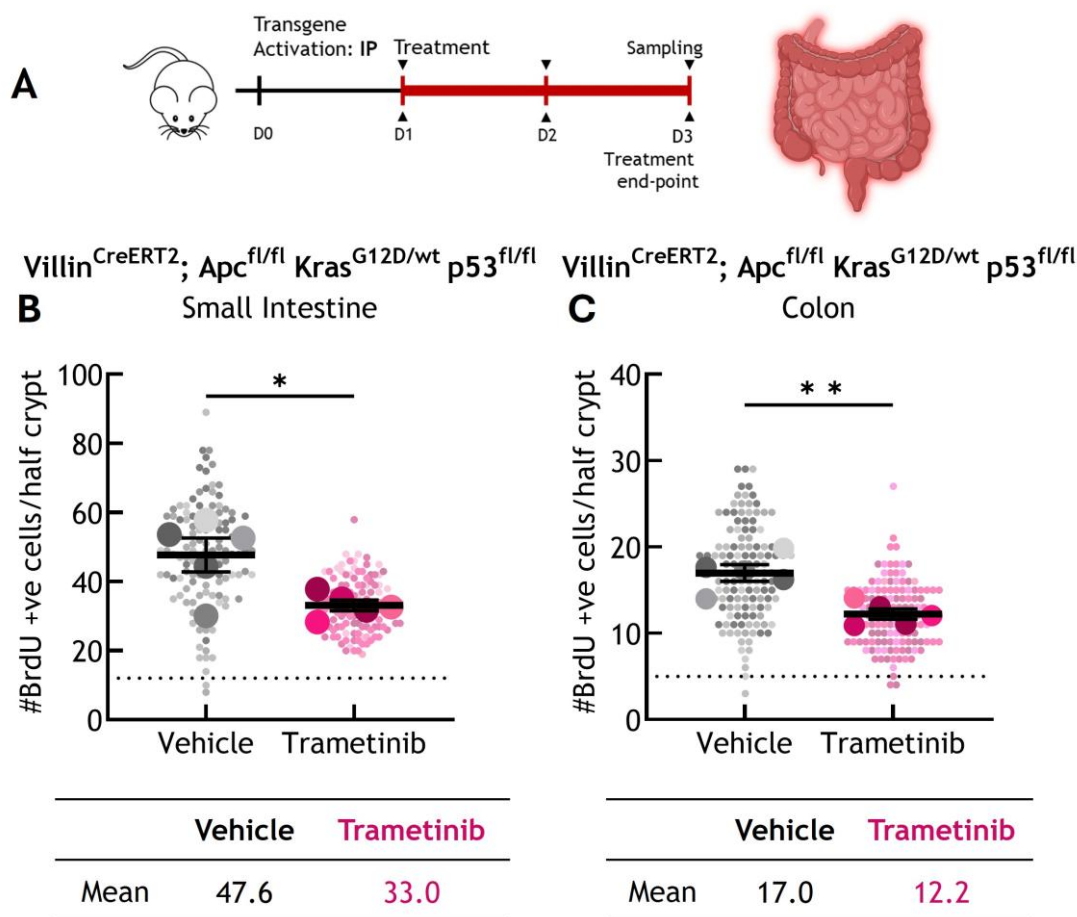


**Figure 4-8: Trametinib suppresses proliferation of hyperproliferative small intestinal and colon crypts of AKP-HOM mice.**

AKP-HOM mice were administered with Tamoxifen (80mg/kg, i.p) on Day 0 and treated with either Vehicle or trametinib (1mg/kg) once daily by oral gavage from Day 1 -3. BrdU was administered 2h before sampling. (A) Illustration of study plan. To assess proliferative potential, number of BrdU positive cells per half crypt (n =25) were quantified from the proximal SI and mid colon. (B) BrdU score in small intestine. (C) BrdU score in colon. Dotted lines are mean BrdU positive cells per half crypt in wildtype crypt. Small dots represent single half-crypts, large dots are means of biological replicates. Small dots represent single half-crypts, large dots are means of biological replicates. Mann-Whitney test. Asterisks represent P values; ns P(>0.05), \* P(<0.05), \*\* P(<0.005), \*\*\* P(<0.001), and \*\*\*\* P(<0.0001).

transgene activation on gut physiology and study the effect of intervention. In my study, trametinib was able to suppress proliferation in both AK- and AKP-HOM mice, both in the small intestine and colon. It further warrants studying the effect of trametinib in a tumour model.

### 4.3.2 Targeting the RAS pathway in Kras driven intestinal tumour model

To understand long-term effects of trametinib in our model, we used the long-term model described in section 3.2.2. Tamoxifen administration leads to heterozygous loss of Apc in AK-HET and AKP-HET mice. While this is not enough to cause tumour initiation, subsequent loss of heterozygosity leads to tumour initiation. Treatment begins 21 days post-tamoxifen induction. Mice are allocated into the following treatment groups: trametinib 0.8mg/kg (T<sub>s</sub>) or vehicle dosed once daily by oral gavage. Mice were treated until they developed clinical signs of end point - weight loss, hunching and anaemia. BrdU (0.25ml, 10mM) was administered 2h before sampling. Tumour scoring was performed by pathological assessment of H&E-stained sections.

#### 4.3.2.1 Response to MEK inhibition in Kras driven intestinal tumour model with functional p53

AK-HET mice have a baseline median survival of 74.5 days post induction (n=10) (Figure 4-9, B). Oncogenic activation of Kras leads to tumour formation in both small intestine and colon. Most of the tumours form in the proximal part of the small intestine and proximal and distal part of the colon. Rectal prolapse is often observed in these mice due to thickening of the distal gut. Hence, these mice are also sampled due to unresolved prolapse apart from other clinical signs such as hunching, paling and weight loss. Treatment was started on 21<sup>st</sup> day post induction to allow tumour initiation in the intestine. As mentioned in Section 3.2.2.2, majority of the tumour burden in this model is primarily composed of colonic tumours (>80%). Trametinib treatment led to significant reduction in colonic tumour burden (Figure 4-10, B&C), which contributed to reduction in overall tumour burden in a dose-dependent manner for trametinib (Figure 4-9, C&D). Interestingly, SI tumours did not respond to trametinib as the tumour burden seemed to increase with trametinib dosage. This increase in SI tumour burden might be due to tumour growth due to survival extension.

A clear dose-dependent reduction in colonic tumour burden was observed. While a dose-dependent reduction in overall tumour burden was observed with trametinib treatment, this effect was more pronounced in the colon.

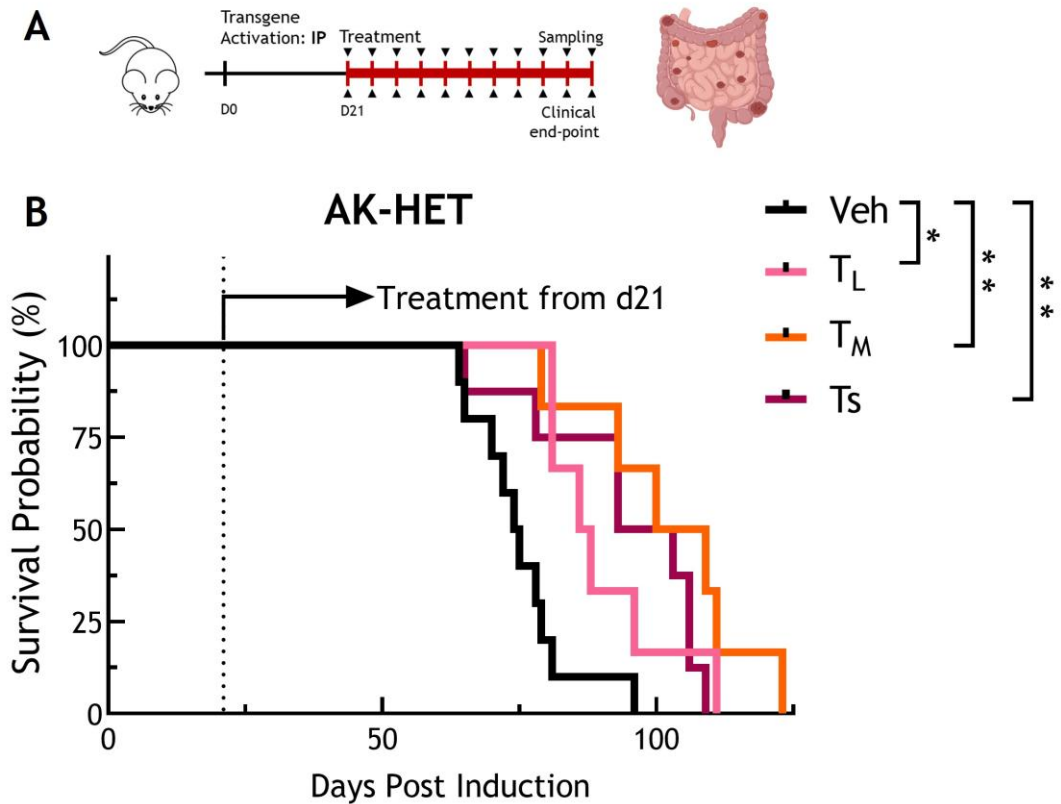
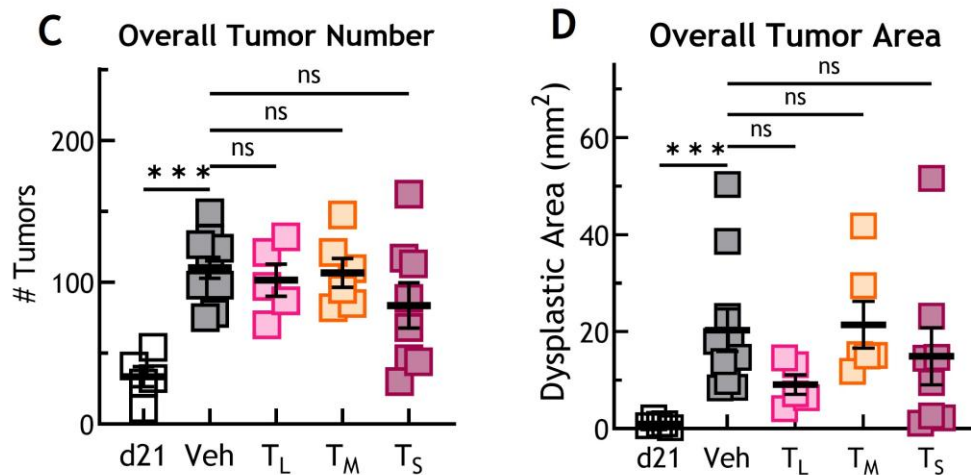


Table 4-2: Summary of median survival

	Vehicle	Trametinib (0.2mg/kg)	Trametinib (0.4mg/kg)	Trametinib (0.8mg/kg)
	Veh	T <sub>L</sub>	T <sub>M</sub>	T <sub>S</sub>
# deaths/events	10	6	6	8
Median Survival	74.5	87	104.5	98
Range	64-96	81-111	79-123	65-109



**Figure 4-9: Trametinib treatment results in up to 30% survival extension in mice bearing Kras driven intestinal tumours with functional p53.**

(A) Illustration of study plan. (B) Survival curve of AK-HET mice post transgene activation by Tamoxifen (80mg/kg; i.p). Mice were treated with Vehicle (black, n=10), low-dose Trametinib 0.2mg/kg (T<sub>L</sub>, light pink, n = 6) or medium-dose Trametinib 0.4mg/kg (T<sub>M</sub>, orange, n = 6) or standard-dose Trametinib 0.8mg/kg (T<sub>S</sub>, dark pink, n = 8) once daily by oral gavage from day 21 post induction and aged until clinical endpoint. Mice treated with Trametinib had up to 30% longer survival compared to Vehicle treated mice (p = 0.006, Log-rank test). Tumour burden quantified by (C) total number of tumours, and (D) total dysplastic area. Asterisks represent P values; ns P(>0.05), \* P(<0.05), \*\* P(<0.005), \*\*\* P(<0.001), and \*\*\*\* P(<0.0001).

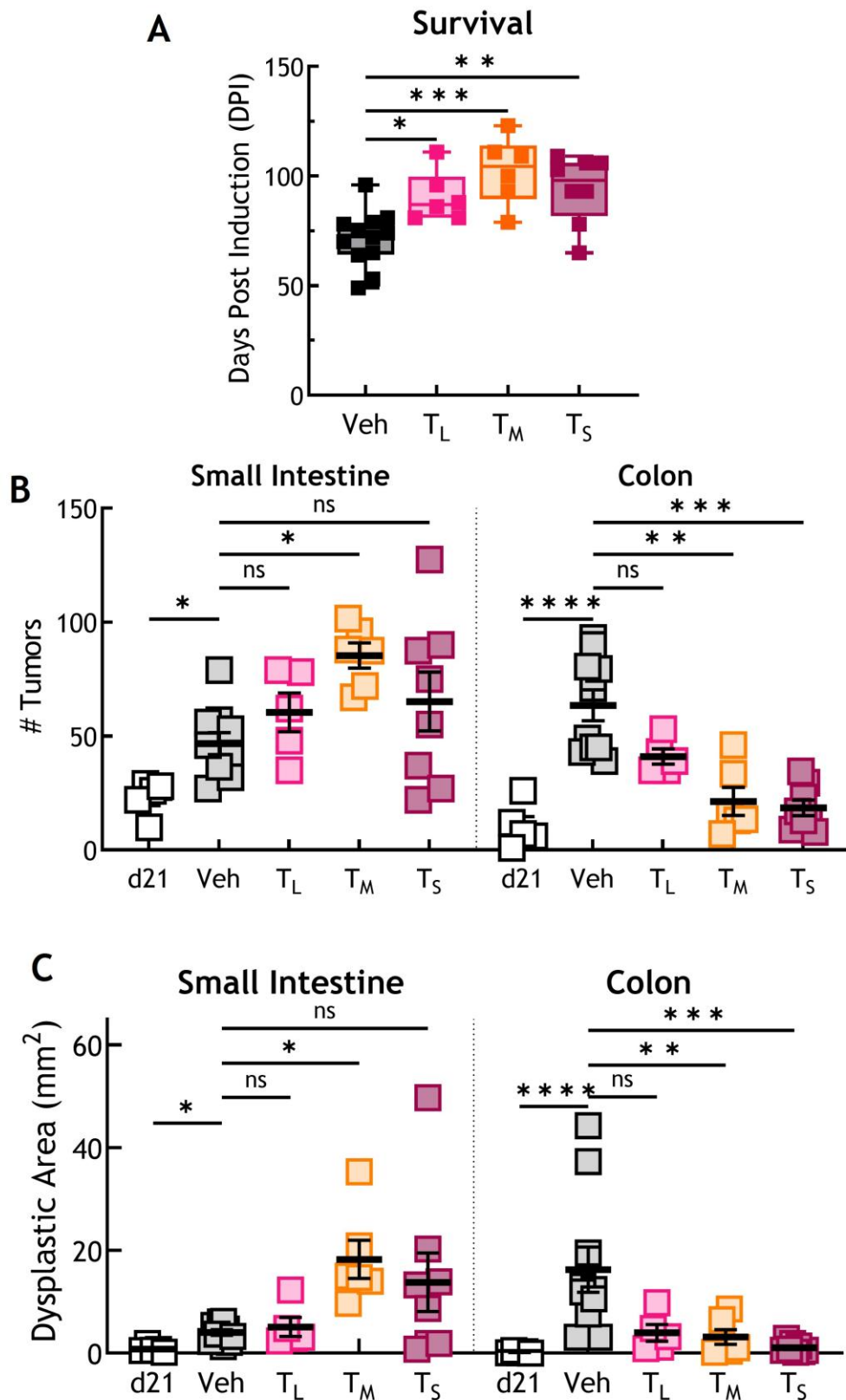


**Figure 4-10: Survival extension in Trametinib treated in AK-HET mice is due to reduction of tumour burden in colon but not small intestine.**

AK-HET mice were sampled on day 21 (d21) to establish baseline tumour burden or treated with Vehicle (Veh, black, n=10), low-dose Trametinib 0.2mg/kg (T<sub>L</sub>, light pink, n = 5), medium-dose Trametinib 0.4mg/kg (T<sub>M</sub>, orange, n = 6), or standard-dose Trametinib 0.8mg/kg (T<sub>S</sub>, dark pink, n = 6) once daily by oral gavage until clinical end-point. (A) Survival plot of AK-HET mice. Tumour burden quantified in small intestine and colon by (B) total number of tumours, and (C) total dysplastic area. One-way ANOVA (Kruskal-Wallis) test. Asterisks represent *P* values; ns *P*>0.05), \* *P*<0.05), \*\* *P*<0.005), \*\*\* *P*<0.001), and \*\*\*\* *P*<0.0001).

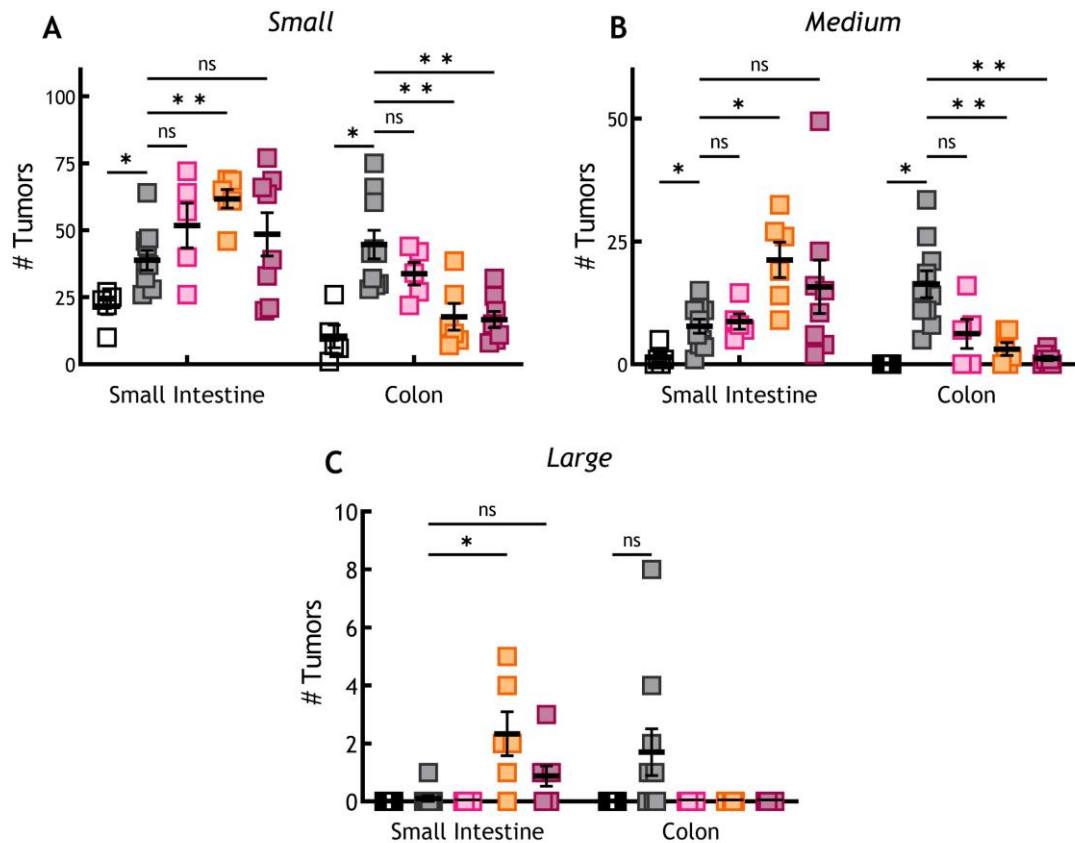


**Figure 4-11: Distribution of tumour burden by size in small intestine and colon.**

AK-HET mice were sampled on day 21 (d21) to establish baseline tumour burden or treated with Vehicle (Veh, black, n=10), low-dose Trametinib 0.2mg/kg (T<sub>L</sub>, light pink, n = 5), medium-dose Trametinib 0.4mg/kg (T<sub>M</sub>, orange, n = 6), or standard-dose Trametinib 0.8mg/kg (T<sub>S</sub>, dark pink, n = 6) once daily by oral gavage. (A-C) Tumours sorted by size, small (<0.1mm<sup>2</sup>), medium (0.1-1.5mm<sup>2</sup>) and large (>1.5mm<sup>2</sup>). One-way ANOVA, Kruskal-Wallis test. Asterisks represent P values; ns P(>0.05), \* P(<0.05), \*\* P(<0.005), \*\*\* P(<0.001), and \*\*\*\* P(<0.0001).

#### 4.3.2.2 Response to MEK inhibition in Kras driven intestinal tumour model with loss of p53

Additional loss of p53 in the intestine, as modelled by our AKP mice, exacerbates tumour burden in both small intestine and colon (200 - 800 tumours) causing significant reduction in survival time (Median 44 DPI, n = 9) post induction in comparison to AK mice (Median 74.5 DPI, n = 6) harbouring wildtype p53. Histopathological assessment of the tumours revealed that tumours in the small intestine are poorly differentiated in comparison to small intestinal tumours in AK mice. Some mice were sampled at d21 post induction to assess baseline tumour burden at treatment onset. While the overall tumour burden ranged between 222 to 617 tumours (n=3) across the whole intestine. Both the small intestinal and colon tumours ranged between small and medium sized tumours. No large tumours were noted. Vehicle treated mice had median survival of 44DPI (Range 33-66 days post induction, n = 9). Overall tumour burden ranged between 200 to 820 tumours across the whole intestine. All small intestinal tumours were either categorised as small

(0.001-0.1mm<sup>2</sup>) or medium (0.1 - 1.5mm<sup>2</sup>) and no large (>1.5mm<sup>2</sup>) tumours were noted in these mice. However, several small intestinal medium sized tumours showed features of high-grade dysplasia. Colon tumours on the other hand were also small - medium sized (Figure 4-14, A&B), although a couple of large sized tumours were noted in 3 out of 6 mice (Figure 4-14, C), suggesting that colonic tumours might have a higher proliferative potential than SI tumours. Colon tumours were also predominately low-grade dysplasia by histopathological assessment.

Mice treated with low-dose trametinib (T<sub>L</sub> 0.2mg/kg, p.o, q.d.) had a median survival of 61 DPI (Range 49 - 67 DPI, n = 5). This survival time post induction is not superior to that of vehicle treated mice (p > 0.05). Overall tumour burden in these mice ranged from 262 to 580 tumours across the whole intestine. Both small intestinal and colon tumour ranged between small and mid-sized tumours. However, no large colonic tumours were noted in contrast to vehicle treated AKP mice, suggesting that trametinib at low doses is still able to suppress tumour growth, although this did not reach statistical significance.

Mice treated with standard-dose trametinib (T<sub>S</sub> 0.8mg/kg, p.o, q.d) had a significant extension in median survival 77.5 DPI (Range 69 - 112 DPI, n = 8, p <0.0001). This extension of survival was complimented with a significant reduction in tumour burden, especially in colon. Overall tumour number in these mice ranged between 31 to 178 tumours across the whole intestine. While the tumour number was significantly lower in both small intestine and colon, this reduction was more pronounced in the colon. Interestingly, I also noted large tumours in small intestine which was not observed in Vehicle or low-dose trametinib treated mice. The extension of survival might have led to some lesions to progress into adenocarcinoma (Figure 4-14, C&D). In T<sub>S</sub> treated mice, colonic tumours better responded treatment compared to small intestinal tumours. 3 out of 5 mice developed adenocarcinomas in the small intestine (Figure 4-14, D).

RZA023.2f - pT3, poorly differentiated, invasive carcinoma, less desmoplasia.

RZA038.3a - pT4, moderate-poorly differentiated, invasive carcinoma, less desmoplasia.

RZA025.2c - pT3, invasive carcinoma, less nuclear pleomorphism.

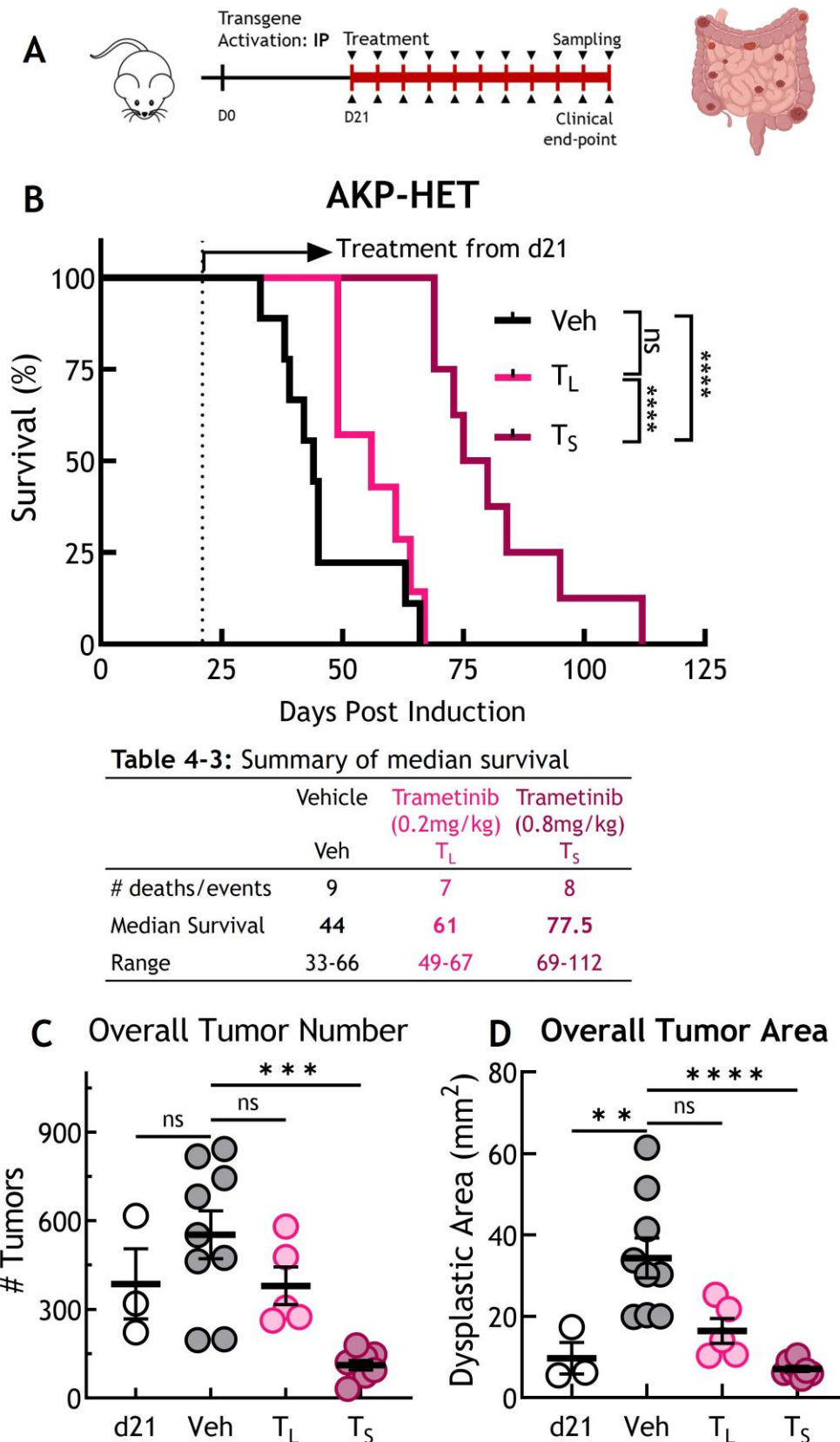


**Figure 4-12: Trametinib treatment results in up to 75% survival extension in mice bearing *Kras* driven intestinal tumours with loss of p53.**

(A) Illustration of study plan. (B) Survival curve of AKP-HET mice post transgene activation by Tamoxifen (80mg/kg; i.p). At Day 21 post induction, some AKP-HET mice were sampled to establish baseline tumour burden (d21) or were treated with Vehicle (black, n=9) or low-dose Trametinib 0.2mg/kg (T<sub>L</sub>, light pink, n = 7) or standard-dose Trametinib 0.8mg/kg (T<sub>S</sub>, dark pink, n = 8) by p.o, q.d and aged until clinical endpoint. Mice treated with Trametinib had upto 75% longer survival compared to Vehicle treated mice (p = 0.0005, Log-rank (Mantel-Cox) test). Tumour burden quantified by calculating (C) overall tumour number, and (D) overall tumour area. One-way ANOVA, Kruskal-Wallis test.

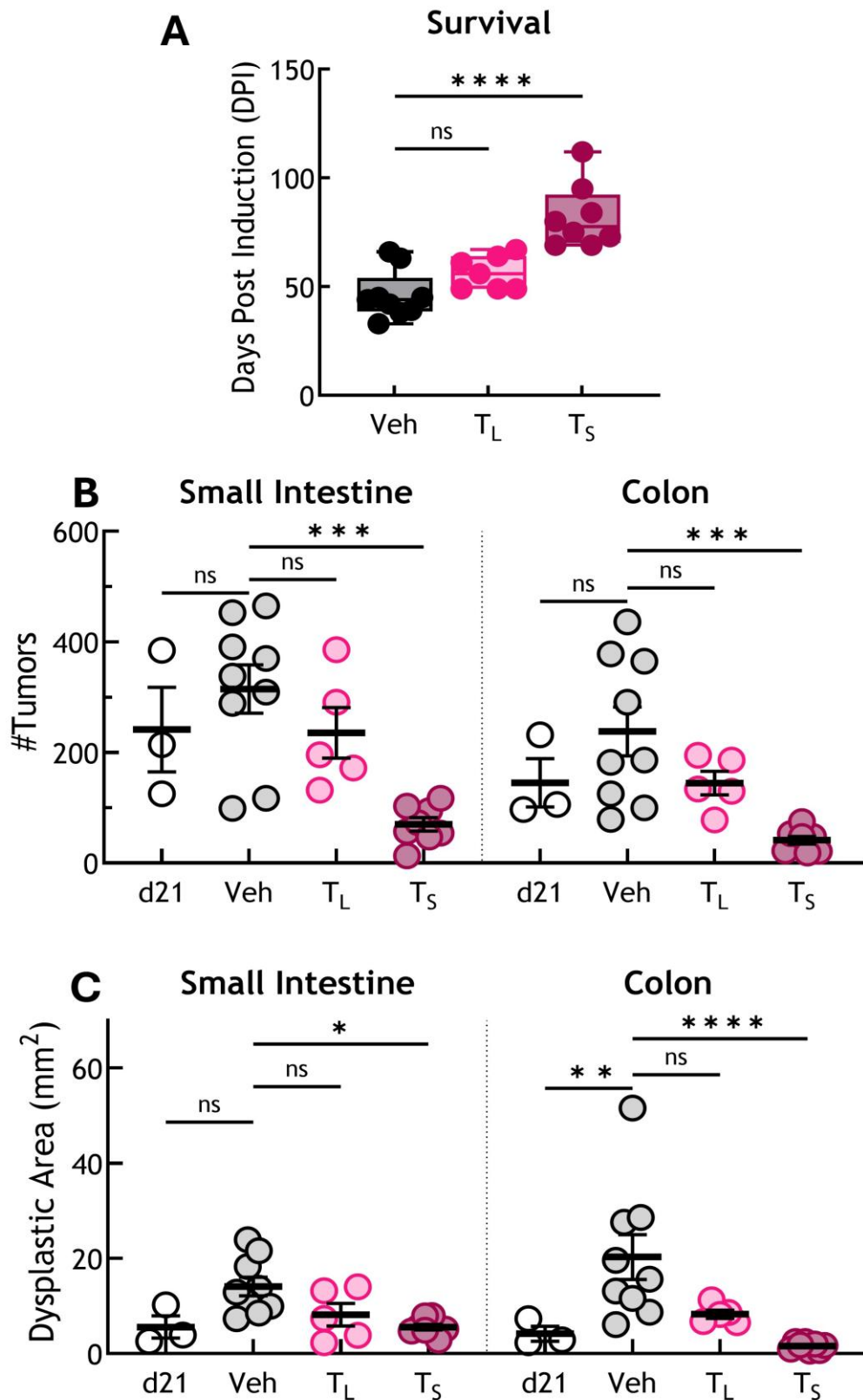


**Figure 4-13: Survival extension in Trametinib treated AKP-HET mice is due to reduction in overall tumour burden.** While this reduction in tumour burden is dose-dependent, it is more pronounced in the colon.

AKP-HET mice were sampled on day 21 (d21) to establish baseline tumour burden or treated with Vehicle (Veh, black, n=10), low-dose Trametinib 0.2mg/kg (T<sub>L</sub>, light pink, n = 5), or standard-dose Trametinib 0.8mg/kg (T<sub>S</sub>, dark pink, n = 6) once daily by oral gavage until clinical endpoint. (A) Survival plot of AKP-HET mice. Tumour burden quantified in small intestine and colon by (B) total number of tumours, and (C) total dysplastic area. One-way ANOVA (Kruskal-Wallis) test.

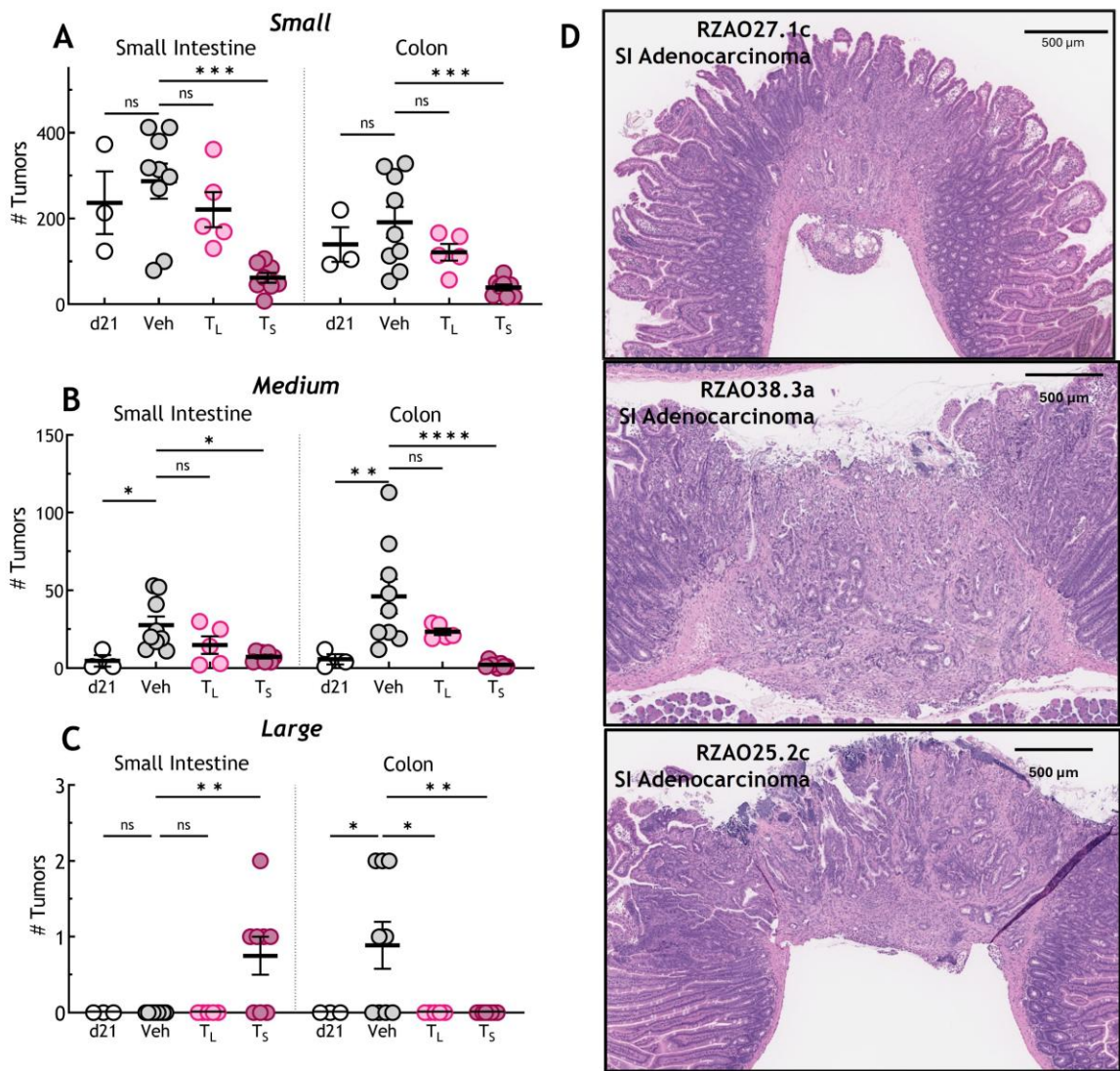


**Figure 4-14: Extension of survival causes progression to adenocarcinoma in some intestinal tumours.**

AKP-HET Mice were sampled on day 21 (d21) to establish baseline tumour burden or treated with Vehicle (Veh, black, n=9) or low-dose trametinib 0.2mg/kg (T<sub>L</sub>, light pink, n = 7) or standard-dose trametinib 0.8mg/kg (T<sub>S</sub>, dark pink, n = 8) once daily by oral gavage and aged until clinical end-point.

Extension of survival reveals tumour progression in some small intestinal tumours that form large adenocarcinomas. This progression to adenocarcinoma is observed only in small intestinal tumours but not colon. Intestinal tumours are sorted by size - (A) small (<0.01mm<sup>2</sup>), (B) medium (0.01-1.5 mm<sup>2</sup>), (C) large (>1.5 mm<sup>2</sup>). (D) Bright-field images of H&E images of advanced adenocarcinoma. One-way ANOVA, Kruskal-Wallis test. Asterisks represent P values; ns P(>0.05), \* P(<0.05), \*\* P(<0.005), \*\*\* P(<0.001), and \*\*\*\* P(<0.0001).

### 4.3.3 Targeting the RAS pathway in Kras driven colon tumour model.

To overcome the limitations of our long-term models in which mice develop multiple tumours throughout the intestine, I studied MAPK dependency in the colon tumour model, where a single tumour is induced in the colon. Development of single tumour extends latency of this model and gives an opportunity for tumour progression.

Histopathological assessment showed well-differentiated tubular adenomas with no detectable invasion, reminiscent of human colon adenomas. This model recapitulates key features of colonic adenomas in a fully immunocompetent environment, allowing fundamental questions of tumour initiation and dependency on key signalling pathways (Roper et al., 2017). To generate a single colonic tumour, 4-Hydroxy Tamoxifen (70µl, 100mM) was injected into the colonic sub-mucosa of A-HOM, AK-HOM and AKP-HOM mice to induce focal transgene induction. Tumours resulting from these mice are referred as A, AK and AKP colon tumours respectively. Mice were monitored for tumour growth by colonoscopy 21-days post induction. Upon confirmation of tumour establishment, mice were treated with Vehicle (0.5% HPMC + 0.1% Tween) or standard-dose trametinib (0.8mg/kg) for 5 days (p.o, q.d.) and sampled at treatment endpoint.

#### **A. Trametinib does not suppress proliferation in an established colon tumour model.**

I have previously shown that Ras driven colon tumours (AK- and AKP) colon tumours have a slightly lesser proliferation rate compared to A-colon tumour, suggesting oncogenic Kras rewires metabolism in the tumour rather than proliferation. I studied if MEK inhibition would reduce proliferation and induce cell death in these tumours. Trametinib treatment has little to no effect in reducing proliferation or Apoptosis in A-colon tumour. Interestingly, trametinib treatment led to an increased proliferation rate in both AK- and AKP-colon tumour (Figure 4-15, B). This increase in proliferation was also coupled with increase in cell death as evidenced by higher cleaved PARP positive cells in the tumours (Figure 4-15, C).

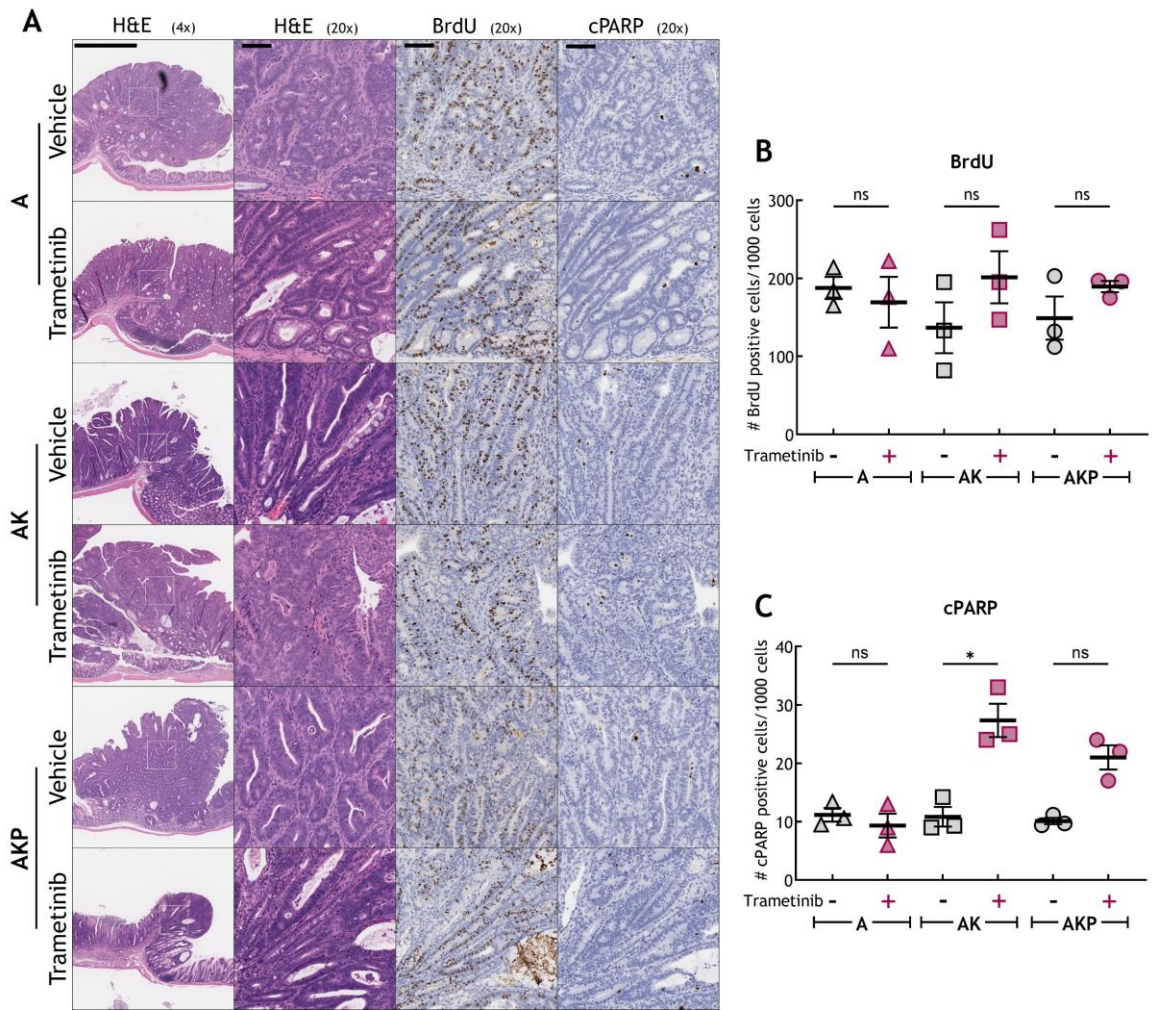


**Figure 4-15: Trametinib treatment does not suppress proliferation in Ras-driven colon tumour model.**

(A) Bright-field images of A-, AK-, and AKP colon tumour model treated with Trametinib(0.8mg/kg) or Vehicle for 5 days post-tumour confirmation. Tissue sections stained with Haematoxylin & Eosin (4x and 20x), BrdU to assess proliferation rate and cPARP to assess rate of cell death. (B) rate of proliferation was assessed by quantifying BrdU positive cells per 1000 dysplastic cells (C) rate of cell death was assessed by counting number of cPARP positive cells per 1000 dysplastic cells. Scale bars for images are: 1mm (4x magnification), and 100µm (20x magnification). Asterisks represent *P* values obtained from One-way ANOVA, Kruskal-Wallis test followed by Dunn's correction; ns (*P*>0.05), \* *P*(<0.05), \*\* *P*(<0.005), \*\*\* *P*(<0.001), and \*\*\*\* *P*(<0.0001).

## B. Trametinib effectively suppresses MAPK activity in Kras-driven colon tumours.

I next checked if the reason for no change in proliferation is due to poor drug target engagement in established tumours. I checked MAPK status with RNAscope analysis of *Dusp6* transcripts in the tumours. This revealed a significant suppression of MAPK activity in Kras driven tumours, AK- and AKP- colon tumours. There was a slight decrease in *Dusp6* in tumours with loss of *Apc* alone (Figure 4-16, B). But this is expected as MEK is a downstream target of Kras. Trametinib effectively suppresses the MAPK pathway in Ras-driven tumour models. Trametinib treatment led to significant suppression of the MAPK pathway as evidenced by reduction in number of *Dusp6* transcripts per cell in both AK- and AKP-colon tumours.

I hypothesised that suppression of the MAPK pathway would lead to shift in fetal progenitor population, as assessed by levels of *Anxa1* transcripts in the tumour. *Anxa1* is an oncofetal marker of revival stem cell population (Tape, 2024). However, no significant changes were observed in *Anxa1* across different tumours and across treatments (Figure 4-16, C).

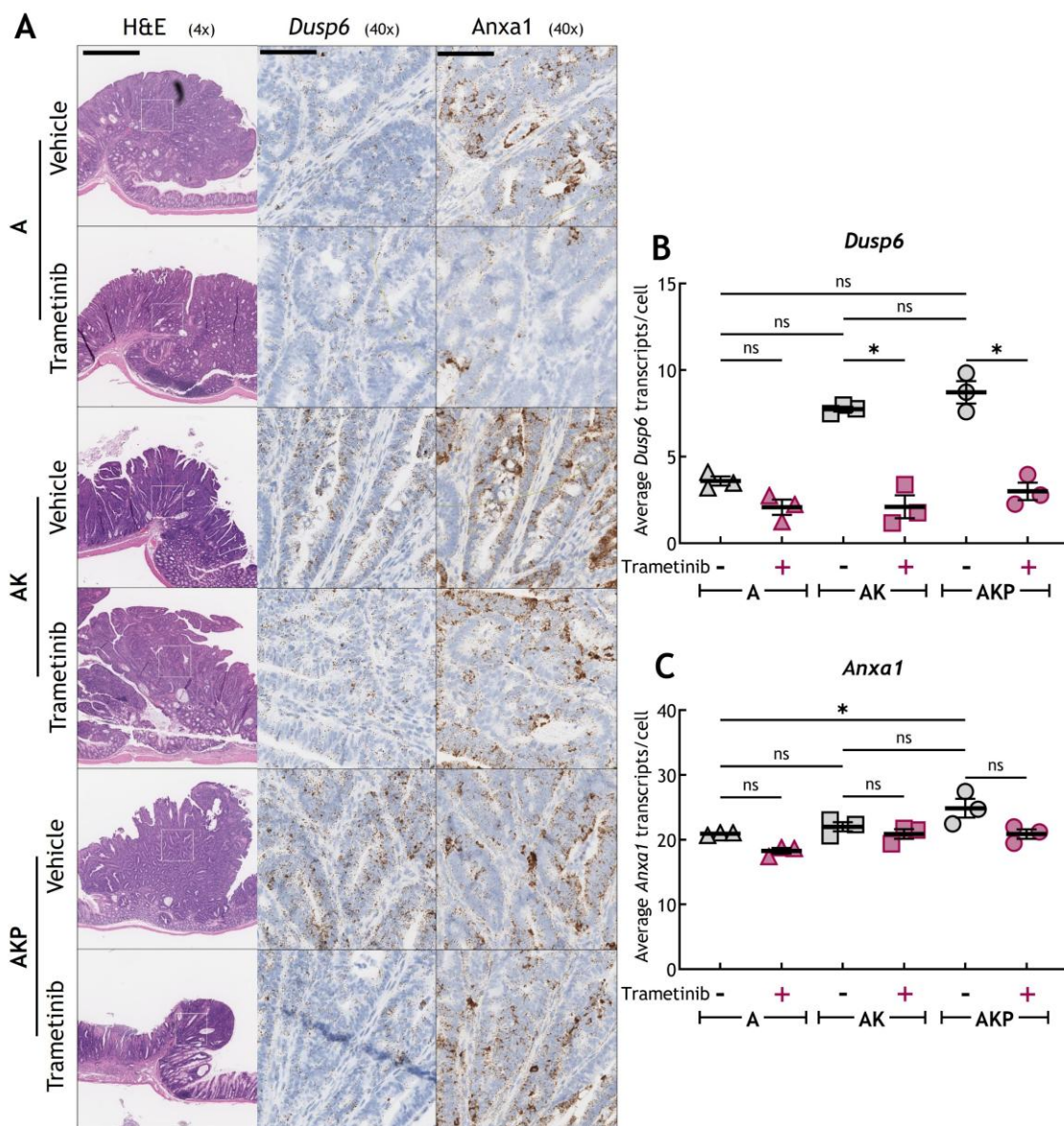


**Figure 4-16: Trametinib suppresses MAPK activity in a Kras driven colon tumour model.**

(A) Bright-field images of A-, AK-, and AKP colon tumour model treated with Trametinib(0.8mg/kg) or Vehicle for 5 days post-tumour confirmation. Tissue sections stained with Haematoxylin & Eosin (4x and 20x), (B) MAPK activity was assessed with RNAscope® analysis of *Dusp6*. (C) Fetal stem cell markers assessed with RNAscope® analysis of *Anxa1*. Scale bars for images are: 1mm (4x magnification), and 100µm (40x magnification). Asterisks represent *P* values obtained from One-way ANOVA, Kruskal-Wallis test followed by Dunn's correction; ns  $P(>0.05)$ , \*  $P(<0.05)$ , \*\*  $P(<0.005)$ , \*\*\*  $P(<0.001)$ , and \*\*\*\*  $P(<0.0001)$ .

### C. Trametinib treatment alters Wnt activity based on p53 status in the colon tumour model.

To assess Wnt signalling activity, I performed RNAscope® analysis of Notum and Axin2 which are markers of high Wnt activity. Notum from Apc mutant cells actively inhibits proliferation of surrounding wildtype cells by its Wnt inhibiting role, driving their differentiation and outcompeting the wildtype cells from the crypt niche (Flanagan et al., 2021). Axin2, part of the  $\beta$ -catenin destruction complex, is a  $\beta$ -catenin/TCF regulated target gene that serves as a feedback inhibitor to modulate high Wnt activity in normal cells. In a normal colon epithelium, Axin2 levels are generally low, however constitutive activation of Axin2 expression by the  $\beta$ -catenin/TCF transcriptional complex is observed

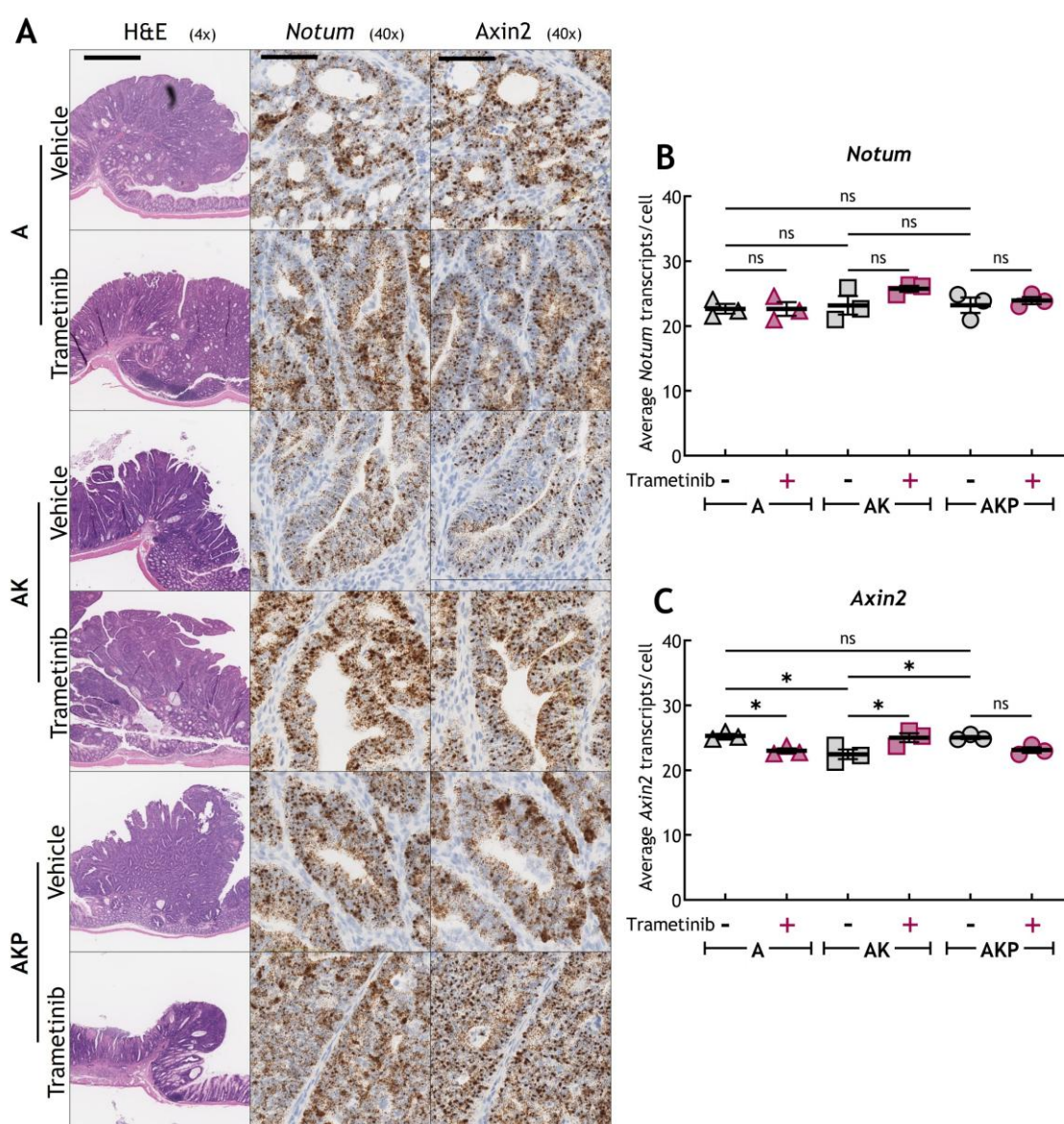


**Figure 4-17: Trametinib treatment alters Wnt signalling activity based on p53 status.** (A) Bright-field images of A-, AK-, and AKP colon tumour model treated with Trametinib (0.8mg/kg) or Vehicle for 5 days post-tumour confirmation. Tissue sections stained with Haematoxylin & Eosin (4x), and Wnt signalling activity was assessed with RNAscope® analysis of (B) Notum and, (C) Axin2. Scale bars for images are: 1mm (4x magnification), and 100 $\mu$ m (40x magnification). Asterisks represent *P* values obtained from One-way ANOVA, Kruskal-Wallis test followed by Dunn's correction; ns *P*(>0.05), \* *P*(<0.05), \*\* *P*(<0.005), \*\*\* *P*(<0.001), and \*\*\*\* *P*(<0.0001).

in CRCs (Klaus and Birchmeier, 2008). In Apc mutant CRCs, high levels of Axin2 promotes, rather than suppresses, a  $\beta$ -catenin/TCF-initiated, EMT program (Wu et al., 2012).

In A- and AKP- colon tumour, where p53 is not activated or is functionally lost, Notum levels remain unchanged upon treatment with trametinib. Moreover, a modest reduction in Axin2 levels were noted upon trametinib treatment (Figure 4-17, B-C).

However, in AK-colon tumour where p53 is functionally activated, an increase in both Notum and Axin2 transcripts were noted upon trametinib treatment (Figure 4-17, B-C). This was also reported by (Solberg et al., 2019) where MEK inhibition increased Wnt/ $\beta$ -catenin activity via YAP in an APC-KRAS mutated cell line.

#### D. Trametinib treatment induces p53 activity in Kras driven colon tumours.

I next assessed how p53 activity is induced across the tumours upon MEK inhibition. As described in section 3.2.3, loss of Apc alone does not induce p53 or its target gene p21

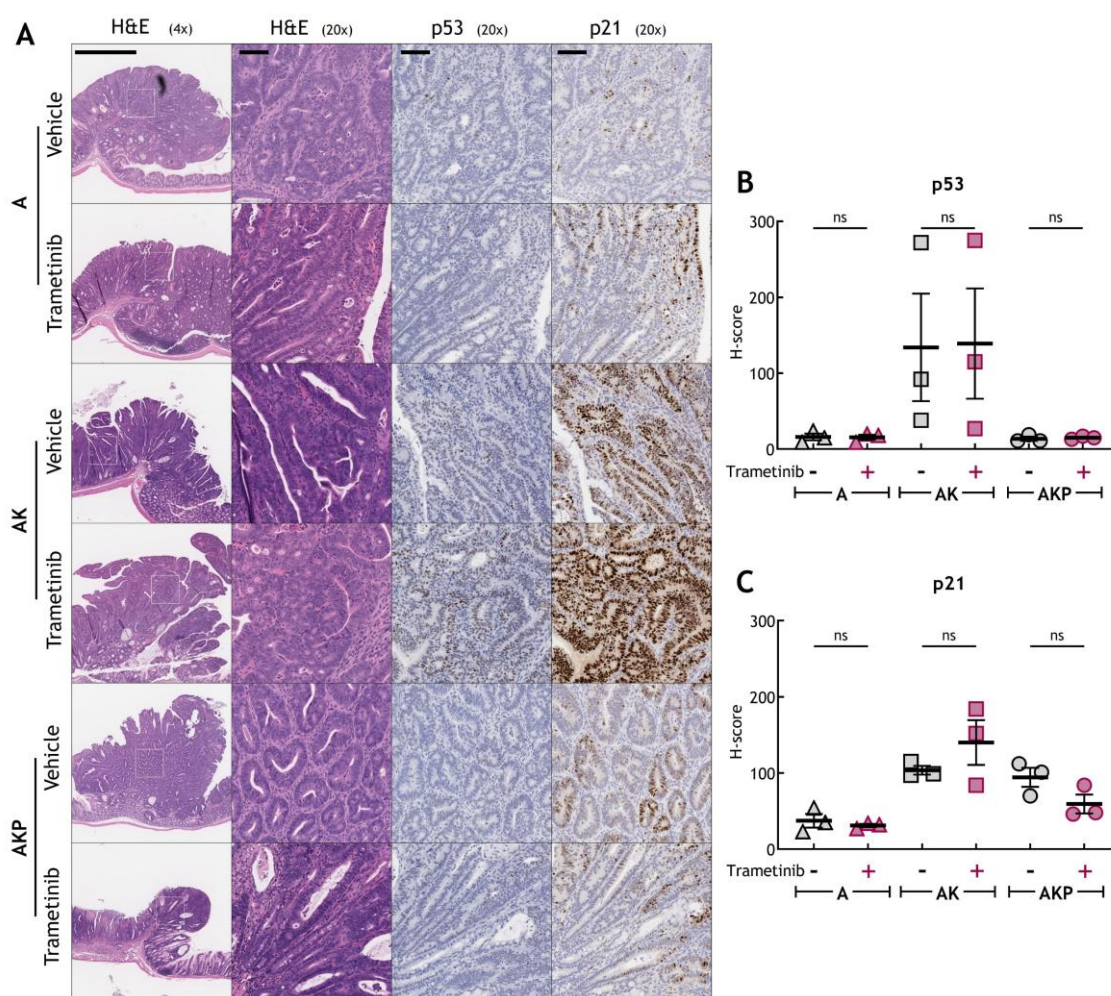


Figure 4-18: Trametinib treatment induces p21 in Ras driven colon tumour with functional p53. (A) Bright-field images of A-, AK-, and AKP colon tumour model treated with Trametinib (0.8mg/kg) or Vehicle for 5 days post-tumour confirmation. Tissue sections stained with Haematoxylin & Eosin (4x and 20x), and p53 activity was assessed with immunohistochemical analysis of (B) p53 and, (C) p21. Scale bars for images are: 1mm (4x magnification), and 100 $\mu$ m (20x magnification). Asterisks represent *P* values obtained from One-way ANOVA, Kruskal-Wallis test followed by Dunn's correction; ns *P*>0.05), \* *P*<0.05), \*\* *P*<0.005), \*\*\* *P*<0.001), and \*\*\*\* *P*<0.0001).

(Figure 4-18, B-C. In tumours with oncogenic Kras and functional p53 (AK-colon tumour), trametinib treatment causes a further increase in p21 level. This suggests a p53 dependent cell cycle arrest and apoptosis activity as evident from the cleaved-PARP levels discussed in section 4.3.3-A.

Interestingly an increase in p21 levels were noted in AKP-colon tumours, which further decreased upon trametinib treatment. This increased in p21 might be due to a p53 independent mechanism (Figure 4-18, C).

### E. Trametinib induces double strand breaks in Ras driven colon tumour with functional p53

I next assessed if cell cycle arrest leads to senescence by studying levels of p16 within the tumours. P16 accumulation is normally observed during G0/G1 cell cycle phase. Depending upon the level of cellular stress, cells undergo either cell cycle arrest or

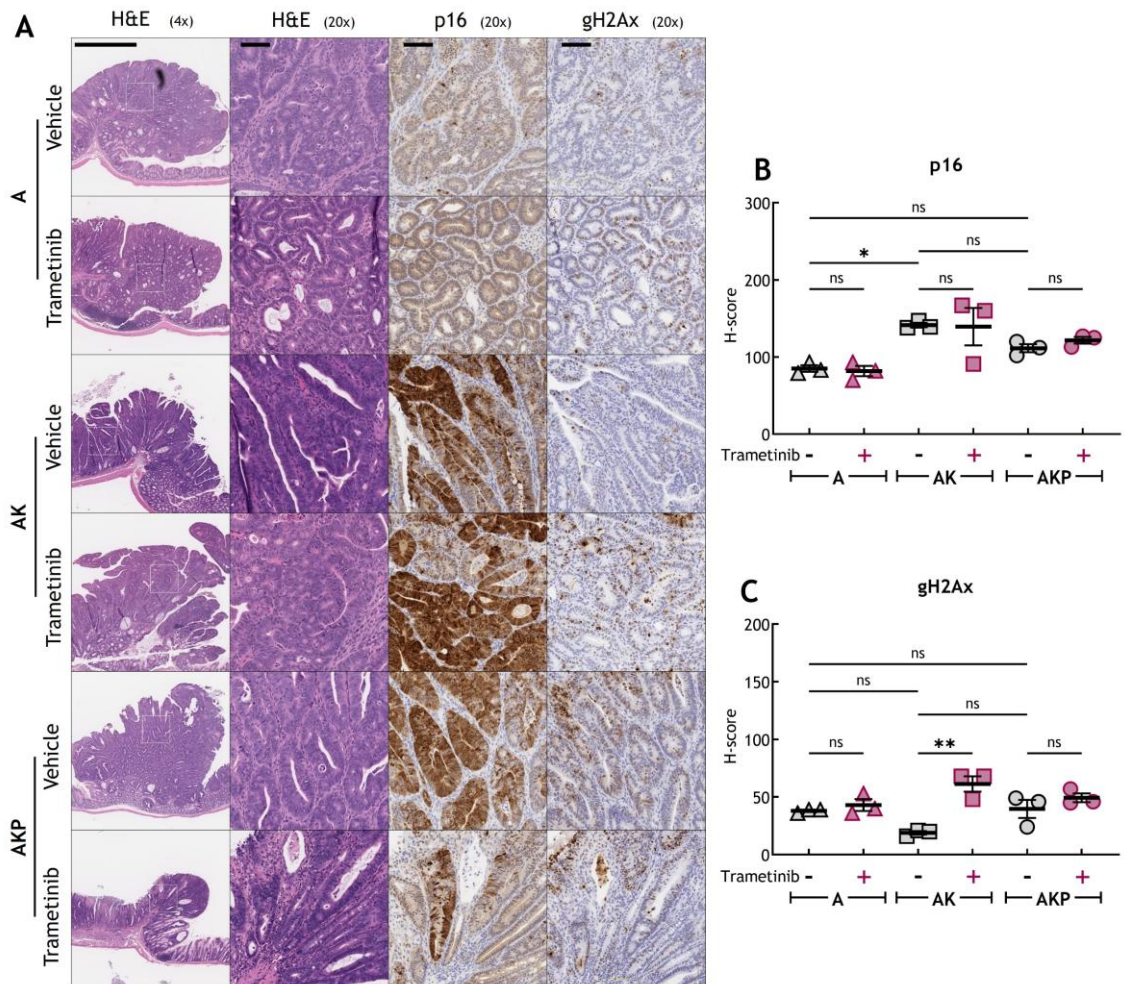


**Figure 4-19: Trametinib treatment induces double strand breaks in Ras driven colon tumour with functional p53.**

(A) Bright-field images of A-, AK-, and AKP colon tumour model treated with Trametinib (0.8mg/kg) or Vehicle for 5 days post-tumour confirmation. Tissue sections stained with Haematoxylin & Eosin (4x and 20x), and senescence and DNA damage was assessed with immunohistochemical analysis of (B) p16 and, (C) gH2Ax. Scale bars for images are: 1mm (4x magnification), and 100µm (20x magnification). Asterisks represent *P* values obtained from One-way ANOVA, Kruskal-Wallis test followed by Dunn's correction; ns  $P(>0.05)$ , \*  $P(<0.05)$ , \*\*  $P(<0.005)$ , \*\*\*  $P(<0.001)$ , and \*\*\*\*  $P(<0.0001)$ .

senescence. Interestingly, an increase in double strand breaks was also observed as noted with an increase in levels of  $\gamma$ H2Ax noted only in AK-colon tumour (Figure 4-19, C). This suggests that p53 might have a role in causing double strand breaks.

All the results described above are preliminary and warrant further validation to understand the role of multiple signalling pathways in an established colon tumour model.

## 4.4 Discussion

Our fruit fly avatar effectively recapitulates clinical observations of resistance to targeted therapies. The single mutant fly line *bynts>rasG12V* responds positively to MEK inhibition via trametinib, whereas the 10-hit fly line *bynts>CPCT036* exhibits only a modest response to trametinib (Figure 3-2 & 4-1). Moreover, no other targeted drugs (binimetinib, regorafenib, dabrafenib, and rapamycin) demonstrated any survival benefit, underscoring that drug resistance is an emergent property of genetically complex tumours. My observations align with other studies that have also noted drug resistance in complex tumour models (Bang et al., 2016).

In line with my findings in fruit fly models, intestinal organoids derived from compound-mutant mice (AKP) demonstrated greater resistance to MEK inhibition compared to single-mutant *Kras* organoids (Figure 4-3). Analyzing key signaling pathways illuminated the role of p53 in modulating drug response over time (Figure 4-4). Both compound-mutant organoids with functional p53 (AK) and those lacking p53 (AKP) exhibited reduced MAPK activity following MEK inhibition at an early time point (6 hours), as indicated by diminished pERK levels. However, apoptosis was notably delayed in AKP organoids. Furthermore, pERK levels displayed distinct dynamics across both organoid types; intriguingly, pERK levels returned to baseline in AK organoids 18 hours post-treatment, while they remained suppressed in AKP organoids. The reduced pERK levels not only reflect decreased MAPK activity and lower proliferation rates but also suggest potential cell cycle arrest or senescence in the AKP organoids, likely stemming from the impaired apoptotic pathway. Cell cycle analysis revealed that organoids lacking functional p53 arrested in the G0/G1 phase upon MEK inhibition, while those with functional p53 underwent apoptosis in the AK organoids (Figure 4-6). These findings underscore the need for further investigations utilizing additional intestinal organoid models to deepen our understanding of these complex dynamics.

In our mouse models, I demonstrate that the response to MEK inhibition is also dependent on the stage of tumour development and treatment onset. At the pre-adenoma stage, represented by our short-term models, hyperproliferative intestinal crypts respond to MEK inhibition irrespective of p53 status. A modest yet significant reduction in proliferation was observed in both AK- and AKP-HOM mice, indicating that dysplastic cells are dependent on the MAPK pathway during early tumour initiation. While this model helps

elucidate important processes in tumour formation, a clinically relevant setting is treatment response in established tumours.

MEK inhibition contributes to survival extension in the Ras-driven intestinal tumour model (Long-term model). Interestingly, contrary to findings reported in several studies and our fly data, mice bearing AKP tumours initially appeared to respond better to MEK inhibition. AKP-HET mice experienced nearly a 70% extension in survival when treated with trametinib, while mice bearing AK tumours showed only a 30% survival extension compared to vehicle-treated mice. This increase in survival was largely due to the reduction in colonic tumour burden in both AK- and AKP-mice.

However, small intestinal tumours exhibited a heterogeneous response to MEK inhibition depending on their p53 status. In mice bearing tumours with functional p53 (AK-HET), survival extension correlated with an increase in small intestinal tumour burden, as mice receiving trametinib had more small intestinal tumours compared to vehicle-treated mice. Conversely, mice with tumours lacking functional p53 (AKP-HET) demonstrated an overall reduction in small intestinal tumour burden, with half developing adenocarcinomas. Notably, adenocarcinoma was observed only in the small intestine, not in the colon, indicating differing tumour progression dynamics between these regions. These differences might be driven by epigenetic changes and differences in microenvironment in small intestine and colon. Thus, the response to MEK inhibition is not solely dependent on mutational background but also on tumour location. Further assessment of proliferation rates and the status of key signalling pathways between small intestinal and colon tumours is warranted.

A significant caveat of our long-term model is that tumours develop throughout the entire intestine, not specifically in the colon, which may not be spatially relevant to human CRC. Moreover, tumours arise at different time points post-Tamoxifen induction, as tumour formation relies on the sporadic loss of the second copy of *Apc*. This complicates the determination of tumour burden at treatment onset and makes it challenging to ascertain whether treatment-resistant lesions initiated before or after treatment began.

To overcome these limitations, I studied MAPK dependency in an established colon tumour model. This model consists of a single spatially resolved colon tumour induced by an injection of 4-hydroxy Tamoxifen (4-OHT) into the colonic submucosa. The colonic tumours in this model were adenomatous polyps with a high degree of differentiation and no invasive features, closely resembling human colonic adenomas and remaining relevant to human CRC. Contrary to the hyperproliferative crypts in our short-term models, the colon tumours exhibited no change in proliferation levels despite a reduction in MAPK activity following MEK inhibition. In the subsequent chapter, I will explore the mechanisms underlying drug resistance.

# Chapter 5 Combination Strategies to target vulnerabilities of KRAS mutant CRCs

While targeted therapies like trametinib initially show promise, resistance frequently develops, hindering long-term treatment success. This chapter investigates a potential strategy to overcome trametinib resistance in mouse models of CRC by combining trametinib with vorinostat. This approach stems from recent research highlighting the role of enhanced drug metabolism, specifically through the glucuronidation pathway, in driving trametinib resistance.

Our recent work (Cong et al., 2023) demonstrated that trametinib-resistant  $RAS^{G12V}$ -APC<sup>i</sup>-P53<sup>i</sup> tumours in fly models (*byn<sup>ts</sup>> ras<sup>G12V</sup> apc<sup>Ri</sup> p53<sup>Ri</sup>*; hereafter RAP) exhibited elevated levels of metabolites associated with the glucuronidation pathway. Glucuronidation, a crucial detoxification process, facilitates drug clearance from the body is normally activated in the liver. Trametinib metabolism is primarily through deacetylation after which it is glucuronidated (Ho et al., 2014). Inhibiting different steps within this pathway, including the HDAC1-mediated deacetylation step using vorinostat, effectively reversed trametinib resistance in our fly and intestinal organoid models. Importantly, this

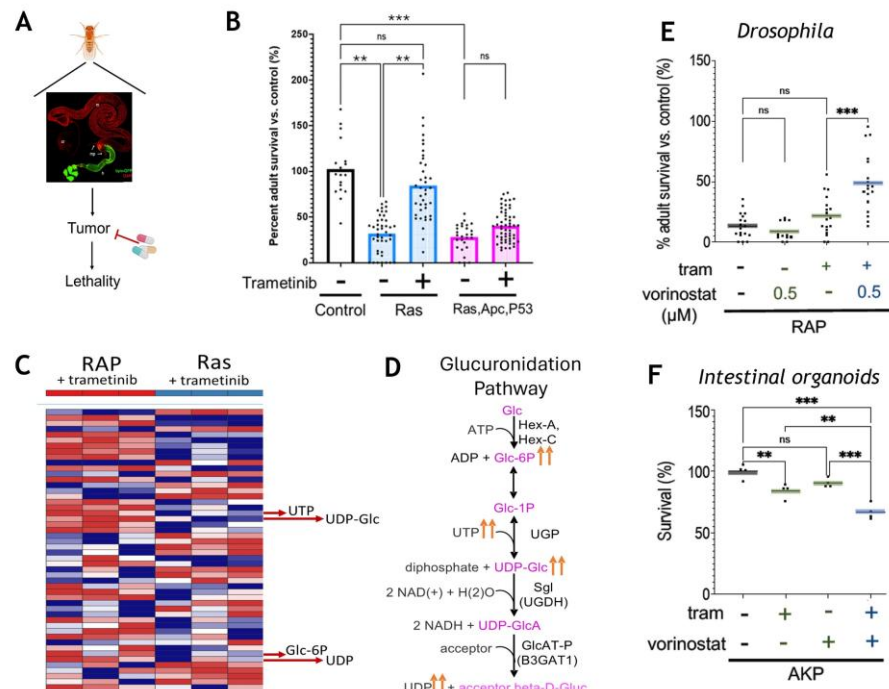


**Figure 5-1: Glucuronidation pathway induces trametinib resistance in Drosophila and mouse intestinal organoids.**

(A) Illustration of rescue from lethality assay. (B) Triple mutant Drosophila (*byn<sup>ts</sup>>RAP*) responds poorly to single agent trametinib. (C) LC/MS analysis in trametinib treated *byn<sup>ts</sup>>Ras* and *byn<sup>ts</sup>>RAP* flies reveal upregulation of metabolites involved in glucuronidation pathway. (D) An overview of the glucuronidation pathway. Addition of vorinostat improves trametinib response in (E) Drosophila and (F) mouse intestinal organoids. (Data generated in collaboration with Dr Bojie Cong and Dr Alejandro H Uribe at University of Glasgow)

resistance mechanism appears to be conserved in KRAS/APC/TP53 CRC models, suggesting potential clinical relevance.

This chapter aims to build upon these findings by examining whether the trametinib/vorinostat combination yields similar results in mouse models of RAS-driven CRC. The results provide critical insights into the translatability of this therapeutic strategy and the development of more effective treatment options for CRC patients.

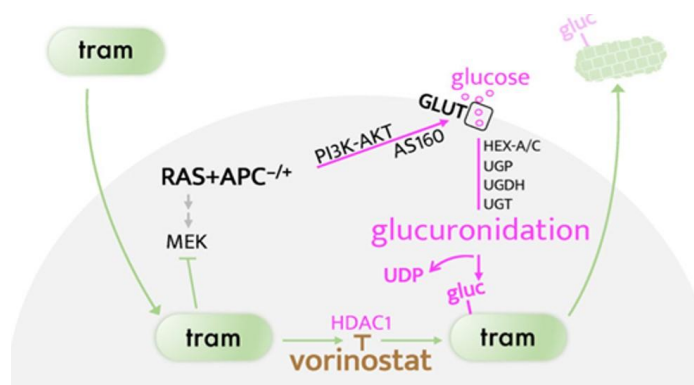


**Figure 5-2: Schematic summary of targeting trametinib glucuronidation by blocking deacetylation step.**

Trametinib (tram) is a potent MEK inhibitor that effectively blocks RAS pathway signaling and oncogenic transformation in preclinical studies. Coactivation of RAS and WNT pathways induces PI3K/AKT signaling, AS160, and GLUT1/4 activation, promoting increased glucose influx into cells. This leads to heightened glucuronidation and clearance of trametinib. Potential therapeutic targets may include HDAC1, as its deacetylation activity is crucial for the glucuronidation process of certain drugs, including trametinib

## 5.1 Dose titration of trametinib

Our studies in *Drosophila* and mouse intestinal organoids show that trametinib is cleared from the tumours by upregulation of the glucuronidation pathway - a toxin clearance pathway. This suggests a possibility of lesser accumulation of trametinib in Tumours compared to normal tissues. Moreover, trametinib, while effective as a MEK inhibitor, is associated with a range of toxicities, including rash, diarrhea, fatigue, and, more seriously, cardiopulmonary issues. These side effects often limit the dosage that can be administered safely to patients. Employing a low-dose trametinib can be a useful as a strategy to mitigate these adverse effects. This approach may also allow for combination with other therapies, enhancing efficacy with manageable side-effect profile.

### 5.1.1 Dose titration of trametinib in short-term model

To understand if HDAC inhibition can increase the availability of unaltered trametinib within tumours, I studied potency of different doses of trametinib in our short-term models to identify dosage of trametinib that can,

A - suppress MAPK activity and reduce proliferation in the hyperproliferative intestinal crypts, or

B - suppress MAPK activity but the dosage isn't optimum to reduce proliferation within the hyperproliferative intestinal compartments.

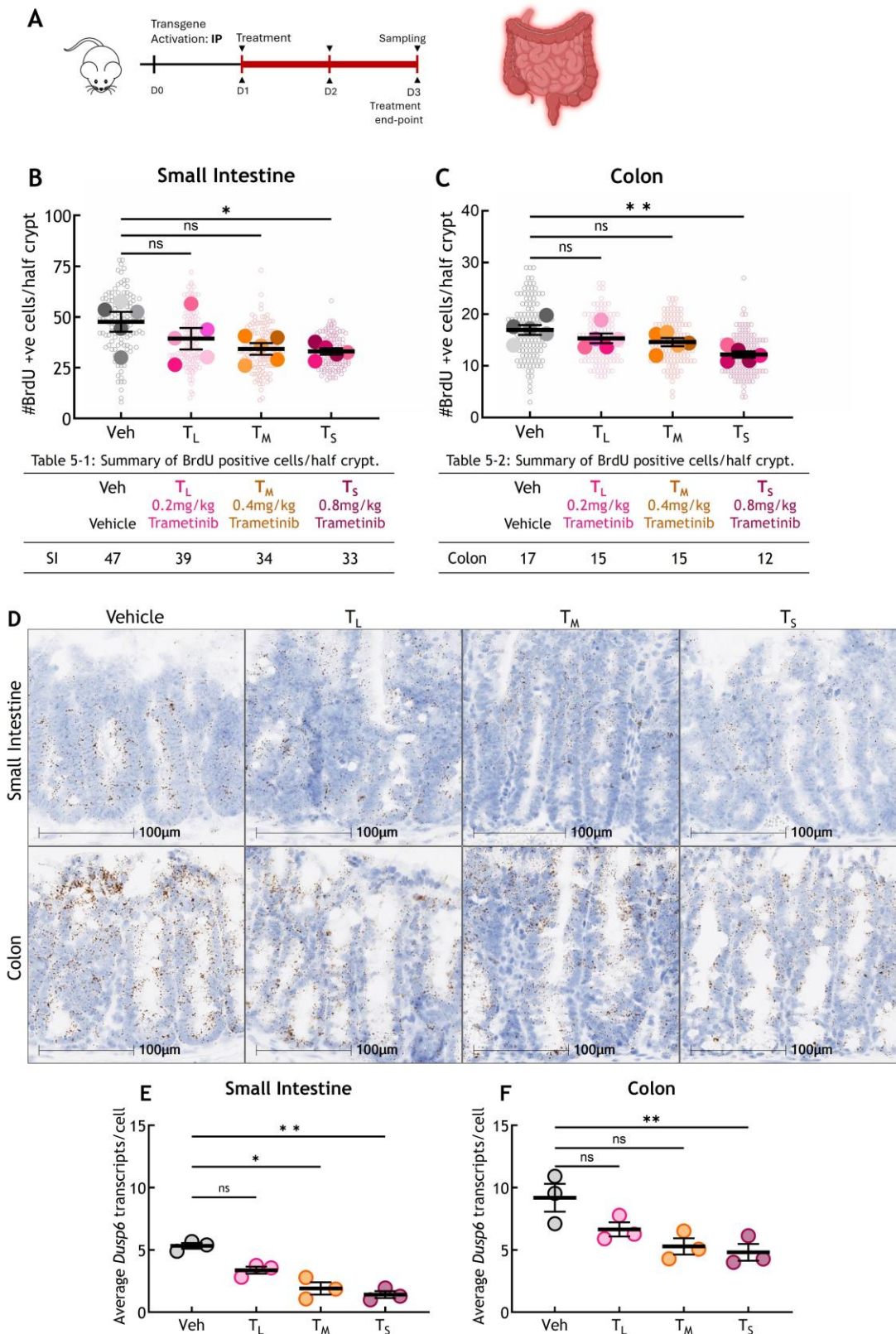


**Figure 5-3: Trametinib has a dose-dependent effect on suppressing proliferation and MAPK activity in the intestinal crypts.**

AKP-HOM mice were administered with 80mg/kg tamoxifen once on Day 0 and treated with Vehicle or various doses of Trametinib - 0.2mg/kg (T<sub>L</sub>) or 0.4mg/kg (T<sub>M</sub>) or 1mg/kg (T<sub>S</sub>) once daily by oral gavage for 3 days. (A) Illustration of study plan. BrdU positive cells per half crypt (n = 25) were quantified from (B) small intestine and (C) colon. Small dots represent single half-crypts, large dots represent mean of biological replicates. Unpaired t test with Welch's correction. Summary of BrdU score in small intestine (Table 5-1) and colon (Table 5-2). (D) Bright-field images of *Dusp6* RNAscope in small intestine and colon. Average *Dusp6* transcripts per cell in (E) small intestine and (F) colon. One-way ANOVA, Kruskal-Wallis test. Asterisks represent *P* values; ns (*P*>0.05), \* (*P*<0.05), \*\* (*P*<0.005), \*\*\* (*P*<0.001), and \*\*\*\* (*P*<0.0001).

AKP-HOM mice were induced as described in Chapter 2.6 and treated with various doses of trametinib - 0.2mg/kg ( $T_L$ , low-dose), or 0.4mg/kg ( $T_M$ , mid-dose) or 1mg/kg trametinib ( $T_S$ , standard-dose) or Vehicle from Day 1 to 3. BrdU (0.25ml, 10mM) was administered 2h before sampling on Day 3. BrdU scoring was performed as described in Chapter 2.6. I also assessed MAPK activity by checking transcript levels of *DUSP6*.

A dose-dependent reduction was observed in number of BrdU score with increasing trametinib dosage. Briefly, mice treated with standard-dose trametinib ( $T_S$ ) had a 30% lower proliferation in both small intestine and colon when compared to Vehicle treated mice (SI:  $33 \pm 1.6$  vs  $48 \pm 5$  BrdU positive cells per half crypt,  $p < 0.05$ ), (Colon:  $12 \pm 0.6$  vs  $17 \pm 1$  BrdU positive cells per half crypt,  $p < 0.005$ ) (Figure 5-3, B-C) (Table 5-1,2). This reduction in proliferation was also accompanied by significant reduction in average *Dusp6* transcripts per cell in small intestine ( $1.4 \pm 0.2$  vs  $5.3 \pm 0.2$ ,  $p < 0.05$ ) and colon ( $4.8 \pm 0.7$  vs  $9.1 \pm 1.1$ ,  $p < 0.05$ ) (Figure 5-3, E-F).

On the other hand, mice treated with low-dose trametinib ( $T_L$ ) had little effect ( $< 20\%$ ) on suppressing crypt proliferation in small intestine ( $39 \pm 5.3$  vs  $48 \pm 5$  BrdU positive cells per half crypt,  $p > 0.05$ ) and colon ( $15.3 \pm 1$  vs  $17 \pm 1$  BrdU positive cells per half crypt,  $p > 0.05$ ) (Figure 5-2, B-C). *Dusp6* transcripts per cell were slightly lower in both small intestine ( $3 \pm 0.2$  vs  $5 \pm 0.4$ ,  $p > 0.05$ ) and colon ( $6.6 \pm 0.6$  vs  $8.3 \pm 1.2$ ,  $p > 0.05$ ) (Figure 5-3, E-F). However, the reduction was not statistically significant.

While this study was useful to determine effect of different doses of trametinib on proliferation, it should be noted that this is a hyperplastic model and not a tumour model. One of the benefits of this model is its shorter latency. It would be prudent to confirm if the same dose dependent trend is observed in tumour models, as described in the next section.

### 5.1.2 Dose titration of trametinib in orthotopic transplantation model

To confirm if trametinib has a similar dose-dependent response in an established Ras driven CRC tumour, I studied the effects of different doses of trametinib in orthotopic transplantation models. There are two major reasons for choosing this model: Early experiments to study glucuronidation pathway were studied on intestinal organoids derived from Villin<sup>CreERT2</sup>; *Apc*<sup>fl/fl</sup> *Kras*<sup>G12D/wt</sup> *Trp53*<sup>fl/fl</sup> mice (Cong et al., 2023). Orthotopic transplantation of these organoid would allow us to further explore the glucuronidation pathway at a whole-organism level, whilst minimising variables. Secondly, difficulty in generating transgenic mice in sufficient numbers would cause a huge delay in completing the study.

C57/BL6J recipient mice were orthotopically transplanted with  $Apc^{fl/fl}$   $Kras^{G12D/wt}$   $p53^{fl/fl}$  organoids into the colonic sub-mucosae (Roper et al., 2017). Post confirmation of tumour by colonoscopy, mice were allocated into one of the following treatment groups - trametinib 0.4mg/kg ( $T_M$ ), trametinib 0.8mg/kg ( $T_S$ ) or Vehicle. Drugs were administered once daily by oral gavage for 5 days. BrdU (0.25ml, 10mM) was administered 2h before sampling at treatment endpoint.

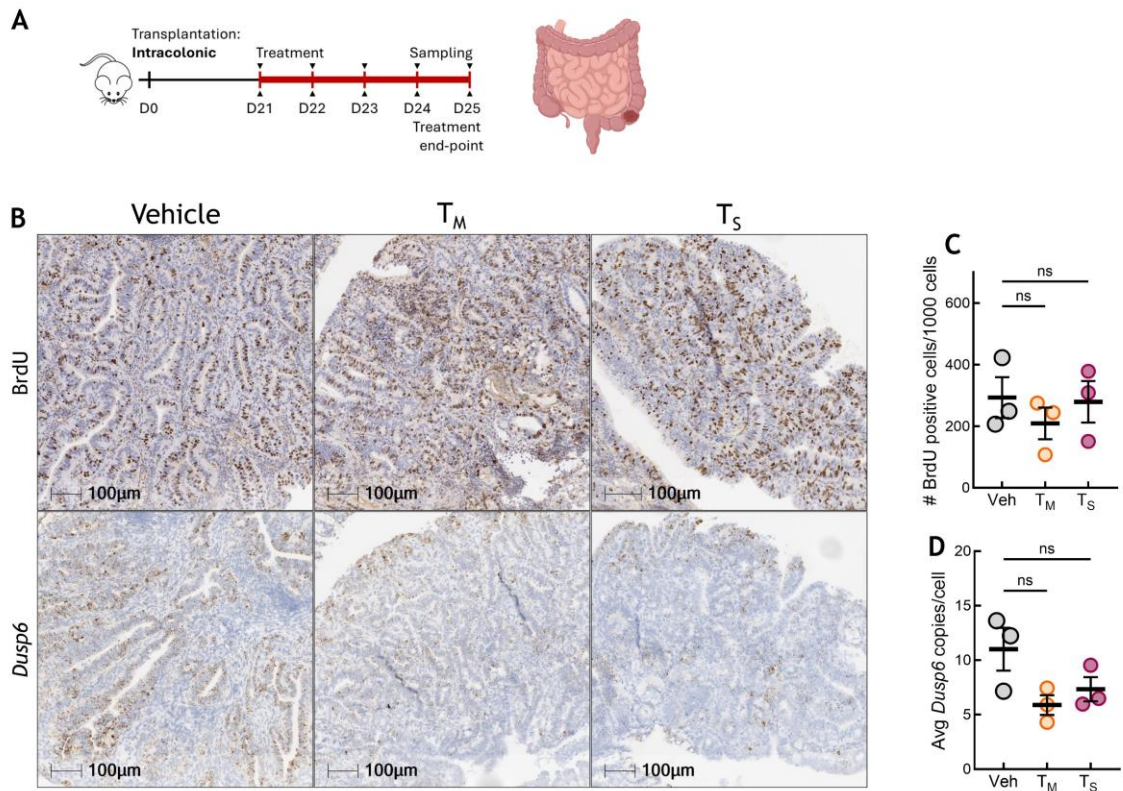


**Figure 5-4: Trametinib has a modest effect on suppressing proliferation in orthotopically transplanted model.**

C57BL/6J mice were intracolonicly transplanted with  $Apc^{fl/fl}$   $Kras^{G12D/wt}$   $Trp53^{fl/fl}$  intestinal organoids. Post tumour establishment mice were treated with different doses of Trametinib ( $T_M$ , 0.4mg/kg or  $T_S$ , 0.8 mg/kg) or Vehicle control for 5 days. 0.25ml BrdU was administered 2h before sampling at treatment endpoint. (A) Illustration of study plan. (B) Bright-field images of tumour stained with BrdU and Dusp6 RNAscope. (C) Number of BrdU positive cells per 1000 dysplastic cells. (D) Average number of Dusp6 transcripts per dysplastic cell. One-way ANOVA, Kruskal-Wallis test. Asterisks represent  $P$  values; ns  $P(>0.05)$ , \*  $P(<0.05)$ , \*\*  $P(<0.005)$ , \*\*\*  $P(<0.001)$ , and \*\*\*\*  $P(<0.0001)$ .

I assessed proliferation rate by scoring BrdU positive cells in the tumour area and measured Dusp6 transcript levels by RNAscope to assess MAPK status. Dusp6 transcript levels were 30 - 40% ( $T_S$  &  $T_M$ ) (Figure 5-4, B&D) lower in mice that received trametinib, but this reduction was not statistically significant. Moreover, the reduction in MAPK activity did not translate to reduction in proliferation of cells as mice that received trametinib had similar proliferation rate compared to Vehicle treated mice (280 vs 293 BrdU positive cells per 1000 dysplastic cells,  $p>0.05$ ,  $n = 3$ ) (Figure 5-4, B&C). These observations were quite interesting, and I chose this model to study how trametinib is metabolised within these tumours.

## 5.2 CRC Orthotopic transplantation for mass spec analysis of trametinib and its metabolites

To determine if concomitant HDAC inhibition (vorinostat) suppresses trametinib metabolism via glucuronidation, I utilised the orthotopic transplanted tumour model. Wildtype (C57BL/6) mice were intracolonicly transplanted with intestinal organoids derived from AKP-HOM mice (Section 3.3.2). Upon tumour confirmation by colonoscopy, mice were allocated into the following treatment groups: trametinib (T<sub>s</sub>, 0.8 mg/kg; n = 5), vorinostat (Vor, 50 mg/kg; n = 5), trametinib and vorinostat (T<sub>s</sub> + Vor, n = 5), or Vehicle (Veh, n = 5). The drugs were administered via oral gavage once daily for five days and mice were sampled at treatment endpoint for metabolite analysis.

I checked accumulation of unaltered trametinib in various tissues using LC-MS analysis. As known from several pharmacokinetics studies, liver consistently had the highest amount of trametinib, and its metabolites compared to other tissues (Figure 5-5, B&F). Corroborating our earlier studies (Cong et al., 2023), mice that received trametinib as a single agent had 40% lower levels of trametinib in the tumour compared to adjacent normal tissue (n = 6, p = 0.006, uncorrected Dunn's test) (Figure 5-4, A), suggesting higher drug clearance in tumour tissue. Addition of vorinostat led to an 80% increase in unaltered trametinib within the tumour (n = 6, p = 0.04, unpaired t-test). However, this increase in trametinib levels upon addition of vorinostat was not observed in other tissues such as adjacent normal tissue, liver and serum.

The first stage of trametinib metabolism involves deacetylation of the drug. With addition of vorinostat, we hoped to suppress deacetylation of trametinib, thereby increasing its unaltered levels within the tumours. Contrary to my supposition, mice that received trametinib and vorinostat combination had higher levels of deacetylated trametinib in liver, stool and colon tumour compared to mice that received single-agent trametinib (Figure 5-5, E-H). However, the levels of deacetylated trametinib was 20-fold lower than parent compound and represented only 2% of unaltered trametinib. While it was encouraging to observe that addition of vorinostat improves levels of trametinib within tumour tissue without affecting other tissues, it is necessary to determine if this translates to reduction in tumour burden and extension of survival in mice bearing *Apc/Kras/p53* driven intestinal tumours. I will be exploring this drug combination in our long-term/ intestinal tumor model.

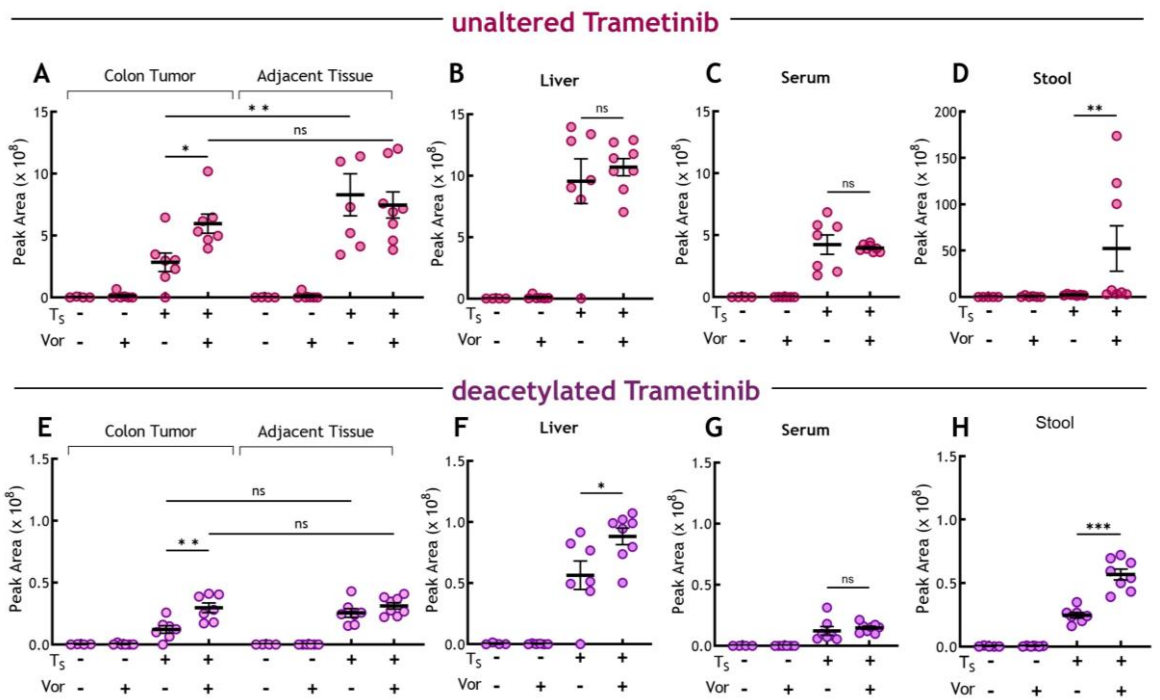


**Figure 5-5: LC-MS analysis revealed low-levels of Trametinib in colon tumour compared to adjacent normal intestine in mice that received trametinib as a single-agent.**

C57BL/6J mice were intracolonicly transplanted with *Apc<sup>fl/fl</sup> Kras<sup>G12D/wt</sup> Trp53<sup>fl/fl</sup>* intestinal organoids. Post tumour establishment mice were treated with Vehicle (Veh, n = 5) or Trametinib 0.2mg/kg (T<sub>L</sub>, n = 5) or vorinostat 50mg/kg (Vor, n = 5) or trametinib and vorinostat (T<sub>L</sub> + Vor, n = 5) once daily by oral gavage for 5 days. Mice were sampled at treatment endpoint and tissues were prepared for LC/MS analysis (described in 2.2.4.4)

Levels of unaltered trametinib (A - D) and deacetylated trametinib (E - H) in colon tumour, adjacent normal intestine, liver, serum and stool. Colon tumors have lower levels of trametinib compared to adjacent normal tissue (A). Addition of vorinostat improves levels of trametinib within the tumor without affect adjacent normal tissue and serum. One-way ANOVA, Kruskal-Wallis test. Asterisks represent *P* values; ns (>0.05), \* *P*<0.05, \*\* *P*<0.005, \*\*\* *P*<0.001, and \*\*\*\* *P*<0.0001).

### 5.3 Combination of trametinib and vorinostat in short-term model

We have established in Section 3.3.1, that treatment with low-dose trametinib (T<sub>L</sub>; 0.2mg/kg) has little effect on suppressing proliferation in intestinal crypts. I tested if concomitant HDAC inhibition with addition of vorinostat would further improve trametinib efficacy in our short-term model. AKP-HOM mice were induced as described in Chapter 2 on Day 0. Following transgene induction, mice were treated with low-dose (T<sub>L</sub>, 0.2mg/kg) with or without vorinostat (50mg/kg) for 3 days (Figure 5-6, A). Vehicle and vorinostat treated mice served as controls. BrdU (0.25ml, 10mM) was administered 2h before sampling at treatment endpoint. I chose this model due to its short latency. Proliferation rate was assessed by BrdU scoring and MAPK activity was assessed by measuring *Dusp6* transcript levels. Addition of vorinostat improved trametinib efficacy in the small intestine but not in the colon.

Mice that received combination of trametinib and vorinostat ( $T_L + Vor$ ) had 40% lower proliferation rate in the small intestinal crypts compared to mice that received trametinib as a single agent (27 vs 45 BrdU positive cells per crypt,  $p < 0.05$ ,  $n = 5$ ) (Figure 5-6, B&C). Interestingly, combination of trametinib and vorinostat had no effect in the colon, possibly due to tumor microenvironment, epigenetics or microbiome. Moreover, mice that received trametinib or vorinostat had similar proliferation rate to that of Vehicle treated mice. While it was encouraging to see that vorinostat was able to improve trametinib efficacy in our short-term hyperproliferative model, it was necessary to determine if this due to suppression of deacetylation of trametinib by vorinostat.

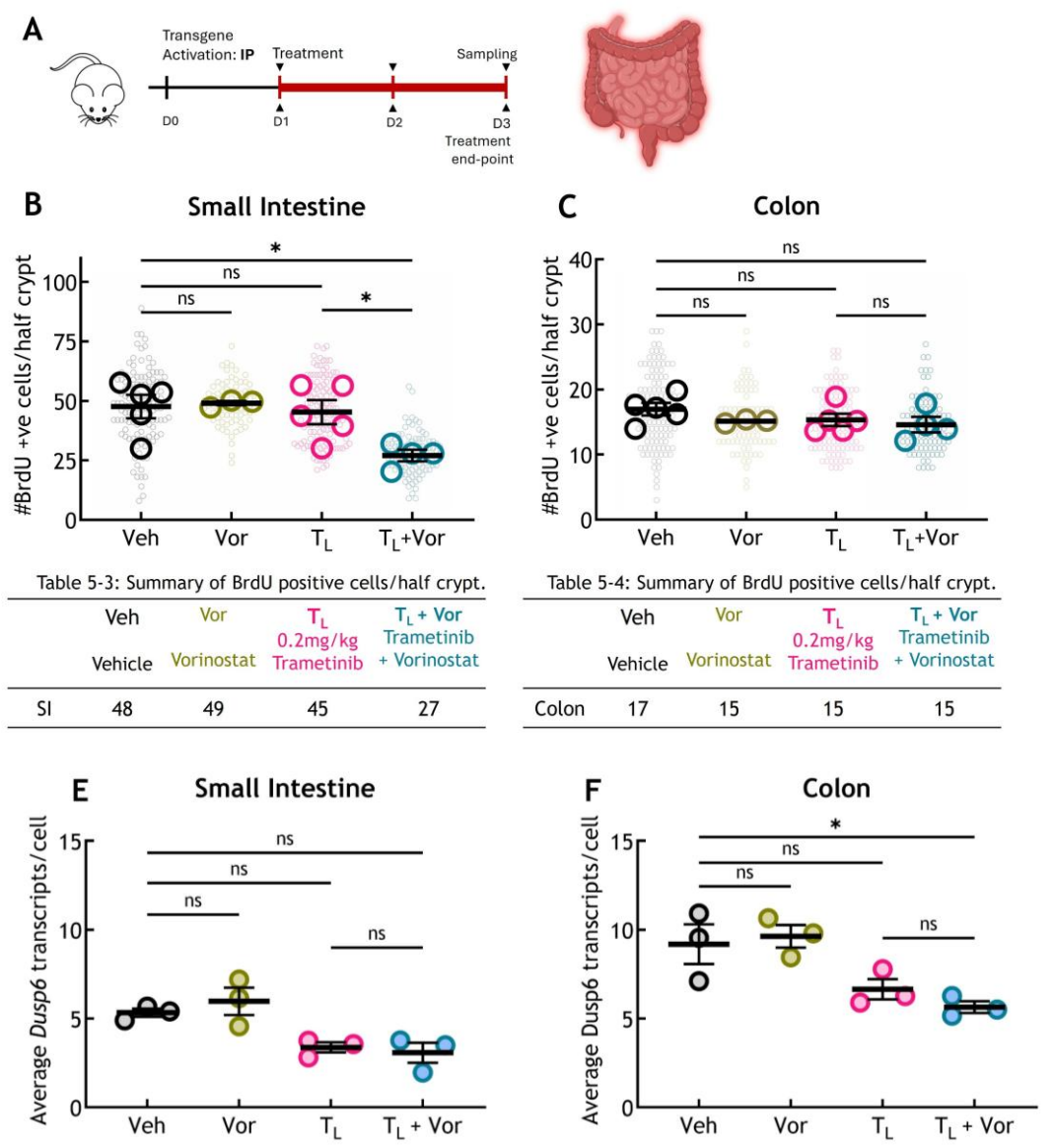


**Figure 5-6: Combination of Trametinib and vorinostat moderately suppresses proliferation in acute hyperplastic intestinal crypts.**

Mice were administered with 80mg/kg tamoxifen once on day0 and treated with Vehicle (Veh,  $n = 5$ ) or Trametinib 0.2mg/kg ( $T_L$ ,  $n = 5$ ) or vorinostat 50mg/kg (Vor,  $n = 3$ ) or Trametinib and vorinostat ( $T_L + Vor$ ,  $n = 4$ ) once daily by oral gavage for 3 days. (A) Illustration of study plan. BrdU positive cells per half crypt ( $n=25$ ) were quantified from, (B) small intestine, (C) Colon. Small dots represent single half crypts, large dots are biological replicates. Average Dusp6 transcripts per cell in (E) small intestine and (F) colon. One-way ANOVA, Kruskal-Wallis test. Asterisks represent  $P$  values; ns  $P(>0.05)$ , \*  $P(<0.05)$ , \*\*  $P(<0.005)$ , \*\*\*  $P(<0.001)$ , and \*\*\*\*  $P(<0.0001)$ .

## 5.4 Combination of trametinib and vorinostat in Long-term model

To determine if combination of trametinib and vorinostat confers survival advantage to mice predisposed to tumour formation, I tested combination of vorinostat with both standard- (0.8mg/kg) and low-dose trametinib (0.2mg/kg).

### 5.4.1 Combination of vorinostat and standard-dose trametinib offers no survival advantage

As discussed in section 3.2.3.2, AKP-HET mice treated with standard-dose trametinib ( $T_S$ , 0.8mg/kg) had 76% extension in survival compared to Vehicle treated mice (77.5 vs 44 days post induction,  $n = 8$ ,  $p < 0.0001$ , Mantel-Cox test) (Figure 5-7, B). This extension in

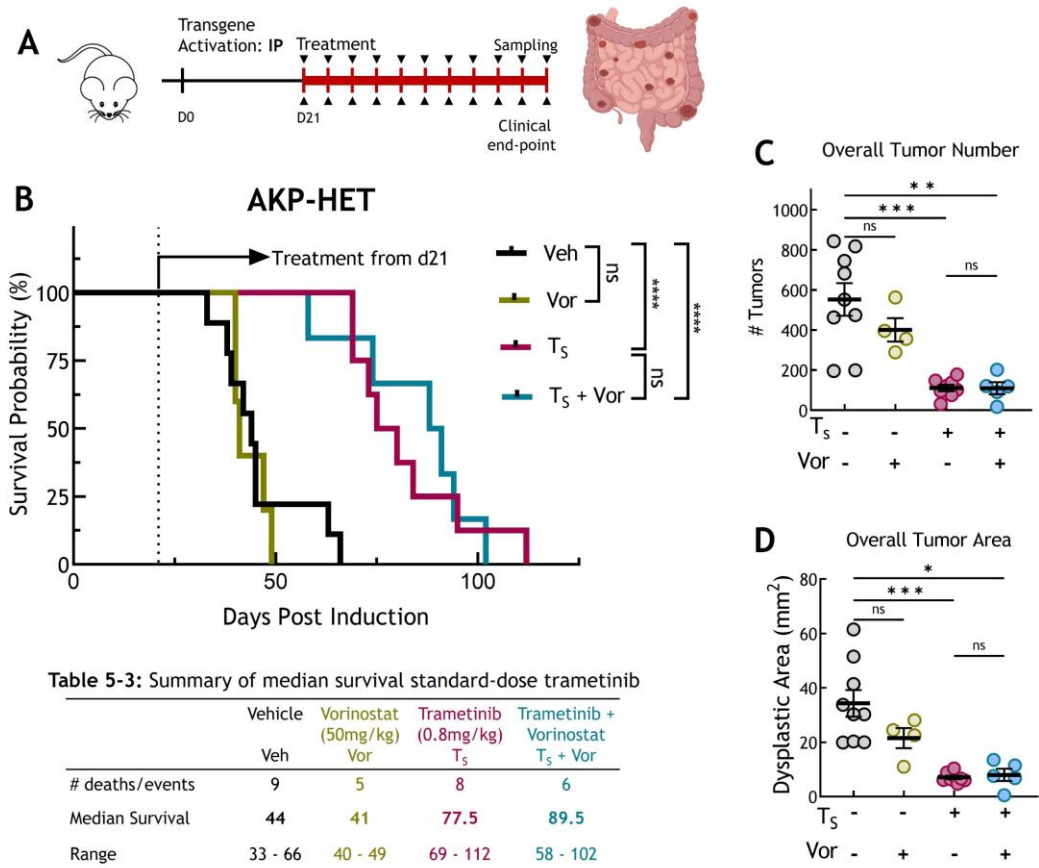


**Figure 5-7: Addition of vorinostat does not contribute to survival extension at standard-dose of Trametinib.**

(A) Illustration of study plan. (B) Survival curve of AKP-HET mice post transgene activation by Tamoxifen (80mg/kg; i.p). At Day 21 post induction, AKP-HET mice were treated with with Vehicle (black,  $n=9$ ) or vorinostat 50mg/kg (Vor, green,  $n = 4$ ) or standard-dose Trametinib 0.8mg/kg ( $T_S$ , dark pink,  $n = 8$ ) or combination of Trametinib and vorinostat ( $T_S + Vor$ , blue,  $n = 6$ ) by p.o, q.d and aged until clinical endpoint. Mice treated with Trametinib and vorinostat ( $T_S + Vor$ ) had similar median survival compared to mice that received Trametinib alone (MS: 89.5 vs 77.5,  $p>0.05$ , Log-rank (Mantel-Cox) test). Tumour burden quantified by calculating (C) overall tumour number, and (D) overall tumour area. One-way ANOVA, Kruskal-Wallis test. Asterisks represent  $P$  values; ns  $P(>0.05)$ , \*  $P(<0.05)$ , \*\*  $P(<0.005)$ , \*\*\*  $P(<0.001)$ , and \*\*\*\*  $P(<0.0001)$ .

survival was also coupled with regression in overall tumour burden. Mice treated with trametinib ( $T_S$ ) had markedly reduced overall tumour burden, specifically observed in reduction of small and medium sized tumours in small intestine and colon. However, 4 out of 8 mice ( $T_S$ ) had developed large adenocarcinomas in the small intestine. This suggested that while trametinib was able to resolve most of the tumours, some tumours escaped drug action representing drug resistant lesions. I sought to check if addition of vorinostat improved the outcomes noticed with trametinib as a single agent. Specifically, extension of survival coupled with regression of tumours.

AKP-HET mice that received vorinostat along with standard dose trametinib ( $T_S + Vor$ ) had a similar median survival compared to mice that received trametinib ( $T_S$ ) as a single agent (Median survival: 89.5 vs 77.5 days post induction,  $n = 6$ ,  $p > 0.05$ , Mantel-Cox test) (Figure 5-7, B).

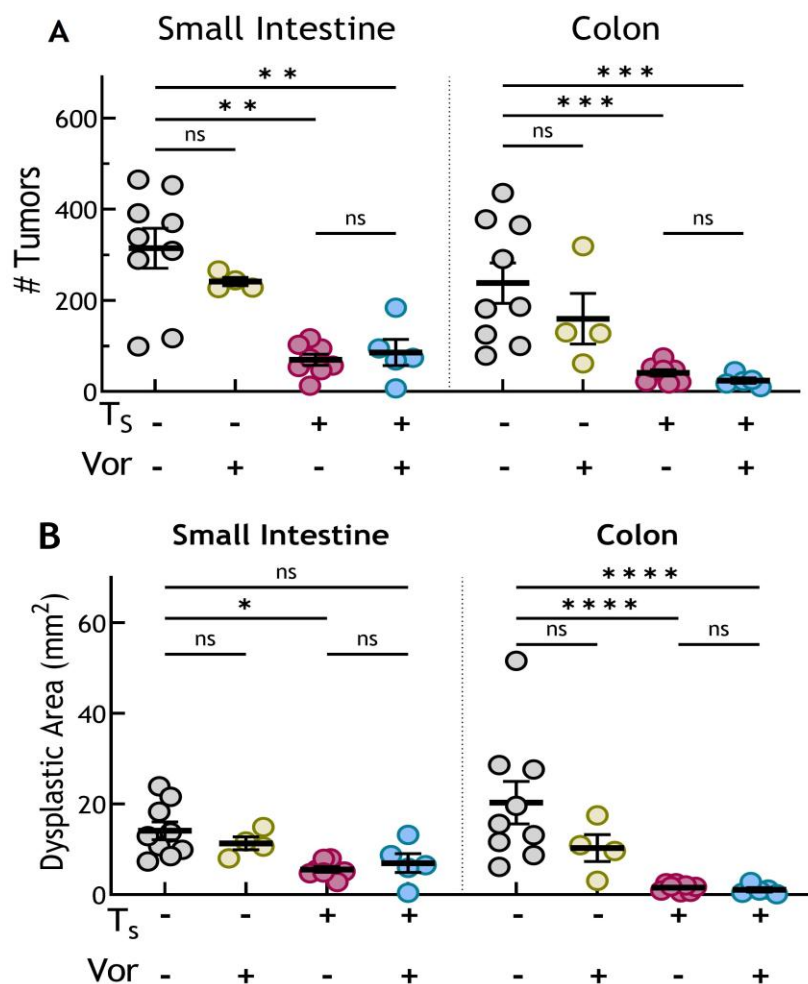


**Figure 5-8: Addition of vorinostat has no additional impact on tumour burden at standard-dose of Trametinib.**

AKP-HET mice were treated with Vehicle (black,  $n=9$ ) or vorinostat 50mg/kg (Vor, green,  $n = 4$ ) or standard-dose Trametinib 0.8mg/kg ( $T_S$ , dark pink,  $n = 8$ ) or combination of Trametinib and vorinostat ( $T_S + Vor$ , blue,  $n = 6$ ) once daily by oral gavage from day 21 post induction and aged until clinical end-point. Mice treated with Trametinib and vorinostat ( $T_S + Vor$ ) had similar tumour burden compared to mice that received Trametinib alone. Tumour burden quantified in small intestine and colon by (B) total number of tumours, and (C) total dysplastic area. One-way ANOVA (Kruskal-Wallis) test. Asterisks represent  $P$  values; ns  $P(>0.05)$ , \*  $P(<0.05)$ , \*\*  $P(<0.005)$ , \*\*\*  $P(<0.001)$ , and \*\*\*\*  $P(<0.0001)$ .

Overall tumour burden was similar in mice that received trametinib with or without vorinostat. Like what was observed in T<sub>S</sub> treated mice, colonic tumours better responded treatment compared to small intestinal tumours. 3 out of 5 mice developed adenocarcinomas in the small intestine (Figure 5-9, D).

RZA027.1c - pT3, moderately differentiated, invasive carcinoma, less desmoplasia.  
 RZA025.5b - pT4, moderate-poorly differentiated, invasive carcinoma, less desmoplasia.  
 RZA027.1a - pT4, invasive carcinoma, less nuclear pleomorphism. We inferred that the reason we were not able to see survival advantage or improvement in tumour regression was because trametinib dosage was already at optimum levels. I wondered if vorinostat addition would be synergistic at low-dose trametinib.

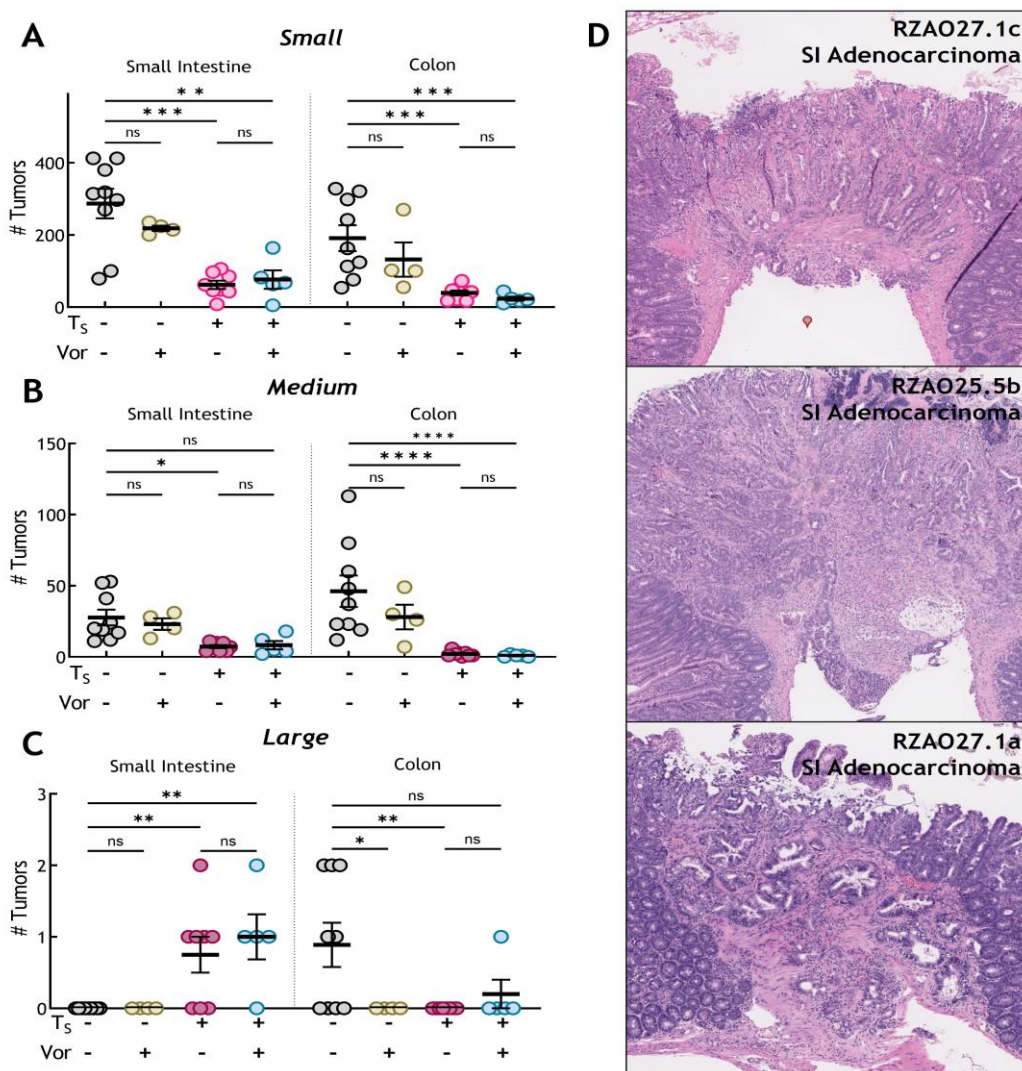


**Figure 5-9: Emergence of drug-resistant lesions is observed in the small intestine of AKP-HET mice**

AKP-HET mice were treated with Vehicle (black, n=9) or vorinostat 50mg/kg (Vor, green, n = 4) or standard-dose Trametinib 0.8mg/kg (T<sub>S</sub>, dark pink, n = 8) or combination of Trametinib and vorinostat (T<sub>S</sub> + Vor, blue, n = 6) once daily by oral gavage from day 21 post induction and aged until clinical end-point. Mice treated with Trametinib and vorinostat (T<sub>S</sub> + Vor) had similar tumour burden compared to mice that received Trametinib alone. Tumour burden quantified in small intestine and colon by (B) total number of tumours, and (C) total dysplastic area. (D) Bright-field images of H&E images of advanced adenocarcinoma. One-way ANOVA (Kruskal-Wallis) test. Asterisks represent P values; ns (P>0.05), \* P(<0.05), \*\* P(<0.005), \*\*\* P(<0.001), and \*\*\*\* P(<0.0001).

## 5.4.2 Combination of vorinostat and low-dose trametinib improves survival

As discussed in section 3.2.3.2, AKP-HET mice treated with low-dose trametinib ( $T_L$ , 0.2mg/kg) had modest survival extension (40%) when compared to Vehicle treated mice (Median Survival = 61 vs 44 days post induction,  $n = 7$ ,  $p > 0.05$ , Mantel-Cox test). Mice sampled at clinical endpoint exhibited significant intestinal tumour burden (average 400 intestinal tumours) while most of them were smaller in size ( $<0.01\text{m}^2$ ).

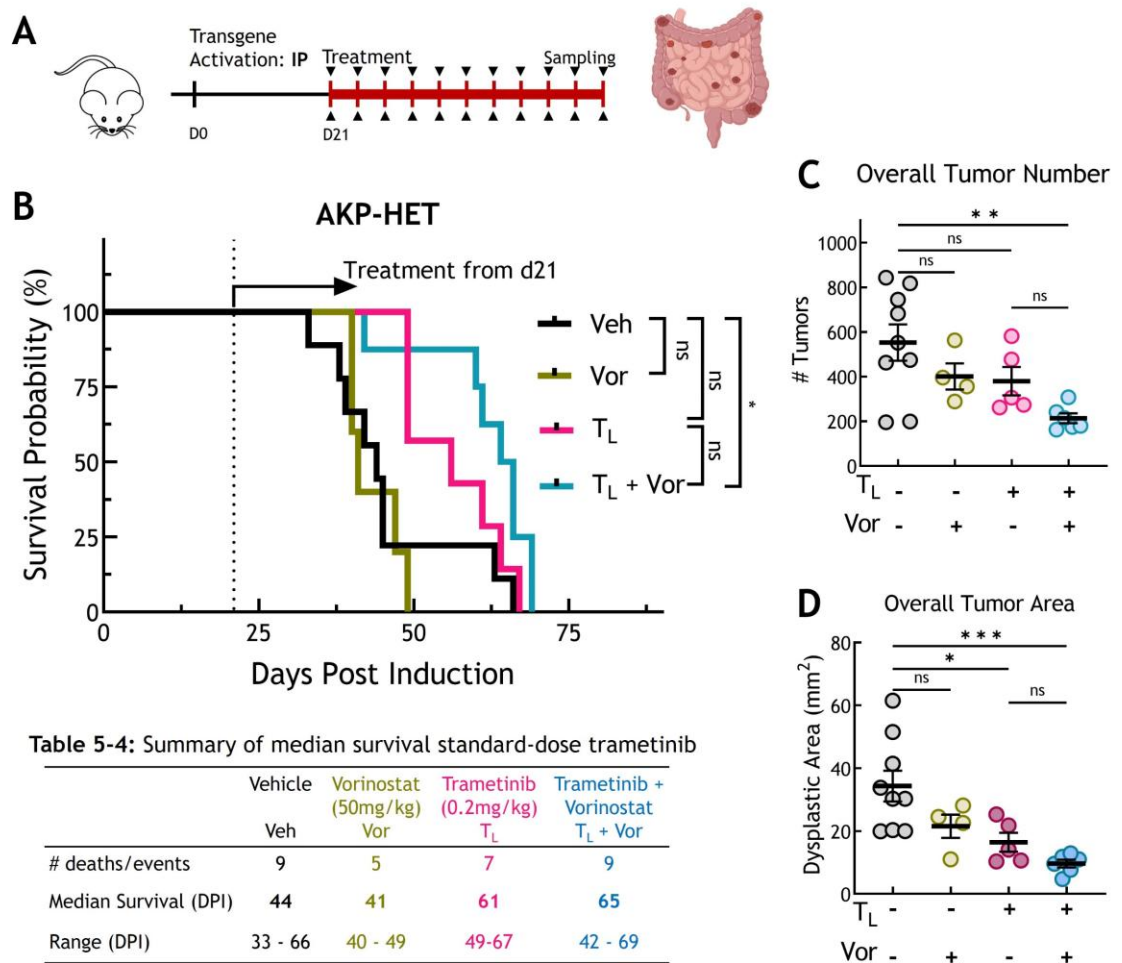


**Figure 5-10: Addition of vorinostat has a modest impact on extension of survival at low-dose Trametinib**

(A) Illustration of study plan. (B) Survival curve of AKP-HET mice post transgene activation by Tamoxifen (80mg/kg; i.p.). At Day 21 post induction, AKP-HET mice were treated with Vehicle (black,  $n=9$ ) or vorinostat 50mg/kg (Vor, green,  $n = 4$ ) or low-dose Trametinib 0.8mg/kg ( $T_L$ , light pink,  $n = 7$ ) or combination of Trametinib and vorinostat ( $T_L + Vor$ , light blue,  $n = 9$ ) by p.o, q.d and aged until clinical endpoint. Mice treated with Trametinib and vorinostat ( $T_L + Vor$ ) had similar median survival compared to mice that received Trametinib alone (MS: 61 vs 65,  $p>0.05$ , Log-rank (Mantel-Cox) test). Tumour burden quantified by calculating (C) overall tumour number, and (D) overall tumour area. One-way ANOVA Kruskal Wallis test. Asterisks represent  $P$  values; ns  $P(>0.05)$ , \*  $P(<0.05)$ , \*\*  $P(<0.005)$ , \*\*\*  $P(<0.001)$ , and \*\*\*\*  $P(<0.0001)$ .

Mice treated with low-dose trametinib and vorinostat ( $T_L + Vor$ ) had a modest yet significant extension in survival (47%) compared to Vehicle treated mice (Median Survival:

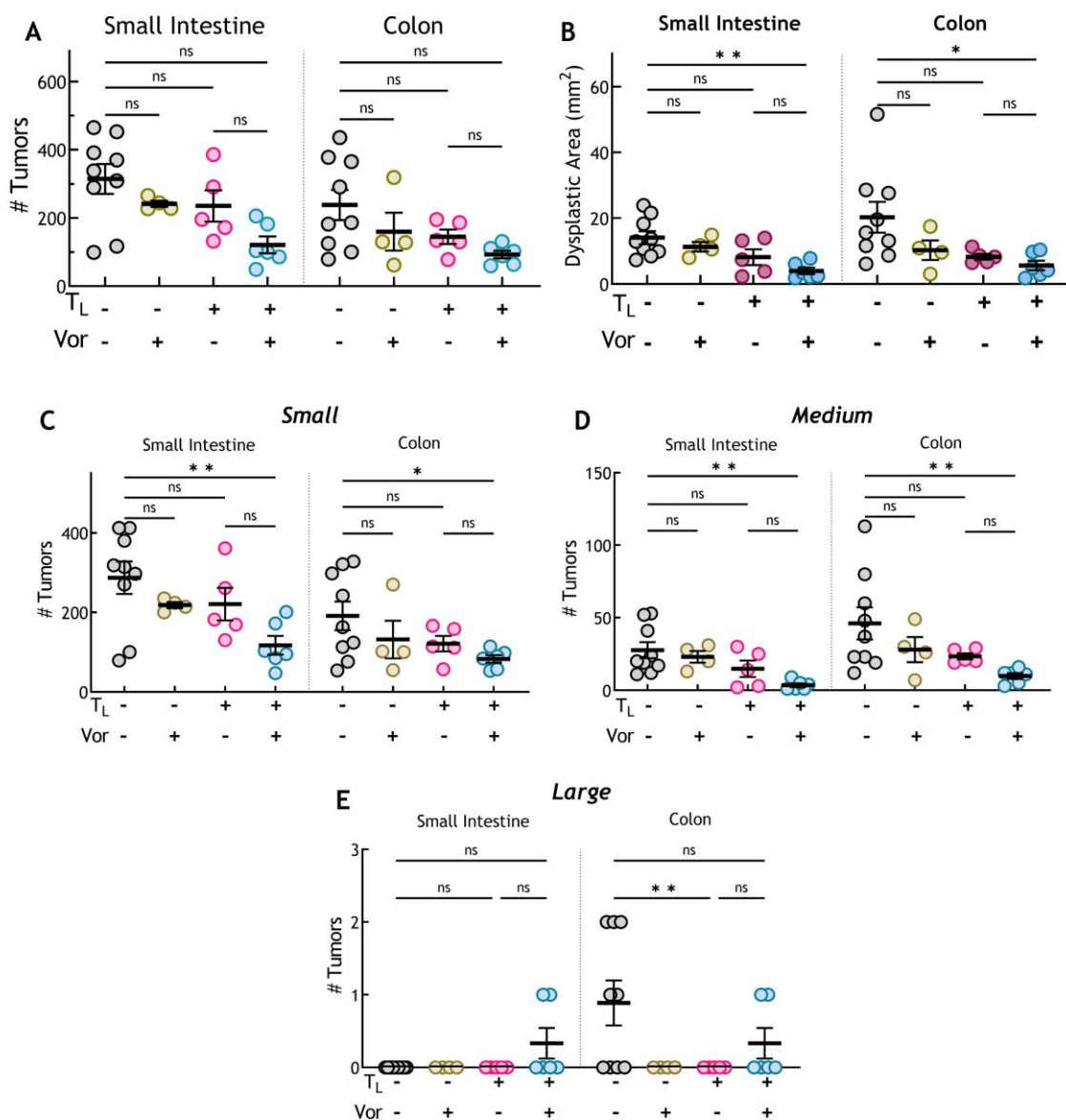


**Figure 5-11: Addition of vorinostat has a modest impact on reduction in tumour burden at low-dose Trametinib.**

AKP-HET mice were treated with Vehicle (black, n=9) or vorinostat 50mg/kg (Vor, green, n = 4) or low-dose Trametinib 0.2mg/kg (TL, light pink, n = 7) or combination of Trametinib and vorinostat (TL + Vor, blue, n = 5) once daily by oral gavage from day 21 post induction and aged until clinical end-point. Mice treated with Trametinib and vorinostat (TL + Vor) had a slightly lower tumour burden compared to mice that received Trametinib alone. One-way ANOVA (Kruskal-Wallis) test. Asterisks represent P values; ns P(>0.05), \* P(<0.05), \*\* P(<0.005), \*\*\* P(<0.001), and \*\*\*\* P(<0.0001).

65 vs 44 days post induction, n = 9, p = 0.03, Log rank test) (Figure 5-8, B). However, median survival was similar to mice that received only trametinib (TL). A reduction in overall tumour burden was also noted in mice that received combination treatment (Figure 5-10, C&D). This reduction in overall tumour burden was contributed by reduction in tumours in the small intestine and colon (Figure 5-9, A-E). While most of the tumours regressed, adenocarcinoma was also noted in mice that received drug combination, suggesting resistance to combination treatment.

## 5.5 Discussion

Resistance to therapy remains one of the most pressing challenges in the treatment of Ras-driven colorectal cancer (CRC). Using *Drosophila* and mouse intestinal organoids, we previously uncovered that glucuronidation—a critical toxin clearance pathway—is upregulated in Ras/Apc/P53-driven CRCs (Cong et al., 2023). Our findings demonstrated that trametinib undergoes metabolism via a two-step process: deacetylation followed by glucuronidation, mirroring observations from studies conducted on CRC patients (Ho et al., 2014). Importantly, we showed that blocking the deacetylation of trametinib using an HDAC inhibitor, vorinostat, effectively suppressed its metabolism.

In this chapter, I explored whether our observations in *Drosophila* and intestinal organoids are recapitulated in mouse models of CRC. LC/MS analysis revealed that AKP colon tumours had lower levels of trametinib compared to adjacent normal tissue (Figure 5-4). Notably, the addition of vorinostat improved trametinib levels within the tumour without affecting other tissues, such as adjacent normal tissue, liver, or serum. This confirms that glucuronidation is upregulated in the tumor tissues and not in other normal tissues. I have also shown that Vorinostat is able to enhance the therapeutic index of trametinib by selectively increasing its availability in tumour tissues.

To further assess whether improved availability of trametinib translates into a better response to MEK inhibition, I considered the pharmacokinetics and half-life of trametinib. Following oral dosing, trametinib has a half-life of approximately four days and is associated with acute toxicities such as rash, diarrhea, fatigue, and liver injury (Welsh and Corrie, 2015). Given this profile, there is a potential risk of exacerbated toxicities if vorinostat increases the circulation of unaltered trametinib in the body. To mitigate this risk, I designed two combinatorial treatment strategies: one with low-dose trametinib and the other with standard-dose trametinib, both in conjunction with vorinostat.

My findings indicate that the improvement in trametinib response is dependent on the stage of the tumour model being studied. In our short-term models, which represent the pre-adenoma stage, the combination of trametinib and vorinostat showed a stronger suppression of proliferation compared to single-agent trametinib, particularly in small intestinal crypts. While this response is promising, it is crucial to determine if a similar effect is observed in more established intestinal tumour models.

In the AKP-HET intestinal tumour models, mice treated with vorinostat and standard-dose trametinib demonstrated a modest survival benefit; however, this extension was not statistically significant. Additionally, treatment arms were underpowered to detect true statistical significance. Notably, mice that survived longer on the combination regimen

also developed adenocarcinomas in the small intestine, suggesting that these treatment-resistant lesions may be independent of the MAPK pathway.

Conversely, intestinal tumour models treated with the low-dose trametinib combination, while not yielding significant survival extensions, showed a marked reduction in tumour burden in terms of both number and area. Mice in this group lived slightly longer, although it is important to note that the study is currently ongoing and underpowered.

Overall, I have identified a drug resistance mechanism and investigated how it can potentially be overcome. While the addition of vorinostat improved the levels of trametinib within the tumours, its impact on reducing tumour burden and enhancing survival was modest. This underscores the complexity of drug resistance in Ras-driven CRC and suggests that further studies are needed to optimize combinatorial therapeutic strategies.

## Chapter 6 Discussion and Outlook

Nearly half of colorectal cancers (CRCs) harbor mutations in the KRAS gene, which significantly limits the effectiveness of standard treatment options (Jones et al., 2017, Yoon et al., 2014). Patients with KRAS mutations poorly respond to targeted therapies, particularly anti-EGFR agents and immune checkpoint inhibitors. In advanced disease, KRAS mutations are associated with worse progression-free survival (PFS) and serve as negative predictors for responses to epidermal growth factor receptor (EGFR) inhibitors (Henry et al., 2021, Modest et al., 2016). Despite several clinical studies, there remains a considerable unmet need for patients with KRAS-mutant cancers, particularly in CRC. Although recent developments of drugs that target KRAS<sup>G12C</sup> have emerged, the majority of KRAS oncoproteins remain undruggable.

The KRAS<sup>G12C</sup> mutation is most prevalent in lung adenocarcinomas (14%), followed by colorectal tumours (5%). Results from phase I/II clinical trials using KRAS<sup>G12C</sup> inhibitors, such as Sotorasib (NCT04303780; CodeBreak 200) and Adagrasib (NCT03785249; KRYSTAL-1), have demonstrated significant responses in about half of lung cancer patients but not in colon cancer patients (de Langen et al., 2023, Yaeger et al., 2023). This discrepancy raises questions about whether these differential responses are a consequence of differences in MAPK dependency of KRAS mutant colorectal cancer.

My thesis research leverages *Drosophila* and mouse models to dissect the cellular and molecular underpinnings of CRC, driven by oncogenic Ras signalling. Here are some of the key observations that emerge from my thesis:

### 6.1 Oncogenic Ras signalling perturbs intestinal homeostasis

In *Drosophila*, oncogenic Ras signalling is sufficient to induce a rapid expansion of the hindgut hyperproliferation zone. Additional mutations in *apc<sup>Ri</sup>* and *p53<sup>Ri</sup>*, as observed in compound mutants, also contribute to this hyperproliferative phenotype (Figure 3-1). This disruption of hindgut homeostasis ultimately results in lethality as the larvae continue to develop to adulthood.

In contrast to our *Drosophila* model, loss of **Apc** is necessary for the disruption of intestinal homeostasis in the mouse model. Oncogenic **Kras** (*Kras<sup>G12D/wt</sup>*) and loss of **p53** (*p53<sup>fl/fl</sup>*) alone are insufficient to perturb intestinal homeostasis. Therefore, all my mouse studies were conducted within a hyperactivated Wnt background.

Our short-term mouse models simulate acute transgene activation, akin to the Big Bang theory of CRC initiation and progression. The acute loss of **Apc** resulted in a doubling of

the proliferation rate in intestinal crypts compared to wild-type controls. Further activation of oncogenic **Kras** drove a rapid hyperproliferation throughout the intestine, leading to a 300% increase in proliferation rate across the intestinal crypts. Due to the disruption of intestinal homeostasis and the severity of the phenotype, these mice were sampled three days post-transgene activation (Figure 3-4).

Loss of **p53** has been implicated in uncontrolled proliferation due to impaired cell-cycle checkpoints and apoptosis. Interestingly, the further loss of **p53** in our short-term model did not result in an increase in proliferation; rather, these crypts exhibited slightly reduced proliferation compared to their wild-type counterparts. This difference was only noted in the small intestine, not in the colon (Figure 3-4).

Given that this is an acute model with a brief time interval between transgene activation and sampling, it likely represents pathway dynamics and tissue dependencies at very early stages of tumour development.

## 6.2 Oncogenic Kras accelerates tumour development in the mouse colon

In our long-term model, transgene activation leads to the formation of multiple tumours throughout the entire intestine. The loss of **Apc** is a prerequisite for tumour development within the intestinal tract. Tumours predominantly arise in the small intestine, with occasional occurrences of colonic polyps (Figure 3-5). Oncogenic **Kras** significantly increases the overall tumour burden and reduces survival by more than 50%. Notably, the formation of tumours is primarily observed in the colon, indicating a critical role for oncogenic **Kras** in colon tumour development (Figure 3-6). Additionally, further loss of **p53** accelerates tumourigenesis across the entire intestine, underscoring the importance of signalling pathways in intestinal tumour development (Figure 3-7).

## 6.3 Oncogenic Kras does not accelerate proliferation in established colon tumours in mice

In our colon tumour model, spatially resolved **Cre** recombination in the colon leads to the formation of a single tumour. Interestingly, the proliferation rates remain comparable across **A-**, **AK-**, and **AKP** colon tumours, despite evidence of increased **MAPK** signaling, as indicated by elevated **Dusp6** transcript levels.

## 6.4 Genetically complex Ras-driven tumours are resistant to MAPK suppression

Our studies in *Drosophila* and mice align with findings reported by several groups, highlighting that drug resistance is an emergent characteristic of genetically complex tumours. This is particularly evident in colorectal cancer, which is highly complex and heterogeneous. As discussed in the previous section, oncogenic Ras signaling disrupts intestinal homeostasis in the larval hindgut. Unless homeostasis is restored, larvae fail to survive to adulthood.

In our experiments, MEK inhibition with trametinib effectively rescues single mutant (Ras alone) larvae, but not genetically complex larvae (Ras-Apc-p53). Moreover, resistance to trametinib was observed in patient-specific *Drosophila* avatars containing additional passenger mutations alongside Ras, Apc, and p53.

## 6.5 MAPK dependency changes during the course of tumour development in mice

In *Kras*<sup>G12D/wt</sup>-driven hyperproliferative crypts, early intervention with MEK inhibition post-transgene activation can suppress proliferation, albeit modestly. However, this suppression diminishes if the treatment onset is delayed, as observed in our colon tumour model, where MEK inhibition ultimately fails to reduce proliferation rates.

## 6.6 Tumour microenvironment impacts response to MAPK suppression

In our long-term models, trametinib treatment significantly reduces the colonic tumour burden in both *Kras*-driven models (AK- and AKP-HET), regardless of p53 status. This reduction in tumour burden is dose-dependent, with both tumour number and size decreasing in proportion to the dosage in both AK- and AKP-HET mice. There is a direct correlation between the extent of tumour reduction and increased survival. Conversely, the response of small intestinal tumours varies.

In AK-HET mice, small intestinal tumours not only increased in number but also in size under trametinib treatment, indicating signs of tumour progression compared to vehicle-treated mice. In contrast, AKP-HET mice displayed a significantly lower tumour burden in the small intestine. Notably, about half of the trametinib-treated AKP-HET mice developed a large adenocarcinoma in the small intestine. It remains unclear whether these lesions initiated before or after the onset of treatment, suggesting potential intrinsic or acquired resistance to MEK inhibition.

It is important to note that these tumours, while differing in location, share the same genetic background and originate from the same site—intestinal crypts. Regional differences in tumour response may be attributed to variations in Wnt signalling levels across different segments of the intestine. (Leedham et al., 2013) reported an intestinal gradient of Wnt and stem cell modulators in murine and human intestines, showing an inverse gradient of the Wnt agonist *Sfrp2* between species. Wnt agonists are notably lower in the colon compared to the small intestine in mice, which could explain the disparate responses of small intestinal tumours compared to colonic tumours. These findings suggest further investigations are needed to clarify the role of Wnt and stem cell modulators in our models.

## 6.7 Colon tumours evade drug response by upregulating a toxin-clearance pathway

LC/MS analysis conducted on our trametinib-resistant *Drosophila* model (*ras-apc-p53* flies) indicated an upregulation in metabolites associated with the glucuronidation pathway. Glucuronidation, a primary mechanism for drug metabolism and clearance, typically occurs in the liver and involves a large family of enzymes known as UDP-glucuronosyltransferases (UGTs). This pathway is responsible for the metabolism of over 70 therapeutic agents and has been implicated as a potential mechanism of anticancer drug resistance, including in colon cancer. However, the complexity of this pathway and the diversity of UGTs involved have historically rendered them challenging targets for intervention.

Our recent findings (Cong et al., 2023) demonstrated that tumours in the trametinib-resistant fly models (*byn<sup>ts</sup>* > *ras<sup>G12V</sup> apc<sup>Ri</sup> p53<sup>Ri</sup>* or RAP) exhibited elevated glucuronidation activity. This process facilitates the rapid clearance of drugs from the body, including trametinib, which undergoes metabolism primarily through deacetylation followed by glucuronidation (Ho et al., 2014). Our experimental interventions targeting HDAC1-mediated deacetylation using vorinostat have successfully reversed trametinib resistance in both fly and intestinal organoid models. This suggests a conserved resistance mechanism across KRAS/APC/TP53 CRC models, highlighting potential clinical implications.

Further exploratory studies were conducted in mouse models of CRC to determine if similar patterns were observable. LC/MS analysis of AKP colon tumours revealed lower levels of trametinib compared to adjacent normal tissue (Figure 5-4). Interestingly, co-administration of vorinostat selectively increased trametinib concentrations within tumour tissues without affecting normal adjacent tissue, liver, or serum levels. This

indicates that vorinostat may enhance the therapeutic efficacy of trametinib by increasing its bioavailability specifically within tumour cells.

Further investigations whether enhanced intratumoural concentration of trametinib translates to improved tumour response, suggest a synergistic effect in our short-term models, which represent pre- or early adenoma stages immediately following transgene activation. However, the extension of survival observed in our long-term tumour models was modest. This raises important questions about the efficacy of this combination therapy in established colon tumours and warrants further investigation to understand the underlying resistance mechanisms.

Throughout this thesis, a consistent theme has emerged: the challenge of drug resistance in Ras-driven CRC. My investigations revealed that the mechanisms of resistance are not merely a consequence of specific mutations, but also involve complex regulatory pathways such as the glucuronidation pathway that governs drug metabolism. By characterizing the pharmacokinetics of trametinib and its metabolites, I highlighted the need for strategies that enhance drug accumulation in tumours while minimizing systemic toxicity.

The combined treatment strategies employed in my studies offer promising avenues for future exploration. The differential responses observed between short-term and long-term models underscore the importance of context in drug efficacy. It is evident that a deeper understanding of the signalling networks involved in drug resistance is necessary to devise more effective therapeutic regimens. While response to early-stage tumours may inform on important processes in tumour formation, the most clinically relevant setting is the treatment of established tumours at late stage. In late-stage tumours we see resistance to targeted therapy. A deeper understanding of late-stage tumours is necessary to unravel more clinically relevant targeting approaches.

## **OUTLOOK**

To build upon the foundational insights gained from this research, I propose the following future experiments designed to deepen our understanding of tumour dynamics.

### **1. Further Investigations into Late-Stage Adenomas and Drug Resistance Mechanisms**

Our colon tumour model effectively mimics drug resistance as observed clinically. Despite significant MAPK pathway suppression by trametinib, these fully established colon tumours continue to proliferate. Previously, I highlighted changes in Wnt signalling contingent upon p53 status. While immunohistochemistry and in situ hybridization have provided a broad overview of signalling pathways and key targets within the tumour, a

more granular analysis is needed. Single-cell sequencing or spatial analysis of A-, AK-, and AKP-colon tumours treated with trametinib could elucidate the interactions between various epithelial and mesenchymal cell populations that contribute to the evasion of drug responses.

## 2. Investigation on the role of tumour microenvironment in drug response.

Our long-term intestinal tumour model has demonstrated differential responses to MAPK suppression by trametinib in small intestinal versus colon tumours. Specifically, Kras-driven colon tumours showed a significant reduction in tumour burden regardless of p53 status. In contrast, the response in small intestinal tumours was inconsistent; those with functional p53 (AK-HET) showed no reduction in tumour burden, whereas those lacking p53 (AKP-HET) exhibited overall reduction but some progressed to adenocarcinomas. This suggests a heterogeneous tumour response to pathway suppression. A limitation of this model is the variable timing of tumour development post-tamoxifen induction, complicating the determination of tumour stage at the clinical endpoint.

To overcome this, we could study spontaneous small intestinal tumours in AK- and AKP-HOM mice, which develop tumours due to leaky Cre activity. Monitoring these mice for clinical signs such as anaemia, which indicates spontaneous tumour development, and enrolling them into treatment groups upon confirmation could help refine treatment plan. Comparing these spontaneous small intestinal tumours to colon tumours induced by intracolonic tamoxifen could highlight differences in late-stage tumour behaviors.

## 3. Investigation on the role of clonal dynamics on drug response using orthotopic transplantation model.

The tumour models discussed in my thesis, while genetically complex, do not exhibit the clonal heterogeneity seen in human colorectal cancers (CRCs). Our studies have focused on genetically homogeneous tumours; thus, understanding the response of a mixed clonal population to therapy could provide new insights into drug resistance mechanisms.

An initial method to explore this could involve orthotopic transplantation of a mix of labeled AK- and AKP-intestinal organoids in equal proportions. Following confirmation of tumour establishment via colonoscopy, treatment could commence. This approach would allow us to assess how multiclonal tumours respond to therapy and potentially guide the development of more effective treatment strategies.

These proposed studies will enhance our understanding of drug resistance mechanisms, the influence of the tumour microenvironment on therapy outcomes, and the impact of clonal diversity on treatment efficacy, thereby informing future therapeutic strategies for CRC.

## 7 Bibliography

- ANDREU, P., COLNOT, S., GODARD, C., GAD, S., CHAFEY, P., NIWA-KAWAKITA, M., LAURENT-PUIG, P., KAHN, A., ROBINE, S., PERRET, C. & ROMAGNOLO, B. 2005. Crypt-restricted proliferation and commitment to the Paneth cell lineage following *Apc* loss in the mouse intestine. *Development*, 132, 1443-51.
- ANDREYEV, H. J., NORMAN, A. R., CUNNINGHAM, D., OATES, J., DIX, B. R., IACOPETTA, B. J., YOUNG, J., WALSH, T., WARD, R., HAWKINS, N., BERANEK, M., JANDIK, P., BENAMOUZIG, R., JULLIAN, E., LAURENT-PUIG, P., OLSCHWANG, S., MULLER, O., HOFFMANN, I., RABES, H. M., ZIETZ, C., TROUNGOS, C., VALAVANIS, C., YUEN, S. T., HO, J. W., CROKE, C. T., O'DONOGHUE, D. P., GIARETTI, W., RAPALLO, A., RUSSO, A., BAZAN, V., TANAKA, M., OMURA, K., AZUMA, T., OHKUSA, T., FUJIMORI, T., ONO, Y., PAULY, M., FABER, C., GLAESENER, R., DE GOEIJ, A. F., ARENDS, J. W., ANDERSEN, S. N., LÖVIG, T., BREIVIK, J., GAUDERNACK, G., CLAUSEN, O. P., DE ANGELIS, P. D., MELING, G. I., ROGNUM, T. O., SMITH, R., GOH, H. S., FONT, A., ROSELL, R., SUN, X. F., ZHANG, H., BENHATTAR, J., LOSI, L., LEE, J. Q., WANG, S. T., CLARKE, P. A., BELL, S., QUIRKE, P., BUBB, V. J., PIRIS, J., CRUICKSHANK, N. R., MORTON, D., FOX, J. C., AL-MULLA, F., LEES, N., HALL, C. N., SNARY, D., WILKINSON, K., DILLON, D., COSTA, J., PRICOLO, V. E., FINKELSTEIN, S. D., THEBO, J. S., SENAGORE, A. J., HALTER, S. A., WADLER, S., MALIK, S., KRTOLICA, K. & UROSEVIC, N. 2001. Kirsten ras mutations in patients with colorectal cancer: the 'RASCAL II' study. *Br J Cancer*, 85, 692-6.
- AWAD, M. M., LIU, S., RYBKIN, I. I., ARBOUR, K. C., DILLY, J., ZHU, V. W., JOHNSON, M. L., HEIST, R. S., PATIL, T., RIELY, G. J., JACOBSON, J. O., YANG, X., PERSKY, N. S., ROOT, D. E., LOWDER, K. E., FENG, H., ZHANG, S. S., HAIGIS, K. M., HUNG, Y. P., SHOLL, L. M., WOLPIN, B. M., WIESE, J., CHRISTIANSEN, J., LEE, J., SCHROCK, A. B., LIM, L. P., GARG, K., LI, M., ENGSTROM, L. D., WATERS, L., LAWSON, J. D., OLSON, P., LITO, P., OU, S.-H. I., CHRISTENSEN, J. G., JÄNNE, P. A. & AGUIRRE, A. J. 2021. Acquired Resistance to KRAS<sup>G12C</sup> Inhibition in Cancer. *New England Journal of Medicine*, 384, 2382-2393.
- BACA, S. C., PRANDI, D., LAWRENCE, M. S., MOSQUERA, J. M., ROMANEL, A., DRIER, Y., PARK, K., KITABAYASHI, N., MACDONALD, T. Y., GHANDI, M., VAN ALLEN, E., KRYUKOV, G. V., SBONER, A., THEURILLAT, J. P., SOONG, T. D., NICKERSON, E., AUCLAIR, D., TEWARI, A., BELTRAN, H., ONOFRIO, R. C., BOYSEN, G., GUIDUCCI, C., BARBIERI, C. E., CIBULSKIS, K., SIVACHENKO, A., CARTER, S. L., SAKSENA, G., VOET, D., RAMOS, A. H., WINCKLER, W., CIPICCHIO, M., ARDLIE, K., KANTOFF, P. W., BERGER, M. F., GABRIEL, S. B., GOLUB, T. R., MEYERSON, M., LANDER, E. S., ELEMENTO, O., GETZ, G., DEMICHELIS, F., RUBIN, M. A. & GARRAWAY, L. A. 2013. Punctuated evolution of prostate cancer genomes. *Cell*, 153, 666-77.
- BAKER, S. J., FEARON, E. R., NIGRO, J. M., HAMILTON, S. R., PREISINGER, A. C., JESSUP, J. M., VANTUINEN, P., LEDBETTER, D. H., BARKER, D. F., NAKAMURA, Y., WHITE, R. & VOGELSTEIN, B. 1989. Chromosome 17 deletions and p53 gene mutations in colorectal carcinomas. *Science*, 244, 217-21.
- BANGI, E., ANG, C., SMIBERT, P., UZILOV, A. V., TEAGUE, A. G., ANTIPIN, Y., CHEN, R., HECHT, C., GRUSZCZYNSKI, N., YON, W. J., MALYSHEV, D., LASPINA, D., SELKRIDGE, I., RAINEY, H., MOE, A. S., LAU, C. Y., TAIK, P., WILCK, E., BHARDWAJ, A., SUNG, M., KIM, S., YUM, K., SEBRA, R., DONOVAN, M., MISIUKIEWICZ, K., SCHADT, E. E., POSNER, M. R. & CAGAN, R. L. 2019. A personalized platform identifies trametinib plus zoledronate for a patient with KRAS-mutant metastatic colorectal cancer. *Science Advances*, 5, eaav6528.

- BANGI, E., MURGIA, C., TEAGUE, A. G. S., SANSOM, O. J. & CAGAN, R. L. 2016. Functional exploration of colorectal cancer genomes using *Drosophila*. *Nature Communications*, 7, 13615.
- BHANOT, P., BRINK, M., SAMOS, C. H., HSIEH, J.-C., WANG, Y., MACKE, J. P., ANDREW, D., NATHANS, J. & NUSSE, R. 1996. A new member of the frizzled family from *Drosophila* functions as a Wingless receptor. *Nature*, 382, 225-230.
- BIDOU, L., BUGAUD, O., BELAKHOV, V., BAASOV, T. & NAMY, O. 2017. Characterization of new-generation aminoglycoside promoting premature termination codon readthrough in cancer cells. *RNA Biology*, 14, 378-388.
- BOU-HANNA, C., JARRY, A., LODE, L., SCHMITZ, I., SCHULZE-OSTHOFF, K., KURY, S., BEZIEAU, S., MOSNIER, J.-F. & LABOISSE, C. L. 2015. Acute cytotoxicity of MIRA-1/NSC19630, a mutant p53-reactivating small molecule, against human normal and cancer cells via a caspase-9-dependent apoptosis. *Cancer Letters*, 359, 211-217.
- BOUTIN, A. T., LIAO, W. T., WANG, M., HWANG, S. S., KARPINETS, T. V., CHEUNG, H., CHU, G. C., JIANG, S., HU, J., CHANG, K., VILAR, E., SONG, X., ZHANG, J., KOPETZ, S., FUTREAL, A., WANG, Y. A., KWONG, L. N. & DEPINHO, R. A. 2017. Oncogenic Kras drives invasion and maintains metastases in colorectal cancer. *Genes Dev*, 31, 370-382.
- BOZIC, I., GEROLD, J. M. & NOWAK, M. A. 2016. Quantifying Clonal and Subclonal Passenger Mutations in Cancer Evolution. *PLoS Comput Biol*, 12, e1004731.
- BRAICU, C., BUSE, M., BUSUIOC, C., DRULA, R., GULEI, D., RADULY, L., RUSU, A., IRIMIE, A., ATANASOV, A. G., SLABY, O., IONESCU, C. & BERINDAN-NEAGOE, I. 2019. A Comprehensive Review on MAPK: A Promising Therapeutic Target in Cancer. *Cancers (Basel)*, 11.
- BRAND, A. H. & PERRIMON, N. 1993. Targeted gene expression as a means of altering cell fates and generating dominant phenotypes. *Development*, 118, 401-415.
- BRAY, F., LAVERSANNE, M., SUNG, H., FERLAY, J., SIEGEL, R. L., SOERJOMATARAM, I. & JEMAL, A. 2024. Global cancer statistics 2022: GLOBOCAN estimates of incidence and mortality worldwide for 36 cancers in 185 countries. *CA: A Cancer Journal for Clinicians*, 74, 229-263.
- BURRELL, R. A., MCGRANAHAN, N., BARTEK, J. & SWANTON, C. 2013. The causes and consequences of genetic heterogeneity in cancer evolution. *Nature*, 501, 338-45.
- CALCAGNO, S. R., LI, S., COLON, M., KREINEST, P. A., THOMPSON, E. A., FIELDS, A. P. & MURRAY, N. R. 2008. Oncogenic *K-ras* promotes early carcinogenesis in the mouse proximal colon. *International Journal of Cancer*, 122, 2462-2470.
- CANCER RESEARCH UK, B. C. S.
- CAO, X., HOU, J., AN, Q., ASSARAF, Y. G. & WANG, X. 2020. Towards the overcoming of anticancer drug resistance mediated by p53 mutations. *Drug Resistance Updates*, 49, 100671.
- CAPONIGRO, G. & SELLERS, W. R. 2011. Advances in the preclinical testing of cancer therapeutic hypotheses. *Nat Rev Drug Discov*, 10, 179-87.
- CHANG, Y.-T., CHIU, I., WANG, Q., BUSTAMANTE, J., JIANG, W., RYCAJ, K., YI, S., LI, J., KOWALSKI-MUEGGE, J. & MATSUI, W. 2023. Loss of p53 enhances the tumor-initiating potential and drug resistance of clonogenic multiple myeloma cells. *Blood Advances*, 7, 3551-3560.
- CHANRION, M., KUPERSTEIN, I., BARRIÈRE, C., EL MARJOU, F., COHEN, D., VIGNJEVIC, D., STIMMER, L., PAUL-GILLOTEAUX, P., BIÈCHE, I., TAVARES, S. D. R., BOCCIA, G.-F., CACHEUX, W., MESEURE, D., FRE, S., MARTIGNETTI, L., LEGOIX-NÉ, P., GIRARD, E., FETLER, L., BARILLOT, E., LOUVARD, D., ZINOVYEV, A. & ROBINE, S. 2014. Concomitant Notch activation and p53 deletion trigger epithelial-to-mesenchymal transition and metastasis in mouse gut. *Nature Communications*, 5, 5005.
- CHAPEAU, E. A., GEMBARSKA, A., DURAND, E. Y., MANDON, E., ESTADIEU, C., ROMANET, V., WIESMANN, M., TIEDT, R., LEHAR, J., DE WECK, A., RAD, R., BARYS, L., JEAY, S., FERRETTI, S., KAUFFMANN, A., SUTTER, E., GREVOT, A., MOULIN, P., MURAKAMI, M., SELLERS, W. R., HOFMANN, F. & JENSEN, M. R. 2017. Resistance mechanisms to

- TP53-MDM2 inhibition identified by in vivo piggyBac transposon mutagenesis screen in an Arf<sup>2212</sup> mouse model. *Proceedings of the National Academy of Sciences*, 114, 3151-3156.
- CIOMBOR, K. K., WU, C. & GOLDBERG, R. M. 2015. Recent Therapeutic Advances in the Treatment of Colorectal Cancer. *Annual Review of Medicine*, 66, 83-95.
- CONG, B., THAKUR, T., URIBE, A. H., STAMOU, E., GOPINATH, S., MADDOCKS, O. & CAGAN, R. 2023. Colon Cancer Cells Evade Drug Action by Enhancing Drug Metabolism. Cold Spring Harbor Laboratory.
- CONG, F., SCHWEIZER, L. & VARMUS, H. 2004. Wnt signals across the plasma membrane to activate the beta-catenin pathway by forming oligomers containing its receptors, Frizzled and LRP. *Development*, 131, 5103-15.
- COOPER, H. S. 2007. Pathologic issues in the treatment of endoscopically removed malignant colorectal polyps. *J Natl Compr Canc Netw*, 5, 991-6.
- CRAYMER, L. 1984. Third multiple six, b structure. *Drosophila Information Service*, 60, 234.
- CUESTA, C., ARÉVALO-ALAMEDA, C. & CASTELLANO, E. 2021. The Importance of Being PI3K in the RAS Signaling Network. *Genes (Basel)*, 12.
- CUTSEM, E. V., KÖHNE, C.-H., HITRE, E., ZALUSKI, J., CHIEN, C.-R. C., MAKHSON, A., D'HAENS, G., PINTÉR, T., LIM, R., BODOKY, G., ROH, J. K., FOLPRECHT, G., RUFF, P., STROH, C., TEJPAN, S., SCHLICHTING, M., NIPPGEN, J. & ROUGIER, P. 2009. Cetuximab and Chemotherapy as Initial Treatment for Metastatic Colorectal Cancer. *New England Journal of Medicine*, 360, 1408-1417.
- DABROWSKI, M., BUKOWY-BIERYLLO, Z. & ZIETKIEWICZ, E. 2018. Advances in therapeutic use of a drug-stimulated translational readthrough of premature termination codons. *Molecular Medicine*, 24, 25.
- DAVIS, A., GAO, R. & NAVIN, N. 2017. Tumor evolution: Linear, branching, neutral or punctuated? *Biochim Biophys Acta Rev Cancer*, 1867, 151-161.
- DE GRAMONT, A., FIGER, A., SEYMOUR, M., HOMERIN, M., HMISSI, A., CASSIDY, J., BONI, C., CORTES-FUNES, H., CERVANTES, A., FREYER, G., PAPAMICHAEL, D., LE BAIL, N., LOUVET, C., HENDLER, D., DE BRAUD, F., WILSON, C., MORVAN, F. & BONETTI, A. 2000. Leucovorin and Fluorouracil With or Without Oxaliplatin as First-Line Treatment in Advanced Colorectal Cancer. *Journal of Clinical Oncology*, 18, 2938-2947.
- DE LANGEN, A. J., JOHNSON, M. L., MAZIERES, J., DINGEMANS, A.-M. C., MOUNTZIOS, G., PLESS, M., WOLF, J., SCHULER, M., LENA, H., SKOULIDIS, F., YONESHIMA, Y., KIM, S.-W., LINARDOU, H., NOVELLO, S., VAN DER WEKKEN, A. J., CHEN, Y., PETERS, S., FELIP, E., SOLOMON, B. J., RAMALINGAM, S. S., DOOMS, C., LINDSAY, C. R., FERREIRA, C. G., BLAIS, N., OBIOZOR, C. C., WANG, Y., MEHTA, B., VARRIEUR, T., NGARMCHAMNANRITH, G., STOLLENWERK, B., WATERHOUSE, D. & PAZ-ARES, L. 2023. Sotorasib versus docetaxel for previously treated non-small-cell lung cancer with KRAS<sup>G12C</sup> mutation: a randomised, open-label, phase 3 trial. *The Lancet*, 401, 733-746.
- DELEO, A. B., JAY, G., APPELLA, E., DUBOIS, G. C., LAW, L. W. & OLD, L. J. 1979. Detection of a transformation-related antigen in chemically induced sarcomas and other transformed cells of the mouse. *Proc Natl Acad Sci U S A*, 76, 2420-4.
- DROSTEN, M., SUM, E. Y. M., LECHUGA, C. G., SIMÓN-CARRASCO, L., JACOB, H. K. C., GARCÍA-MEDINA, R., HUANG, S., BEIJERSBERGEN, R. L., BERNARDS, R. & BARBACID, M. 2014. Loss of p53 induces cell proliferation via Ras-independent activation of the Raf/Mek/Erk signaling pathway. *Proceedings of the National Academy of Sciences*, 111, 15155-15160.
- DUFFY, J. B. 2002. GAL4 system in drosophila: A fly geneticist's swiss army knife. *genesis*, 34, 1-15.
- EL MARJOU, F., JANSSEN, K. P., HUNG-JUNN CHANG, B., LI, M., HINDIE, V., CHAN, L., LOUWARD, D., CHAMBON, P., METZGER, D. & ROBINE, S. 2004. Tissue-specific and inducible Cre-mediated recombination in the gut epithelium. *genesis*, 39, 186-193.
- FAES, S. & DORMOND, O. 2015. PI3K and AKT: Unfaithful Partners in Cancer. *Int J Mol Sci*, 16, 21138-52.

- FANGER, G. R., JOHNSON, N. L. & JOHNSON, G. L. 1997. MEK kinases are regulated by EGF and selectively interact with Rac/Cdc42. *The EMBO Journal*, 16, 4961-4972-4972.
- FEARON, E. R. & VOGELSTEIN, B. 1990. A genetic model for colorectal tumorigenesis. *Cell*, 61, 759-67.
- FLANAGAN, D. J., PENTINMIKKO, N., LUOPAJÄRVI, K., WILLIS, N. J., GILROY, K., RAVEN, A. P., MCGARRY, L., ENGLUND, J. I., WEBB, A. T., SCHARAW, S., NASREDDIN, N., HODDER, M. C., RIDGWAY, R. A., MINNEE, E., SPHYRIS, N., GILCHRIST, E., NAJUMUDEEN, A. K., ROMAGNOLO, B., PERRET, C., WILLIAMS, A. C., CLEVERS, H., NUMMELA, P., LÄHDE, M., ALITALO, K., HIETAKANGAS, V., HEDLEY, A., CLARK, W., NIXON, C., KIRSCHNER, K., JONES, E. Y., RISTIMÄKI, A., LEEDHAM, S. J., FISH, P. V., VINCENT, J.-P., KATAJISTO, P. & SANSOM, O. J. 2021. NOTUM from Apc-mutant cells biases clonal competition to initiate cancer. *Nature*, 594, 430-435.
- FLOQUET, C., DEFORGES, J., ROUSSET, J.-P. & BIDOUE, L. 2011. Rescue of non-sense mutated p53 tumor suppressor gene by aminoglycosides. *Nucleic Acids Research*, 39, 3350-3362.
- FOX, D. T. & SPRADLING, A. C. 2009. The *Drosophila* Hindgut Lacks Constitutively Active Adult Stem Cells but Proliferates in Response to Tissue Damage. *Cell Stem Cell*, 5, 290-297.
- GÂNDARA, R. M. C., MAHIDA, Y. R. & POTTEN, C. S. 2012. Regional Differences in Stem and Transit Cell Proliferation and Apoptosis in the Terminal Ileum and Colon of Mice After 12 Gy. *International Journal of Radiation Oncology\*Biophysics*, 82, e521-e528.
- GRIM, J. E., KNOBLAUGH, S. E., GUTHRIE, K. A., HAGAR, A., SWANGER, J., HESPELT, J., DELROW, J. J., SMALL, T., GRADY, W. M., NAKAYAMA, K. I. & CLURMAN, B. E. 2012. Fbw7 and p53 cooperatively suppress advanced and chromosomally unstable intestinal cancer. *Mol Cell Biol*, 32, 2160-7.
- GRIZZI, F. & CHIRIVA-INTERNATI, M. 2006. Cancer: looking for simplicity and finding complexity. *Cancer Cell International*, 6, 4.
- GUINNEY, J., DIENSTMANN, R., WANG, X., DE REYNIÈS, A., SCHLICKER, A., SONESON, C., MARISA, L., ROEPMAN, P., NYAMUNDANDA, G., ANGELINO, P., BOT, B. M., MORRIS, J. S., SIMON, I. M., GERSTER, S., FESSLER, E., DE SOUSA E MELO, F., MISSIAGLIA, E., RAMAY, H., BARRAS, D., HOMICKO, K., MARU, D., MANYAM, G. C., BROOM, B., BOIGE, V., PEREZ-VILLAMIL, B., LADERAS, T., SALAZAR, R., GRAY, J. W., HANAHAHAN, D., TABERNERO, J., BERNARDS, R., FRIEND, S. H., LAURENT-PUIG, P., MEDEMA, J. P., SADANANDAM, A., WESSELS, L., DELORENZI, M., KOPETZ, S., VERMEULEN, L. & TEJPAR, S. 2015. The consensus molecular subtypes of colorectal cancer. *Nature Medicine*, 21, 1350-1356.
- HAIGIS, K. M., KENDALL, K. R., WANG, Y., CHEUNG, A., HAIGIS, M. C., GLICKMAN, J. N., NIWA-KAWAKITA, M., SWEET-CORDERO, A., SEBOLT-LEOPOLD, J., SHANNON, K. M., SETTLEMAN, J., GIOVANNINI, M. & JACKS, T. 2008. Differential effects of oncogenic K-Ras and N-Ras on proliferation, differentiation and tumor progression in the colon. *Nature Genetics*, 40, 600-608.
- HALBERG, R. B., KATZUNG, D. S., HOFF, P. D., MOSER, A. R., COLE, C. E., LUBET, R. A., DONEHOWER, L. A., JACOBY, R. F. & DOVE, W. F. 2000. Tumorigenesis in the multiple intestinal neoplasia mouse: redundancy of negative regulators and specificity of modifiers. *Proc Natl Acad Sci U S A*, 97, 3461-6.
- HANAHAHAN, D. & WEINBERG, R. A. 2011. Hallmarks of cancer: the next generation. *Cell*, 144, 646-74.
- HANSEN, A. R., MASSARD, C., OTT, P. A., HAAS, N. B., LOPEZ, J. S., EJADI, S., WALLMARK, J. M., KEAM, B., DELORD, J. P., AGGARWAL, R., GOULD, M., YANG, P., KEEFE, S. M. & PIHA-PAUL, S. A. 2018. Pembrolizumab for advanced prostate adenocarcinoma: findings of the KEYNOTE-028 study. *Annals of Oncology*, 29, 1807-1813.
- HASSAN, C., ZULLO, A., RISIO, M., ROSSINI, F. P. & MORINI, S. 2005. Histologic risk factors and clinical outcome in colorectal malignant polyp: a pooled-data analysis. *Dis Colon Rectum*, 48, 1588-96.

- HAY, M., THOMAS, D. W., CRAIGHEAD, J. L., ECONOMIDES, C. & ROSENTHAL, J. 2014. Clinical development success rates for investigational drugs. *Nat Biotechnol*, 32, 40-51.
- HENRY, J. T., COKER, O., CHOWDHURY, S., SHEN, J. P., MORRIS, V. K., DASARI, A., RAGHAV, K., NUSRAT, M., KEE, B., PARSEGHIAN, C., PANT, S., JEYAKUMAR, N., ZHU, L., NISHIOKA, Y., FOGELMAN, D., WOLFF, R. A., HONG, D., OVERMAN, M. J., VAUTHEY, J., KOPETZ, S. & JOHNSON, B. 2021. Comprehensive Clinical and Molecular Characterization of KRAS (G12C)-Mutant Colorectal Cancer. *JCO Precis Oncol*, 5.
- HERNÁNDEZ, A. R., KLEIN, A. M. & KIRSCHNER, M. W. 2012. Kinetic responses of  $\beta$ -catenin specify the sites of Wnt control. *Science*, 338, 1337-40.
- HIENTZ, K., MOHR, A., BHAKTA-GUHA, D. & EFFERTH, T. 2017. The role of p53 in cancer drug resistance and targeted chemotherapy. *Oncotarget*, 8, 8921-8946.
- HO, M. Y. K., MORRIS, M. J., PIRHALLA, J. L., BAUMAN, J. W., PENDRY, C. B., ORFORD, K. W., MORRISON, R. A. & COX, D. S. 2014. Trametinib, a first-in-class oral MEK inhibitor mass balance study with limited enrollment of two male subjects with advanced cancers. *Xenobiotica*, 44, 352-368.
- HU, Z., SUN, R. & CURTIS, C. 2017. A population genetics perspective on the determinants of intra-tumor heterogeneity. *Biochim Biophys Acta Rev Cancer*, 1867, 109-126.
- HUMPHRIES, A., CERESER, B., GAY, L. J., MILLER, D. S., DAS, B., GUTTERIDGE, A., ELIA, G., NYE, E., JEFFERY, R., POULSOM, R., NOVELLI, M. R., RODRIGUEZ-JUSTO, M., MCDONALD, S. A., WRIGHT, N. A. & GRAHAM, T. A. 2013. Lineage tracing reveals multipotent stem cells maintain human adenomas and the pattern of clonal expansion in tumor evolution. *Proc Natl Acad Sci U S A*, 110, E2490-9.
- IMAMURA, Y., MORIKAWA, T., LIAO, X., LOCHHEAD, P., KUCHIBA, A., YAMAUCHI, M., QIAN, Z. R., NISHIHARA, R., MEYERHARDT, J. A., HAIGIS, K. M., FUCHS, C. S. & OGINO, S. 2012. Specific mutations in KRAS codons 12 and 13, and patient prognosis in 1075 BRAF wild-type colorectal cancers. *Clin Cancer Res*, 18, 4753-63.
- INFANTE, J. R., FECHER, L. A., FALCHOOK, G. S., NALLAPAREDDY, S., GORDON, M. S., BECERRA, C., DEMARINI, D. J., COX, D. S., XU, Y., MORRIS, S. R., PEDDAREDDIGARI, V. G., LE, N. T., HART, L., BENDELL, J. C., ECKHARDT, G., KURZROCK, R., FLAHERTY, K., BURRIS, H. A., 3RD & MESSERSMITH, W. A. 2012. Safety, pharmacokinetic, pharmacodynamic, and efficacy data for the oral MEK inhibitor trametinib: a phase 1 dose-escalation trial. *Lancet Oncol*, 13, 773-81.
- JACKSON, E. L., WILLIS, N., MERCER, K., BRONSON, R. T., CROWLEY, D., MONTOYA, R., JACKS, T. & TUVESON, D. A. 2001. Analysis of lung tumor initiation and progression using conditional expression of oncogenic *K-ras*. *Genes & Development*, 15, 3243-3248.
- JANSSEN, K. P., ALBERICI, P., FSIHI, H., GASPAR, C., BREUKEL, C., FRANKEN, P., ROSTY, C., ABAL, M., EL MARJOU, F., SMITS, R., LOUVARD, D., FODDE, R. & ROBINE, S. 2006. APC and oncogenic KRAS are synergistic in enhancing Wnt signaling in intestinal tumor formation and progression. *Gastroenterology*, 131, 1096-109.
- JOANITO, I., WIRAPATI, P., ZHAO, N., NAWAZ, Z., YEO, G., LEE, F., ENG, C. L. P., MACALINAO, D. C., KAHRAMAN, M., SRINIVASAN, H., LAKSHMANAN, V., VERBANDT, S., TSANTOULIS, P., GUNN, N., VENKATESH, P. N., POH, Z. W., NAHAR, R., OH, H. L. J., LOO, J. M., CHIA, S., CHEOW, L. F., CHERUBA, E., WONG, M. T., KUA, L., CHUA, C., NGUYEN, A., GOLOVAN, J., GAN, A., LIM, W.-J., GUO, Y. A., YAP, C. K., TAY, B., HONG, Y., CHONG, D. Q., CHOK, A.-Y., PARK, W.-Y., HAN, S., CHANG, M. H., SEOW-EN, I., FU, C., MATHEW, R., TOH, E.-L., HONG, L. Z., SKANDERUP, A. J., DASGUPTA, R., ONG, C.-A. J., LIM, K. H., TAN, E. K. W., KOO, S.-L., LEOW, W. Q., TEJPAN, S., PRABHAKAR, S. & TAN, I. B. 2022. Single-cell and bulk transcriptome sequencing identifies two epithelial tumor cell states and refines the consensus molecular classification of colorectal cancer. *Nature Genetics*, 54, 963-975.
- JONES, R. P., SUTTON, P. A., EVANS, J. P., CLIFFORD, R., MCAVOY, A., LEWIS, J., ROUSSEAU, A., MOUNTFORD, R., MCWHIRTER, D. & MALIK, H. Z. 2017. Specific mutations in

- KRAS codon 12 are associated with worse overall survival in patients with advanced and recurrent colorectal cancer. *Br J Cancer*, 116, 923-929.
- JONKERS, J., MEUWISSEN, R., VAN DER GULDEN, H., PETERSE, H., VAN DER VALK, M. & BERNIS, A. 2001. Synergistic tumor suppressor activity of BRCA2 and p53 in a conditional mouse model for breast cancer. *Nature Genetics*, 29, 418-425.
- KASTAN, M. B., ZHAN, Q., EL-DEIRY, W. S., CARRIER, F., JACKS, T., WALSH, W. V., PLUNKETT, B. S., VOGELSTEIN, B. & FORNACE, A. J., JR. 1992. A mammalian cell cycle checkpoint pathway utilizing p53 and GADD45 is defective in ataxia-telangiectasia. *Cell*, 71, 587-97.
- KAYHANIAN, H., GOODE, E., SCLAFANI, F., ANG, J. E., GERLINGER, M., GONZALEZ DE CASTRO, D., SHEPHERD, S., PECKITT, C., RAO, S., WATKINS, D., CHAU, I., CUNNINGHAM, D. & STARLING, N. 2018. Treatment and Survival Outcome of BRAF-Mutated Metastatic Colorectal Cancer: A Retrospective Matched Case-Control Study. *Clin Colorectal Cancer*, 17, e69-e76.
- KESHELAVA, N., ZUO, J. J., CHEN, P., WAIDYARATNE, S. N., LUNA, M. C., GOMER, C. J., TRICHE, T. J. & REYNOLDS, C. P. 2001. Loss of p53 Function Confers High-Level Multidrug Resistance in Neuroblastoma Cell Lines<sup>1</sup>. *Cancer Research*, 61, 6185-6193.
- KLAUS, A. & BIRCHMEIER, W. 2008. Wnt signalling and its impact on development and cancer. *Nat Rev Cancer*, 8, 387-98.
- KÖHNE, C. H., VAN CUTSEM, E., WILS, J., BOKEMEYER, C., EL-SERAFI, M., LUTZ, M. P., LORENZ, M., REICHARDT, P., RÜCKLE-LANZ, H., FRICKHOFEN, N., FUCHS, R., MERGENTHALER, H. G., LANGENBUCH, T., VANHOEFER, U., ROUGIER, P., VOIGTMANN, R., MÜLLER, L., GENICOT, B., ANAK, O. & NORDLINGER, B. 2005. Phase III study of weekly high-dose infusional fluorouracil plus folinic acid with or without irinotecan in patients with metastatic colorectal cancer: European Organisation for Research and Treatment of Cancer Gastrointestinal Group Study 40986. *J Clin Oncol*, 23, 4856-65.
- KOSTADINOV, R. L., KUHNER, M. K., LI, X., SANCHEZ, C. A., GALIPEAU, P. C., PAULSON, T. G., SATHER, C. L., SRIVASTAVA, A., ODZE, R. D., BLOUNT, P. L., VAUGHAN, T. L., REID, B. J. & MALEY, C. C. 2013. NSAIDs modulate clonal evolution in Barrett's esophagus. *PLoS Genet*, 9, e1003553.
- KOYAMA, S. & KIKUCHI, A. 2001. Ras interaction with RalGDS effector targets. *Methods Enzymol*, 332, 127-38.
- KRESS, M., MAY, E., CASSINGENA, R. & MAY, P. 1979. Simian virus 40-transformed cells express new species of proteins precipitable by anti-simian virus 40 tumor serum. *J Virol*, 31, 472-83.
- KUBOKI, Y., FAKIH, M., STRICKLER, J., YAEGER, R., MASUISHI, T., KIM, E. J., BESTVINA, C. M., KOPETZ, S., FALCHOOK, G. S., LANGER, C., KRAUSS, J., PURI, S., CARDONA, P., CHAN, E., VARRIEUR, T., MUKUNDAN, L., ANDERSON, A., TRAN, Q. & HONG, D. S. 2024. Sotorasib with panitumumab in chemotherapy-refractory KRAS(G12C)-mutated colorectal cancer: a phase 1b trial. *Nat Med*, 30, 265-270.
- LAMBERT, J. M., LAMBERT, Q. T., REUTHER, G. W., MALLIRI, A., SIDEROVSKI, D. P., SONDEK, J., COLLARD, J. G. & DER, C. J. 2002. Tiam1 mediates Ras activation of Rac by a PI(3)K-independent mechanism. *Nat Cell Biol*, 4, 621-5.
- LAMBERT, J. M. R., GORZOV, P., VEPRINTSEV, D. B., SÖDERQVIST, M., SEGERBÄCK, D., BERGMAN, J., FERSHT, A. R., HAINAUT, P., WIMAN, K. G. & BYKOV, V. J. N. 2009. PRIMA-1 Reactivates Mutant p53 by Covalent Binding to the Core Domain. *Cancer Cell*, 15, 376-388.
- LANE, D. P. & CRAWFORD, L. V. 1979. T antigen is bound to a host protein in SV40-transformed cells. *Nature*, 278, 261-3.
- LAUGHON, A. & GESTELAND, R. F. 1984. Primary structure of the *Saccharomyces cerevisiae* GAL4 gene. *Mol Cell Biol*, 4, 260-7.
- LAVOIE, H. & THERRIEN, M. 2015. Regulation of RAF protein kinases in ERK signalling. *Nature Reviews Molecular Cell Biology*, 16, 281-298.

- LAWRENCE, M. S., STOJANOV, P., POLAK, P., KRYUKOV, G. V., CIBULSKIS, K., SIVACHENKO, A., CARTER, S. L., STEWART, C., MERMEL, C. H., ROBERTS, S. A., KIEZUN, A., HAMMERMAN, P. S., MCKENNA, A., DRIER, Y., ZOU, L., RAMOS, A. H., PUGH, T. J., STRANSKY, N., HELMAN, E., KIM, J., SOUGNEZ, C., AMBROGIO, L., NICKERSON, E., SHEFLER, E., CORTÉS, M. L., AUCLAIR, D., SAKSENA, G., VOET, D., NOBLE, M., DICARA, D., LIN, P., LICHTENSTEIN, L., HEIMAN, D. I., FENNELL, T., IMIELINSKI, M., HERNANDEZ, B., HODIS, E., BACA, S., DULAK, A. M., LOHR, J., LANDAU, D. A., WU, C. J., MELENDEZ-ZAJGLA, J., HIDALGO-MIRANDA, A., KOREN, A., MCCARROLL, S. A., MORA, J., CROMPTON, B., ONOFRIO, R., PARKIN, M., WINCKLER, W., ARDLIE, K., GABRIEL, S. B., ROBERTS, C. W. M., BIEGEL, J. A., STEGMAIER, K., BASS, A. J., GARRAWAY, L. A., MEYERSON, M., GOLUB, T. R., GORDENIN, D. A., SUNYAEV, S., LANDER, E. S. & GETZ, G. 2013. Mutational heterogeneity in cancer and the search for new cancer-associated genes. *Nature*, 499, 214-218.
- LEEDHAM, S. J., RODENAS-CUADRADO, P., HOWARTH, K., LEWIS, A., MALLAPPA, S., SEGDIRSAS, S., DAVIS, H., JEFFERY, R., RODRIGUEZ-JUSTO, M., KESHAV, S., TRAVIS, S. P., GRAHAM, T. A., EAST, J., CLARK, S. & TOMLINSON, I. P. 2013. A basal gradient of Wnt and stem-cell number influences regional tumour distribution in human and mouse intestinal tracts. *Gut*, 62, 83-93.
- LENGYEL, J. A. & IWAKI, D. D. 2002. It Takes Guts: The Drosophila Hindgut as a Model System for Organogenesis. *Developmental Biology*, 243, 1-19.
- LEVINE, A. J. 2019a. The many faces of p53: something for everyone. *Journal of Molecular Cell Biology*, 11, 524-530.
- LEVINE, A. J. 2019b. Targeting Therapies for the p53 Protein in Cancer Treatments. *Annual Review of Cancer Biology*, 3, 21-34.
- LEYSTRA, A. A., DEMING, D. A., ZAHM, C. D., FARHOUD, M., OLSON, T. J. P., HADAC, J. N., NETTEKOVEN, L. A., ALBRECHT, D. M., CLIPSON, L., SULLIVAN, R., WASHINGTON, M. K., TORREALBA, J. R., WEICHERT, J. P. & HALBERG, R. B. 2012. Mice Expressing Activated PI3K Rapidly Develop Advanced Colon Cancer. *Cancer Research*, 72, 2931.
- LINZER, D. I. & LEVINE, A. J. 1979. Characterization of a 54K dalton cellular SV40 tumor antigen present in SV40-transformed cells and uninfected embryonal carcinoma cells. *Cell*, 17, 43-52.
- LIU, C., LI, Y., SEMENOV, M., HAN, C., BAEG, G. H., TAN, Y., ZHANG, Z., LIN, X. & HE, X. 2002. Control of beta-catenin phosphorylation/degradation by a dual-kinase mechanism. *Cell*, 108, 837-47.
- LONGLEY, D. B., HARKIN, D. P. & JOHNSTON, P. G. 2003. 5-Fluorouracil: mechanisms of action and clinical strategies. *Nature Reviews Cancer*, 3, 330-338.
- LOWENSTEIN, E. J., DALY, R. J., BATZER, A. G., LI, W., MARGOLIS, B., LAMMERS, R., ULLRICH, A., SKOLNIK, E. Y., BAR-SAGI, D. & SCHLESSINGER, J. 1992. The SH2 and SH3 domain-containing protein GRB2 links receptor tyrosine kinases to ras signaling. *Cell*, 70, 431-42.
- LUEBECK, E. G. & MOOLGAVKAR, S. H. 2002. Multistage carcinogenesis and the incidence of colorectal cancer. *Proc Natl Acad Sci U S A*, 99, 15095-100.
- MALEY, C. C. 2007. Multistage carcinogenesis in Barrett's esophagus. *Cancer Lett*, 245, 22-32.
- MALLETTE, F. A. & FERBEYRE, G. 2007. The DNA damage signaling pathway connects oncogenic stress to cellular senescence. *Cell Cycle*, 6, 1831-6.
- MARTIN, L., GRIGORYAN, A., WANG, D., WANG, J., BREDA, L., RIVELLA, S., CARDOZO, T. & GARDNER, L. B. 2014. Identification and Characterization of Small Molecules That Inhibit Nonsense-Mediated RNA Decay and Suppress Nonsense p53 Mutations. *Cancer Research*, 74, 3104-3113.
- MATALLANAS, D., BIRTWISTLE, M., ROMANO, D., ZEBISCH, A., RAUCH, J., VON KRIEGSHEIM, A. & KOLCH, W. 2011. Raf family kinases: old dogs have learned new tricks. *Genes Cancer*, 2, 232-60.
- MENG, L., THAPA, R., DELGADO, M. G., GOMEZ, M. F., JI, R., KNEPPER, T. C., HUBBARD, J. M., WANG, X., PERMUTH, J. B., KIM, R. D., LABER, D. A. & XIE, H. 2023. Association of

- Age With Treatment-Related Adverse Events and Survival in Patients With Metastatic Colorectal Cancer. *JAMA Network Open*, 6, e2320035.
- MICCHELLI, C. A. & PERRIMON, N. 2006. Evidence that stem cells reside in the adult *Drosophila* midgut epithelium. *Nature*, 439, 475-9.
- MICHAELIS, M., ROTHWEILER, F., BARTH, S., CINATL, J., VAN RIKXOORT, M., LÖSCHMANN, N., VOGES, Y., BREITLING, R., VON DEIMLING, A., RÖDEL, F., WEBER, K., FEHSE, B., MACK, E., STIEWE, T., DOERR, H. W., SPEIDEL, D. & CINATL, J. 2011. Adaptation of cancer cells from different entities to the MDM2 inhibitor nutlin-3 results in the emergence of p53-mutated multi-drug-resistant cancer cells. *Cell Death & Disease*, 2, e243-e243.
- MODEST, D. P., RICARD, I., HEINEMANN, V., HEGEWISCH-BECKER, S., SCHMIEGEL, W., PORSCHE, R., STINTZING, S., GRAEVEN, U., ARNOLD, D., VON WEIKERSTHAL, L. F., GIESSEN-JUNG, C., STAHLER, A., SCHMOLL, H. J., JUNG, A., KIRCHNER, T., TANNAPFEL, A. & REINACHER-SCHICK, A. 2016. Outcome according to KRAS-, NRAS- and BRAF-mutation as well as KRAS mutation variants: pooled analysis of five randomized trials in metastatic colorectal cancer by the AIO colorectal cancer study group. *Ann Oncol*, 27, 1746-53.
- MOSER, A. R., MATTES, E. M., DOVE, W. F., LINDSTROM, M. J., HAAG, J. D. & GOULD, M. N. 1993. ApcMin, a mutation in the murine Apc gene, predisposes to mammary carcinomas and focal alveolar hyperplasias. *Proc Natl Acad Sci U S A*, 90, 8977-81.
- MOSER, A. R., PITOT, H. C. & DOVE, W. F. 1990. A dominant mutation that predisposes to multiple intestinal neoplasia in the mouse. *Science*, 247, 322-4.
- NAGY, A. 2000. Cre recombinase: the universal reagent for genome tailoring. *Genesis*, 26, 99-109.
- NAJUMUDEEN, A. K., CETECI, F., FEY, S. K., HAMM, G., STEVEN, R. T., HALL, H., NIKULA, C. J., DEXTER, A., MURTA, T., RACE, A. M., SUMPTON, D., VLAHOV, N., GAY, D. M., KNIGHT, J. R. P., JACKSTADT, R., LEACH, J. D. G., RIDGWAY, R. A., JOHNSON, E. R., NIXON, C., HEDLEY, A., GILROY, K., CLARK, W., MALLA, S. B., DUNNE, P. D., RODRIGUEZ-BLANCO, G., CRITCHLOW, S. E., MROWINSKA, A., MALVIYA, G., SOLOVYEV, D., BROWN, G., LEWIS, D. Y., MACKAY, G. M., STRATHDEE, D., TARDITO, S., GOTTLIEB, E., TAKATS, Z., BARRY, S. T., GOODWIN, R. J. A., BUNCH, J., BUSHELL, M., CAMPBELL, A. D. & SANSOM, O. J. 2021. The amino acid transporter SLC7A5 is required for efficient growth of KRAS-mutant colorectal cancer. *Nat Genet*, 53, 16-26.
- NAKAYAMA, M. & OSHIMA, M. 2019. Mutant p53 in colon cancer. *Journal of Molecular Cell Biology*, 11, 267-276.
- NAVIN, N., KRASNITZ, A., RODGERS, L., COOK, K., METH, J., KENDALL, J., RIGGS, M., EBERLING, Y., TROGE, J., GRUBOR, V., LEVY, D., LUNDIN, P., MĀNĚR, S., ZETTERBERG, A., HICKS, J. & WIGLER, M. 2010. Inferring tumor progression from genomic heterogeneity. *Genome Res*, 20, 68-80.
- NEUMANN, J., ZEINDL-EBERHART, E., KIRCHNER, T. & JUNG, A. 2009. Frequency and type of KRAS mutations in routine diagnostic analysis of metastatic colorectal cancer. *Pathology - Research and Practice*, 205, 858-862.
- NIGRO, J. M., BAKER, S. J., PREISINGER, A. C., JESSUP, J. M., HOSTETTER, R., CLEARY, K., BIGNER, S. H., DAVIDSON, N., BAYLIN, S., DEVILEE, P. & ET AL. 1989. Mutations in the p53 gene occur in diverse human tumour types. *Nature*, 342, 705-8.
- OCANA, A., PANDIELLA, A., SIU, L. L. & TANNOCK, I. F. 2010. Preclinical development of molecular-targeted agents for cancer. *Nat Rev Clin Oncol*, 8, 200-9.
- OLIVIER, M., HOLLSTEIN, M. & HAINAUT, P. 2010. TP53 mutations in human cancers: origins, consequences, and clinical use. *Cold Spring Harb Perspect Biol*, 2, a001008.
- OREN, M., REICH, N. C. & LEVINE, A. J. 1982. Regulation of the cellular p53 tumor antigen in teratocarcinoma cells and their differentiated progeny. *Mol Cell Biol*, 2, 443-9.
- OVERMAN, M. J., MCDERMOTT, R., LEACH, J. L., LONARDI, S., LENZ, H.-J., MORSE, M. A., DESAI, J., HILL, A., AXELSON, M., MOSS, R. A., GOLDBERG, M. V., CAO, Z. A., LEDEINE, J.-M., MAGLINTE, G. A., KOPETZ, S. & ANDRÉ, T. 2017. Nivolumab in patients with metastatic DNA mismatch repair-deficient or microsatellite instability-

- high colorectal cancer (CheckMate 142): an open-label, multicentre, phase 2 study. *The Lancet Oncology*, 18, 1182-1191.
- PIERRE, S., BATS, A. S. & COUMOUL, X. 2011. Understanding SOS (Son of Sevenless). *Biochem Pharmacol*, 82, 1049-56.
- PINSON, K. I., BRENNAN, J., MONKLEY, S., AVERY, B. J. & SKARNES, W. C. 2000. An LDL-receptor-related protein mediates Wnt signalling in mice. *Nature*, 407, 535-8.
- POTTEN, C. S. 1998. Stem cells in gastrointestinal epithelium: numbers, characteristics and death. *Philos Trans R Soc Lond B Biol Sci*, 353, 821-30.
- PRAHALLAD, A., SUN, C., HUANG, S., DI NICOLANTONIO, F., SALAZAR, R., ZECCHIN, D., BEIJERSBERGEN, R. L., BARDELLI, A. & BERNARDS, R. 2012. Unresponsiveness of colon cancer to BRAF(V600E) inhibition through feedback activation of EGFR. *Nature*, 483, 100-3.
- PUNT, C. J., KOOPMAN, M. & VERMEULEN, L. 2017. From tumour heterogeneity to advances in precision treatment of colorectal cancer. *Nat Rev Clin Oncol*, 14, 235-246.
- RIM, E. Y., CLEVERS, H. & NUSSE, R. 2022. The Wnt Pathway: From Signaling Mechanisms to Synthetic Modulators. *Annu Rev Biochem*, 91, 571-598.
- ROPER, J., TAMMELA, T., CETINBAS, N. M., AKKAD, A., ROGHANIAN, A., RICKELT, S., ALMEQDADI, M., WU, K., OBERLI, M. A., SÁNCHEZ-RIVERA, F. J., PARK, Y. K., LIANG, X., ENG, G., TAYLOR, M. S., AZIMI, R., KEDRIN, D., NEUPANE, R., BEYAZ, S., SICINSKA, E. T., SUAREZ, Y., YOO, J., CHEN, L., ZUKERBERG, L., KATAJISTO, P., DESHPANDE, V., BASS, A. J., TSICHLIS, P. N., LEES, J., LANGER, R., HYNES, R. O., CHEN, J., BHUTKAR, A., JACKS, T. & YILMAZ, Ö. H. 2017. In vivo genome editing and organoid transplantation models of colorectal cancer and metastasis. *Nature Biotechnology*, 35, 569-576.
- ROSEN, L. S., LORUSSO, P., MA, W. W., GOLDMAN, J. W., WEISE, A., COLEVAS, A. D., ADJEI, A., YAZJI, S., SHEN, A., JOHNSTON, S., HSIEH, H. J., CHAN, I. T. & SIKIC, B. I. 2016. A first-in-human phase I study to evaluate the MEK1/2 inhibitor, cobimetinib, administered daily in patients with advanced solid tumors. *Invest New Drugs*, 34, 604-13.
- RUSSO, A., BAZAN, V., IACOPETTA, B., KERR, D., SOUSSI, T. & GEBBIA, N. 2005. The TP53 colorectal cancer international collaborative study on the prognostic and predictive significance of p53 mutation: influence of tumor site, type of mutation, and adjuvant treatment. *J Clin Oncol*, 23, 7518-28.
- RYOO, H. D., GORENC, T. & STELLER, H. 2004. Apoptotic Cells Can Induce Compensatory Cell Proliferation through the JNK and the Wingless Signaling Pathways. *Developmental Cell*, 7, 491-501.
- SABAPATHY, K. & LANE, D. P. 2018. Therapeutic targeting of p53: all mutants are equal, but some mutants are more equal than others. *Nat Rev Clin Oncol*, 15, 13-30.
- SAHA, M. N., CHEN, Y., CHEN, M. H., CHEN, G. & CHANG, H. 2014. Small molecule MIRA-1 induces in vitro and in vivo anti-myeloma activity and synergizes with current anti-myeloma agents. *British Journal of Cancer*, 110, 2224-2231.
- SANCHO, R., JANDKE, A., DAVIS, H., DIEFENBACHER, M. E., TOMLINSON, I. & BEHRENS, A. 2010. F-box and WD repeat domain-containing 7 regulates intestinal cell lineage commitment and is a haploinsufficient tumor suppressor. *Gastroenterology*, 139, 929-41.
- SANSOM, O. J., MENIEL, V., WILKINS, J. A., COLE, A. M., OIEN, K. A., MARSH, V., JAMIESON, T. J., GUERRA, C., ASHTON, G. H., BARBACID, M. & CLARKE, A. R. 2006. Loss of Apc allows phenotypic manifestation of the transforming properties of an endogenous K-ras oncogene in vivo. *Proceedings of the National Academy of Sciences*, 103, 14122-14127.
- SANSOM, O. J., REED, K. R., HAYES, A. J., IRELAND, H., BRINKMANN, H., NEWTON, I. P., BATTLE, E., SIMON-ASSMANN, P., CLEVERS, H., NATHKE, I. S., CLARKE, A. R. & WINTON, D. J. 2004. Loss of Apc in vivo immediately perturbs Wnt signaling, differentiation, and migration. *Genes & Development*, 18, 1385-1390.

- SATO, T., VAN ES, J. H., SNIPPERT, H. J., STANGE, D. E., VRIES, R. G., VAN DEN BORN, M., BARKER, N., SHROYER, N. F., VAN DE WETERING, M. & CLEVERS, H. 2011. Paneth cells constitute the niche for Lgr5 stem cells in intestinal crypts. *Nature*, 469, 415-418.
- SATO, T., VRIES, R. G., SNIPPERT, H. J., VAN DE WETERING, M., BARKER, N., STANGE, D. E., VAN ES, J. H., ABO, A., KUJALA, P., PETERS, P. J. & CLEVERS, H. 2009. Single Lgr5 stem cells build crypt-villus structures in vitro without a mesenchymal niche. *Nature*, 459, 262-5.
- SCHIRRIPA, M., NAPPO, F., CREMOLINI, C., SALVATORE, L., ROSSINI, D., BENSI, M., BUSINELLO, G., PIETRANTONIO, F., RANDON, G., FUCÀ, G., BOCCACCINO, A., BERGAMO, F., LONARDI, S., DEI TOS, A. P., FASSAN, M. & LOUPAKIS, F. 2020. KRAS G12C Metastatic Colorectal Cancer: Specific Features of a New Emerging Target Population. *Clin Colorectal Cancer*, 19, 219-225.
- SCHULZ-HEDDERGOTT, R. & MOLL, U. M. 2018. Gain-of-Function (GOF) Mutant p53 as Actionable Therapeutic Target. *Cancers (Basel)*, 10.
- SHIBATA, H., TOYAMA, K., SHIOYA, H., ITO, M., HIROTA, M., HASEGAWA, S., MATSUMOTO, H., TAKANO, H., AKIYAMA, T., TOYOSHIMA, K., KANAMARU, R., KANEGAE, Y., SAITO, I., NAKAMURA, Y., SHIBA, K. & NODA, T. 1997. Rapid colorectal adenoma formation initiated by conditional targeting of the Apc gene. *Science*, 278, 120-3.
- SHIEH, S. Y., IKEDA, M., TAYA, Y. & PRIVES, C. 1997. DNA damage-induced phosphorylation of p53 alleviates inhibition by MDM2. *Cell*, 91, 325-34.
- SIEGEL, R. L., MILLER, K. D., GODING SAUER, A., FEDEWA, S. A., BUTTERLY, L. F., ANDERSON, J. C., CERCEK, A., SMITH, R. A. & JEMAL, A. 2020. Colorectal cancer statistics, 2020. *CA: A Cancer Journal for Clinicians*, 70, 145-164.
- SIEGMUND, K. D., MARJORAM, P., TAVARÉ, S. & SHIBATA, D. 2009. Many colorectal cancers are "flat" clonal expansions. *Cell Cycle*, 8, 2187-93.
- SIEGMUND, K. D., MARJORAM, P., TAVARÉ, S. & SHIBATA, D. 2011. High DNA methylation pattern intratumoral diversity implies weak selection in many human colorectal cancers. *PLoS One*, 6, e21657.
- SIEVERS, C. K., ZOU, L. S., PICKHARDT, P. J., MATKOWSKYJ, K. A., ALBRECHT, D. M., CLIPSON, L., BACHER, J. W., POOLER, B. D., MOAWAD, F. J., CASH, B. D., REICHELDERFER, M., VO, T. N., NEWTON, M. A., LARGET, B. R. & HALBERG, R. B. 2017. Subclonal diversity arises early even in small colorectal tumours and contributes to differential growth fates. *Gut*, 66, 2132-2140.
- SIMKENS, L. H., VAN TINTEREN, H., MAY, A., TEN TIJE, A. J., CREEMERS, G. J., LOOSVELD, O. J., DE JONGH, F. E., ERDKAMP, F. L., ERJAVEC, Z., VAN DER TORREN, A. M., TOL, J., BRAUN, H. J., NIEBOER, P., VAN DER HOEVEN, J. J., HAASJES, J. G., JANSEN, R. L., WALS, J., CATS, A., DERLEYN, V. A., HONKOOOP, A. H., MOL, L., PUNT, C. J. & KOOPMAN, M. 2015. Maintenance treatment with capecitabine and bevacizumab in metastatic colorectal cancer (CAIRO3): a phase 3 randomised controlled trial of the Dutch Colorectal Cancer Group. *Lancet*, 385, 1843-52.
- SOLBERG, N. T., MELHEIM, M., STRAND, M. F., OLSEN, P. A. & KRAUSS, S. 2019. MEK Inhibition Induces Canonical WNT Signaling through YAP in KRAS Mutated HCT-15 Cells, and a Cancer Preventive FOXO3/FOXO1 Ratio in Combination with TNKS Inhibition. *Cancers (Basel)*, 11.
- SORICH, M. J., WIESE, M. D., ROWLAND, A., KICHENADASSE, G., MCKINNON, R. A. & KARAPETIS, C. S. 2015. Extended RAS mutations and anti-EGFR monoclonal antibody survival benefit in metastatic colorectal cancer: a meta-analysis of randomized, controlled trials. *Ann Oncol*, 26, 13-21.
- SOTTORIVA, A., KANG, H., MA, Z., GRAHAM, T. A., SALOMON, M. P., ZHAO, J., MARJORAM, P., SIEGMUND, K., PRESS, M. F., SHIBATA, D. & CURTIS, C. 2015. A Big Bang model of human colorectal tumor growth. *Nat Genet*, 47, 209-16.
- SOTTORIVA, A., SPITERI, I., SHIBATA, D., CURTIS, C. & TAVARÉ, S. 2013. Single-molecule genomic data delineate patient-specific tumor profiles and cancer stem cell organization. *Cancer Res*, 73, 41-9.

- STAAL, F. J. & SEN, J. M. 2008. The canonical Wnt signaling pathway plays an important role in lymphopoiesis and hematopoiesis. *Eur J Immunol*, 38, 1788-94.
- STIEWE, T. & HARAN, T. E. 2018. How mutations shape p53 interactions with the genome to promote tumorigenesis and drug resistance. *Drug Resistance Updates*, 38, 27-43.
- STRONG, L. C., WILLIAMS, W. R. & TAINSKY, M. A. 1992. The Li-Fraumeni syndrome: from clinical epidemiology to molecular genetics. *Am J Epidemiol*, 135, 190-9.
- SUZUKI, Y., NG, S. B., CHUA, C., LEOW, W. Q., CHNG, J., LIU, S. Y., RAMNARAYANAN, K., GAN, A., HO, D. L., TEN, R., SU, Y., LEZHAVA, A., LAI, J. H., KOH, D., LIM, K. H., TAN, P., ROZEN, S. G. & TAN, I. B. 2017. Multiregion ultra-deep sequencing reveals early intermixing and variable levels of intratumoral heterogeneity in colorectal cancer. *Mol Oncol*, 11, 124-139.
- TAI, A.-S., PENG, C.-H., PENG, S.-C. & HSIEH, W.-P. 2018. Decomposing the subclonal structure of tumors with two-way mixture models on copy number aberrations. *PLOS ONE*, 13, e0206579.
- TAKASHIMA, S., MKRTCHYAN, M., YOUNOSSI-HARTENSTEIN, A., MERRIAM, J. R. & HARTENSTEIN, V. 2008. The behaviour of *Drosophila* adult hindgut stem cells is controlled by Wnt and Hh signalling. *Nature*, 454, 651-5.
- TAPE, C. J. 2024. Plastic persisters: revival stem cells in colorectal cancer. *Trends in Cancer*, 10, 185-195.
- TCGA 2012. Comprehensive molecular characterization of human colon and rectal cancer. *Nature*, 487, 330-337.
- TEJPAR, S., CELIK, I., SCHLICHTING, M., SARTORIUS, U., BOKEMEYER, C. & VAN CUTSEM, E. 2012. Association of KRAS G13D tumor mutations with outcome in patients with metastatic colorectal cancer treated with first-line chemotherapy with or without cetuximab. *J Clin Oncol*, 30, 3570-7.
- THOMSEN, M., GUREN, M. G., SKOVLUND, E., GLIMELIUS, B., HJERMSTAD, M. J., JOHANSEN, J. S., KURE, E., SORBYE, H., PFEIFFER, P., CHRISTOFFERSEN, T., GUREN, T. K. & TVEIT, K. M. 2017. Health-related quality of life in patients with metastatic colorectal cancer, association with systemic inflammatory response and RAS and BRAF mutation status. *Eur J Cancer*, 81, 26-35.
- TOLCHER, A. W., PENG, W. & CALVO, E. 2018. Rational Approaches for Combination Therapy Strategies Targeting the MAP Kinase Pathway in Solid Tumors. *Mol Cancer Ther*, 17, 3-16.
- UCHI, R., TAKAHASHI, Y., NIIDA, A., SHIMAMURA, T., HIRATA, H., SUGIMACHI, K., SAWADA, G., IWAYA, T., KURASHIGE, J., SHINDEN, Y., IGUCHI, T., EGUCHI, H., CHIBA, K., SHIRAISHI, Y., NAGAE, G., YOSHIDA, K., NAGATA, Y., HAENO, H., YAMAMOTO, H., ISHII, H., DOKI, Y., IINUMA, H., SASAKI, S., NAGAYAMA, S., YAMADA, K., YACHIDA, S., KATO, M., SHIBATA, T., OKI, E., SAEKI, H., SHIRABE, K., ODA, Y., MAEHARA, Y., KOMUNE, S., MORI, M., SUZUKI, Y., YAMAMOTO, K., ABURATANI, H., OGAWA, S., MIYANO, S. & MIMORI, K. 2016. Integrated Multiregional Analysis Proposing a New Model of Colorectal Cancer Evolution. *PLoS Genet*, 12, e1005778.
- VAN CUTSEM, E., LANG, I., FOLPRECHT, G., NOWACKI, M., BARONE, C., SHCHEPOTIN, I., MAUREL, J., CUNNINGHAM, D., CELIK, I. & KOHNE, C. 2010. Cetuximab plus FOLFIRI: Final data from the CRYSTAL study on the association of KRAS and BRAF biomarker status with treatment outcome. *Journal of Clinical Oncology*, 28, 3570-3570.
- VAN NOORT, M., MEELDIJK, J., VAN DER ZEE, R., DESTREE, O. & CLEVERS, H. 2002. Wnt signaling controls the phosphorylation status of beta-catenin. *J Biol Chem*, 277, 17901-5.
- VASSILEV, L. T., VU, B. T., GRAVES, B., CARVAJAL, D., PODLASKI, F., FILIPOVIC, Z., KONG, N., KAMMLOTT, U., LUKACS, C., KLEIN, C., FOTOUHI, N. & LIU, E. A. 2004. In Vivo Activation of the p53 Pathway by Small-Molecule Antagonists of MDM2. *Science*, 303, 844-848.
- VOGELSTEIN, B., LANE, D. & LEVINE, A. J. 2000. Surfing the p53 network. *Nature*, 408, 307-10.

- VOGELSTEIN, B., PAPADOPOULOS, N., VELCULESCU, V. E., ZHOU, S., DIAZ, L. A., JR. & KINZLER, K. W. 2013. Cancer genome landscapes. *Science*, 339, 1546-58.
- WELSH, S. J. & CORRIE, P. G. 2015. Management of BRAF and MEK inhibitor toxicities in patients with metastatic melanoma. *Ther Adv Med Oncol*, 7, 122-36.
- WU, X., BAYLE, J. H., OLSON, D. & LEVINE, A. J. 1993. The p53-mdm-2 autoregulatory feedback loop. *Genes Dev*, 7, 1126-32.
- WU, Z.-Q., BRABLETZ, T., FEARON, E., WILLIS, A. L., HU, C. Y., LI, X.-Y. & WEISS, S. J. 2012. Canonical Wnt suppressor, Axin2, promotes colon carcinoma oncogenic activity. *Proceedings of the National Academy of Sciences*, 109, 11312-11317.
- XUE, J. Y., ZHAO, Y., ARONOWITZ, J., MAI, T. T., VIDES, A., QERIQI, B., KIM, D., LI, C., DE STANCHINA, E., MAZUTIS, L., RISSO, D. & LITO, P. 2020. Rapid non-uniform adaptation to conformation-specific KRAS(G12C) inhibition. *Nature*, 577, 421-425.
- YAEGER, R., WEISS, J., PELSTER, M. S., SPIRA, A. I., BARVE, M., OU, S.-H. I., LEAL, T. A., BEKAI-SAAB, T. S., PAWELETZ, C. P., HEAVEY, G. A., CHRISTENSEN, J. G., VELASTEGUI, K., KHEOH, T., DER-TOROSSIAN, H. & KLEMPNER, S. J. 2023. Adagrasib with or without Cetuximab in Colorectal Cancer with Mutated *KRAS* G12C. *New England Journal of Medicine*, 388, 44-54.
- YATES, L. R., GERSTUNG, M., KNAPPSKOG, S., DESMEDT, C., GUNDEM, G., VAN LOO, P., AAS, T., ALEXANDROV, L. B., LARSIMONT, D., DAVIES, H., LI, Y., JU, Y. S., RAMAKRISHNA, M., HAUGLAND, H. K., LILLENG, P. K., NIK-ZAINAL, S., MCLAREN, S., BUTLER, A., MARTIN, S., GLODZIK, D., MENZIES, A., RAINE, K., HINTON, J., JONES, D., MUDIE, L. J., JIANG, B., VINCENT, D., GREENE-COLOZZI, A., ADNET, P. Y., FATIMA, A., MAETENS, M., IGNATIADIS, M., STRATTON, M. R., SOTIRIOU, C., RICHARDSON, A. L., LØNNING, P. E., WEDGE, D. C. & CAMPBELL, P. J. 2015. Subclonal diversification of primary breast cancer revealed by multiregion sequencing. *Nat Med*, 21, 751-9.
- YOON, H. H., TOUGERON, D., SHI, Q., ALBERTS, S. R., MAHONEY, M. R., NELSON, G. D., NAIR, S. G., THIBODEAU, S. N., GOLDBERG, R. M., SARGENT, D. J. & SINICROPE, F. A. 2014. KRAS codon 12 and 13 mutations in relation to disease-free survival in BRAF-wild-type stage III colon cancers from an adjuvant chemotherapy trial (N0147 alliance). *Clin Cancer Res*, 20, 3033-43.
- YOSHII, S., NOJIMA, M., NOSHO, K., OMORI, S., KUSUMI, T., OKUDA, H., TSUKAGOSHI, H., FUJITA, M., YAMAMOTO, H. & HOSOKAWA, M. 2014. Factors associated with risk for colorectal cancer recurrence after endoscopic resection of T1 tumors. *Clin Gastroenterol Hepatol*, 12, 292-302.e3.
- ZACHE, N., LAMBERT, J. M. R., RÖKAEUS, N., SHEN, J., HAINAUT, P., BERGMAN, J., WIMAN, K. G. & BYKOV, V. J. N. 2008. Mutant p53 targeting by the low molecular weight compound STIMA-1. *Molecular Oncology*, 2, 70-80.
- ZHANG, Y. & WANG, X. 2020. Targeting the Wnt/ $\beta$ -catenin signaling pathway in cancer. *Journal of Hematology & Oncology*, 13, 165.
- ZHAO, J., NASSAR, M. A., GAVAZZI, I. & WOOD, J. N. 2006. Tamoxifen-inducible NaV1.8-CreERT2 recombinase activity in nociceptive neurons of dorsal root ganglia. *Genesis*, 44, 364-71.
- ZHONG, Y., KATAVOLOS, P., NGUYEN, T., LAU, T., BOGGS, J., SAMBRONE, A., KAN, D., MERCHANT, M., HARSTAD, E., DIAZ, D., COSTA, M. & SCHUTTEN, M. 2016. Tankyrase Inhibition Causes Reversible Intestinal Toxicity in Mice with a Therapeutic Index < 1. *Toxicol Pathol*, 44, 267-78.
- ZHOU, X., HAO, Q. & LU, H. 2019. Mutant p53 in cancer therapy—the barrier or the path. *Journal of Molecular Cell Biology*, 11, 293-305.
- ZHU, G., PAN, C., BEI, J. X., LI, B., LIANG, C., XU, Y. & FU, X. 2020. Mutant p53 in Cancer Progression and Targeted Therapies. *Front Oncol*, 10, 595187.

# Appendix

- Cong B, Thakur T, Uribe AH, Stamou E, Gopinath S, Maddocks O, Cagan R. Colon Cancer Cells Evade Drug Action by Enhancing Drug Metabolism. bioRxiv [Preprint]. 2023 Dec 23:2023.12.21.572817. doi: 10.1101/2023.12.21.572817. PMID: 38187524; PMCID: PMC10769412.
- Cong B, Stamou E, Pennel K, Thakur T, Mckenzie M, Matly A, Gopinath S, Edwards J, Cagan R. WNT Signalling Promotes NF- $\kappa$ B Activation and Drug Resistance in KRAS-Mutant Colorectal Cancer. bioRxiv [Preprint]. 2023 Dec 23:2023.12.21.572810. doi: 10.1101/2023.12.21.572810. PMID: 38187607; PMCID: PMC10769410.